THE DEVELOPMENT OF A REVERSIBLE AND FINITELY VARIABLE CAMBER WINDSURF FIN

by

Simon Barry Fagg

Thesis submitted in partial fulfilment of the requirement of Bournemouth University for the Degree of Doctor of Philosophy

Bournemouth University

September 1997

The Development of a Reversible and Finitely Variable Camber Windsurf Fin

Abstract

An investigation was undertaken to identify and develop a practical method for improving the lift to drag ratio (L/D) of the contemporary windsurf fin.

It was established that the contemporary windsurf fin is at an advanced stage of evolution and that a fundamental reworking of the design is required to attain significant L/D gains. In particular the symmetrically foiled cross-section (required for equal performance on each sailing tack) limits the performance potential of the device.

The benefits of using camber in the design of lifting sections for high lift and low drag are well known. Traditional variable camber lifting surfaces utilise leading and trailing edge flap technologies to vary the geometry (camber) of the cross-section. However, this method for generating variable camber is not considered to be suitable or practical for the windsurf fin, primarily due to the increases in drag associated with conventional flaps. An alternative approach for developing a variable camber windsurf fin is therefore considered.

It is proposed to use hydroelastic tailoring techniques to realise a reversible and finitely variable camber cross section for the fins used in the sport of windsurfing. The camber in the cross-section is invoked by the pressure differential acting on the two surfaces of the fin when it is at an incidence angle to the freestream. The magnitude of the camber is adaptive and responds passively by design, material usage and sailor input.

As part of the preliminary investigation a computer based analysis tool was developed to perform the two dimensional investigation into the coupling effect between the fluid flow and the hydroelastically tailored cross section. Based on the outcome of this work a prototype windsurf fin employing a hydroelastic cross section was fabricated and tested.

Results from this preliminary investigation establish the potential for using a hydroelastically tailored cross-section to significantly increase the L/D performance of a windsurf fin of nominal surface area (when compared with contemporary designs).

CONTENTS

APPENDICES

4

FIGURES LIST

TABLES LIST

ACKNOWLEDGEMENTS

NOMENCLATURE

Abbreviations

2D	Two Dimensional
3D	Three Dimensional
CFD	Computational Fluid Dynamics
CFSAT	Coupled Fluid and Structural Analysis Tool
GFRP	Glass Fibre Reinforced Plastic
HTWF	Hydroelastically Tailored Windsurf Fin
FEA	Finite Element Analysis
FSW	Forward Swept Wing
MAW	Mission Adaptive Wing
NLF	Natural Laminar Flow

Symbols

AR	Aspect Ratio (b^2/S)
b	Span of Lifting Surface
c	Chord Length
c_p	Minimum Pressure Coefficient
C_d	Section Drag Coefficient
C_D	Wing Drag Coefficient
C_{Di}	Induced Drag
C_l	Section Lift Coefficient
C_L	Wing Lift Coefficient
$C_L(\alpha)$	Lift Coefficient at an Incidence Angle
$C_L(0)$	Lift due to Camber at Zero Incidence Angle
C_{Lmax}	Maximum Lift Coefficient
D	Wing Drag (N)
K	Planform Efficiency Constant

L	Wing Lift (N)
L/D	Wing Lift to Drag Ratio
p	Local Static Pressure
p_0	Freestream Flow Pressure
p_v	Vapour Pressure of Fluid
R_e	Reynolds Number
S	Area of Lifting Surface
t	Airfoil Thickness
t/c	Thickness Ratio
u	Local Flow Velocity at a Point in the Flow
U_c	Critical Flow Velocity
u_0	Freestream Flow Velocity
α	Incidence Angle
α_{ef}	Effective Incidence Angle
α_g	Geometric Incidence Angle
α_i	Induced Incidence Angle
π	pi (3.14159) 5 d.p.
σ	Cavitation Number
$\sigma_{(c)}$	Critical Cavitation Number
υ	Kinematic Viscosity (m^2s^{-1})

1.0   Introduction

Windsurfing is a spectacular mass participant sport in which the energy of the wind is used to propel the sailor over the surface of the water (Figure 1.1). The sport has grown rapidly since its origins in the late 1960s as can be seen by the development of the Professional Windsurfing Association (PWA) World Tour competition series and by the inclusion of the sport in the Olympic Games.

The original windsurfers were cumbersome and slow, bearing little resemblance to the modern equipment which is substantially lighter, more efficient and capable of propelling the sailor to speeds in excess 80 km/h (45 knots).

1.1   The Equipment Used in the Sport of Windsurfing

The equipment used in the sport of windsurfing consists of a sail assembly which is joined to the board by means of a flexible universal joint. The sail assembly comprises a mast, boom and sail-cloth. The board is similar to a conventional surfboard and comprises a hull, fin(s) on the underside of the hull and footstraps to enable the sailor stay in contact with the equipment at high speeds. The sailor uses bodyweight and rig movements in conjunction with footsteering techniques to control the speed and direction of the craft.

1.1.1   The Evolution of the Equipment

The search for effective high-speed marine, land and air vehicles has a long history. The search for higher speeds and improved overall efficiency can be cited as the primary driving forces behind the development of the windsurfing equipment [123].

In the early days of the sport, the windsurfing equipment was very similar to dinghy craft in that a 'soft' sail and displacement type hull were employed. A displacement hull of nominally constant wetted length is however notoriously poor for high speed vessels

because the magnitude of viscous resistance increases rapidly due to its dependence on velocity squared (v^2), where for a flat plate;

$$Drag \approx \frac{1}{2}\rho v^2 SC_D \tag{1.1}$$

We should recognise that C_D will vary with Reynolds's Number (i.e. especially whether laminar or turbulent flow) and with pressure and induced drag. C_D cannot therefore be regarded as a constant.

To limit the rate of increase in resistance with increasing forward speed there are three philosophies that can be used for the design of the hull [6] [18] [27] [43] [66] [142].

1. Use a planing hull design in which the hull is raised in the water, by the application of a dynamic supporting force, thereby reducing the wetted surface area.

2. Use hydrofoils in which the hull is raised clear of the water by the dynamic force of the immersed foils.

3. Use an air cushion (hovercraft) to raise the hull clear of the water.

1.1.1.1 The Planing Hull Windsurfer

The use of a planing hull design on windsurf boards was introduced in the late 1970s and has proven to be effective in reducing the drag of the hull and elevating the attainable speeds of the complete assembly. Windsurfers supported by dynamic forces such as through the use of hydrofoils or air cushions have not been successfully developed.

In conjunction with hull developments, advancements in sail and fin technology have had an equally positive effect in improving the efficiency of the complete assembly and the attainable speed [64] [144].

Over the years the equipment has evolved through a process of 'inspired trial and error', whereby feedback from the sailors is used as the primary source of information for the sail, hull and fin designers. This is not as unconventional as it may first seem based on the fact that until very recently the evolution and design of aircraft wings was similarly described by Dillner et al [37] as a process of, *'enlightened cut and try'*, relying almost exclusively on the use of empirical data and information acquired by physical flow testing techniques. Marchaj [99] expands on this point by stating,

'unlike the airplane, whose development resulted from the close co-operation of scientists and technologists, the modern racing yacht has been evolved almost entirely by the concerted efforts of enthusiastic skippers, designers and sailmakers with little direct reference to basic scientific principles. In fact, yacht designing and particularly sailmaking , have been working to a rule of thumb - a very good rule of thumb - based on hundreds of years of accumulated experience. '

Garrett [61] concludes that, *'A good measure of the state of development of a device is to look at the variation in its design. Items that have reached an advanced stage of evolutionary development are all very similar in design'*. This scenario is particularly true in the sport of windsurfing where the design of the fin has remained nominally the same for many years. Burkett [19] points out, *'modern race and wave fins are all fairly similar in design and function....with the differences (between the various designs) being very subtle indeed so that you should not expect a revolutionary surprise when changing between these various modern fins'*.

From this it can be concluded that the contemporary windsurf fin is at an advanced stage of evolution and that alternative design approaches are required to realise further significant performance gains.

Significant performance gains in the ultimate speed of the windsurf assembly could be realised through a reduction in the drag of the fin [123]. Other land based and hard water (ice) sail powered vehicles (land yachts, ice yachts and land surfers) are capable of speeds well in excess of the windsurfer [99] (greater than 160 km/h), with the same mode of locomotion. The difference in speed between these craft is therefore attributable to the larger magnitudes of parasitic drag associated with the fin and hull. A reduction in drag will also enhance the acceleration potential of the equipment.

For this reason development work into the design of the hull and the fin is an ongoing process of practical interest to competitive sailors. The fin is in fact one of the easiest components to change and is capable of having the greatest effects on overall performance [31].

Because the fins are at an advanced stage of development (in their current format) a radical reworking of the design is required to see any noticeable performance gains [36]. Pillet [109] even goes as far as to suggest that the fins of the future will need to become intelligent and adaptive to meet this requirement.

1.1.2   Global Model of the Windsurfer Assembly

To enable a better understanding of the role of the fin as part of the complete windsurfer assembly a mathematical model of the system needs to be developed.

In any discussion of the mechanics of marine vehicles great care must be taken to define a model of the system and system boundaries accurately. Systems involving natural phenomena such as that of the ocean, or atmosphere are notoriously difficult to investigate [27]. For this reason approximations and assumptions are often made, such as ignoring the

influence of the surface waves and only considering parts of the problem in a two dimensional sense.

The modeling of a dynamic system, such as the windsurfer, is particularly problematic due to the interaction of the sailor and the equipment, as well as the natural environment of the air, water and air/water interface. In particular the wave motions towards the surface of the sea can greatly affect the loading and hence the performance of the fin. Although this type of unsteady loading has been successfully modeled by Hugo and Jumper,[76] it is felt that the generation of such a dynamic model is beyond the scope of this work. Therefore, an alternative simplified steady state model is employed [135].

These models indicate the primary interactions between the components of the windsurf board (as shown in Figure 1.2) and the required balancing of forces for controlled and steady navigation.

1.1.3   The Role of the Windsurf Fin

The primary role of the windsurf fin is to produce a lifting force to counteract the sideways force of the sail, as well as providing directional control and stability[16][17][24][26][80][81][82][99]. Without the fin the complete assembly would be pushed downwind under the action of the sail.

With the modern planing hull designs the wetted length is reduced to a minimum (as compared with a displacement type hull), thereby elevating the role of the fin in generating the required sideways force.

The magnitudes of the lifting force generated by the fin used on a modern planing hull windsurfer vary between 300 N and 600 N [16][17][135]. The magnitudes of drag generated by the fin typically vary between 20 N and 50 N (the drag from the fin accounts for approximately one sixth of the total drag, - with the drag due to windage and the drag of the hull accounting for the rest).

Generally, the surface area of the fin is selected to match the surface area of the sail which means that a larger sail will require the use of a larger fin for comfortable sailing. There are however no set rules governing fin selection as this is very much down to personal preference, sailing stance and the prevailing conditions.

1.2   The Disciplines in the Sport of Windsurfing

In most sports there exist specialised disciplines and events. In the sport of cycling a multitude of separate and distinctive disciplines exist, such as mountain biking, speed trialing and pursuit to name but a few. Each of these disciplines places a set of distinctive requirements on the rider and the equipment such that the equipment is tailored to suit the mode of use. Due to this tailoring of the equipment, a bicycle optimised for one discipline is unlikely to perform well in another.

The same scenario exists in the sport of windsurfing where there are four distinctive disciplines and types of competition sailing.

1. Wave Sailing
2. Course Racing
3. Slalom Racing
4. Speed Sailing

Generally, for the racing type disciplines the equipment is designed to be highly efficient, which in the case of the fins means that high aspect ratio, 'upright' designs are used [64][96]. In wave sailing, the equipment is 'detuned' through the introduction of rake and lower aspect ratios, which although detrimental in terms of hydrodynamic efficiency does make the fin more 'user friendly' and maneuverable.

Although the design details of the board, fin and sail can vary considerably for each discipline, the fundamental principles governing the operation and interaction of the

equipment components is the same for each discipline. Therefore it is possible to consider the work as being applicable for each of the separate disciplines in the sport.

1.3   Design Aim

The overall aim of the research project is to establish a practical and realistic method (or methods) for improving the hydrodynamic operational efficiency of the conventional windsurf fin.

Improvements in the performance of the new design (or design feature) will be gauged in terms of a net gain in the ratio of lift to drag (L/D) achieved in comparison with the existing contemporary designs.

1.4   The Research Program

The program of research was as follows;

1. To research the role and operation of contemporary windsurf fins.

2. To investigate the most suitable approaches for increasing the lift and/or reducing the drag generated by a windsurf fin of a nominal surface area.

3. To propose a practical method for increasing the lift and/or reducing the drag generated by a windsurf fin of a nominal surface area.

4. To investigate the effectiveness of the proposed design solution.

5. To fabricate a prototype windsurf fin for testing and evaluation of the proposed design solution.

Figure 1.1   Planing Windsurf Board

Sail
Sideways
Force

Sailor
Weight

Fin Lift

Aerodynamic
Drag

Lift

Sail
Forward
Force

Trim Angle

Board and
Fin Drag

Fin Lift

Board Sideways Force

Board and
Fin Drag

Yaw Angle

Direction
of Advance

Sail
Forward
Force

Sail Side Force
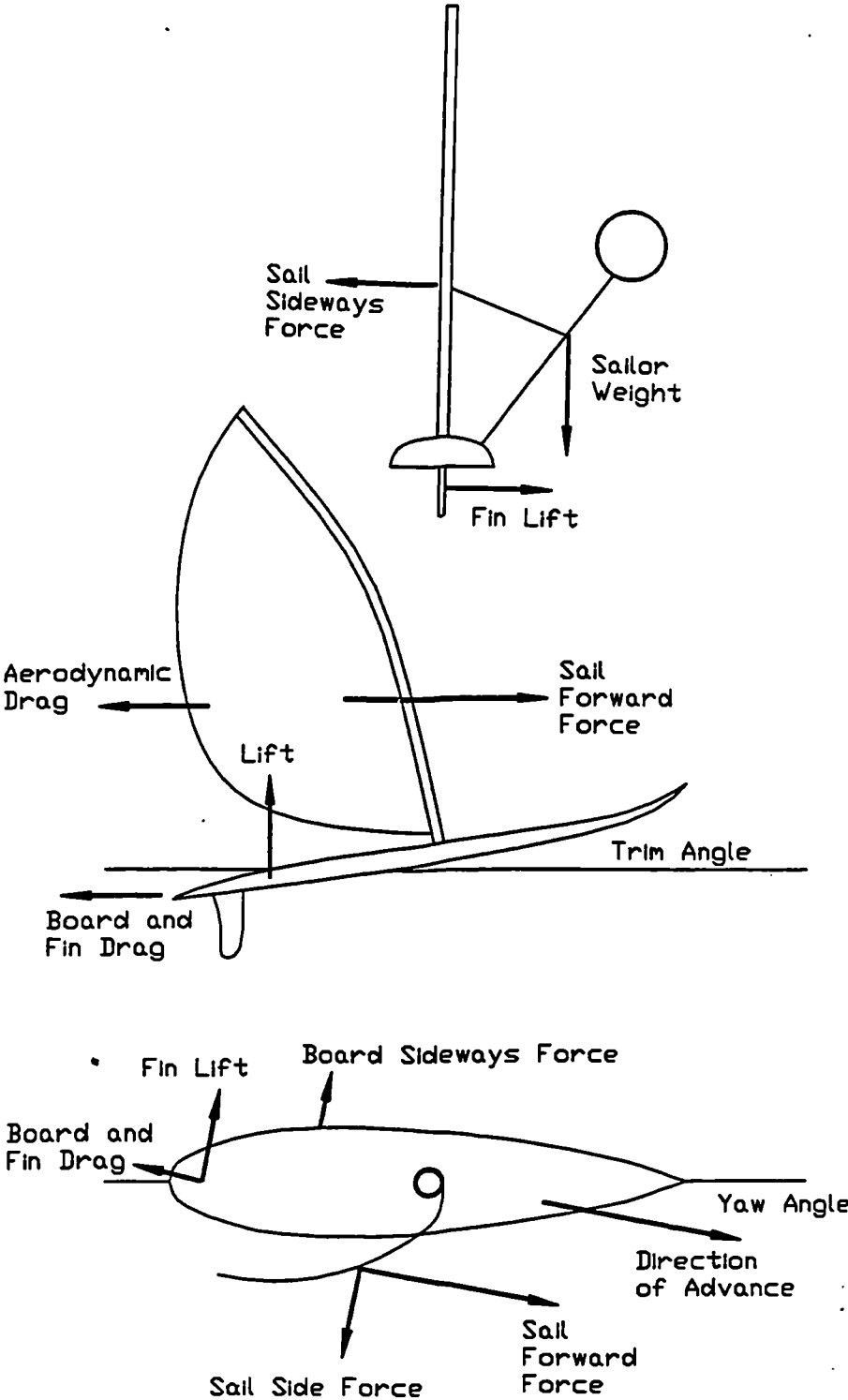
Figure 1.2 Primary Forces Acting on the Windsurf Assembly.

22

2.0   The Conventional Windsurf Fin

Literature specific to the design and operation of the windsurf fin is generally limited to articles in the 'Windsurfing Press'. Although these provide a good insight into the views held by many within the sport they do not necessarily represent a thorough and scientific examination of the subject area.

2.1   The Anatomy of the Conventional Windsurf Fin

The windsurf fin is located on the underside of hull of the board and is fully immersed in the water under normal steady sailing conditions. If this immersion is not maintained, flow separation and spinout (severe loss of lift also referred to as stall) due to ventilation will be experienced by the fin as air is able to pass into the low pressure region of the fin thereby destroying the integrity of the flow [121].

The operation of the fin on a windsurfer can be considered as analogous to the operation of the keel on a sailing boat. Two of the primary functions performed by the keel are [61][99];

1. To generate a hydrodynamic sideforce at minimum additional drag to balance the opposite aerodynamic sideforce produced by the sails.

2. To secure good directional stability and balance in rough seas.

Function 1 is a commensurable quality which can be determined and measured quantitatively in terms of lift and drag, whereas **function 2** is about 'feel' and is therefore subjective and incommensurable in nature, making it difficult to gage and compare accurately.

Assessing the performance of a windsurf fin is problematic as the success of a design can be as much about its 'feel' as about the actual hydrodynamic efficiency [47] [64].

23

Determining the incommensurable nature and 'feel' of any item of sporting equipment (such as a football, a racquet, a bat and particularly a fin) is beyond the scope of this work. This project is therefore solely concerned with evaluating the commensurable quantities of the lift and drag generated by the fin.

2.2   Flow Around the Windsurf Fin

The nature of the flow around an object immersed in a moving fluid (or an object moving through a stationary fluid) is governed by the geometric shape, its orientation to and speed in the flow, as well as other flow parameters such as depth of immersion [78], temperature, viscosity, density and the localised pressure.

For a streamlined shape, the nature and pattern of the flow can be established through experimental techniques and/or reference to empirical data. Following recent advances in computer technology it is also possible to predict the nature of the flow using Computational Fluid Dynamics (CFD) techniques [4].

It has also been demonstrated that classical airfoil theory can be employed to predict the lift and drag generated by a finite length windsurf fin [78][135].

2.3   The Format and Operation of the Conventional Windsurf Fin

The geometric features of a range of contemporary windsurf fins are shown in Figure 2.1, clearly illustrating the diversity of planforms that have evolved for the disciplines within the sport. Figure 2.2 shows the nomenclature used to describe the geometric features of a windsurf fin. The non-dimensional planform of a hydrofoil can be uniquely defined in terms of the following three parameters [98];

1. Aspect Ratio (AR) - ratio of mean span to chord.
2. Taper Ratio - Ratio of tip chord to root chord.
3. Rake Angle (or sweep angle).

2.4   Two Dimensional Flow Characteristics of the Windsurf Fin

To simplify the analysis of a lifting surface it is convenient to consider the theoretical two dimensional operation of the cross section in isolation from the three dimensional flow effects due to the shape of the planform.

Due to the velocity changes in the flow around the cross section the localised pressure values vary in accordance with Bernoulli's equation;

$$p + \frac{1}{2}\rho U^2 = p_0 + \frac{1}{2}\rho U_0^2 = CONSTANT \qquad (2.1)$$

By using the velocity fluctuations and Bernoulli's equation a plot of the pressure field around a foil section can be generated, as shown in Figure 2.3. This illustrates the pressure differential between the upper and lower surfaces, as well as indicating the location of the minimum and maximum pressure. The regions of favourable (decreasing) and adverse (increasing) pressure gradients are also visible.

The lift and drag components of a two dimensional cross section can be provided in a non-dimensional form as follows;

$$C_l = \frac{LIFT}{\frac{1}{2}\rho S v^2} \qquad (2.2)$$

$$C_d = \frac{DRAG}{\frac{1}{2}\rho S v^2} \qquad (2.3)$$

The lift and drag coefficients (C_l and C_d) vary with the incidence angle of the cross section to the freestream. A plot of the C_l and C_d versus angle of incidence (Figure 2.4) is often used to describe the aerodynamic characteristics of the cross section.

The plot of C_l versus angle of incidence rises linearly until it reaches a maximum when the section stalls. The linear section of the C_l versus angle of incidence plot is often referred to as the lift slope of the section.

The C_d versus angle of incidence is approximately parabolic for angles of attack (below stall) and has a minimum value at low values of C_l.

The optimum operating angle of incidence for the cross section corresponds to the value of maximum Lift to Drag (L/D) ratio.

A conventional windsurf fin uses a streamlined and symmetrical cross-section which is designed to operate with equal efficiency on both sailing tacks (exceptions to this rule exist, such as the asymmetric sections used for one tack speed sailing [39] as well as the unconventional "Quattro" Fin by Gun Sails which features four alternately asymmetric sections over the span).

A symmetrical section can only develop lift if it is oriented with an angle of incidence to the freestream (whereas a cambered section will produce lift even at zero angle of incidence; with its lift also being a function of increasing angle of incidence). Other lifting surfaces which are designed to work in one direction only normally use a cambered section (fixed and variable).

For a symmetrically foiled cross-section an approximation of the C_l value as a function of incidence angle (before the onset of flow separation) is provided by the following formula [99],

$$C_l = 0.11(1+\frac{t}{c})\alpha \qquad\qquad (2.4)$$

26

This approximation serves to show that the maximum thickness and angle of incidence to the freestream are the governing parameters on the performance of a symmetrically foiled profile.

The location of the maximum thickness has been shown to have a minimal effect on the lift curve slope, but will influence the point of stall and hence C_{Lmax} [1]. There are however practical limits in using the body thickness (t/c) and angle of incidence alone to increase the value of C_{Lmax}.

For a 'general use' symmetrical cross section this would seem to be when the t/c ratio is approximately 12% and the angle of incidence is in the range of 6° - 9° [1] (corresponding with the maximum L/D value).

This establishes that the streamlining of the section has a minimal effect on the lift curve slope (before stall). Therefore the primary function of streamlining is to reduce the magnitudes of drag produced. It is therefore concluded that, *'streamlining can be considered as an engineering problem of enormous practical consequences where every effort to delay or avoid flow transition or separation can pay handsomely in terms of reduced drag, power required or increased velocity'* [99].

The drag generated by a streamlined cross section is referred to as profile drag and consists of the viscous effects (friction drag) and pressure change effects (pressure or wake drag). The primary reason for streamlining the cross section is to reduce the pressure drag (frictional drag is governed by the surface area and Reynolds Number although this too is influenced by the location of the transition point which in turn is determined by the shape of the foil section).

Minimal pressure drag is attained by reducing the size of the wake behind the section by ensuring that the flow remains attached to the foil surface as much as is possible. This is achieved by avoiding excessive contour changes and adverse pressure gradients.

The design of the cross section and hence the nature of the pressure gradients can also be used to increase the region of laminar flow. By using a favourable pressure gradient the transition to turbulent flow can be delayed, thereby reducing the magnitude of frictional drag. Figure 2.5 shows a plot of the measured frictional drag values for a number of flat plates. This indicates that based on Reynolds Number (R_e) alone, transition normally occurs between $R_e = 5 \times 10^5$ and 2×10^6 for a flow over a flat plate.

Based on a typical range of sailing speeds between 10 ms^{-1} and 20 ms^{-1} the Reynolds number for a windsurf fin can be derived as follows;

$$R_e = \frac{Ul}{\upsilon} \qquad (2.5)$$

where;

      l is the length of the body (typically 0.1m at base of fin)

      v is the kinematic viscosity of the fluid (1.19×10^{-6} m^{2}s^{-1} for salt water at 15°)

Giving;

      $R_e = 8.4 \times 10^5$ (at a velocity of 10 ms^{-1})

      $R_e = 1.7 \times 10^6$ (at a velocity of 20 ms^{-1})

This indicates that based on R_e alone a typical windsurf fin operating at a speed of 10 ms^{-1} would be likely to develop a partially turbulent flow. At a speed of 20 ms^{-1} the extent of the region of turbulent flow is likely to increase substantially (although it must be considered that for sailing at this elevated speed a fin with a smaller surface area and hence chord length (l) would be employed, which would reduce the value of R_e).

This assumption of transition from a laminar to turbulent flow is based on calculations for a flat plate. In the case of the windsurf fin transition is more likely to be triggered by the presence of the adverse pressure gradient.

The start of an adverse pressure gradient normally coincides with the point of maximum thickness and so this can be considered as the most likely point at which the flow will change from a laminar to a turbulent flow. Contemporary windsurf fins typically have the maximum thickness located between 30% to 50% of the chord distance from the nose. To further increase the regions of laminar flow it is therefore preferable to move the point of maximum thickness rearwards such that a favourable pressure gradient is maintained over a larger region of the foil surface. Again there are limitations to moving the maximum thickness rearwards as a sufficiently long region is required for the pressure recovery to satisfy the Kutta-Jowkowski condition (equal velocity) at the trailing edge [44].

2.4.1 Stall

As the angle of incidence is increased for a foil section the streamlining effect diminishes and eventually flow separation, or stall, occurs with a dramatic reduction in lift and increase in drag [107].

The mathematical theory of ideal fluids yields no information about the expected separation for even the most simple cases. In addition the point at which the stall takes place is sensitive to the Reynolds number, as well as the ambient turbulence of the fluid and the roughness of the foil [107].

The prediction of the angle of incidence at which C_{Lmax} and stall occurs is therefore a difficult task. Experimental techniques have established typical stalling angles of between 9° and 14° for a contemporary windsurf fins [16][17][26][135].

2.4.2 Cavitation

In any discussion involving hydrofoils the phenomena of cavitation needs to be considered. According to Dimotakis and Shen [38], the occurrence of cavitation produces undesirable changes in hydrodynamic performance, noise generation and physical damage. Therefore the ability to predict the occurrence of cavitation becomes an important engineering

problem. Because the physical processes involved with cavitation inception are complex, the prediction of cavitation performance has relied heavily on model experiments and extrapolation of these results to other scales.

In theory, cavitation occurs when the local flow pressure drops to the vapour pressure of water resulting in the formation of bubbles and cavities. This will occur if the velocity of the windsurf fin is sufficiently high, since pressure is a decreasing function of fluid velocity and incidence angle. In principle cavitation will commence when;

$$p_0 \leq p_v \tag{2.6}$$

or,

$$\sigma = \frac{p_0 - p_v}{\frac{1}{2}\rho U^2} \leq 0 \tag{2.7}$$

Particles in the water and surface imperfections mean that the pressure at which cavitation commences is higher than the theoretical value of zero [32]. For this reason the critical cavitation number (σ_c) is determined empirically. The critical velocity (U_c) at which cavitation will occur on a hydrofoil section can then be determined as follows;

$$U_c = \left[\frac{p_0 - p_v}{\frac{1}{2}\rho(\sigma_c - c_p)} \right]^{0.5} \tag{2.8}$$

For a windsurf fin at the surface of the sea the following figures are taken;

p_0 = 100 kPa at sea surface

p_v = 1.8 kPa for sea water of density (ρ) 1025 kgm^{-3}

σ_c = 0 (although realistically a higher number would be expected for a hydrofoil operating in a marine environment)

c_p = -0.5 (From 12.66% (t/c) Eppler foil e836 at α = 2° [6](2))

Giving;

$$U_c = 19.6 \text{ ms}^{-1} \text{ (approximately 37.8 knots)}$$

This indicates that for high speed sailors the windsurf fin is currently operating well within the domain of cavitation. Clayton and Bishop [27] confirm this by stating that the maximum operating speed of conventional sub-cavitating hydrofoils sections (as used on windsurf fins) is in the region of 20 ms^{-1} (approximately 40 knots). However, they also describe how the operational limits of conventional foils can be extended to 30 ms^{-1} (approximately 60 knots) through the use of delayed cavitation cross sections which have a more even pressure distribution on the suction surface.

Rogers [121] considers that the maximum attainable speed before cavitation for a conventional windsurf fin will be in the region of 50 knots (approximately 25 ms^{-1}) if a suitable cross section and planform is employed.

Crimi [32] supports this by demonstrating that the onset of cavitation can be delayed through the use of leading edge sweep. It is shown that it is the flow component normal to the leading edge that is the most influential factor in cavitation inception (as is the case in forestalling the compressibility effects on high speed aircraft[20]). Therefore the speed for cavitation inception on a finite length hydrofoil varies inversely as the cosine of the sweep angle. There are however limitations with using sweep (to delay cavitation inception) due to the associated increases in drag and reductions in wing lift effectiveness [20].

Beyond a speed of 30 ms^{-1} a supercavitating type foil section is required. This is shown in Figure 2.6 alongside typical sub-cavitating and delayed cavitation foil sections. At these speeds special techniques, such as the use of intentional cavitation devices [83], are then required to optimise the performance.

2.5   Three Dimensional Flow Effects

In a 2D flow the lifting surface is considered to be infinite in length such that there are no spawns components of velocity flow. However, with a finite length lifting surface deviations from the two dimensional flow exist. Due to the pressure differential at the tip of a finite length lifting surface the fluid tends to flow around from the region of high pressure to low pressure as shown in Figure 2.7. The result of this is threefold [72];

1. The foil surface near the tip is much less efficient at producing lift
2. This decrease in lift is accompanied by an increase in drag
3. The additional disturbing fluid movement developing towards the tip(s) modifies the direction of the oncoming flow near the foil, hence the effective angle of incidence along the foil span changes, as do lift and drag.

The downwash induced by the three dimensional flow causes a downward flow modification to the direction of the freestream, thus reducing the effectiveness of the lifting section. Additionally, these three dimensional flow effects result in a tip vortex and an additional drag referred to as induced drag.

For an elliptical wing the angle of incidence of the foil is reduced to a new effective value;

$$\alpha_{ef} = \alpha_g - \alpha_i \qquad (2.9)$$

substituting $$\alpha_i = \frac{C_L}{\pi AR} \qquad (2.10)$$

to give
$$\alpha_{ef} = \alpha_g - \frac{C_L}{\pi AR}\,(Radians) \qquad\qquad (2.11)$$

or
$$\alpha_{ef} = \alpha_g - 18.24 \times \frac{C_L}{\pi AR}\,(Degrees) \qquad\qquad (2.12)$$

The magnitude of the induced drag due to the three dimensional flow effects is given by;

$$C_{Di} = \frac{C_L^2}{\pi AR} \qquad\qquad (2.13)$$

where C_{Di} is the induced drag to the 3D flow effects.

These equations for the effective incidence angle and induced drag show the crucial role played by the planform in terms of lift and drag performance. A plot of the lift coefficient (C_l) as a function of AR is shown in Figure 2.8, with a similar plot of the drag coefficient (C_d) shown in Figure 2.9. This illustrates the reduction in lift effectiveness and increases in drag associated with a reduction in AR. The benefits of increasing the aspect ratio to reduce the influence of the 3D flow effects are thereby established.

2.6   Scope of the Investigation

The previous sections have established the fundamental features and operational characteristics of the conventional windsurf fin. Determining the theoretical stalling and cavitational characteristics of hydrofoils is complex and can be considered to be somewhat specialist topic areas. For this reason it is not proposed to undertake a detailed investigation into the cavitating and stalling characteristics of the contemporary windsurf fin. Instead the work will be concerned with the pre-stall range of incidence angles (nominally $\leq 10°$) and the sub-cavitating range of sailing speeds (nominally $\leq 20\ ms^{-1}$).
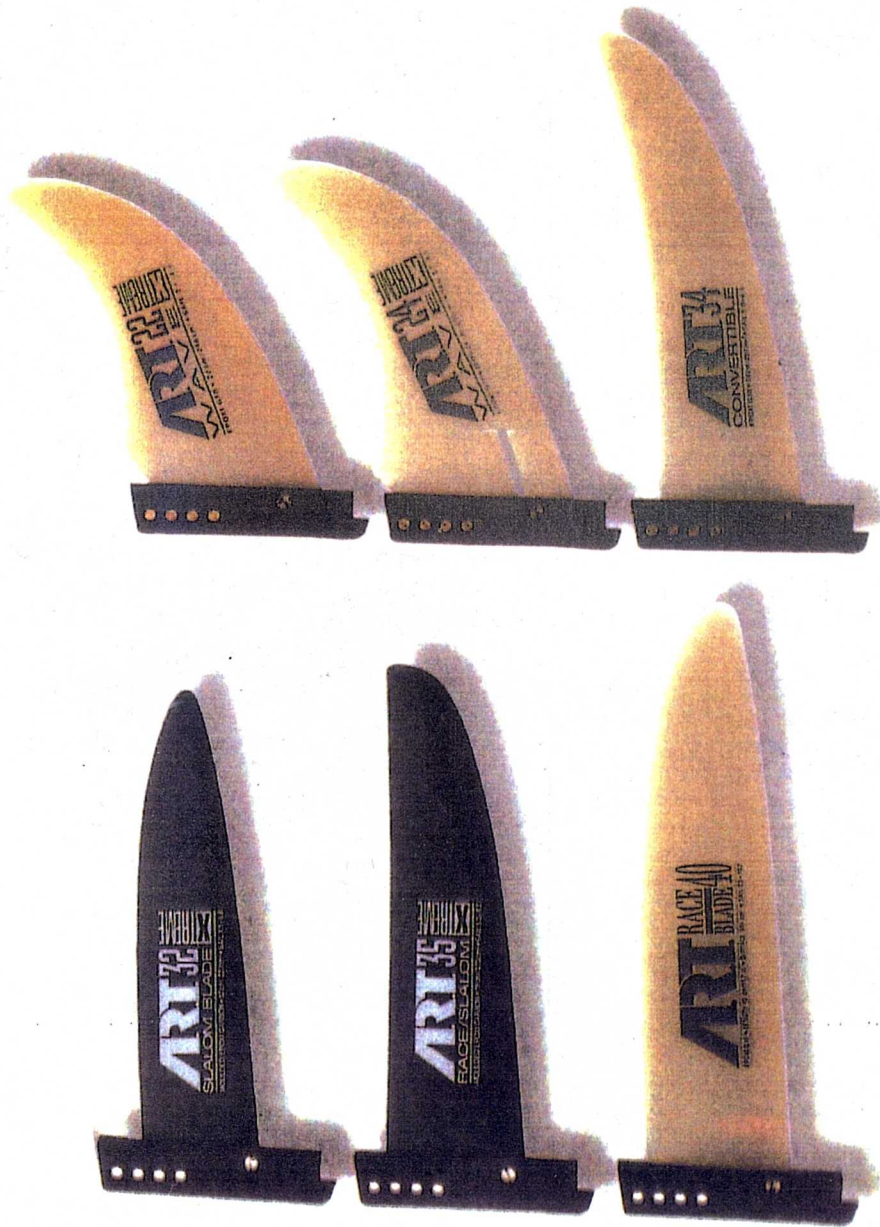
Figure 2.1   A Range of Contemporary Windsurf Fins
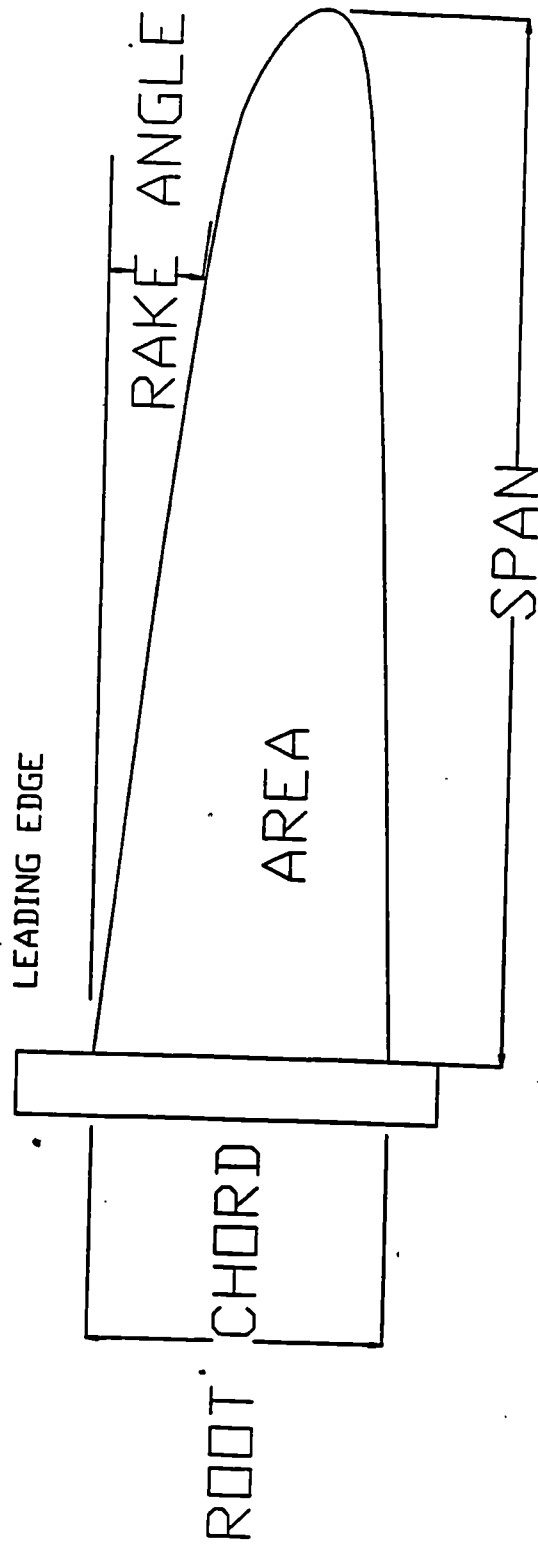
Figure 2.2   Windsurf Fin Nomenclature
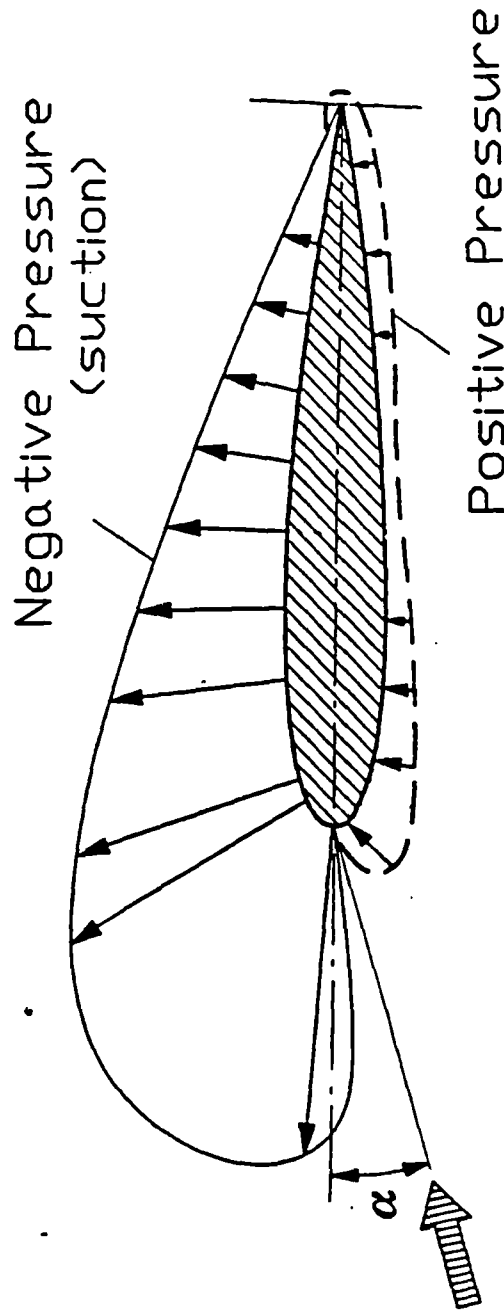
Figure 2.3   Pressure Field Around Foil Section
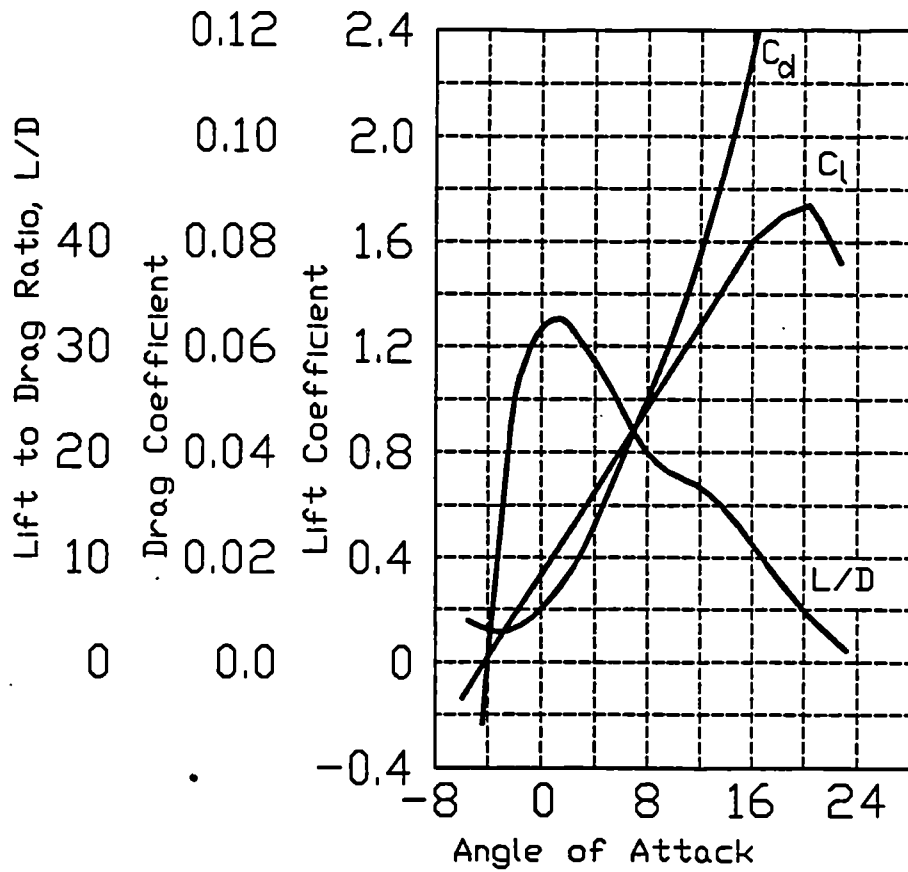
Figure 2.4   Typical Section Characteristics
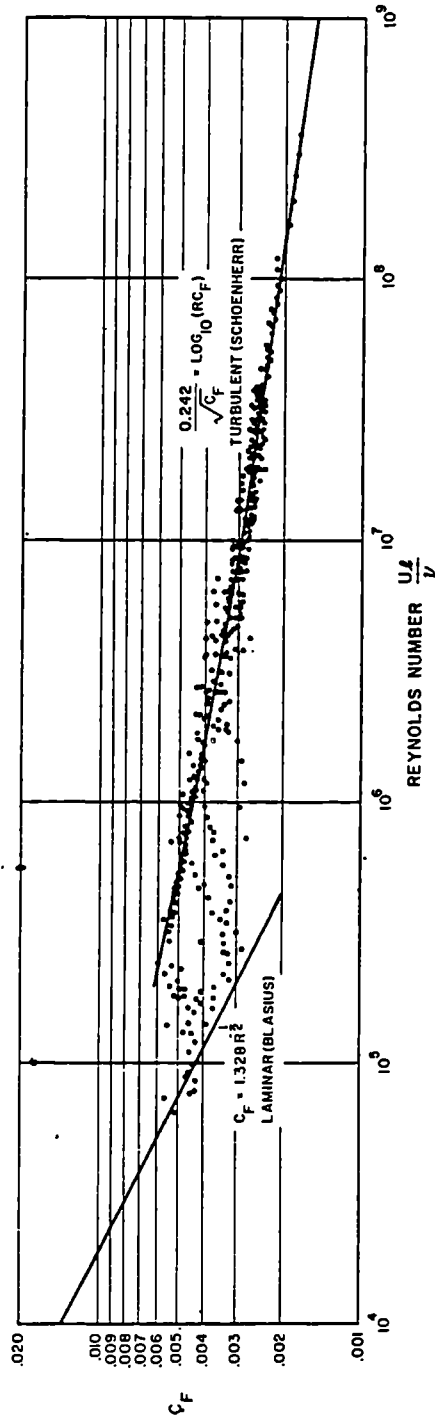
Figure 2.5 Measured Coefficient of Friction for a Number of Flat Plates

38

Sub-cavitation: < 20 m s^{-1}

Delayed cavitation: $20 - 30$ m s^{-1}

Supercavitation: > 30 m s^{-1}
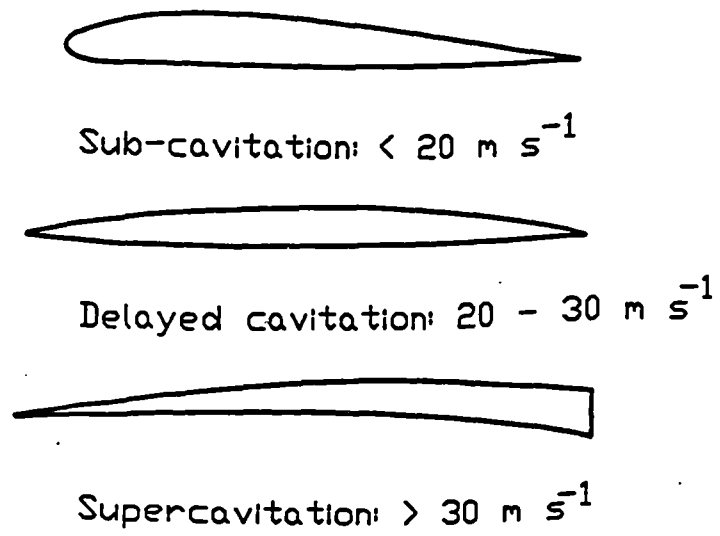
Figure 2.6   Hydrofoil Sections

Low Pressure Flow

High Pressure Flow

Relatively Low Pressure

Tip
Vortex

Relatively High Pressure
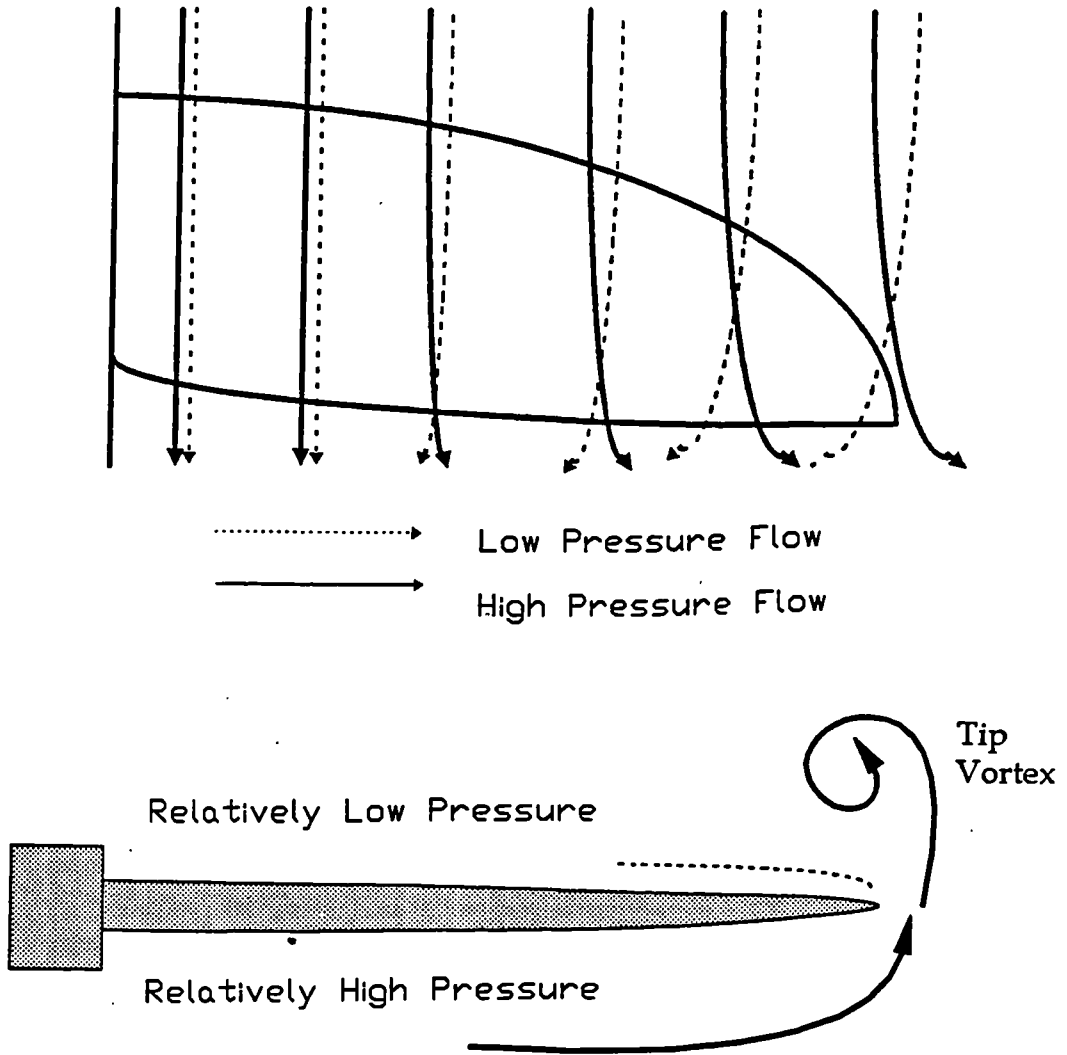
Figure 2.7   Three Dimensional Flow Effects
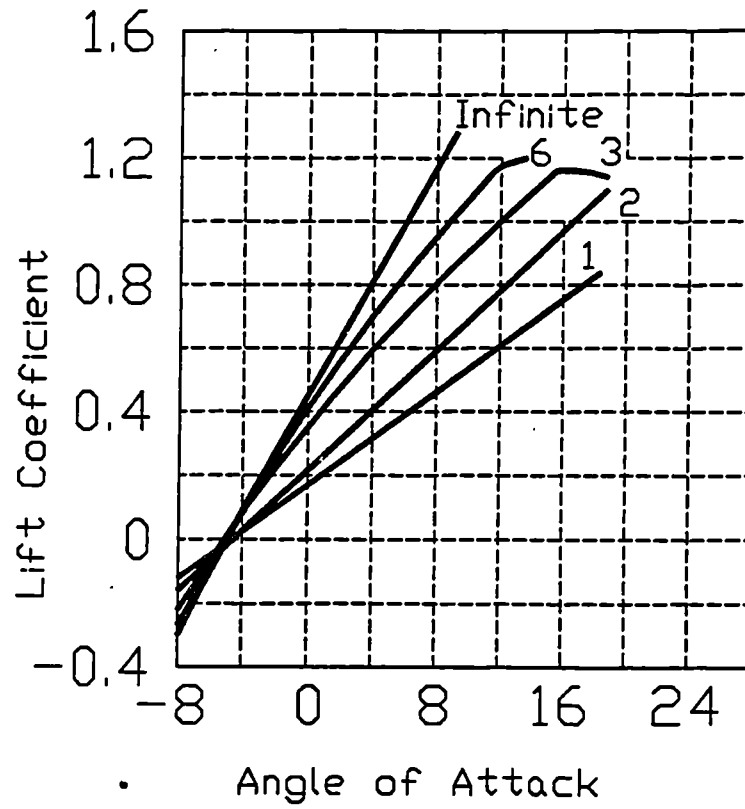
Figure 2.8   Effect of Aspect Ratio on Lift Curve Slope
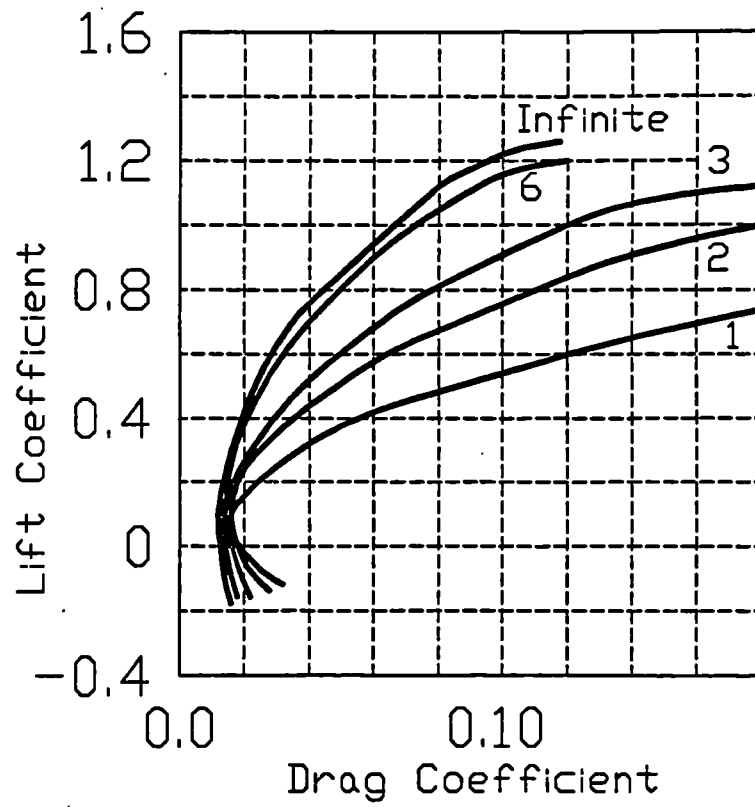
Figure 2.9 Effect of Aspect Ratio on Drag Polar

3.0   Literature Review

3.1   General Approaches for Optimising the Performance of Lifting Surfaces

The format and operation of the conventional windsurf fin has been established. Consideration is now given to the approaches for realising further gains in the lift to drag ratio (L/D) of the device.

A gain in L/D will be realised by employing geometrical features that optimise the two dimensional performance characteristics of the cross section and/or minimise the magnitude and influence of the three dimensional flow effects.

To improve the L/D ratio it will be necessary to adopt one or both of the following approaches;

1. Increase the lift produced by a nominal surface area.

2. Reduce the drag produced by a nominal surface area.

These two goals are however not mutually exclusive. Although a laminar flow is better for low drag at low incidence angles, a turbulent boundary layer is more resistant to flow separation at high lift, thereby increasing the value of maximum lift (C_{Lmax}) that can be generated [59].

3.2   General Approaches for Increasing Lift

In terms of increasing the lift of a wing type device there are three main approaches [21];

1. Increase the camber of the section.
2. Increase the effective wing area.
3. Boundary layer Control.

3.3   General Approaches for Reducing Drag

In terms of reducing the drag of a lifting surface the four main approaches are [138];

1. Skin friction reduction.
2. Pressure drag reduction.
3. Induced drag reduction.
4. Interference drag reduction.

The suitability and effectiveness of these approaches to drag reduction will be a function of the Reynolds number and hence the characteristics of the boundary layer flow.

For the following three ranges of Reynolds numbers the most suitable methods of frictional drag reduction are [59];

1. **For $R_e < 10^6$.** Reduce the near wall momentum (assuming a laminar flow) by boundary layer blowing/heating/cooling [118].

2. **For $10^6 < R_e < 4 \times 10^7$.** Delay boundary layer transition.

3. **For $R_e > 10^7$.** Reduce skin friction for turbulent boundary layers with riblets, Large Eddy Break-up Devices (LEBUs), geometric modifications, relaminarisation, introduction of foreign substance, synergism [3].

Typically the windsurf fin operates at Reynolds numbers varying between 8×10^5 and 1.6×10^6. This indicates that the methods for reducing the frictional drag of the fin by delaying boundary layer transition are the most relevant to this work.

The technologies, approaches and methods for achieving high lift and/or low drag can be generally termed as active or passive [129][130]. The distinction is that in an active system

there is a requirement for some form of energy input and control, whereas in a passive system the operation of the device is autonomous in nature.

For the current work it is a requirement that any of the high lift and/or low drag devices will not require an auxiliary power source. This does not necessarily restrict the scope of the study exclusively to passive devices as it may be possible to use the sailor to provide a limited form 'active' input. It is however not considered appropriate to utilise an active method which requires the inclusion of an auxiliary power source.

3.4   Optimising the Conventional Windsurf Fin

Assuming that the windsurf fin is to be restricted to its current format of fixed planform and cross section, the approaches available for optimising the performance of the device are limited to;

1. Modifications to the cross section geometry.
2. Modifications to the planform geometry.
3. Modifications to the surface finish.

3.4.1 Design Variables for a Symmetrical Cross Section

The requirement for equal operation in two directions restricts changes in the design of the cross sections to modifications to the nose shape and pressure distribution (thickness distribution).

Eppler and Shen [46] discuss various aspects of the design of symmetrical foil sections for hydrofoils. They conclude that the symmetrical cross section most suitable for hydrofoil applications, *'is that shape which can be operated with the craft speed as high as possible without cavitation, and which can tolerate velocity fluctuations as large as possible imposed by rough waters or during manoeuvring'.*

At low incidence angles, a thin profile (<10% t/c) has the potential for a small wake with an associated reduction in total drag. If the thickness is further reduced to that of a flat plate the drag results almost exclusively from surface friction effects (at low incidence angles). Although this is beneficial in terms of a reduction in wake drag at low incidence angles, performance at higher incidence angles will be compromised. This is due to the sharper leading edge profile (if the maximum thickness is located typically rearwards) which at elevated incidence angles is prone to leading edge separation and stall. This means that the attainable C_{Lmax} is limited in comparison with a thicker profile.

In contrast, a thicker streamlined profile (>15% t/c) has the potential for maintaining an attached flow at higher incidence angles (assuming a suitable nose profile is used). This increases the potential for a higher C_{Lmax} and hence total lift, but this is at the expense of an increase in wake drag at lower incidence angles.

A comprehensive collection of data on the experimental characteristics of symmetrical cross sections is provided by Abbott and Doenhoff [1]. From this comes the conclusion that a maximum thickness ratio of approximately 12% provides the best compromise in terms of both lift and drag performance over a large range of incidence angles for symmetrical sections. Venn [144] corroborates this by stating that most windsurf fins feature a t/c of between 10% and 12% of the chord length.

The position of maximum thickness normally governs the point of transition from a laminar to a turbulent flow due to the adverse pressure gradient in this region. This is highly significant as the skin friction associated with a turbulent flow is higher than that associated with a laminar flow. To exploit the low skin friction drag associated with a laminar flow a series of cross sections known as Natural Laminar Flow (NLF) profiles have been developed.

A NLF profile uses passive techniques and geometric features to maintain extended regions of laminar flow. The simplest technique for maintaining laminar flow over the foil surface

is to capatilise on the stabilising effect that favourable pressure gradient has on laminar boundary layers.

Research work on NLF profiles dates back to the 1930s when NACA developed the 6 series of airfoils [46]. These NACA 6 series airfoils are characterised by a more rearward position of maximum thickness thereby promoting an extended region of favourable pressure gradient in which a laminar flow can be maintained. This rearward movement of maximum thickness reduces the pressure recovery region, resulting in large adverse pressure gradients. One of the most suitable techniques for dealing with a large adverse pressure is the Stratford type recovery [44](Stratford established the theoretical minimum length required for a pressure recovery).

The drag polar for a NLF profile features a 'bucket' of low drag values corresponding with the incidence angles at which long runs of laminar flow are maintained. Achieving these flows on aircraft wings in the 'real world' can be problematic because the construction techniques (riveted panels) and small imperfections on the leading edge (insect debris) tend to upset the laminar flow.

Jones and Khalid [79] detail how the advent of composite material technology in the 1970's led to resurgence of interest in NLF profiles for military aerospace applications, although unfortunately the results of much of this work is classified.

Work by Somers [133] at Lockheed has confirmed the low drag advantages of NLF profiles and how the success of a NLF profile is highly sensitive to the design and subsequent fabrication method. A NLF profile developed by Somers [133] has been tested and shown to have no detrimental performance characteristics even if the laminar flow is not maintained.

Eppler and Shen [45][46] detail the development of a series of symmetrical hydrofoils which are designed for large regions of laminar flow. The operational efficiency and benefits of the laminar flow are however limited to incidence angles up to approximately 4°.

NLF profiles are therefore not suited for applications where high C_{Lmax} values are required. This is primarily due to the early stall associated with the sharp nose shape. To obtain the benefits of a NLF profile the incidence angles must therefore be constrained to those corresponding to the low drag bucket, which is generally in the range of -4° $< \alpha >$ 4° (for a symmetrical section).

Based on the fact that the windsurf fin is typically sailed at an incidence angle of 6° (upwards) it is unlikely that the low drag benefits of using a NLF profile will be realised.

The NLF profile is therefore not considered to be suitable for optimising the overall L/D performance of the windsurf fin.

It is more common for the position of maximum thickness (for windsurf fins) to be located at between 30% and 40% of the chord length [24][62]. This seems to provide the best compromise in terms of a short run of laminar flow and an attainable C_{Lmax}. Garrett [61] supports this by stating, *'the symmetrical sections most used in sailing are those whose maximum thickness occurs at 30% the chord length'.*

So far the discussion has been concerned with the general profile shape in terms of the value and location of maximum thickness. However, the nose shape of the foil section is also a design variable which can be used to tailor the performance of symmetrical cross sections.

The leading edge shape affects the character of the flow, which in turn determines the range of incidence angles in which separation and stall will occur. Any considerable sharpening of the nose results in an increase in the local flow velocity, which encourages leading edge separation and consequently stall and loss of lift. With a suitable shape of nose such an eventuality might be delayed or even avoided.

Rogers [121] discusses the types of nose shape commonly found on windsurf fins. These are shown in Figure 3.1 and are referred to as sharp, moderate and blunt nose shapes. The

benefits at low incidence angles of a sharper leading edge shape have already been established as have the stalling characteristics which make this feature unsuitable for generating large C_{Lmax} values at high incidence angles.

To avoid a leading edge stall a more rounded nose shape can be employed. This reduces the flow velocities in the vicinity of the nose, thereby enabling the cross section to operate satisfactorily over a larger range of incidence angles. A rounded nose shape is however less efficient at lower incidence angles due to the region of high pressure that builds up in front of the foil (due to the less efficient splitting of the freestream flow). Therefore the selection of a suitable nose shape is highly dependent on the range of incidence angles over which the cross section is to be employed. For low drag over a range of low incidence angles a sharper nose profile can be used, whereas for a large range of incidence angles a more rounded nose profile is preferred (at the expense of an increase in drag for low incidence angles).

The 'Boa Stick' windsurf fin was designed in Canada and is claimed to have a novel cross section profile which has been 'extensively tank tested' [33] (it has not been possible to source this test data). The cross section itself is of a higher thickness chord ratio (14%) than comparable fins produced by other manufacturers, with the position of maximum thickness located in an unusually forward position (25%) and the nose shape is blunt, probably to delay the onset of leading edge stall. The cross section also features a concave trailing edge curve design which is presumably used to develop a Stratford type recovery.

A summary of the cross section design variables parameters is provided in Table 3.1.

PARAMETER	INCREASING VALUES	DECREASING VALUES
Thickness Ratio (t/c)	• **Increases Stall Angle** • **Increases Form Drag** • **Increases Volume**	• **Reduces Stall Angle** • **Reduce Drag at Zero Angle of Attack**
Position of Maximum Thickness	• **Reduces Drag at Zero Angle of Attack**	• **Increases Lift to Drag Ratio**
Leading Edge Radius	• **Increases Lift to Drag Ratio**	• **Reduces Drag at Zero Angle of Attack**
Trailing Edge Thickness	• **Increases Lift** • **Decreases Lift to Drag Ratio (max. trailing edge thickness = 0.1t)**	• **Minimum (knife edge) Best**

TABLE 3.1   Airfoil Design Parameters and their Effect on Performance

3.4.2   Design Variables for the Planshape of the Windsurf Fin

The planshape influences the magnitude and nature of the three dimensional flow effects. In the sport of windsurfing a number of distinctive shapes of planform have 'evolved' to satisfy the requirements of the different disciplines found within the sport (as shown in Figure 2.1). This illustrates that the ultimate hydrodynamic efficiency is not always a governing factor in determining the 'overall performance' of a fin. For some disciplines, sea states and wind strengths it is often preferable to detune the fin by reducing the aspect ratio and introducing sweep, thereby rendering the fin more 'user-friendly' and controllable.

For the current work the aim is simply to optimise the efficiency of the planform by reducing the detrimental 3D flow effects.

Reconsideration is given to the formulae for induced drag (C_{Di}) and effective incidence angle (α_{ef}) (2.12 and 2.13) with the inclusion of a span efficiency constant (K) based on the sweep angle, taper ratio and geometric twist.

$$C_{Di} = \frac{C_L^2}{\pi ARK} \qquad (3.1)$$

$$\alpha_{ef} = \alpha_g - 18.24 \times \frac{C_L}{\pi ARK}(Degrees) \qquad (3.2)$$

This shows the dependence of C_{Di} and α_{ef} on;

1. The coefficient of lift squared (C_L^2).
2. The efficiency of the planform (K).
3. The aspect ratio of the fin (AR).

Due to the increase in C_{Di} as a function of C_L^2 it is beneficial to keep the angle of incidence as low as possible to reduce the induced drag.

Garrett [61] considers that for boats which are sailed upright, the keel should have deep high aspect ratio with no sweepback (rake angle). Sweep is beneficial as it reduces the influence of the free surface [78] and improves stall characteristics, however there is a penalty to be paid in that any amount of sweep entrains larger magnitudes of drag due to lift, as well as reducing the lift curve slope. Normally when sweep is used on high performance windsurf fins it is to compensate for the planing attitude of the board (normally 6° to 8°) and *'to add a modicum of control'* [31].

In terms of the efficiency of the planform, Munk [105] establishes that a theoretical minimum value of C_{Di} is obtained for a constant downwash across the span (K = 1). The simplest method for achieving a constant downwash is with an elliptical lift distribution

with no sweep. An elliptical lift distribution is readily obtained by using an elliptical planform (with a constant chord and no geometric twist).

The use of elliptical planforms is already prevalent in the sport of windsurfing with most of the manufacturers producing a range of fins to this general shape (Figure 2.1). This indicates that in terms of hydrodynamic efficiency the optimum planshape is already being employed.

The question has to be raised as to why the elliptical planform is seldom seen in nature? Contrary to Munk's theories for minimum induced drag, it is common for the most agile and efficient birds and sea animals to employ crescent shaped lifting surfaces which can be considered to be *sculpted by 100 million years of evolution*'.

Burkett [19] investigated the performance of aft swept wing tips and claims that induced drag reductions of 4% are feasible for a suitable wing tip design on an otherwise planar wing. This aft swept wing tip design was subsequently used by Dornier on one of their medium size passenger aircraft.

Van Dam [140] has also investigated the crescent wing shape and claimed a theoretical 8% reduction in C_{Di} for a crescent moon shape planform of AR = 7 when compared with Munk's theoretical minimum for an elliptical planform. He concludes that this results from nonplanar shape due to the angle of attack of the wing and its wake.

Zimmer [152] similarly predicts an 8% reduction in induced drag for crescent wings with his vortex lattice method.

An investigation by Smith and Kroo [132] sought to establish the accuracy and validity of the previous theoretical work into the crescent shaped wing. A series of computational models were generated in which the surface panel densities and model planforms were varied. These tests established the sensitivity of the panel method to differing wing planforms and panel densities. From this it was concluded that it is difficult to determine

the magnitudes of induced drag from computational methods with sufficient accuracy to assess the influence of wing tip modifications. This therefore questions the dramatic induced drag reductions demonstrated by the computational methods of Van Dam [140] and Zimmer [152].

Ashenburg and Weihs [5] support Smith and Kroo [132] by demonstrating that the induced drag of a crescent planform is equal but not less than an elliptical planform.

To further investigate the accuracy of the panel method, van Dam et al [141][145] subsequently conducted a wind tunnel investigation of the crescent planform. In this investigation an elliptical and crescent wing model were tested at $R_e = 1.7 \times 10^6$. For all attached flows, the crescent wing exhibited less (3.9% reduction) induced drag for a given lift force and wing span. This reduction in induced drag is believed to result from '*the favourable influence of the trailing wake deformations on the pressure distribution of the highly swept outboard region of the crescent wing*'.

In conjunction with the general shape of the planform, the aspect ratio greatly influences the performance of a lifting surface. As the aspect ratio of a lifting surface increases, the influence of the 3D flow effects diminish. This is shown in Figures 2.8 and 2.9 which illustrate the non linear reduction in drag and increase in lift effectiveness as a function of increasing aspect ratio. For hydrodynamic efficiency it is therefore beneficial to increase the aspect ratio to a practical limit. In terms of the windsurf fin, this practical limit is determined by the trade off between increasing hydrodynamic efficiency and limiting the magnitude of the fin generated moment arm. The maximum aspect ratio is therefore a function of two independent factors;

1. The ability of the fin to maintain structural integrity as the span increases [24].

2. The ability of the sailor to resist the larger turning moment associated with a high aspect ratio windsurf fin [127]. A conventional displacement hull yacht heels over due to the action of the sail and the keel. Excessive heeling is however undesirable for a planing windsurf hull and so the sailor must

physically oppose and counteract the moment generated by the fin on the rear of the board. There is obviously a finite limit to the magnitude (and duration) of turning moment that the sailor can resist with muscular input alone.

The aspect ratio of the commercially available high performance windsurf fins has remained at nominally the same value $(10 > AR_{cf} > 13)$ for the past few years. This indicates that the optimum aspect ratio in terms of structural integrity, hydrodynamic performance and sailor controllability has already been established.

3.4.3 The Surface Finish

It has long been known that the surface roughness, especially near the leading edge, has a large influence on the performance characteristics of wing sections [1]. The C_{Lmax} in particular, is sensitive to leading-edge roughness.

Broers et al [16] conducted an investigation into the influence of the surface finish on the performance of windsurf fins. It was found that windsurf fins featuring a gloss finish were prone to leading edge aeration and stall at a lower incidence angle than the windsurf fins featuring sanded or 'Ribcoated' finishes. The sanded and 'Ribcoat' fins demonstrated the tendency to break the air pockets into smaller 'bubbles' which were then discharged downstream, thereby delaying separation. In general the sanded and Ribcoated fins stalled later than the gloss finish fins and demonstrated an improvement in the lift to drag ratio.

3.4.4 The Design Triangle

The foregoing discussion identifies the potential methodologies for optimising the conventional windsurf fin by means of modifications to the section, planshape and surface finish. The optimisation of the fin is however dependent on the performance requirements of the envisaged discipline or mode of use. Therefore a design 'triangle' is shown in Figure 3.2 which indicates the three primary performance characteristics of the fin (control,

speed, pointing ability) and the manner in which the design variables are tailored to achieve these performance traits.

This 'triangle' serves to illustrate the contradictory requirements for optimising a conventional windsurf fin for more than one performance criteria.

3.5   Alternative Approaches for Optimising the Lift/Drag Ratio of the Windsurf Fin

It is concluded that through a process of continual development, refinement and evolution over the past twenty years, the cross section, planshape and surface finishes of the contemporary windsurf fin have evolved in to what may be termed near optimal formats.

This does not necessarily mean that further performance gains can not, and will not be realised by further work into these individual parameters, rather that it may be more profitable to investigate other methods for realising substantial performance improvements.

For this reason consideration is given to what may be termed 'alternative' methods for enhancing the performance of the windsurf fin.

3.5.1   Boundary Layer Control Methods

The term 'boundary layer control' includes any mechanism or process through which the boundary layer of a fluid is caused to behave differently than it normally would were the flow developing naturally along a smooth straight surface [59]. The control device could be passive, requiring no auxiliary power, or active requiring energy expenditure.

3.5.1.1 Compliant Surfaces

Research into the use of compliant surfaces to reduce frictional drag was triggered by the initial work by Kramer [87][88][89] into the apparent swimming efficiency of dolphins and his

55

belief that this resulted from the 'low drag' characteristics of their skin. The compliant surface (Figure 3.3) was developed and is claimed at certain Reynolds numbers to reduce the drag when compared with a rigid reference model. Kramer hypothesised that this resulted from the damping of the fluid adjacent to the compliant surface thereby delaying the transition from a laminar to a fully turbulent flow.

Benjamin [9] conducted a theoretical study into the problem. He identified three possible forms of flow instability and established that the suppression of one instability by the flexible surface is likely to let in another. This theoretical study indicates that the success of a compliant surface is critically dependent on the choice of properties for the flexible medium and that it is only likely to operate in a limited freestream velocity. He also concluded that a contradictory set of requirements were required for the flexible medium. Landahl [91] expanded on this early theoretical work by Benjamin without an obvious or further conclusion.

Fisher and Blick [56] constructed a compliant surface with a flexible plastic skin over an aluminium plate and found a reduction in the boundary layer turbulence intensities. They did not however measure the effect of this on the skin friction drag.

Blick with Walters [11] found a reduction in the boundary layer turbulence intensities and an apparent thickening of the laminar boundary layer on a subsequent compliant surface model. There was however no change in the mixing length when compared with the rigid reference model. No reductions in drag were found.

Hiroyuki and Taneda [67] investigated the effect of a flexible layer on the boundary layer stabilisation by measuring the skin friction drag on flat plates with flexible surfaces. These tests showed that the flexible surface plates always have the larger skin friction drag than the rigid surface plates, both at the flow transition and where the boundary layer is fully turbulent. It was concluded that the evidence for drag reduction with a flexible surface was not found in their experiments.

The basis of Kramer's early work was the apparent efficiency of the dolphin based upon his estimates of the muscular power and the 'observed' swimming speeds. These estimates would seem to be highly erroneous based upon the work of Lang [92] into the swimming speeds and power of dolphins. Through a series of swimming experiments with tamed animals he has established that there is nothing unusual in the way of low drag associated with the dolphin's skin.

The potential benefits of using a compliant surface for a windsurf fin do need to be considered carefully. In the first instance the total surface area of the fin is limited and as such there are limited gains to be realised with an extended region of laminar flow. It could be concluded that the optimum length of laminar flow is already being achieved by virtue of the favourable pressure gradient on the forward part of the foil section. If the assumption is made that a compliant surface could be successfully implemented into the design of the fin, it would also be necessary to include some means for triggering the change to a turbulent flow in advance of the adverse pressure region, if a laminar flow seperation (stall) is to be avoided.

3.5.1.2 Drag Reducing Polymer Solutions and Surface Coatings

Bornhoft et al [35] quantitatively tested the Sea Slide SB Drag Reducing Paint on a series of windsurf board hulls. They report test data from the Ocean Engineering Department of Rhode Island demonstrating drag reductions of between 8% and 14% for the paint. It was found that in choppy sailing conditions there was no advantage from applying the paint to the hull as board speed in these conditions is, 'as much about skill and strength' as anything else. In smoother waters a performance advantage with the Sea Slide coated board was noted.

The drag reducing properties of polysaccharides and other high polymers produced by bacteria, algae and other marine organisms has long been recognised. Hoyt [74] provides a summary of the theoretical and experimental work into fish slimes which indicates a reduction in the wall shear stresses and a delay in flow transition. Attempts at coating

planks or fish shaped bodies with fish slimes have been unsuccessful due to the fact that the friction reducing properties of these natural slimes rapidly deteriorates once removed from the living animal.

Bragg et al [13] conducted a series of experiments on a number of plates and a dynamometer coated with soluble polymeric coatings. Establishing the accuracy of these tests was problematic due to the inherent dilution of the flow tank water with the polymeric solutions. No drag reductions were shown for single side coated plates although the double sided plate did show a 17% reduction at a Reynolds number of 4.1×10^6, leading to a drag increase of 6% at Reynolds number of 12.3×10^6. The rotating dynamometer provided a more suitable means for testing the solutions. However, the best torque reduction with the soluble polymeric solution was '30% less than half that obtained with pre-mixed solutions'.

Kay [84] discusses how it has been known for many years that the addition of certain chemicals to water will considerably reduce the skin friction of any object moving therein (Toms Effect, 1949). Some of these solutions have in fact been used in test tank to vary the Reynolds number. Hoyt [75] provides a summary of work into polymer drag reduction. By the addition of a few parts per million of dissolved macromolecules the fluid friction and hence drag can be considerably reduced (up to 65% by the addition of 30 parts per million of ethylene oxide).

Alfredsson and Johansson [3] and Marchaj [99] discuss the practical implications of using polymer technology in an open sea environment. The solution to this problem is to secrete small amounts of the polymer solution from small holes towards the leading edge of the immersed body. This would require the provision of a storage tank as well as some form of discharge or secretion system. This alone would make this technology unsuitable for the sport of windsurfing, even before consideration is given to the phenomenal cost and pollution resulting from the use of polymeric solutions.

The change in fluid viscosity due to the use of polymeric solutions also has implications in terms of the nature of the flow. A reduction in the frictional drag of the water will allow the flow to move faster, which according to Bernoulli's theorem results in an increase in the negative pressure intensities. This increase in localised negative pressures in turn is likely to result in premature flow separation and possibly an earlier inception of cavitation. Hoyt [75] confirms this effect by describing the modifications to the pressure distribution and fundamental changes in lift forces due to the injection of polymeric solutions from the surface of a foil. Under suitable conditions the lift to drag ratio can be increased, although this is highly dependent on the location of the ejection point.

A final consideration regarding polymeric solutions is that the governing body of yacht racing and windsurfing (the IYRU) has banned the use of polymer solutions and soluble polymeric coatings in Rule 63.

3.5.1.3 Active Boundary Layer Flow Control

The drag of a cross section can be determined by integrating the forces acting on the body surfaces. These consist of the pressure drag due to the pressure (normal) forces and the friction drag due to the shear (tangential) forces.

In a subsonic flow the pressure drag is originated mainly by boundary layer separation resulting in an increase in the size of the wake. To suppress or avoid this phenomenon boundary layer suction in the adverse pressure region can be employed.

In addition to suction techniques, blowing tangentially to the surface in the direction of the freestream can reduce the wall shear stresses and hence surface friction.

By using a combination of suction and blowing techniques it is therefore possible to reduce both the pressure and friction drag.

Poll et al [111] demonstrated the benefits of using suction techniques for boundary layer stabilisation. It was found that transition could be moved to the minimum pressure location by the application of suction in the vicinity of the transition point.

Due to the requirement for an auxiliary power source these active boundary layer control systems are considered to be unsuitable for use on a windsurf fin.

3.5.1.4 Porous Wings

As an alternative to the active boundary layer control techniques, a passive boundary layer control system involving a fully porous wing has shown the potential for higher values of C_{Lmax} [102]. By allowing air to 'bleed' into the flow through holes in the skin surface the magnitude of the leading edge suction peak is substantially reduced thereby delaying the onset of leading edge stall. A wind tunnel investigation was performed to study the effects of porosity on an NACA 0012 airfoil section. It was found that when compared with the solid reference model, the porous version tended to exhibit multipoint adaptive techniques. The leading edge pressure peak was reduced and the suction over the middle section of the chord was increased. It was however found that the porosity reduced the lift curve slope as well as increasing the drag at a given section normal force coefficient, resulting in poor lift/drag performance at pre-stall incidence angles (when compared with a rigid reference model).

Poll et al [110] describe how a porous surface needs to be as close to fully 'porous' as possible to operate in the desired manner. This is achieved for aeronautical applications by the use of specialised laser drilling techniques to develop the sufficiently small and accurate spaced holes in the wing structure.

In a marine environment it is not clear as to how the size of the holes might need to be changed, whether they would be susceptible to contamination or whether they would act as the trigger point for cavitation (due to the localised high flow velocities through them and the discontinuity on the surface). The porous system has so far only been developed for

symmetrical (one flying direction) applications and as such the effect of a fully porous surface on the two surfaces would need to be investigated.

Even though the porous wing technology offers the potential for an improved C_{Lmax} the detrimental effect on L/D at pre-stall incidence angles means that it is not suitable for achieving the aims of the project.

3.5.1.5 Electromagnetic Damping .

A novel approach to boundary layer stabilisation has been developed in which electromagnetic forces are used to suppress turbulence in a flow [10]. The technique is based on the generation of a Lorentz Force in the flow from the interaction of an electrical flow and magnetic field. This is achieved through the use of a permanent or electromagnetic field across the flow and parallel to the surface which acts with the surface electrodes to generate the Lorentz Force. The resulting Lorentz force acts perpendicular to the surface and is claimed to 'pin down the vortices, thus reducing the mean and fluctuating turbulence'. A corresponding increase in turbulence is generated if the electric field is reversed, thus providing the technology to steer or manoeuvre marine vehicles without the need for conventional control surfaces. No figures are provided to quantify the magnitudes of the changes in overall drag (the British Technology Group are currently developing the concept for potential commercial applications and as such the result of their work is proprietary) and so no firm conclusions can be made about the potential effect this will have on the performance of the windsurf fin.

This electromagnetic damping technology is unsuitable for use in the scope of the current work due to the requirement for an auxiliary power source.

3.5.1.6 Optimised Use Of Materials

By varying the material contents of the windsurf fin it is possible to vary the structural integrity and elastic behaviour of the design. By making the fin more resistant to torsional

bending and twisting, it is claimed that the hydrodynamic performance is enhanced, although this is at the expense of user-friendliness and control [64].

The 'Voodoo Fin' is novel due to the material combinations which are used to develop twist over the span. The fin features a glass fibre and resin composite internal skeleton over which a plastic covering of general airfoil shape is bonded. Although it appears similar to many other fins on first visual inspection, the construction technique allows the trailing edge to twist off significantly in use. This, it is claimed, improves the pointing ability of the fin. A sailing test of the Voodoo Fin [33] found that it continually outpointed similar conventional rigid fins and that, *'you can definitely feel the twist working, particularly when approaching the point of stall'*. Although this may be beneficial in terms of 'controllability' the use of geometric twist will always result in an increment in drag, which is undesirable within the realms of the current work.

Investigation into the influence of the material properties on the performance of a range of windsurf fins have been conducted [17][26]. As part of this work a number of windsurf fins were constructed in which the spanwise stiffness was tailored through the use of composite materials such that the fins deformed and twisted in differing manners. Although tentatively it was found that the fins with flexible tips performed better at angles below 4° (when compared with the reference model) it was also established that these findings were inconclusive and that no obvious conclusion could be found. This could be in part due to the complex and combined interaction of the bending and twisting behaviour of the fins when in use.

3.5.2 Tip Vortex Control and Suppression Devices

The existence of a tip vortex and its detrimental effects on the performance of a finite length lifting surface was noted by Lanchester in 1897 when he filed his British Patent no. 3608 for "Capping Planes" to inhibit the flow of air around the tip from high pressure to low pressure region. The tip vortex resulting from these 3D flow effects is a source of energy loss and as such minimising its size and/or extracting some of this vortex energy is

of particular interest. It has been demonstrated that, *'even relatively small alterations on the tip geometry can have a distinct influence on the polar curve* '[152]. The majority of the work into tip devices has been concerned with;

1. Reducing the induced drag by modifying the tip vortex.

2. Extracting energy from the tip vortex core.

3. Reducing the roll-up characteristics of the vortex so as to minimise its effect on following lifting surfaces (i.e. following aircraft and cascaded systems such as helicopter blades).

A comprehensive evaluation of the methods used to modify the geometry and nature of the tip vortex is provided by Dunham [41]. It is established that these methods can be either active or passive and include devices such as wing tip sails, disc flow spoilers, mass injection systems, variable camber and twist wings as well as porous wing tip sections.

3.5.2.1 Reducing Induced Drag with Wing Tip Devices

The governing factor on the magnitude of C_{Di} is the distance between the vortex cores (in the case of a lifting surface with two free ends). Therefore the shorter the distance between the vortex cores of a lifting surface, the greater the downwash and hence the magnitude of induced drag.

The logical method for reducing the induced drag of a windsurf fin is to move the vortex core further away from the underside of the hull. An increase in span (tip extension) would seem to be the most obvious solution for this, however it has been shown by Flechner et al [57] that on an equal basis of even effects of wing bending moment coefficients and increased wing weight, tip devices produce substantially greater reductions in drag coefficients at near design conditions than simple extensions. However, Chen et al [25] point out that at off design conditions the performance of a wing fitted with tip devices is often worse than for the bare wing alone.

An investigation into the use of wing tip strakes established that a dihedral angle is required for successful operation and that they are beneficial for any aspect ratio and speed [97]. These conclusions are however based upon a comparison with a bare wing and do not take into account the increased aspect ratio resulting from the fitment of the strakes.

A typical wing tip sail configuration in Figure 3.4. When employed on modern aircraft tip sails have shown near design reductions in induced drag of 17% for the KC-135 [152], 14% for the Airbus [152] and up to 29% for an experimental test aircraft using a cascade of sails [134]. This indicates that even when consideration is given to the increase in wing weight and frictional drag the benefit of these wing tip devices is still tangible.

The wing tip devices described so far are optimised for flight in one direction (and usually optimised for one incidence angle) only. Due to their asymmetry they would not be able to operate effectively in the other direction. This limits the applicability of these designs to the windsurf fin, unless a process could be found to reverse the geometry of the tip devices for each sailing tack. Additionally the off design performance is worse than the bare wing alone.

In an attempt to overcome the limited operational range and poor off-design performance of conventional tip devices, Colling [29] investigated an articulated winglet design. The winglet features adjustable cant, yaw, toe-in/out and rudder angle. The goal of adjusting the cant, toe and rudder for optimised performance over a greater range of flight conditions was not realised. Only one optimum configuration was obtained. This indicates that an adjustable winglet has no performance advantage over a rigid device. It is therefore unlikely that a winglet can be made to adapt for optimised performance over a range of flight conditions.

As an alternative to wing tip sails, Acosta et al [2] and Duan et al [40] investigated the novel Ring Wing Tip shown in Figure 3.5. A reduction in induced drag was demonstrated even though the original project goal of reducing the far field tangential velocities was not achieved with this design. It was found that at design conditions the increase in parasitic

drag due to the extra surface area was offset by the associated reduction in induced drag. The tests were performed on a low AR wing where the 3D flow effects are highly influential. It is therefore concluded that the device works best at high angles of attack (>8°), on low aspect ratio wings and that large aspect ratios would mitigate its use. Due to the effective high aspect ratio of the windsurf fin it is unlikely that the use of a Ring Wing Tip would result in any significant performance gains.

One of the simplest symmetrical tip devices is the end plate originally proposed by Lanchester. The 'Foiler' windsurf fin (by Fins International, France) features a simple flat plate tip device. The effectiveness of this tip device on the performance of the fin has not been established, although Wadlin et al [203] only noted small gains in L/D due to the use of an end plate on a hydrofoil (it was also established that the geometry of the end plate needs to be adaptive (for optimal performance) in response to changing incidence angles and flow velocities). The 'Foiler Fin' was introduced in 1994 but is no longer in production. Derivatives of this design have not emerged. To the knowledge of the author, the fin was not used by the professional 'Team Riders' in competitions (normally the Windsurfing Press will publicise any innovations or new design features that are introduced). This would seem to indicate that the concept was not successful (in its format) at enhancing the performance of the windsurf fin. This conclusion is supported by the low efficiency rating of the simple end plate when compared with other tip devices [146][152].

Another windsurf fin featuring what could be considered as a tip device is the 'Hobert Fin' shown in Figure 3.6. This fin features three holes located in the tip which are described as being able to *"break up the tip vortex which causes increased drag"* [81]. The efficiency of this fin is questionable due to the fact that the holes were implemented as a marketing 'gimmick' rather than as an established and proven concept [115]. This tip design feature has not appeared on any subsequent fins.

As an alternative to using a fixed tip device Chen et al [25] propose the use of wing tip jets to modify the flow field near the wing tip. A preliminary study demonstrated that the tip

jet demonstrates performance gains similar to winglets. However, the requirement for an additional power source makes this technology unsuitable for the sport of windsurfing.

The benefits of employing tip devices on the windsurf fin would therefore seem to be limited due to;

1. The requirement for equal operation on both sailing tacks (symmetrical tip device).

2. The high effective aspect ratio of the windsurf fin.

3.5.2.2 Extracting Energy from the Tip Vortex

It is possible to consider the tip vortex as an energy source which can be exploited by a suitable tip device [99][134][143]. One of the better known examples is Van Oossanen's [143] restricted draft winged keel used on the America's Cup boat 'Australia II'. The success of this yacht and the performance gains attributed to the keel are well publicised but need to be tempered by the fact that the winged keel was just part of the substantial development work used to realise the final boat. This work included a new reverse tapered keel, reduced hull length and increased sail area, as well as the winged keel itself. It is therefore suggested that the Australia II boat *"worked due to a combination of factors and not simply by adding a winged keel to a conventional design"* [99]. The applicability of the winged keel technology to the windsurf fin can be further questioned by Van Oossanen himself who states, *'the winglet keel has very few advantages to offer over a deep fin keel '*[143].

3.5.2.3 Reducing Tangential Velocities in the Tip Vortex

In general the approaches for reducing the tangential far field velocities associated with wing tip vortices have not been very successful [41][131]. They can however be used to modify the near field tangential velocities and show the potential for delaying vortex roll up. The limited delay in vortex roll up is showing benefits for cascaded lifting systems such as helicopter blades. Dunham [41] describes how the impingement of the preceding

blade vortex helps to alleviate the problem of 'Blade Slap'. The BERP Helicopter Blade is a successful example of this work into modifying the tip vortex characteristics to improve aerodynamic efficiency [147].

The primary aim of reducing the tangential velocities is to reduce the hazard this causes for following aircraft. However, in the context of the windsurfer, the effect of the far field tangential velocities are not considered to be relevant.

3.5.3 Slots and Multifoils

Slots and multi element foils are commonly employed as high lift devices on aircraft wings. The interaction of the individual foil components raises the combined angle of incidence at which the complete system can work, thereby improving the attainable value of C_{Lmax}.

Slotted and multi element windsurf fins have been in existence for many years. These design features are used to make the fin more 'spinout' (delay leading edge stall) resistant and to aid with control [47]. It is acknowledged that slots and multifoils are 'noticeably' slower due to the increase in drag [31]. For this reason their use is restricted to wave sailing and recreational fins where control and spinout resistance is preferred to ultimate hydrodynamic efficiency.

Slots and multi-element foils are therefore not suitable for improving the (pre-stall) lift to drag ratio of windsurf fins.

3.5.4 Variable Geometry Approaches

Designing an airfoil for an optimum condition means that it performs less well at off design conditions. The use of variable geometry (or adaptive wing) technology involves the ability to change the geometry of the wing or lifting surface in response to changing lift

and/or drag requirements. These changes in geometry can be applied to both the planform and the cross section.

The mechanisms and control processes for variable geometry wings can be complex. For a variable geometry system to be successful the additional complexity and weight of the activating mechanism must not outweigh the gains in operational flexibility associated with optimising the wing for a range of conditions.

3.5.4.1 Variable Geometry Lifting Surfaces in Nature

In nature there are a diverse range of creatures using variable geometry surfaces to fly and swim. Insects use a combination of variable twist and camber in their highly flexible wing structures to take to the air as do birds who have the capability to vary the camber and planform of the wing through muscular movements [95]. This allows birds to optimise the performance of their wings for high and low speed flight. The same is true of flying mammals such as bats which use flexible membrane wings. In the water fish, dolphins and whales change the geometry of their bodies, fins, flippers and tails for propulsion and manoeuvring.

3.5.4.2 Man Made Variable Geometry Wings Mechanical-Flexible Approach

Excluding the use of balloons, man's initial attempts at flying were largely based on the mimicking of nature, which would now seem to be a false economy based on the statement that, *'it is probable that no animal in the history of the world which has had to fly professionally has ever weighed more than about 13 kg '* [149].

Even in our modern world of computer logic and exotic composite materials man has not been able to truly replicate the flapping wings of birds, insects and mammals.

Perhaps the closest man has come to flying naturally is with the aid of hang-gliders and parapentes [30]. The wings on these aircraft demonstrate a subtle form of variable geometry

through the use of aeroelastic tailoring. The variable geometry is seen in the cross section and the planform as a result of the dynamic surface pressure loads. This variation in geometry is beneficial as it introduces camber into the wing. The amount of aeroelastic deformation is carefully limited in the case of the hang-glider by control lines and stiffening battens. Hang-glider and parapente wings are only capable of soaring flight and are not capable of flapping in the same manner as insects, birds and bats. Instead they have to exploit thermal currents and updrafts to ascend.

The technique of aeroelastic tailoring is also used for marine sails such as those found on windsurfers. The sail can in fact be considered as one of the earliest examples of a man made, variable geometry lifting surface. By using rigging tension and reefing techniques the surface area and cross section of the sail can be controlled by the crew [61][99].

The variable geometry devices on modern aircraft have evolved over many years into their current highly effective formats and designs. The approaches to man made variable geometry wings are well documented and can be grouped into the following classifications [129][130].

1. Trailing edge devices (flaps)
2. Leading edge devices (leading edge flap, slots, droop nose)
3. Flexible surface technologies (parapentes, Mission Adaptive Wing (MAW))
4. Aeroelastic tailoring techniques (variable twist)
5. Variable sweep and area wing technologies

All of these design features are used to allow the aircraft wing to be tailored or optimised for more than one flight condition. Some of these techniques are passive whereas others require the use of auxiliary power and control systems.

3.5.4.3 Approaches to Variable Camber

Since the early history of manned flight the use of increasing camber to increase wing lift has been recognised. In general the addition of camber is always beneficial for producing lift and the benefit grows with increasing camber [90].

The Wright brothers used variable geometry on their early aircraft by wing-warping, coupled with rudder deflection to obtain lateral control. The Sopwith Baby featured automatic trailing edge flaps restrained by bungee chords allowing the flaps to be streamlined for high speeds and deployed at low speeds for take off and landing [104].

Historically aircraft designers have seen the use of variable camber to increase the operational flexibility (and manoeuvre-performance-enhancing) of aircraft as an area worthy of investigation. According to Siewart and Whitehead [128] and Ferris [54] camber is recognised as one of the most important parameters affecting the lifting characteristics of wings. Increasing the camber of the wing to achieve increased lift has been common practice since the 1920s [12] (although recently the variation of camber to improve the 'off design' performance has also been the subject of much work).

The approaches to variable camber can be divided into two categories, namely;

1. The 'Conventional Flap and Slat' Systems
2. The 'Flexible Surface' Systems

Each approach to variable camber has its advantages and disadvantages and associated effect on the design of the lifting surface.

According to Newman [107] the lift coefficient for a foil section can be written in the general format;

$$C_L(\alpha) = C_L(0) + 2\pi\alpha \qquad (3.3)$$

This illustrates the decomposition of lift into terms of the lift due to the basic thickness form at an angle of incidence and the contribution to lift due to the mean line. This illustrates how camber can be used to increase the C_L of a foil section (to certain limits).

The ideal angle of attack for a foil section corresponds to the situation where the forward stagnation point of the foil coincides with the leading edge [107]. This is normally achieved by the use of a leading edge flap or droop nose feature.

With regards to the camber distribution, it has been shown that leading edge camber is required to elevate the values of C_{Lmax}, whereas trailing edge camber is effective at raising the C_L value over a range of angles of attack [1]. The use of trailing edge flap alone will reduce C_{Lmax} (Figure 3.7) due to the increased circulation which increases the local flow velocities at the nose leading to earlier stall. To increase the C_{Lmax} it is therefore necessary to use a leading edge device in conjunction with a trailing edge flap.

3.5.4.4 The 'Conventional Flap and Slat' Systems

The most common approaches to conventional flap and slat systems can be grouped into the following categories [72][100];

    1. Trailing Edge Flap Systems
- The plain flap.
- The split flap.
- The zap flap.
- Slotted flaps (single and multiple).
- The Fowler flap.
- The Youngman flap

2. Leading Edge Devices

- Leading edge flap.
- Fixed leading edge modification.
- Kreuger flap.
- 'Slat without slot'
- Handley-Page slat

The relative effect of some of these high lift devices on lift and drag are shown in Figures 3.8 and 3.9. The favourable effect of curvature induced by the flaps is apparent, although the corresponding increase in drag associated with these devices needs to be considered carefully.

To deal with the conflicting requirements of wing lift coefficient during cruise condition and field performance, aircraft have used camber inducing devices in the forms of various flap and slat systems to increase C_{Lmax}. This can be thought of as using wing camber in a 'fixed' way. That is, a certain flap and slat position is selected for a portion of the flight and then the aircraft is changed in pitch to achieve any further increase or decrease in lift.

Recently, ways of using these 'conventional' camber devices have been looked at for flight phases other than just take-off and landing. For example the use of variable camber for improving the lift capability of fighter aircraft in manoeuvring conditions has led to the development of 'manoeuvre flaps', such as those used on the Northrop F-5.

Increasing wing lift by deflection of the ailerons in the symmetrical sense, so that they become flaperons, is another form of using conventional controls for variable camber operation. On the F16 for example the ailerons are given a 20° downward bias when the landing gear is lowered to improve field performance, thereafter operating up and down about this new datum for roll control.

Rao [116] details the use and design of variable camber as a gust load alleviation system for the Airbus A300. The system uses sensors to alter the camber of the wing in response to

72

gust loadings, thereby reducing the acceleration and fatigue experienced by the aircraft and passengers.

Levinsky and Palco [93] tested a Self Optimising Flexible Technology (SOFT) wing model in a wind tunnel to see the effectiveness of this multi-element design. The wing itself consisted of multiple leading and trailing edge flaps which in combination provide a smoother form of camber than conventional mechanical devices. The shape of the wing is continually monitored and updated by a computer to achieve optimum performance characteristics at nominal flight conditions. Although there were problems with wing shape repeatability in the early tests, these were largely resolved by a new software algorithm.

Ferris [54] performed a series of wind tunnel tests on a multi-segmented combined variable camber and twist wing. The wing incorporated movable leading and trailing-edge segments whose swept hinge lines provided maximum camber variations at the outboard leading edge and movable trailing-edge segments whose swept hinge lines provided maximum camber variations near the inboard trailing edge. It was concluded that all forms of leading edge camber were successful at reducing drag at lift coefficients up to 0.4. The maximum lift coefficient was increased by approximately 18% and at higher lift coefficients the camber was effective in reducing the drag and the trailing edge camber gave large increases in lift coefficient. The practicalities of producing a full scale wing were not discussed.

Pendleton et al [108] developed an Active Flexible Wing (AFW) model for an F-16 derivative wing. The AFW project is a joint NASA and Rockwell International effort to demonstrate aeroelastic control through the application of digital active controls technology. The AFW model features multi-segmented leading and trailing edge control surfaces designed to improve the in-flight manoeuvre capability of the aircraft. Tests on the 1/5th scale model wing successfully demonstrated the potential to increase the wing generated control by the multi-segmented leading and trailing edge segments. The segments also help to increase the overall stiffness of the wing and minimise the effects of

aeroelasticity. Subsequent work by Cole et al [28] evaluated the potential of the AFW for actively suppressing flutter and controlling manoeuvre loads.

Rao [116] proposes a variable camber system for the Airbus which ensures a smooth and continuous profile throughout the range of camber shapes without requiring the use of flexible surfaces. There were however no practical suggestions as to how this variable camber system might be realised. An investigation was performed using rigid two dimensional and three dimensional models in a wind tunnel. Lift gains comparable with a conventional trailing edge flaps were demonstrated although the drag figures were largely inconclusive due to fabrication problems with the models and inaccuracies with the measuring equipment.

The use of flaps has been extended to the marine environment and used for hydrofoils and rudders [45][103][150]. Kerwin and Mandel [85] discuss that *'although the beneficial effect of flaps in enhancing the lifting characteristics of control surfaces has long been recognised in aerodynamics, there appears to be very limited systematic experimental data available on flapped control surfaces with proportions suitable for marine applications'*. Following a series of tests on flapped hydrofoils, they conclude;

1. Root gap, flap gap and type of root mounting have a significant effect on hydrodynamic characteristics.

2. Large flaps in association with a fixed skeg can yield maximum lift coefficients that are as large as those of zero flap all movable hydrofoils, but at the expense of increased drag and hinge moment.

3. A doubly movable hydrofoil (i.e. droop nose and flap at rear) with even a small flap has a much larger maximum lift coefficient than an all movable hydrofoil with zero flap.

4. The size of the flap in the range between 20% and 50% of total hydrofoil area has little influence on maximum lift.

5. The 59% increase in maximum lift achieved by a 20% flap doubly all movable hydrofoil compared with a zero flap hydrofoil is achieved at the expense of about a 250% increase in drag.

6. Flap balance is detrimental to maximum lift.

7. Drag coefficient at zero lift increases with flap size.

8. Comparison at fixed values of lift coefficient indicate that a doubly all movable hydrofoil with a 20% flap has less drag than a zero flap hydrofoil at lift coefficients greater than 0.6 and comparable drag at lower lift coefficients. The disadvantages of the doubly all movable hydrofoil are its increased hinge moments, mechanical complexity and possible maintenance difficulties.

This indicates that for optimum performance from a flapped hydrofoil the forward region needs to be drooped into the flow and the slot gap between the flap and the main foil needs to be kept to a minimum.

Wilson [150], Molland [103] and Eppler and Shen [45] support these conclusions as they all report a significant penalty in drag through the use of flaps on hydrofoils. It is also confirmed that the hinge line generates a large negative pressure peak which can cause premature flow seperation and the premature inception of cavitation. Since the surface smoothness is normally defined in fractions of a millimetre it follows that no joint can be considered as being smooth.

A flapped windsurf fin is proposed by Dugdale [82]. The proposed system uses an articulated pad on the deck of the board to drive a flap on the rear of the fin via a series of linkages. A patent application has been submitted for the concept but a prototype windsurfer is yet to be constructed. However, for this system to be fully effective would require the incorporation of a leading edge flap. This would further add to the mechanical complexity and weight of the proposed design. Other problems are envisaged for a flapped windsurf fin such as the ability of the sailor to maintain smooth control of the flap at high speeds over rough waters, as well as the ability of the sailor to set the optimum flap angle for a given speed and incidence angle.

3.5.4.5 The 'Flexible Surface' Approach

According to Rogallo et al [120] the origins of flexible wings for aircraft applications can be traced back to the late 1940s when the first completely flexible wing was created. The shape of these flexible wings is maintained by the balance of airload forces on the surfaces and the tension in the support lines and other localised stiffening devices. The continuation of this pioneering work has led to the development of modern hang-gliders and paragliders.

Fink [55] investigated a flexible sailwing concept in a wind tunnel and concluded;

1. The fabric of the sail maintains a smooth airfoil contour over the unstalled range of incidence angles.
2. The sailwing can achieve maximum lift to drag ratios comparable with similar conventional hard wings.
3. The lift curve slope for a sailwing is unusually steep at low incidence angles (indicating the contribution to lift of the induced camber).
4. Modifications to the tautness of the sail with the rigging wires has a noticeable effect on the aerodynamic characteristics.

Interest in flexible wings for other aircraft as an alternative to conventional flaps has stemmed from the need to reduce the local flow velocities and other detrimental effects associated with discontinuous aerodynamic surfaces. Theoretically this will result in a smooth camber system with less drag than a comparable mechanical device. This has resulted in a number of investigations into variable camber systems which are based on an ability to physically deform a flexible skin on a rigid subframe.

The Beatty B-5 sailwing incorporated a flexible surface approach employing a deformable Dural plate on the upper surface (first 75% of chord) in conjunction with a 20% rear flap. The curvature of the Dural plate was increased by 'pushing' the trailing edge forwards with battery driven (12V) mechanical linkages. The transition time from a thick high cambered

76

section to a thin low cambered section was approximately 5 seconds. This transition time means that the camber is not truly adaptive and as such is 'set' for a portion of the flight regime (i.e. climb). The actual performance of this flexible surface approach was disappointing due to breaks in the wings skin. This resulted in early transition of the flow which had a profound effect as the cross section had been designed originally to support a high degree of laminar flow. The use of a battery along with the complexity of the mechanical system and the slow transition time limits the applicability of this system to the windsurf fin.

For transport aircraft wings, the work of Redeker et al [117] considered a theoretical 'adaptive aerofoil', equipped with a flexible uppersurface. This aerofoil could be adjusted for different flow conditions such that a shock free pressure distribution could be obtained at all conditions, resulting in an optimum aerofoil cruise performance. (This team did not however offer any suggestions as to the design of a practical mechanism to produce this uppersurface profile). Theoretical and experimental tests were carried out on a series of 3 aerofoils, having the same shape, with the exception of a certain portion of the uppersurface. Each uppersurface region was designed to give a shock-free pressure distribution at three different Mach numbers. The case for an adaptive aerofoil was therefore inconclusive because shock-free pressure distributions could not be obtained experimentally, and most of the advantages could be achieved by an aerofoil designed for a single Mach number i.e. the particular aerofoil used as a basis for the work was too sensitive to off-design conditions.

Flexible skins allowing modifications to the camber over the entire chord are not necessary (nor practical) for most applications, although there are some notable and successful exceptions, including the previously mentioned conventional marine sails, hang-glider and parapente wings. However, most 'flexible surface' type variable camber systems limit the area of flexing to the leading (drag reduction) and trailing edge (lift increment) regions.

Early examples of a 'flexible surface' approach in the world of aeronautics are the RAEVAM and VARICAM systems developed by the Royal Aerospace Establishment and

by British Aerospace Warton. These are simply a development of the manoeuvre flaps. They both feature a flexible skin on the uppersurface which allows a more gentle change in the curvature than conventional mechanical flaps.

Military aircraft are prime candidates for highly effective variable camber systems because they spend a fair proportion of their time away from their design point. Two operational examples of a truly 'flexible surface' type variable camber are the F-111 Mission Adaptive Wing (MAW) fighter and the Grumman X-29 Forward Swept Wing (FSW) technology demonstrator [14][15][104][124].

The F-111-MAW was designed to incorporate continuous hydraulically powered variable camber on the leading and trailing edges. Dual digital computers controlled the flap positions in either manual or automatic mode. The wing is built around a fixed wing box structure with Glass Fibre Reinforced Plastic (GFRP) flexible leading and trailing edge surfaces (as shown in Figure 3.10). The GFRP panels provide uppersurface continuity as the camber changes, with sliding plates being used on the underside (i.e. the top panels bending without extension and the lower ones sliding to accommodate the shortening).

The entire wing system is controlled by the on-board computer and can be set to a number of different flight modes. Changing the flight mode instructs the computer to optimise certain aspects of the wing configuration for cruise, manoeuvre or gust alleviation.

During cruise the camber is configured by the computer for minimum drag, or maximum lift-to-drag (L/D) ratio by tailoring the profile until no further increase in forward velocity is achieved.

During Manoeuvre, the wing camber configures itself for maximum L/D in the turn for a sustained maneuver (without losing speed or height). As the aircraft reaches its maximum 'g' loading the trailing edge camber of the outboard section is reduced, and therefore so is the lift in this region, thereby reducing the root bending moment. Manoeuvre enhancement achieves a more rapid entry into turns as it uses a form of 'Direct Lift'.

Gust alleviation is used to reduce the effects of turbulence with the associated improvements in weapon aiming capability. This feature helps to reduce the workload and increase the effectiveness of the pilot.

The development work on the MAW finished in the early 1990s and it is not clear whether the system is to be implemented in service aircraft.

The X-29 Technology Demonstrator combines a number of novel wing design features. These include Forward Sweep Wings (FSW) that are aeroelastically tailored, full authority canards, digital flight control system, relaxed static stability, as well as a flexible variable camber system. The camber system extends over the rear 25% of the chord with a double hinge, combination flaperon and lead-tab. At subsonic speeds the camber of the wing is increased with increasing lift requirements. This raises the aerodynamic efficiency for minimal drag. At supersonic speeds the camber is straightened. Due to the interaction of the various technologies on the aircraft it is not possible to establish the effectiveness of the variable camber system in isolation from the other novel features used in this wing [124].

Wright [151] and Haddock [65] propose the variable camber foil sections shown in Figures 3.11 and 3.12 respectively. The mechanical complexity of these systems again limits their applicability to the windsurf fin.

One problem associated with flexible wings is the limited maximum lift coefficient (C_{Lmax}). McRae [100] states that the C_{Lmax} for a 'clean' wing is approximately 1.8, whereas the use of a simple split flap can increase this to 2.2, with even further gains possible from other high lift flap systems.

3.5.4.6 Aeroelastic and Hydroelastic Tailoring

'Trees sway in the wind, sails and flags flutter, so may airplane wings' [58].

Aeroelasticity is the study of the effect of aerodynamic forces on elastic bodies. The same phenomenon exists in water and is termed hydroelasticity.

Aeroelastic and hydroelastic tailoring is the technique of using the dynamic loads experienced in flight to modify the geometry of the lifting surface to realise beneficial performance characteristics. These techniques can be used to induce camber, twist and elongation in various lifting surfaces.

The phenomenon of aeroelastic tailoring has been addressed by industry, university and government investigators through analyses, model tests and full scale flight programs because it is acknowledged that stability requirements are as important as strength for most flight vehicles. In general the work into aeroelasticity has been concerned with flutter suppression and twist induction/reduction.

Flutter occurs when the exciting forces acting on a body are equal to the restoring forces. These exciting forces are generally unsteady aerodynamic loads and are counteracted by the stiffness of the body. Flutter is characterised as a self excited, self sustained oscillation that occurs at a specific dynamic pressure which can lead to control problems, fatigue and structural damage.

Parametric studies by Popelka et al [112] show that the gains from composite tailoring can be limited because of the conflicting structural safety design requirements. It was found that excessive reductions in weight can allow the structure to deform appreciably, leading to stability problems and/or flutter.

Chiu and Van Den Bersselaar [26] and Broers et al [16][17] investigated the performance of a range of windsurf fins in which the spanwise twisting characteristics were varied by

tailoring the composite materials used in the lay-up process. The result of these tests were inconclusive and it is therefore not possible to establish the effectiveness of this technology for the windsurf fin. This does not necessarily mean that the use of hydroelastic tailoring is not suitable for the windsurf fins, rather that it has not yet been proven to be successful.

A common form of aeroelastic tailoring is in the conventional marine sail where the dynamic loading of the wind is used to tailor the profile of the cross section from one side of the mast to the other. The use of stiffening battens as well as rigging devices enables the magnitude and nature of the camber to be regulated by the crew. The technology and theory behind the use of aeroelastic tailoring for marine sails is not well established and can in fact be considered to be more of a *skill based upon rules of thumb and many years of accumulated experience* [99]. Sail design is further complicated by wind gradients, material characteristics and class rules. Although the sail is in effect a 'snap-through' variable camber device, Garrett [61] describes how the magnitude of camber in the sail can be governed by the slackness ratio, which is a measurement of the amount by which the trailing edge can move as a ratio of the chord length.

Garrett [61] also explores the performance benefits of double surface sails, which are most commonly used on hang-gliders. These sails are formed by wrapping the sail cloth around a circular edge (the mast) and bringing the two sides together to form a sharp trailing edge [55][101][136]. As with a conventional sail, the magnitude of camber in a double surface sail is a function of the slackness ratio. A comparative test with double surface and single surface sails of constant 10.6 % camber ratio at a Reynolds number of 1.5×10^5 established that at low incidence angles the drag is very similar. However at high incidence angles the single sail has much more drag than the double skinned sails and is also prone to stall earlier (15°) than the double surface sails (21°). The lift coefficient of the double surface sail is also considerably better than the single surface sail. The main problem with the double surface sail is the lack of structural integrity provided by the unstayed mast.

Gaide [60] has filed a United States Patent 4,537,143 for a variable camber windsurf fin as shown in Figure 3.13. The design features two deformable side walls which are mounted

to a rigid and stiff centre wall exclusively at the leading edge. According to the inventor *'an optimal hydrodynamic flow profile is automatically generated, depending on the prevailing pressure situations between luff and leeward side'*. To hold the side walls in position and to regulate their shape, the design embodies a water vacuum pump to vary the voidal pressures. There is however no explanation as to how this vacuum pump might be incorporated on a windsurf board. Additionally the rigid central column will limit the extent of the possible camber shapes and the sliding trailing edges form discontinuities which are likely to result in an increase in drag. The patent was filed in 1982 but further information has not come to light. This leads to the conclusion that the concept was not successful in the described format.

Widnall et al [148] filed a patent for a Flexible Tailored Elastic Airfoil Section as shown in Figure 3.14. The device comprises an elastic streamlined structure with a stiffness distribution along the chord and span tailored to provide a desirable cambered shape in operation. The magnitude of the camber is limited by the design of the pivotal axes and a sliding section at the rear. If employed on a windsurf fin these mechanical features could be prone to contamination (saline deposits and sand) unless they are suitably enclosed. Additionally the wear in this type of pivotal axis is likely to be high unless a suitable form of bearing is used. It has not been possible to source further information on this device due to its proprietary nature.

Ehlers [42] proposes an aeroelastically tailored lifting surface in which a feedback control system is used to apply voltages to embedded piezoelectrics in direct proportion to the wing root loads. This results in a lifting surface in which the torsional stiffness and section geometry is adaptive in response to the surface loading. A theoretical investigation indicates that the lift effectiveness of a wing can be increased or decreased by controlling this feedback gain. Physical testing of the concept has not been performed. The requirement for an auxiliary power source makes this technology unsuitable for the sport of windsurfing.

3.5.4.7 Variable Sweep and Surface Area

The contradictory requirements of high and low speed operation has led to the development of variable sweep and area lifting surfaces. The concept for the variable-sweep wing is generally attributed to Dr. Barnes Wallis (1944).

Traditionally the use of variable sweep and surface area in the aerospace industry is used on supersonic aircraft to;

- Improve the low speed performance by increasing the span and reducing the sweep angle.
- Improve the high speed manoeuvrability in transonic flight.
- Enhance the aerodynamic efficiency in supersonic flight.
- Postpone the onset of local supersonic flow to higher transonic speed.

Variable sweep can be similarly used on hydrofoils to delay the onset of cavitation as it is the flow component normal to the leading edge which governs the cavitation number [32] (although because the current work is concerned with the sub-cavitating operational range this approach is not required).

Along with the conventional approaches to variable sweep, Housh et al [73] describe a Scissor Wing variable sweep wing. This configuration features two independently sweeping-wing surfaces which are shown to have a higher total lift to drag ratio than a conventional single-swept wing in the subsonic region. The drag of this configuration is however higher than the single wing. Although this is beneficial for decreasing the landing speeds of aircraft it is nonetheless unsatisfactory for the performance of a windsurf fin.

There are a number of documented approaches to variable geometry surface area and rake windsurf fins. The most common of these is the daggerboard used on beginner and long race boards. The daggerboard is normally pivoted so that the sweep angle and surface area

can be varied by the sailor. The daggerboard can also be fully swept and retracted into the hull of the board if required.

Van der Berg developed variable surface area fins for planing short boards in which the fin is pushed and pulled through the deck of the board by the sailor [82]. Problems with the mechanical system (vibration and aeration of the fin through the slot gap) limited the performance of this design. Further work on the mechanism failed to overcome these problems and the idea was abandoned.

Kinnaird [86] filed a patent application (GB 2 255 937 A) for a windsurf fin with a fulcrum mechanism in which the inclination and extent of downward projection of the fin is variable (as shown in Figure 3.15). As with the system used by Van der Berg, the extent of the sweep and retraction of the fin is regulated by the sailor. The system was tested by Gilmore [62] who commented, *'to say you feel the extra area is an understatement. The additional lift you get from another four inches of carbon foil is extraordinary and the board's pointing ability is improved dramatically'*. There were however a number of problems associated with this system, including difficulties in operating the device at sailing speeds, small particle contamination of the fulcrum and sliding mechanisms as well as general wear and 'freeplay'. The concept has not been a commercial success and has not been adopted by other windsurf board manufacturers.

These documented approaches to variable surface and rake windsurf fins establish the potential for optimising the lift and drag performance for a variety of sailing conditions. In terms of ultimate hydrodynamic efficiency, the approach by Kinnaird is considered too inappropriate for realising an increase in the lift to drag ratio due to the incorporation of variable sweep (sweep will always entrain a penalty in terms of an increase in induced drag). There are however a number of problems associated with these systems which has resulted in the concepts being abandoned. In addition to the wear and clogging of the sliding mechanisms, aeration of the fin and difficulty in operating the devices, the requirement for a specially adapted board (to accept the variable geometry fin system) has limited the operational and commercial success of these approaches.
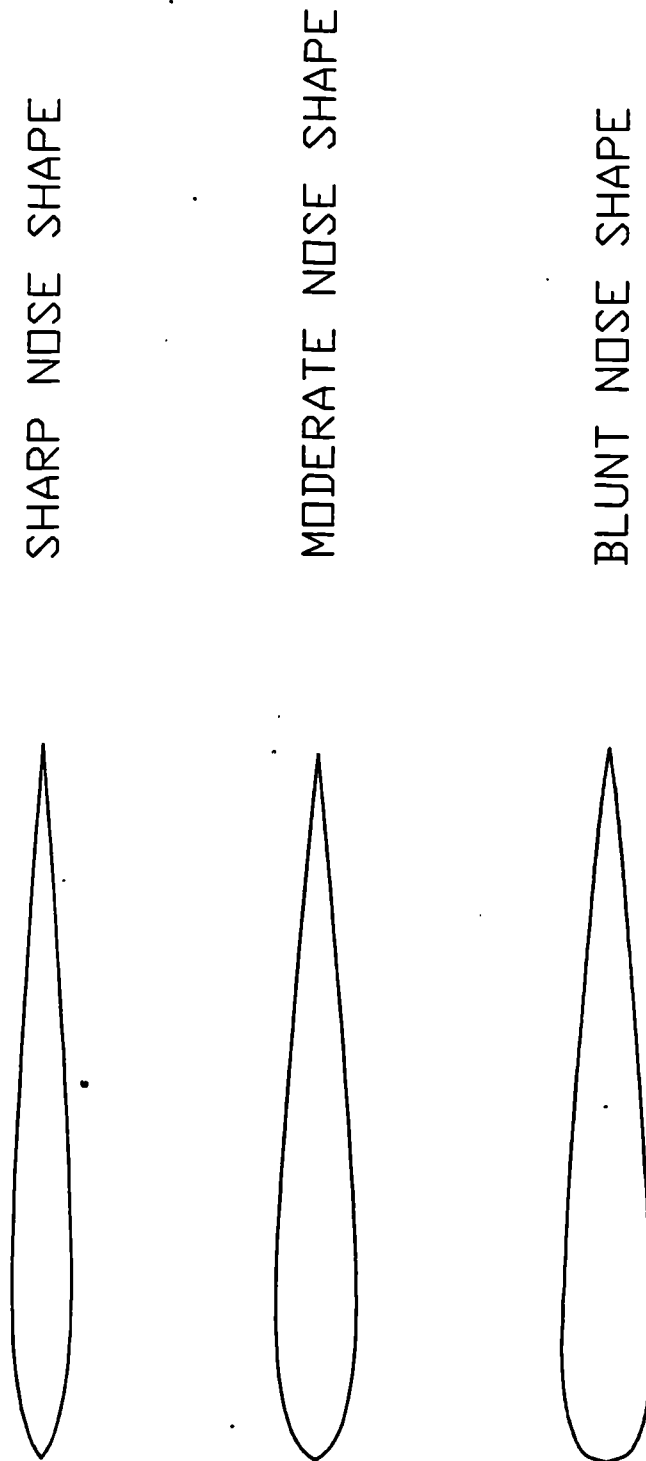
Figure 3.1   Nose Shapes
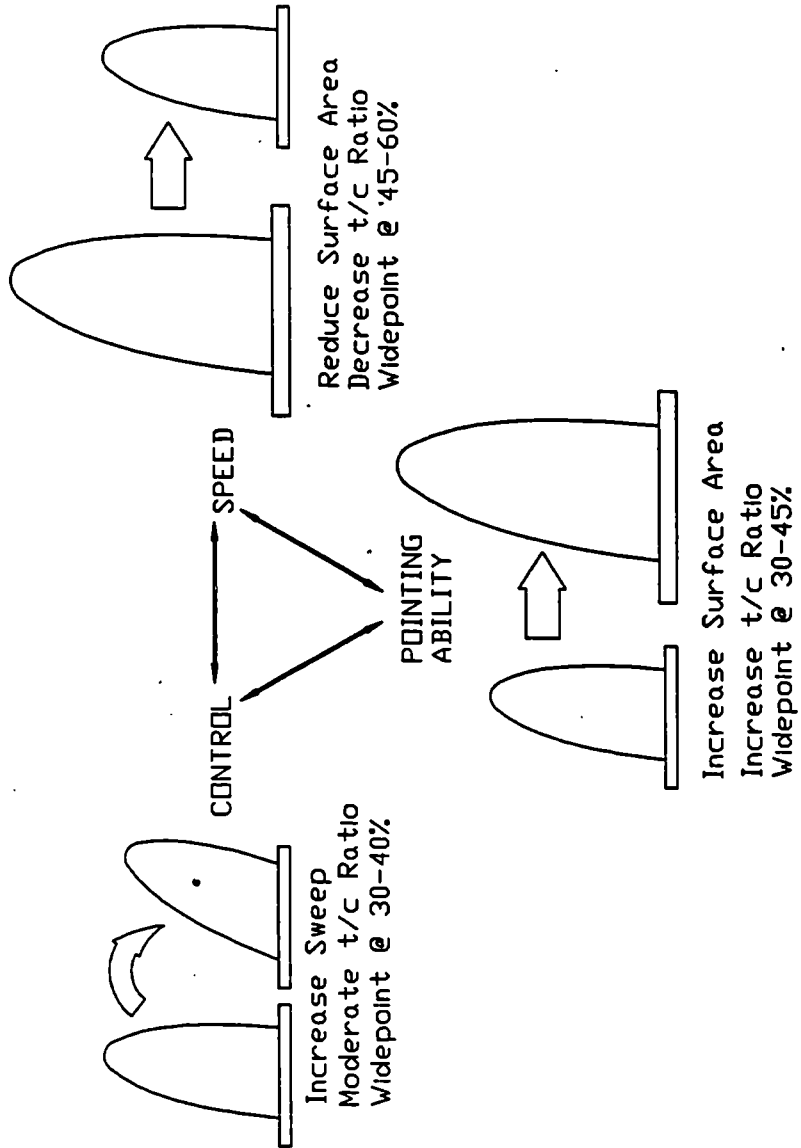
Figure 3.2   Windsurf Fin Design Triangle

3.0

2.0

1.5

1.0

.8

.6

.4

FULLY TURBULENT

FULLY LAMINAR

A

D

B

C

REYNOLDS NUMBER x 10

4 6 8 10 15 20

CROSS SECTION

SEAMLESS HOSE

DIAPHRAGM AND STUBS

RIGID STRUCTURE

60 40 20 20

CUT THROUGH STUBS

80 40

69
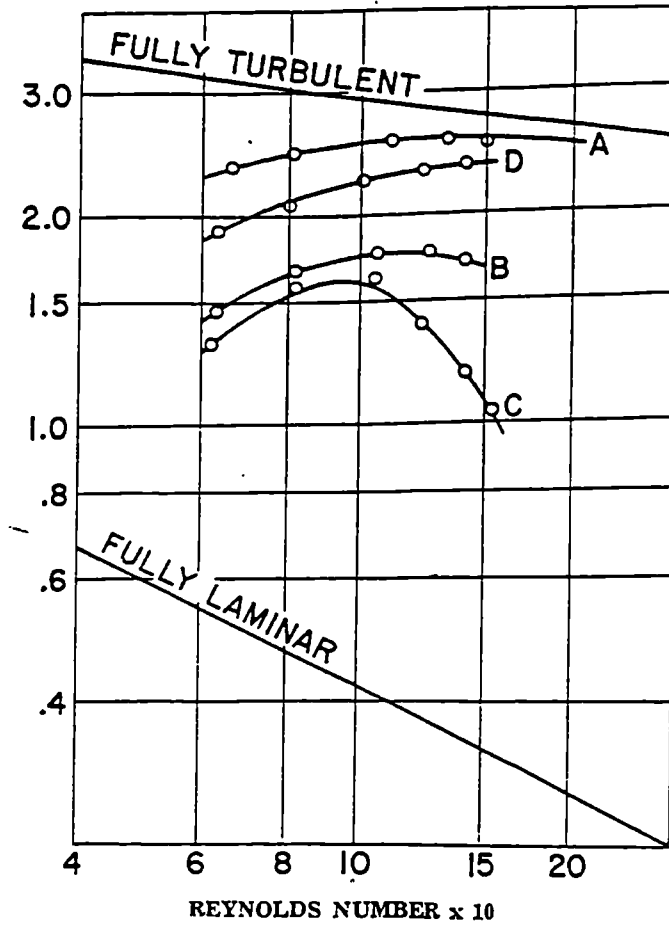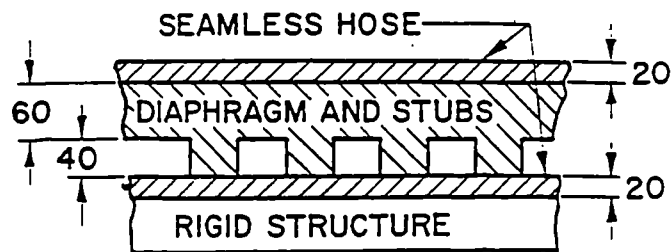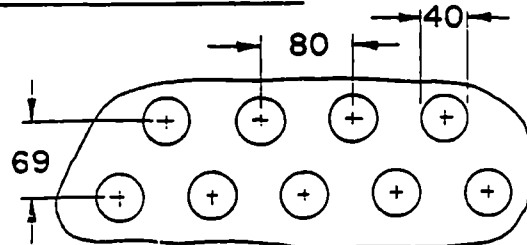
Figure 3.3   Compliant Surface
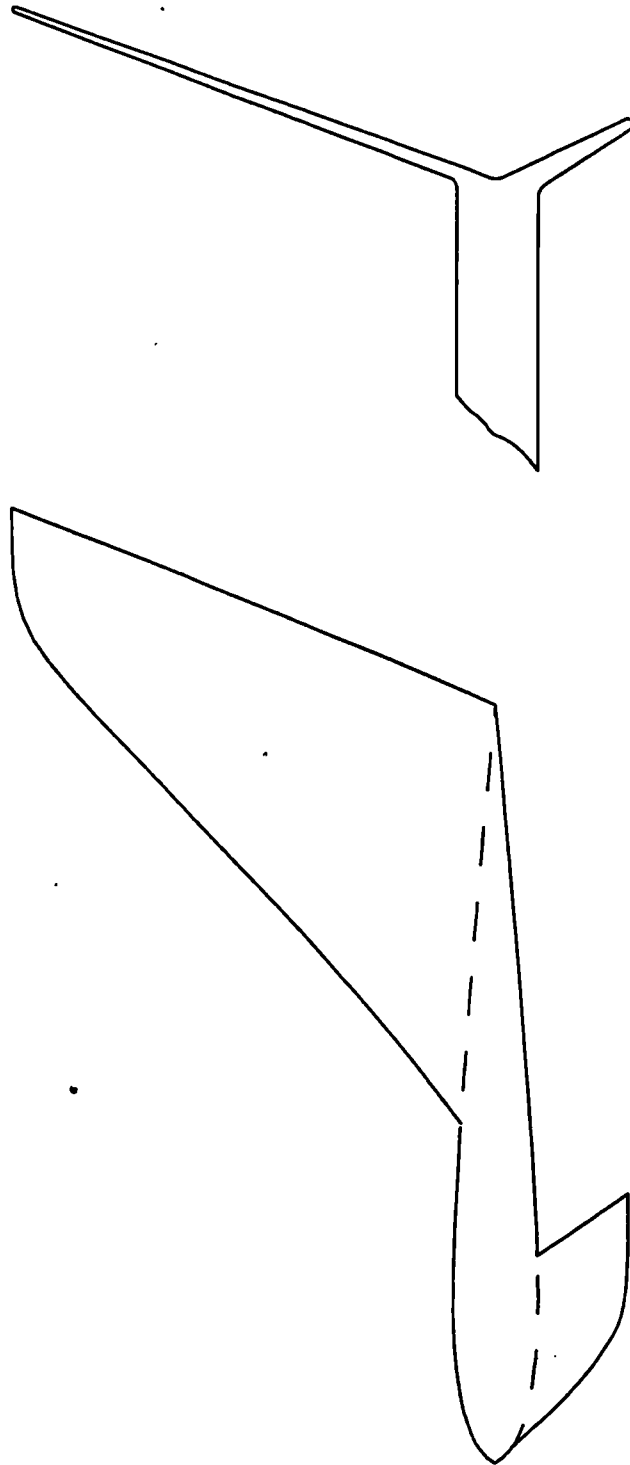
Figure 3.4   A Wing Tip Sail
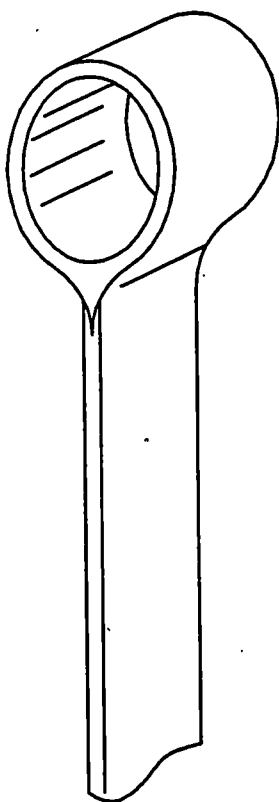
Figure 3.5   Ring Wing Tip

Figure 3.6   The Hobert Fin
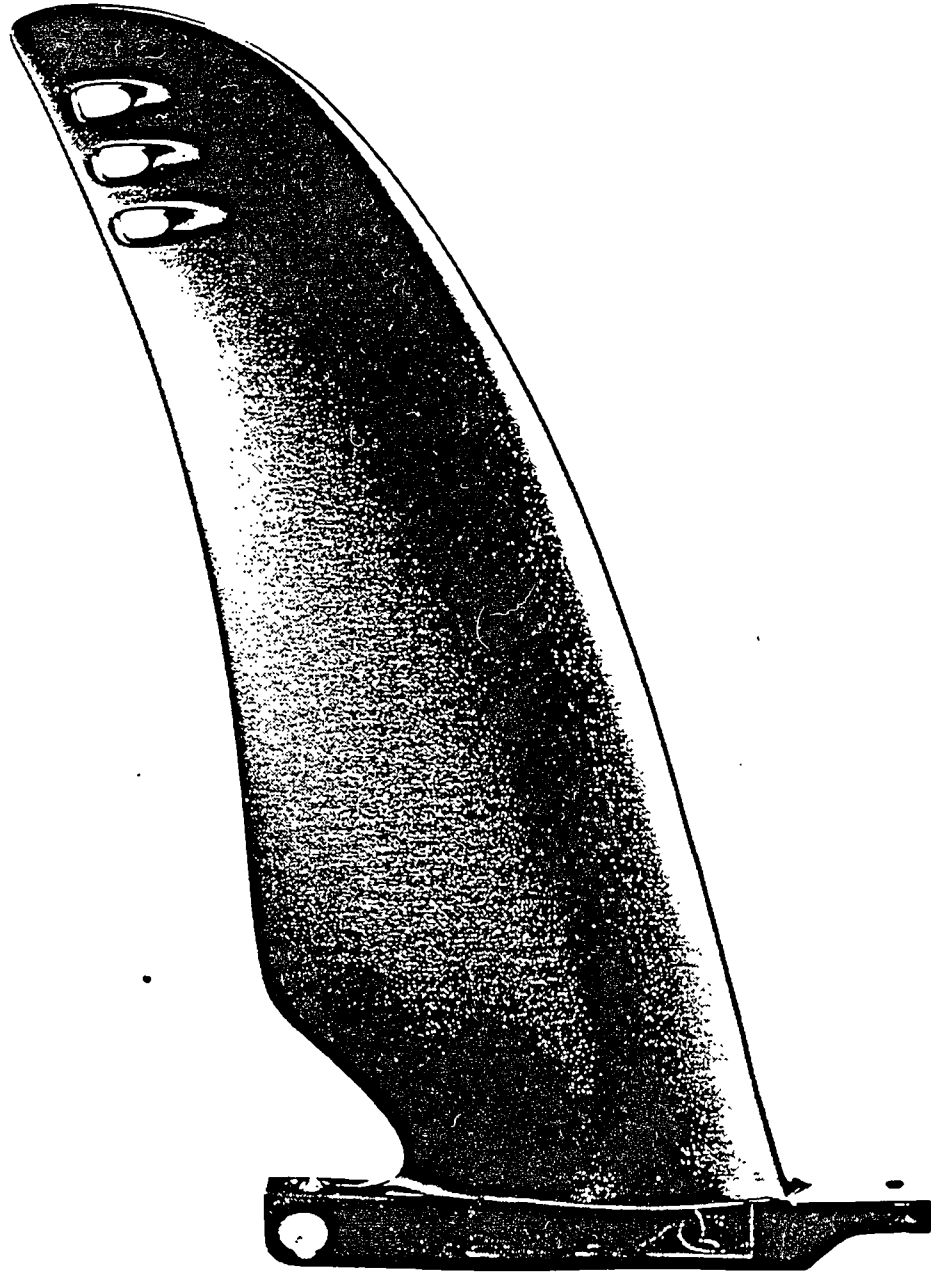
Difference due to trailing edge flap
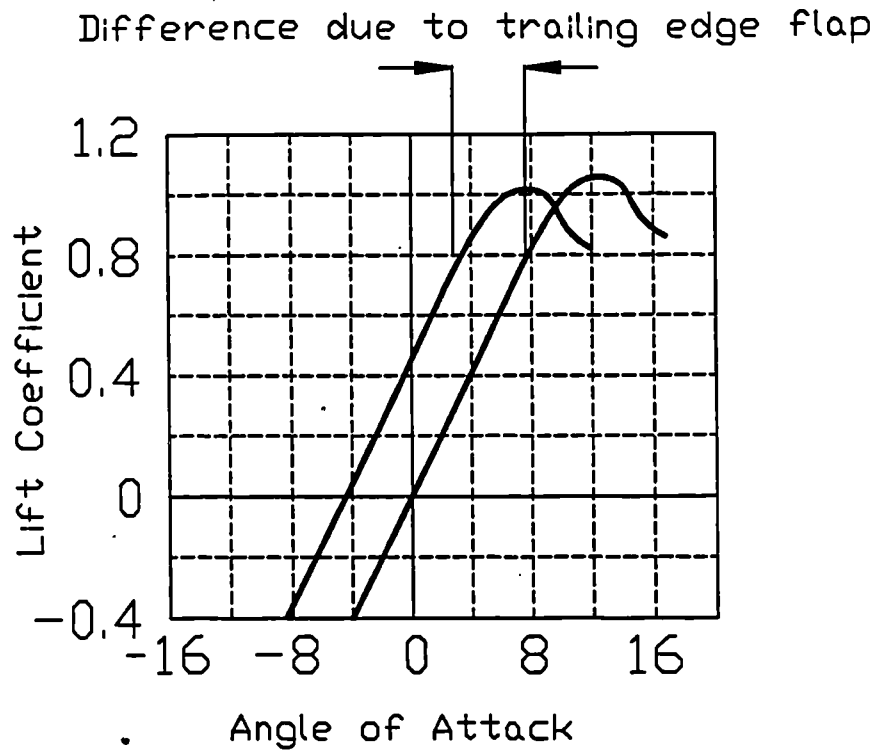
Figure 3.7 Difference in Lift Curve Slopes due to a Trailing Edge Flap (adapted from 'Theory of Wings Sections', Abbott and Doenhoff.)

91
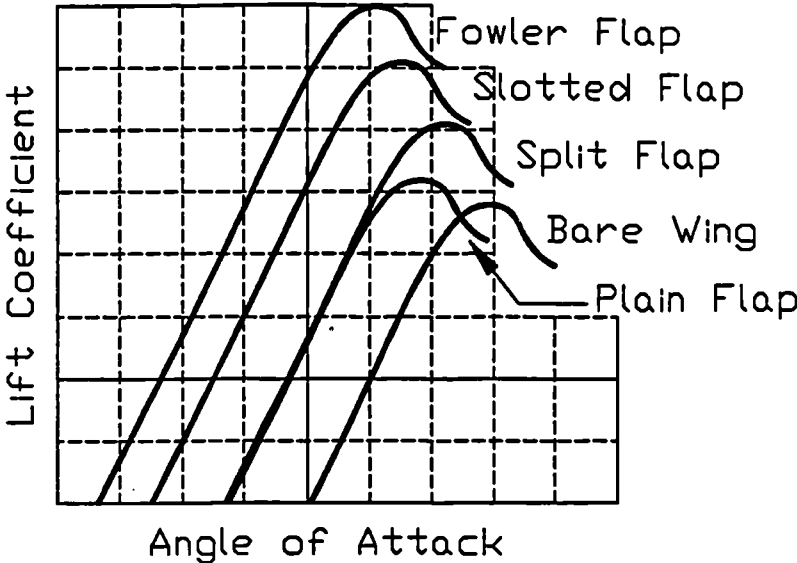
Figure 3.8   Effect of Different Flaps on Lift Curve Slope (adapted from 'Theory of Wings
Sections', Abbott and Doenhoff.)

92
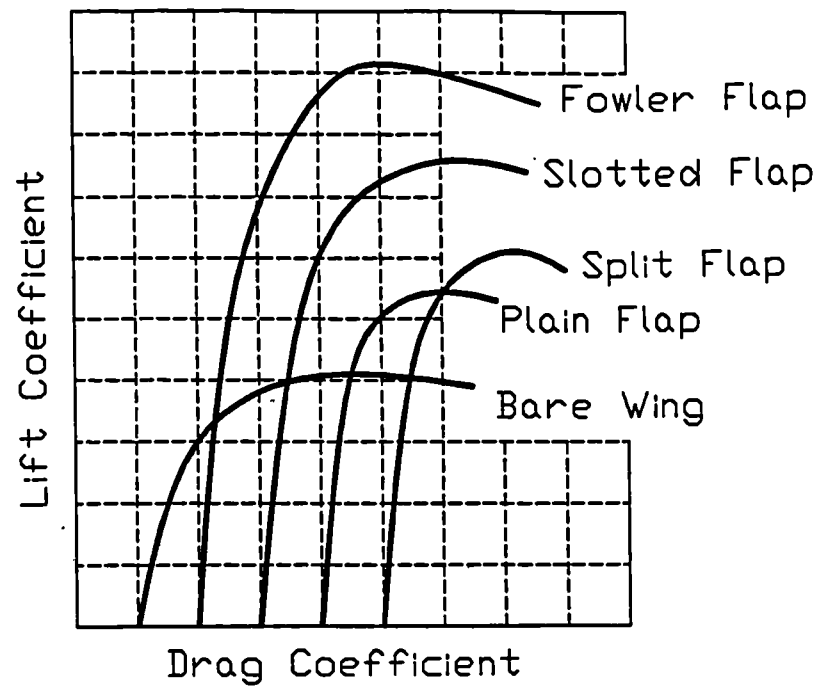
Figure 3.9   Effect of Different Flaps on Drag Polars (adapted from 'Theory of Wings Sections', Abbott and Doenhoff.)
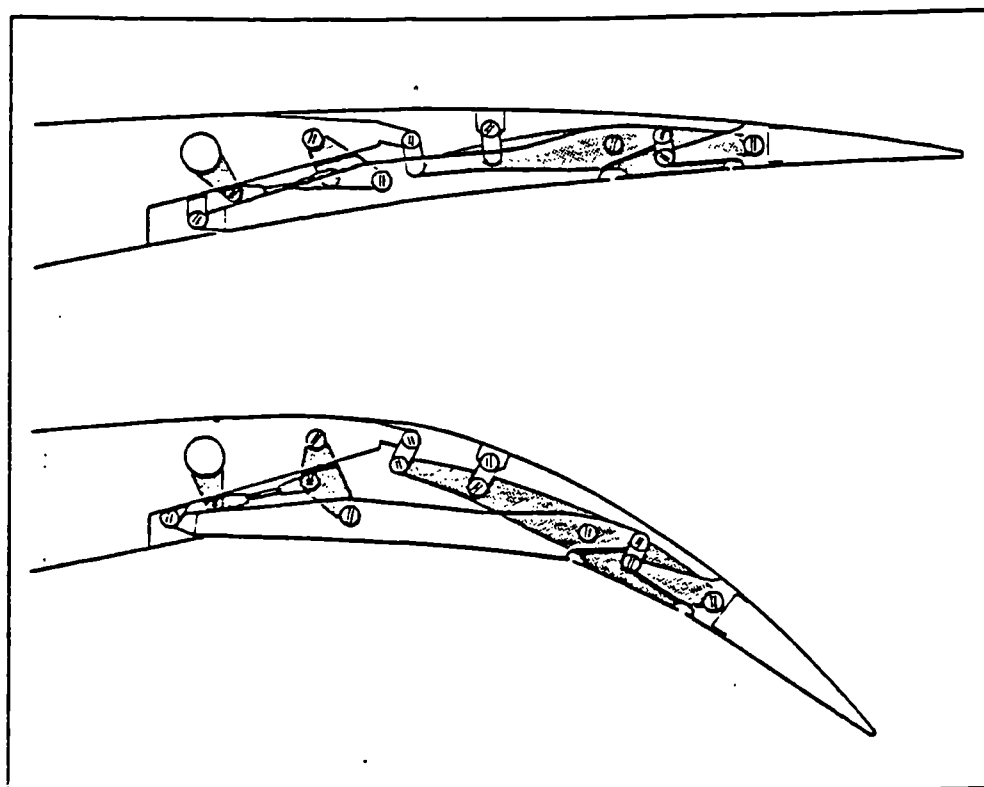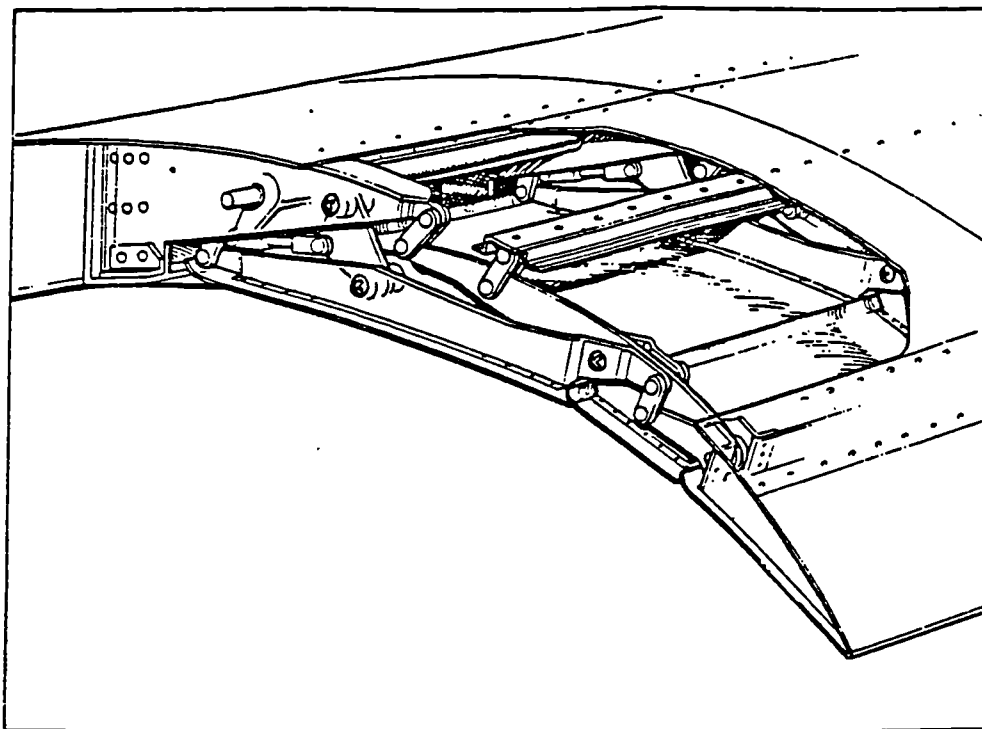
Figure 3.10   The Mission Adaptive Wing
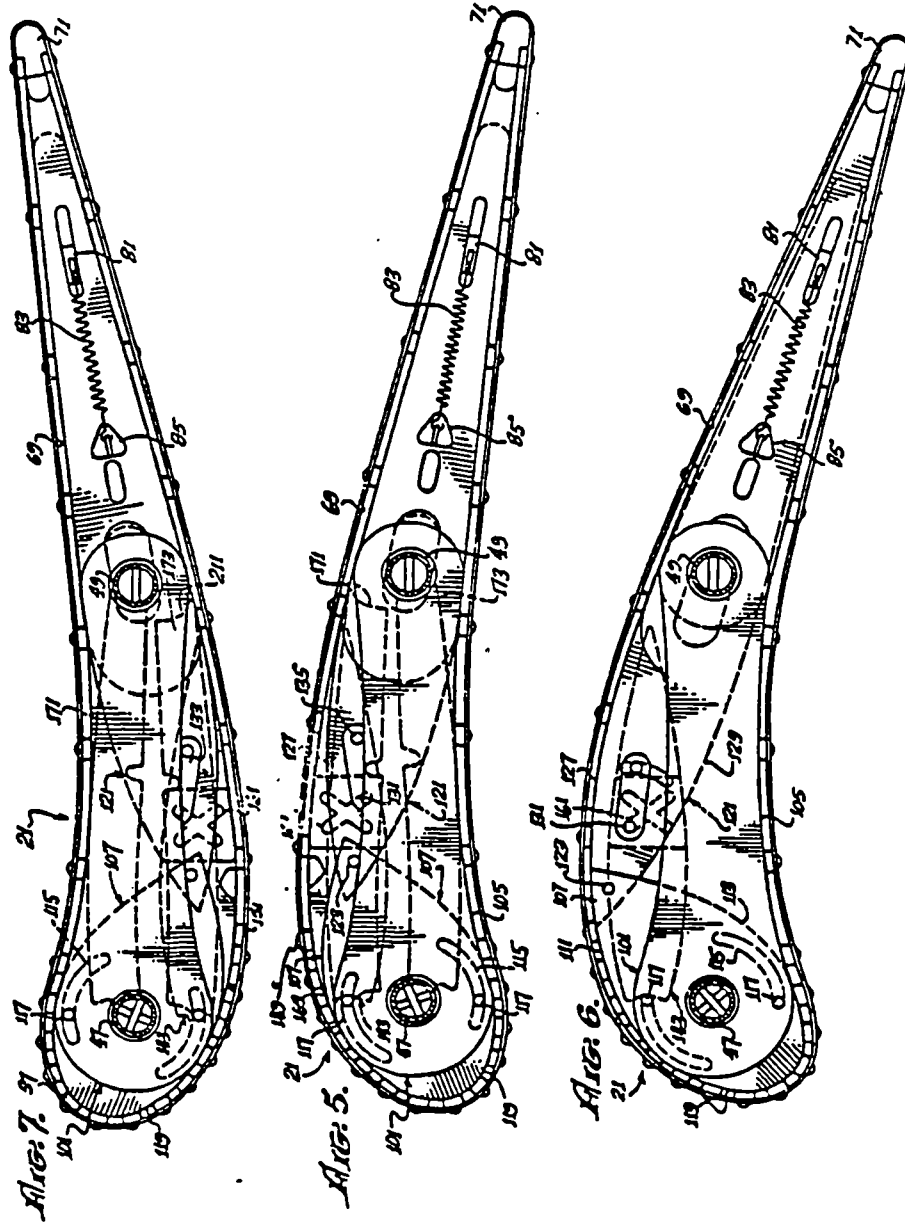
Figure 3.11   Flexible Surface Wing Section
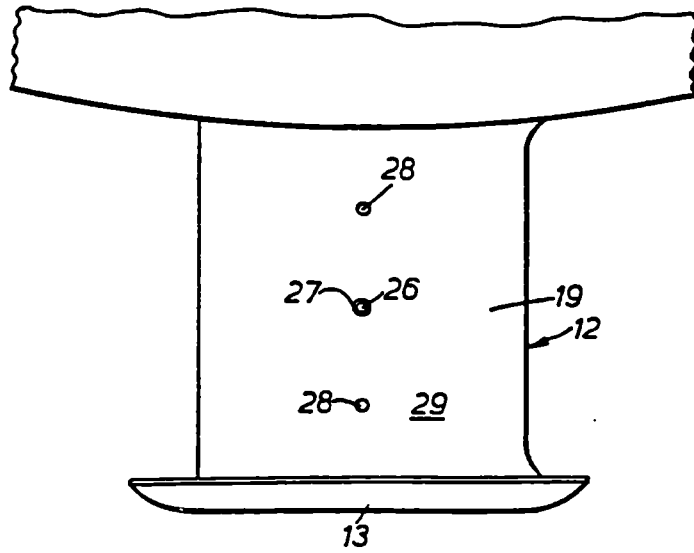
FIG. 2.
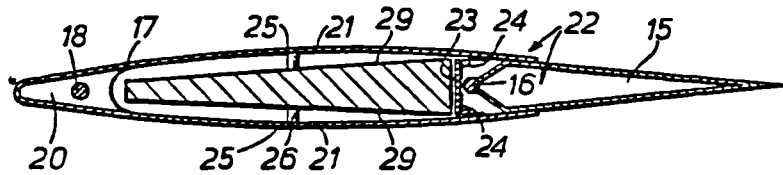
FIG. 3.

Figure 3.12   Variable Camber Hydrofoil

96
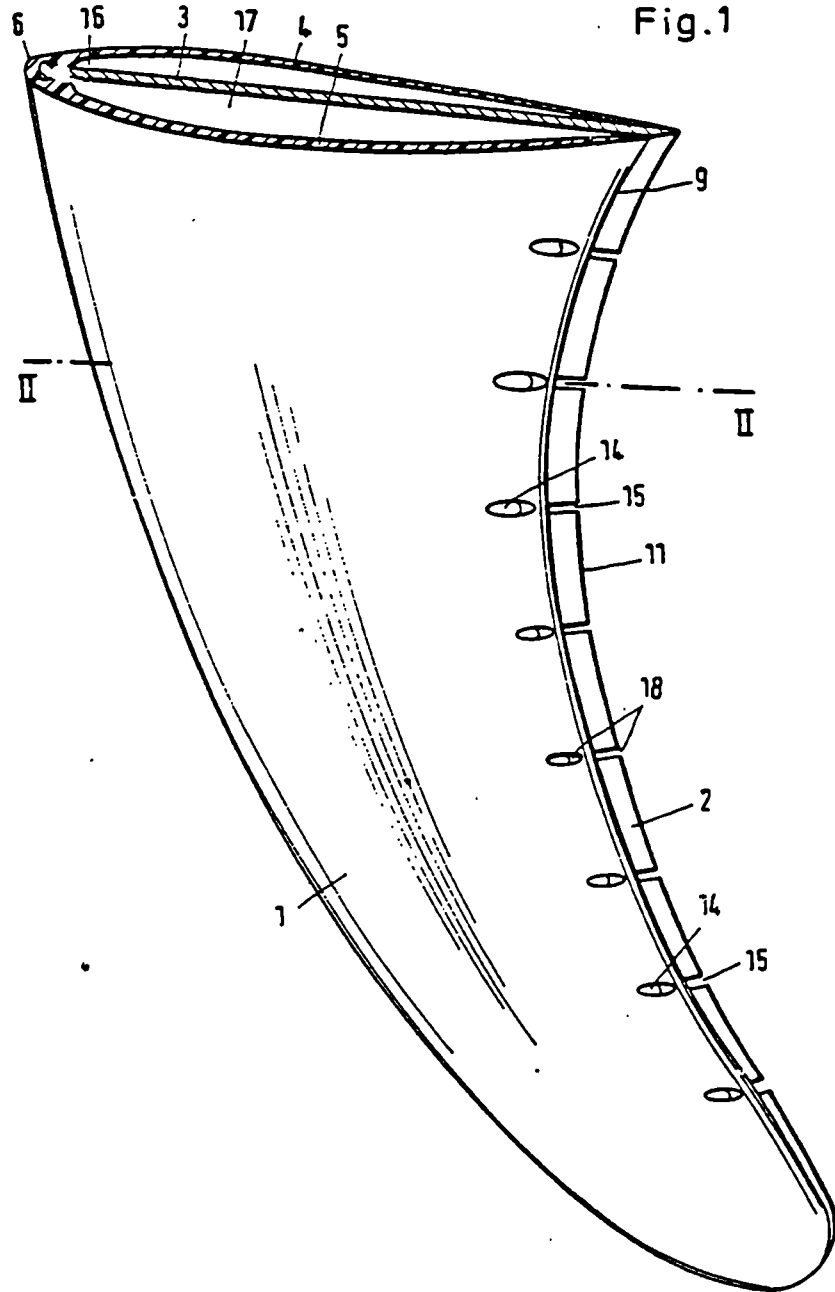
Figure 3.13   Variable Camber Windsurf Fin
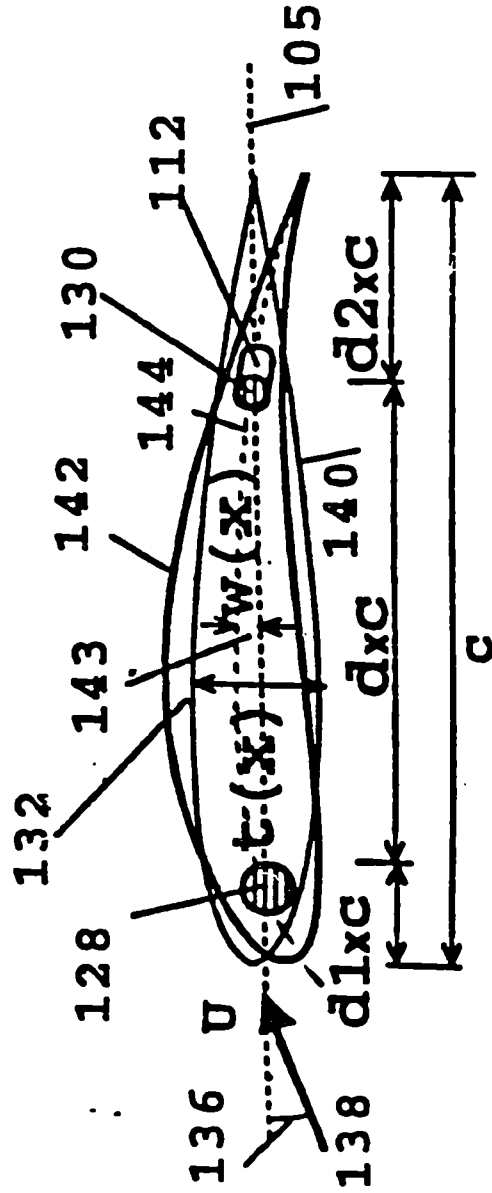
Figure 3.14   Flexible Tailored Elastic Airfoil Section
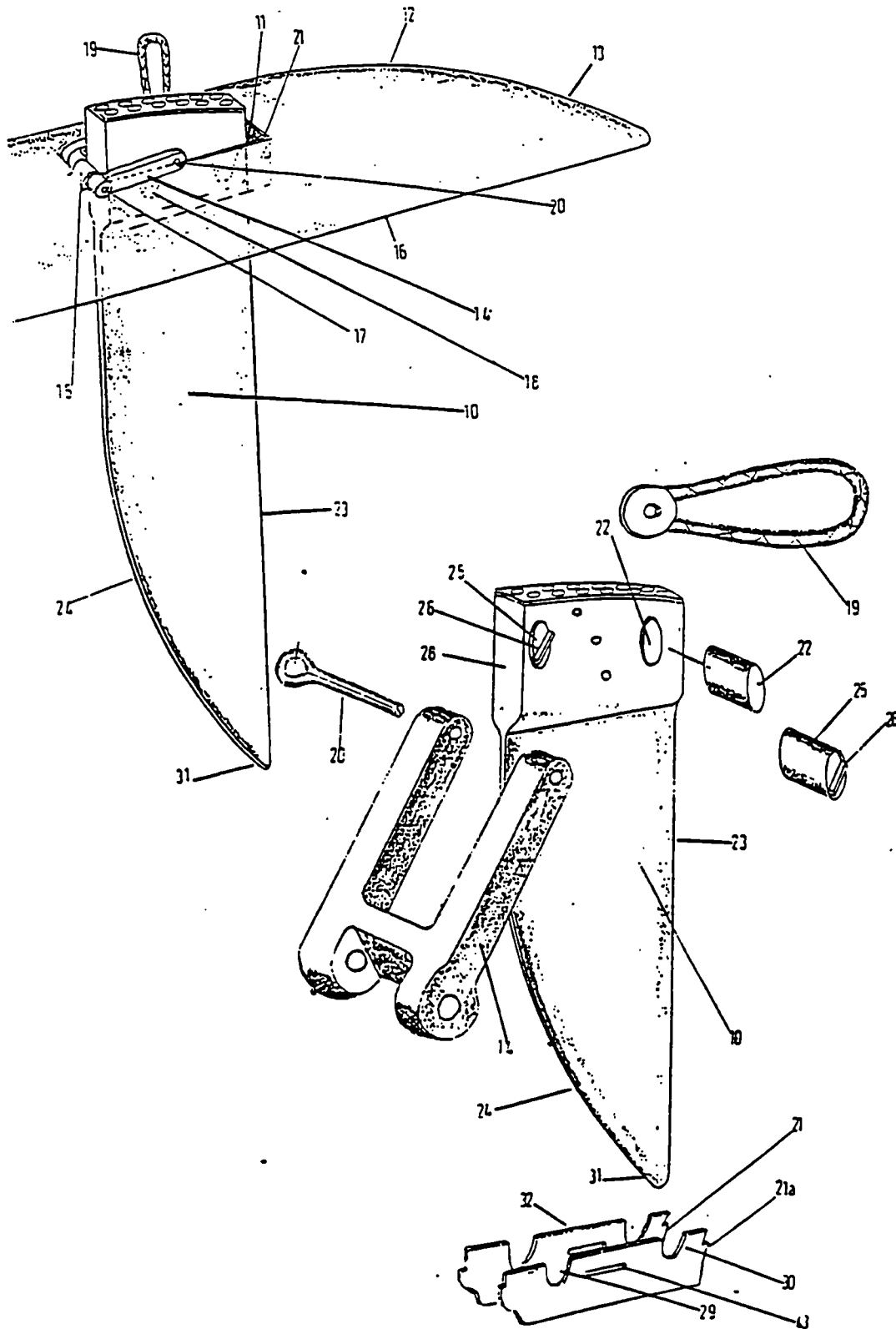
Figure 3.15 Variable Rake and Surface Area Windsurf Fin

4.0   The Design Solution

The previous sections discussed the design and role of contemporary windsurf fins as well as investigating potential methodologies for increasing the L/D ratio of the device (for pre-stall conditions). A summary of this work is provided below;

1. The windsurf fin requires multipoint operational capabilities to perform satisfactorily over a wide range of incidence angles (on both sailing tacks) and sailing speeds.

2. The windsurf fin is at an advanced stage of evolution within the constraints of a fixed geometry device. Only minor gains in the L/D ratio will be attained by further refinements to the planshape, symmetrical cross section and surface finish.

3. Active boundary layer control technologies offer the potential for increasing the L/D ratio of the conventional windsurf fin at pre-stall incidence angles. These technologies can also be employed to delay the onset of leading edge stall. The implementation of active boundary layer control methods is impractical for the windsurf fin primarily due to the requirement for an auxiliary power source.

4. Passive boundary layer control technologies offer limited C_{Lmax} gains, but this is at the expense of an increase in C_d and reduction in C_l effectiveness for pre-stall incidence angles.

5. Tip devices offer the potential for C_{Di} reductions at specific design conditions, but are likely to be highly detrimental to performance (increases in drag) at off design conditions. The most effective tip devices are asymmetric and exhibit the highest performance gains on low AR lifting surfaces where the 3D flow effects are significant. The use of variable geometry tip devices to increase the operational range of tip devices has not been shown to be successful. The high (effective) AR of the windsurf fin and the requirement for equal operation on both tacks (requiring

the use of a symmetrical tip device) limits the potential performance gains associated with tip devices.

6. Variable rake and surface area technologies provide the means for fundamentally altering the lift and drag characteristics of windsurf fins. Previous work in this area has failed to develop a successful design (both commercially and operationally), due to the impractical nature of the design solutions.

7. Variable camber technologies offer the potential for dramatically enhancing the C_l and C_d characteristics of the fin. Although there are documented proposals for variable camber windsurf fins it has not been possible to source the existence of a functioning device.

From the foregoing discussion it is clear that a fundamental reworking of the windsurf fin is needed to realise any significant gains in the lift to drag ratio.

To satisfy this requirement it can be argued that what is really needed is not a rigid and symmetrical cross section windsurf fin for predetermined sailing speeds and course of sailing, but a finitely adjustable and variable camber section which can be trimmed and tuned effectively by the sailor to cope with a great variety of sailing speeds and course directions.

An adjustable cross section will then satisfy the contradictory C_l and C_d requirements of close hauled sailing (high C_{Lmax}) and of reaching (low C_l and C_d). This indicates that a certain amount of 'elasticity' is required in the design of the cross section.

Although this may be considered a demanding design problem, a successful solution would result in a windsurf fin which allows the sailor to intelligently trim and tune the camber in the cross section for the course direction and speed in the same manner as is already used on conventional marine sails.

4.1   Approaches for a Variable Camber Windsurf Fin

The camber of a cross section is recognised as one of the most important characteristics of a lifting surface. The obvious approach for developing a variable camber system for the windsurf fin would be with conventional leading and trailing edge flaps, actuated and controlled by mechanical linkages. This approach is proposed by Dugdale, but a fully functioning windsurfer featuring a variable camber fin has not been fabricated.

There are however a number of problems associated with using conventional flaps in a marine environment which in turn limits their applicability to the windsurf fin. These are summarised as follows;

1. The physical size of the conventional windsurf fin is highly restrictive. Typically a maximum thickness of approximately 12 mm is found in the base region and this decreases rapidly along the span. The implementation of a control and linkage mechanism within these constraints is likely to be problematic. This is supported by Kerwin et al [85] who discuss the problems of *mechanical complexity and possible maintenance difficulties'* associated with a double flap hydrofoil. Additionally, due to the density of the water the pressures (F/A) generated and experienced by a lifting surface in a marine environment are considerably higher than a comparable device operating in an airflow. This has obvious structural implications.

2. The difficulty for the sailor in actively controlling the magnitude of the flap displacement. It is unlikely that the sailor will be able to make finite adjustments to the flap system with a deck operated system as proposed by Dugdale (it is more likely that a 'snap through' approach will need to be adopted). Even if it is possible to develop a finitely variable system, the ability of the sailor to determine and then implement the optimum flap position for a given sailing condition has to be questioned.

3. Wear in the system and contamination by deposits. Continuous use in a marine environment will lead to contamination by saline deposits and possibly by sand. It is envisaged that suitable gaskets or similar devices will be required to avoid damage to the internal mechanisms and contact surfaces.

4. The high velocity peaks associated with the sharp edges at the junction of conventional flaps. The hinge line of the flap causes premature transition to a turbulent flow and act as the trigger point for cavitation inception.

5. The high drag associated with conventional flapped systems. Most of the conventional flap systems for aerospace applications are designed to produce high levels of drag (when deployed) as this helps to reduce the landing speed of the aircraft. Within the realms of the current work an increase in drag is undesirable.

These points indicate that even if the mechanical complexity of a flap system can be addressed, the discontinuity between the flap and the main hydrofoil will result in a significant increase in drag and could possibly lead to an earlier inception of cavitation.

To overcome these drag problems a mechanically driven flexible surface could be used. However, the engineering complexity of the existing flexible surface approaches is an order of magnitude greater than a conventional flap system, which would seem to make it an even more inappropriate and impractical solution to the problem.

Another approach to variable camber is the passive 'snap-through' designs such as the marine sail, which has an excess of material and assumes a curved shape under load. When an angle of incidence is selected and a load generated, the sail snaps through to a pre-determined fixed non-symmetric aerodynamic shape, providing some lift due to the camber and some due to the incidence angle. Additional increments of lift are provided by changes in the angle of incidence. The sail does however suffer from stability problems at low incidence angles when the excess material is prone to flutter and vibration.

The use of snap through camber devices again restricts the potential hydrodynamic performance as it is acknowledged that there is, '*no best camber for all sailing conditions. The skill of the helmsman is shown by the way in which he modifies the sail flow to suit particular demands*' [99].

This therefore leads to the conclusion that a suitable camber system for the windsurf fin needs to be;

1. Finitely variable, with a smooth surface contour.
2. Adjustable by the sailor whilst sailing.

4.2   The Hydroelastically Tailored Windsurf Fin (HTWF)

To meet the requirements of a finitely variable and adjustable camber system for the windsurf fin, a novel concept (patent application FAGG, S. B. - GB 9600137.5) [49] is proposed.

The camber in the section of the Hydroelastically Tailored Windsurf Fin (HTWF) is adaptive and responds passively by design and material usage, commonly known as hydroelastic tailoring, in response to the dynamic surface loads. The design of the section is such that increases in camber are associated with increases in lift.

In operation the HTWF section derives a proportion of the lift from the induced camber shape, thereby delivering higher lift than a symmetrical foil at the same incidence angle. It is also an aspect of the proposed design that the change in geometry is accomplished passively, that is without employing an actuating mechanism, and that this change in geometry occurs equally well for positive and negative load. This means that no fundamental modifications to the hull of the windsurf board are required and that the HTWF can be retrospectively fitted.

104

The use of increasing camber to increase the lift generated at a nominal incidence angle has the effect of increasing the lift curve slope. This means that nominal increases in lift will result from smaller changes in incidence angle than would be required for a symmetrical or fixed camber system. In general this will allow the windsurf board to be sailed at lower leeway angles than with a comparable rigid and symmetrical foil.

In conjunction with the envisaged gains in lift it is also an aspect of the design to reduce the section drag by rotating or 'drooping' the nose into the flow as this is more efficient for splitting the freestream.

A cross-sectional view of the proposed HTWF configuration is shown in Figure 4.1. The configuration is of general aerofoil shape and features;

1. A rigid internal framework, to be referred to as the skeleton.
2. An elastomer flexible covering.

The internal skeleton comprises two regions;

1. The rear support.
2. The mast.

The rear support is nominally rigid and immovable and provides structural integrity to the cross section. The mast also provides structural integrity, as well as forming a pivotal axis about which the flexible elastomer covering and hence the nose region rotates.

The flexible elastomer covering provides the streamlined outer profile shape as well as filling the void (slot gap) between these two supporting members. Due to elastomer's material characteristics it is able to flex and deform in this region under the influence of the surface pressure loads, resulting in a section with 'floating' geometric and hydrodynamic characteristics.

The elastic properties of the elastomer ensures that it assumes a symmetrical profile when at rest or under the influence of a symmetrical loading (when the incidence angle is zero). The magnitude of deformation in the elastomer is proportional to the surface pressure loading (to the linear limit of the elastomer material).

4.2.1   Method of Operation

The method of operation for the hydroelastically tailored fin is analogous to a conventional marine sail in that the pressure differential between the two surfaces is used to induce geometry changes in the cross section. It does however differ from the sail in that the camber shape is finitely variable and is not predetermined and fixed (i.e. not a 'snap through' design). Figure 4.2(a) shows the surface pressure loads on a symmetrical airfoil (at an incidence angle to the freestream). These surface pressure loads will induce structural deformations in the directions indicated by the arrows in Figure 4.2(b). The cross-section will then take on the asymmetric shape shown in Figure 4.2(c). It is then assumed that the asymmetric shape will be stabilised by the rearward movement of the negative pressure peak (due to the camber shape). This demonstrates how the deformations in the flexible elastomer and the rotation about the pivotal mast will be used to;

1. Invoke camber in the cross section.
2. Rotate or 'droop' the nose into the flow.

The resulting section shape from these structural deformations will then satisfy the requirements for high lift and low drag.

Marchaj [99] discusses how the use of a suitable nose shape and camber over the front part of the section can be used to avoid increases in drag and flow seperation. Ideally the curvature at the leading edge should be adjustable to achieve an 'ideal' or smooth entry (tangential to the camber line at the nose) over a range of incidence angles. Smith [129][130]

reinforces this by discussing how high lift is best achieved by keeping the nose angle of attack low with a 'droop' nose design.

In addition to the reductions in drag and increments in lift, the drooping nose should delay the onset of cavitation by reducing the magnitude of the negative pressure peak at the leading edge. This feature will also help to delay leading edge seperation thereby increasing the attainable C_{Lmax}.

The magnitude and nature of the camber in the HTWF concept is a function of the cross section design and the surface pressure loads which in turn are a function of;

1. The velocity of the section through the water.
2. The incidence angle of the section to the freestream.
3. The geometric features and material usage in the section.

The design of the section is such that the sailor will use conventional sailing techniques to regulate the magnitude of the camber in the section. By sheeting the sail in and out the speed of the complete assembly and hence the fin through the water can be varied. In addition to this, conventional footsteering techniques will be used to vary the incidence angle of the fin to the freestream.

4.2.2 The HTWF Design Variables

Variations in C_l and C_d are primarily dependent on the foil section geometry, its surface contour and thickness at the leading edge. Changes or modifications to any of these parameters will result in an associated and unique velocity and pressure distribution for that specific profile shape. Determining an optimum or suitable velocity and pressure distribution is therefore dependent upon the design variables for the HTWF cross section.

It has been established that the sailor will use conventional footsteering techniques to vary the surface pressure loads on the section. The resulting camber shape will therefore be a function of;

    1. The geometric features of the cross section.

    2. The material usage in the cross section.

In theory an infinite number of configurations can be developed. However, for this preliminary investigation the design variables (Figure 4.3) will be limited to changes in;

    1. The initial outer profile geometry.

    2. The position of the pivotal mast (as a percentage of the chord length (p/c)).

    3. The size of the slot gap (as a percentage of the chord length (s/c)).

    4. The stiffness of the flexible elastomer covering.

The position of the rear support (r/c) is fixed at 80% of the chord length for all configurations. This results in a gradual tapering out of the rear support towards the slot gap (s/c) which will help to avoid discontinuities in the surface due to the gradual 'tapering-in' of the elastomer.

The radius of the pivotal mast is defined as 3 mm for all configurations, even though in reality the radius will be enlarged for the thicker sections. This is primarily to reduce the number of variables being considered.

4.2.3   Theoretical Performance Characteristics

With the format of the HTWF configuration established, consideration is given to the potential performance characteristics of the proposed design solution.

To explain the performance potential of the HTWF section it is assumed that suitable geometries and materials are used to enable the configuration to adopt 'known' outer

profile geometries at specified incidence angles. Based on this assumption, it is hypothesised that a HTWF configuration featuring a NACA 0012 section profile can be designed to assume nominally the same outer profile as the NACA 23012 (moderate camber) at an incidence angle of 5° and nominally the same outer profile as the NACA 4412 (large camber) at an incidence angle of 8° (as shown in Figure 4.4).

Figure 4.5 shows the lift curves of these three NACA sections and Figure 4.6 shows the corresponding drag polars. If the assumption is made that the HTWF configuration is able to smoothly vary the camber shape from one section to the other due to a changing incidence angle, the lift curve and drag polar of the hypothetical HTWF section would follow the loci shown.

This would result in a steepening of the lift curve slope and a reduction in the profile drag at increasing incidence angles (when compared with a rigid NACA 0012 section). By using this approach the lift to drag ratio of the fin will be optimised for the pre-stall range of incidence angles.

4.3   Evaluating the HTWF concept

'All the mathematical sciences are founded on relations between physical laws and laws of numbers, so that the aim of exact science is to reduce the problems of nature to the determination of quantities by operations with numbers', James Clerk Maxwell, 1856.

The previous section outlined hypothetical performance characteristics for the HTWF cross section. To assess the performance of the device, particularly the hydroelastic coupling effect, a suitable analysis method is required. Due to the number of design variables, the infancy of the concept and budgetary constraints, a computational based analytical method was devised for this preliminary investigation by the author and Xavier Velay [50][51][52][53].

To reduce the complexity of the analysis process the problem domain was modelled in 2D, in which it is assumed that the section has infinite span such that there is no spanwise (3D)

flow component. By adopting this approach the complexity of the computational model is reduced considerably. It should however be realised that a 3D spanwise flow component may in reality influence the sectional performance characteristics.

4.3.1   Coupled Fluid and Structural Analysis Tool (CFSAT)

The Coupled Fluid Structural Analysis Tool (CFSAT) is a 2D computer based analytical method developed specifically for this research project (sample listing provided in Appendix D). The CFSAT consists of a computer code which automatically integrates and runs two separate software packages (Flotran CFD and ANSYS FEA by Swanson Analysis Systems) into a single iterative process. The structure of the CFSAT is shown in Figure 4.7, illustrating the four main stages of the analysis, namely;

1. Definition of initial geometry from the stored parametric data
2. Flow analysis
3. Structural analysis
4. Convergence checks

Both the ANSYS and Flotran programs are Finite Element packages. The structural analysis of the ANSYS program is based on the Stress-Strain relationships. The stress is related to the strain by:

$$\{\sigma\} = [D]\,\{\varepsilon\} \tag{4.1}$$

where: $\{\sigma\}$ = stress vector = $[\,\sigma_x\ \sigma_y\ \sigma_z\ \sigma_{xy}\ \sigma_{yz}\ \sigma_{xz}\,]$

[D] = elasticity matrix

$\{\varepsilon\}$ = strain vector = $[\,\varepsilon_x\ \varepsilon_y\ \varepsilon_z\ \varepsilon_{xy}\ \varepsilon_{yz}\ \varepsilon_{xz}\,]$

The strains may be related to the nodal displacements by:

$$\{\varepsilon\} = [B]\,\{u\} \tag{4.2}$$

where: [B] = strain-displacement matrix, based on the element shape functions

$\{u\}$ = nodal displacement vector

To evaluate the structural strain and stress we compute the element integration point by combining equations (4.1) and (4.2).

The fluid analysis of the Flotran program is defined by the laws of conversation of mass, momentum, and energy. These laws are expressed in terms of partial differential equations which are discretized with a finite element based technique. Assumptions about the fluid and the analysis are as follows:

1. The fluid is Newtonian.

2. There is only one phase.

3. The problem domain does not change.

4. The user must determine: (a) if the problem is laminar or turbulent; (b) if the flow is incompressible or compressible.

From the law of conservation of mass comes the continuity equation:

$$\frac{\partial \rho}{\partial t} + \frac{\partial (\rho V_x)}{\partial x} + \frac{\partial (\rho V_y)}{\partial y} + \frac{\partial (\rho V_z)}{\partial z} = 0 \qquad (4.3)$$

where: Vx, Vy and Vz = components of the velocity vector in the x, y and z

directions, respectively

ρ = density

x, y,z = global Cartesian coordinate

t = time

The Navier-Stokes equations are written in terms of a Newtonian fluid, where the shear stress is a linear function of the velocity gradients.

$$\frac{\partial (\rho u_i)}{\partial t} + \frac{\partial (\rho u_j u_i)}{\partial x_j} = -\frac{\partial P}{\partial x_i} + \rho g_i + \frac{\partial}{\partial x_j}\left[\mu \frac{\partial u_i}{\partial x_j}\right] + \frac{\partial}{\partial x_j}\left[\mu \frac{\partial u_j}{\partial x_i}\right] \qquad (4.4)$$

where: u_i, u_j = components of the velocity vector in the i and j directions,

respectively

ρ = density

x_i, x_j = global Cartesian coordinate

P = pressure

μ = viscosity

g_i = components of the acceleration due to gravity

If internal effects are great enough with respect to viscous effects, the flow may be turbulent. This means that the instantaneous velocity is fluctuating at every point in the flow field. The velocity is thus expressed in terms of a mean value and a fluctuating component:

$$V_x = \overline{V_x} + V_x{}'$$

where: $\overline{V_x}$ = mean component of velocity in x-direction

$V_x{}'$ = fluctuating component of velocity in x-direction

If an expression such as this is used for the instantaneous velocity in the Navier-Stokes equations, the equations may then be time averaged.

For numerical accuracy reasons, the algorithm solves for a relative pressure rather than an absolute pressure. Considering the possibility that the equations are solved in a rotating coordinate system, the defining expression for the relative pressure is:

$$P_{abs} = P_{ref} + P_{rel} - \rho \, \{g\} \cdot \{r\} + 1/2 \, \rho \, (\{\omega\} \times \{\omega\} \times \{r\}) \cdot \{r\}$$

where: P_{abs} = absolute pressure

P_{ref} = reference pressure

P_{rel} = relative pressure

$\{g\}$ = acceleration vector due to gravity

$\{r\}$ = position vector of the fluid particle with respect to the rotating coordinate system

$\{\omega\}$ = constant angular velocity vector of the coordinate system

For the derivation of the fluid flow matrices a segregated and sequential solution algorithm is used. This means that element matrices are formed, assembled and the resulting system solved for each degree of freedom separately. development of the matrices proceeds in two parts. In the first, the form of the equations is achieved and an approach taken towards evaluating all the terms. Next, the segregated solution algorithm is outlined and the element matrices are developed from the equations.

4.3.1.1 Computational Fluid Dynamics (CFD)

The field of theoretical fluid dynamics has been developing since the seventeenth century. In support of this pure theory, the discipline of experimental fluid dynamics developed in the twentieth century. Based on the data from these pure and experimental fields as well as the advent of the modern high speed computer, the third approach of Computational Fluid Dynamics (CFD) has developed.

The use of CFD in its current format is not a replacement for pure theory or applied experiment, as there will always be a need for these other approaches. CFD does in fact complement these other techniques in a synergistic manner [4].

CFD is therefore a computer based analytical tool with which it is possible to carry out numerical experiments.

However, because the computations are mathematical assumptions and approximations based on empirical test data, the limitations of a computer based analysis need to be known and the results interpreted carefully. The same considerations apply to wind tunnel tests due to the effects of wall interferences, model accuracies and Reynolds Number, particularly for simulated two dimensional flows [69]. The differences between a wing in free flight and a low aspect ratio model in a flow tank are significant. These effects can show the potential to increase at higher incidence angles. The differences between individual flow tunnels also has an influence on the test data, as can the presence of a wake rake measuring device [44]. Baubeau and Latorre [8] describe how it can be difficult to establish a baseline condition from experiments due to the following difficulties associated with tank testing;

- Manufacturing an accurate profile
- Obtaining a smooth surface finish
- Generating two dimensional flow conditions
- Level of turbulence in incoming flow

- Interpretation of the boundary layer conditions from oil film patterns or holographic plates.

These findings are supported by Marchaj [99] who states, *'One should realise that any performance prediction based on towing tank and wind tunnel results is subject to inevitable error and uncertainty'*.

Van Dam et al [141] confirms the problem of erroneous data resulting from inaccuracies in the model. He found different lift and drag values for a supposedly symmetrical wing test model in the upside down and right side up positions.

Eppler therefore concludes [44];

- An airfoil should never be applied without a computer analysis.
- It is more reliable to compare two different airfoils by data obtained from the same computer program than by tests from different wind tunnels.

The basis of these conclusions are that with a computer based analysis;
- The effect of minor modifications to the airfoil can be studied easily and with good reliability.
- The angle of incidence and fluid properties (Reynolds Number, Turbulence model) can be changed rapidly.
- The tailoring of the airfoil can be accelerated considerably.
- The analysis is extremely cheap (comparatively) and always provides additional information.

Anderson [4] supports these conclusions by stating that CFD constitutes a new 'third approach' to analysing fluid dynamic problems which is equal to pure theory and pure experiment. This does not make it a replacement for either pure theory or pure experiment, rather a synergistically complementary process. CFD results are directly analogous to wind tunnel results obtained in a laboratory, representing sets of data for given flow

conditions, configurations and Reynolds numbers. The computer based analysis is therefore a tool with which you can perform numerical experiments.

Housh et al [73] describe the nature of their computer based analysis of the scissor wing geometry and conclude that, *'the qualitative values may be suspect in some cases however, the trends are not and when this code is used to compare two different geometries, firm conclusions may be drawn'.*

4.3.1.2 Finite Element Analysis (FEA)

According to Fagan [48] the finite element method is not a new technique but was first introduced in the 1950s, and has been continually developed and improved since then. It is now an extremely sophisticated tool for solving numerous engineering problems and is widely used an accepted in many branches of the industry for the analysis of structures and solids [7]. Many aircraft components and hence total machines are certified and given airworthiness certificates through the results of finite element models [48].

4.3.1.3 Definition of the Initial Geometry

The program is structured such that the following variables are stored parametrically by the operator;

- Cross section geometry (geometric features, material properties)
- Fluid properties (Velocity, density, angle of attack, turbulence model, pressure)
- Domain properties (model volume, line divisions, mesh refinement)

By using a parametric based programming language the cross section, fluid and domain properties can be changed rapidly. The external geometry of the cross section is defined by 60 keypoints (29 uppersurface, 29 lowersurface, 1 leading edge and 1 trailing edge) which are splined together. The internal features of the cross section are specified by 20 keypoints. The material properties of the cross section (Young's modulus and Poisson

ratio) are also stored as parameters. The outer limits of the flow domain are calculated as a function of the chord length. This ensures that the recommended distance between the cross section and the limits of the flow domain are set in accordance with a freestream type simulation as shown in Figure 4.8 [113]. A mapped mesh is generated in the flow domain as is shown in Figure 4.9. The concentration of the meshing is refined in the area adjacent to the cross section in accordance with CFD recommendations. By using a mapped mesh the analysis time and memory requirements are reduced considerably when compared with a free mesh type analysis [4].

4.3.1.4 Flow Analysis

Prior to the flow analysis boundary conditions are applied to the mesh. The boundary conditions are;

- Velocities at the outer limits of the flow domain (10 ms^{-1} at a user defined incidence angle)
- Boundary edges of outer profile (flow velocity 0 ms^{-1})
- Pressure values at the flow outlet (pressure = 0)

The flow analysis is performed when the boundary conditions and program controls have been set. On completion of the analysis the calculated surface pressure integrals on the cross section are used to derive the section lift and drag coefficients (C_l and C_d). The pressure integrals are then stored and used as the load set for the subsequent structural analysis. Figure 4.10 and Figure 4.11 show typical post processing plots from the CFD method.

4.3.1.5 Structural Analysis

Following the flow analysis a finite element model of the cross section (Figure 4.9) is used to predict the anticipated structural deformations in the cross section due to the flow pressures. To do this the pressure forces from the flow analysis are loaded and applied to

114

the corresponding elements on the FEA model. The other boundary conditions (zero displacement on the skeleton) are also applied. The material properties of the cross section are specified and the structural analysis invoked.

The FEA analysis calculates the anticipated nodal displacement in the model as a result of the surface pressure loads. This data is used to determine the predicted change in the section geometry. The modified geometry is stored and used in the subsequent flow analysis to establish the changes in the flow resulting from the new geometry.

4.3.1.6 Convergence Checks

The convergence checks are used to determine if and when the shape of the cross section has stabilised. The options available for determining the level of convergence are;

- Measuring the change in coefficient of lift and drag (δC_l and/or δC_d) as compared with the previous flow analysis.
- Measuring the change in structural deformation as compared with the previous structural analysis.

Alternatively a pre-set number of looping commands can be used to terminate the analysis.

4.3.2   Accuracy and Validity

The validity of the model depends on how faithfully the physical problem is represented in the computer, whilst the accuracy depends on how close the resulting values are to a theoretically or experimentally derived value.

REAR SUPPORT

FLEXIBLE ELASTOMER COVERING

SLOT GAP

MAST
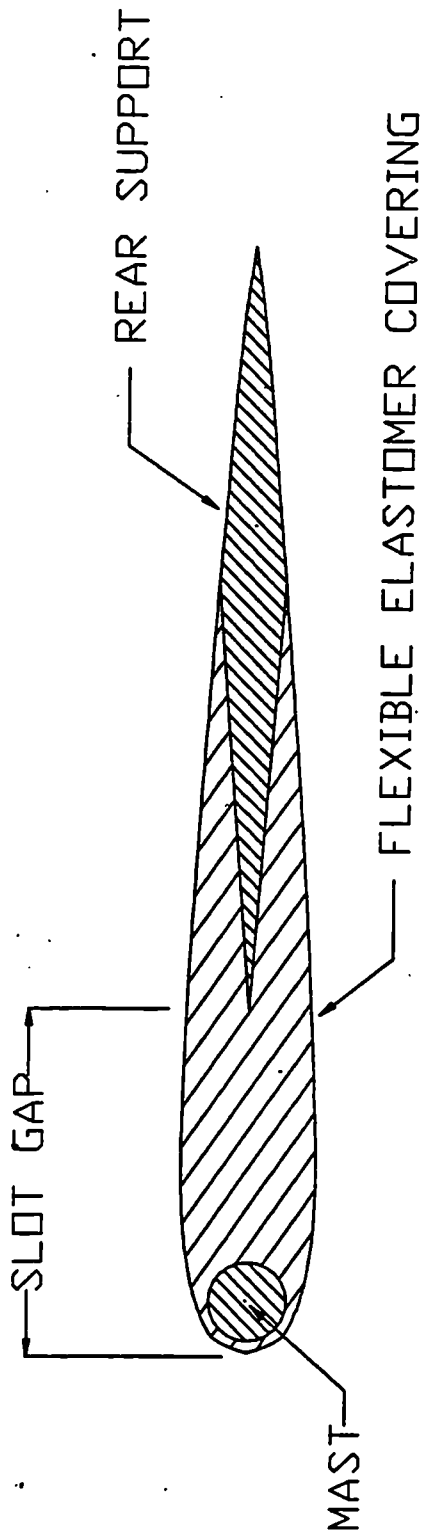
Figure 4.1 The Hydroelastically Tailored Windsurf Fin Cross Section
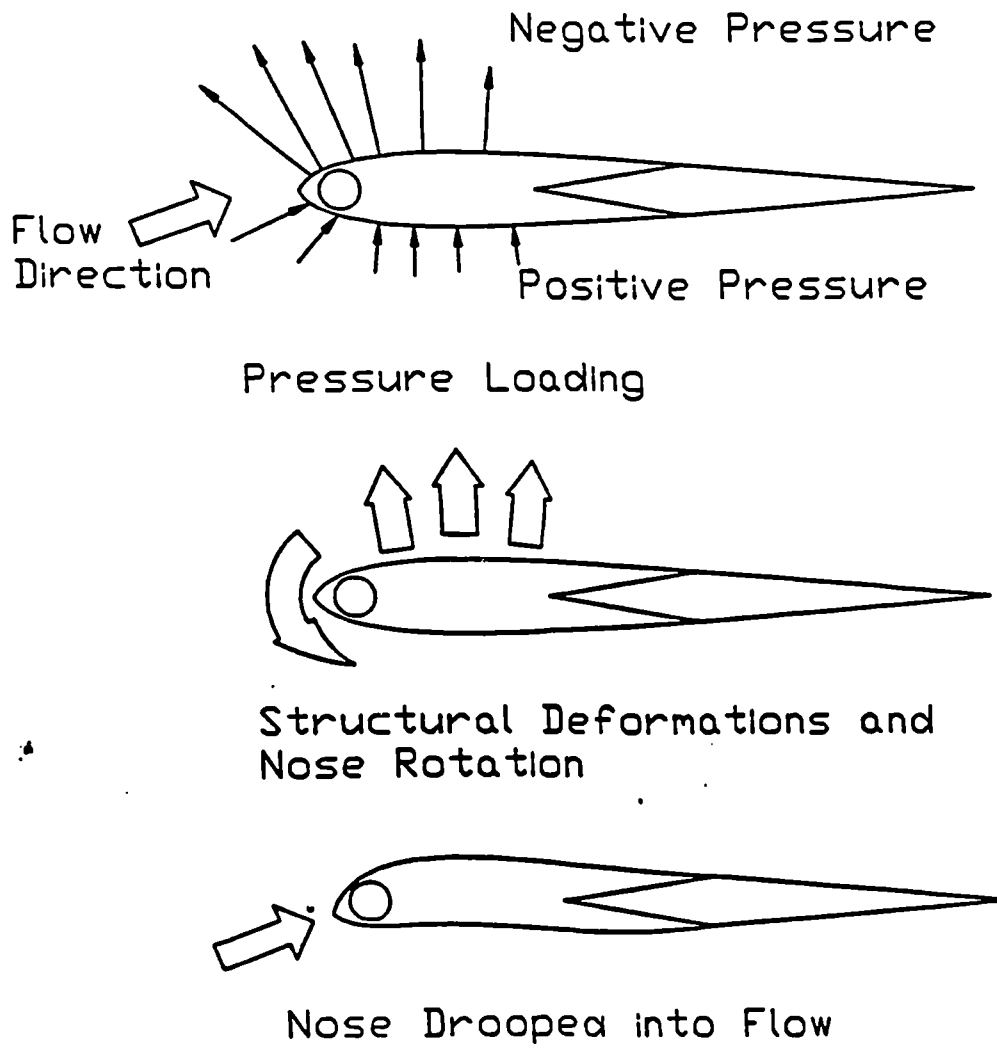
Figure 4.2   Method of Operation for HTWF

117
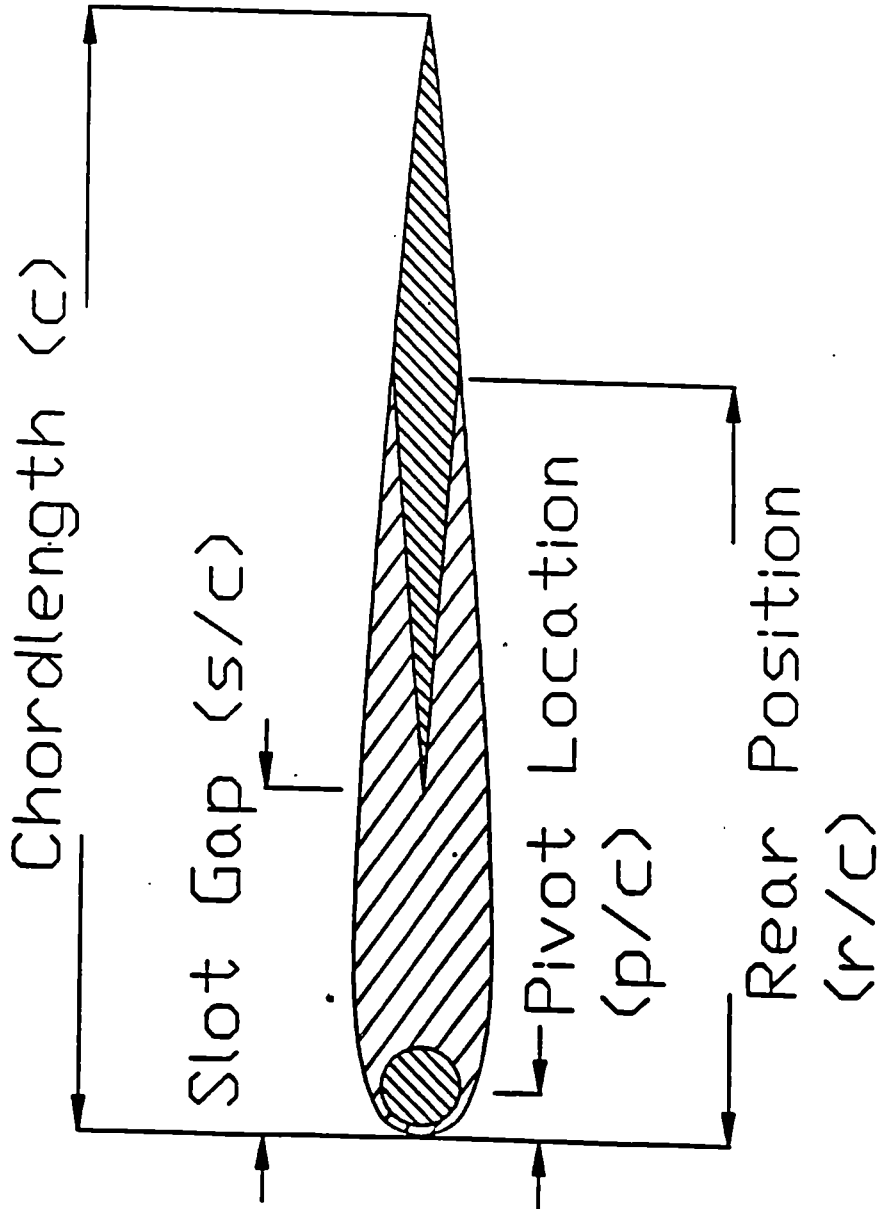
Figure 4.3   HTWF Design Variables

118

INCREASING CAMBER

No Incidence Angle

NACA 0012

Moderate Incidence Angle
(5 degrees)

NACA 23012

High Incidence Angle
(> 8 degrees)

NACA 4412
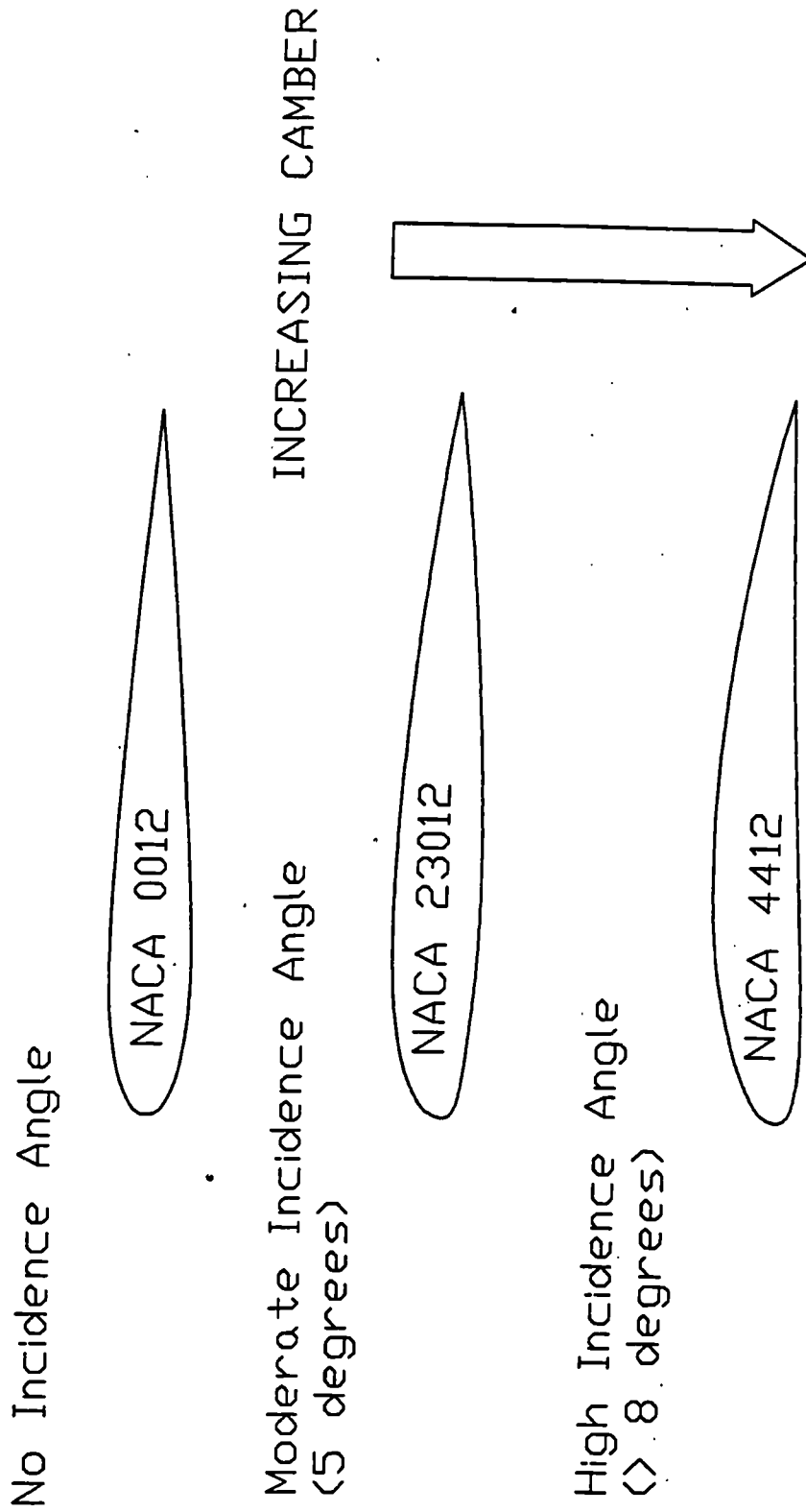
Figure 4.4   Theoretical Shapes for HTWF

THEORETICAL
HTWF
CONFIGURATION
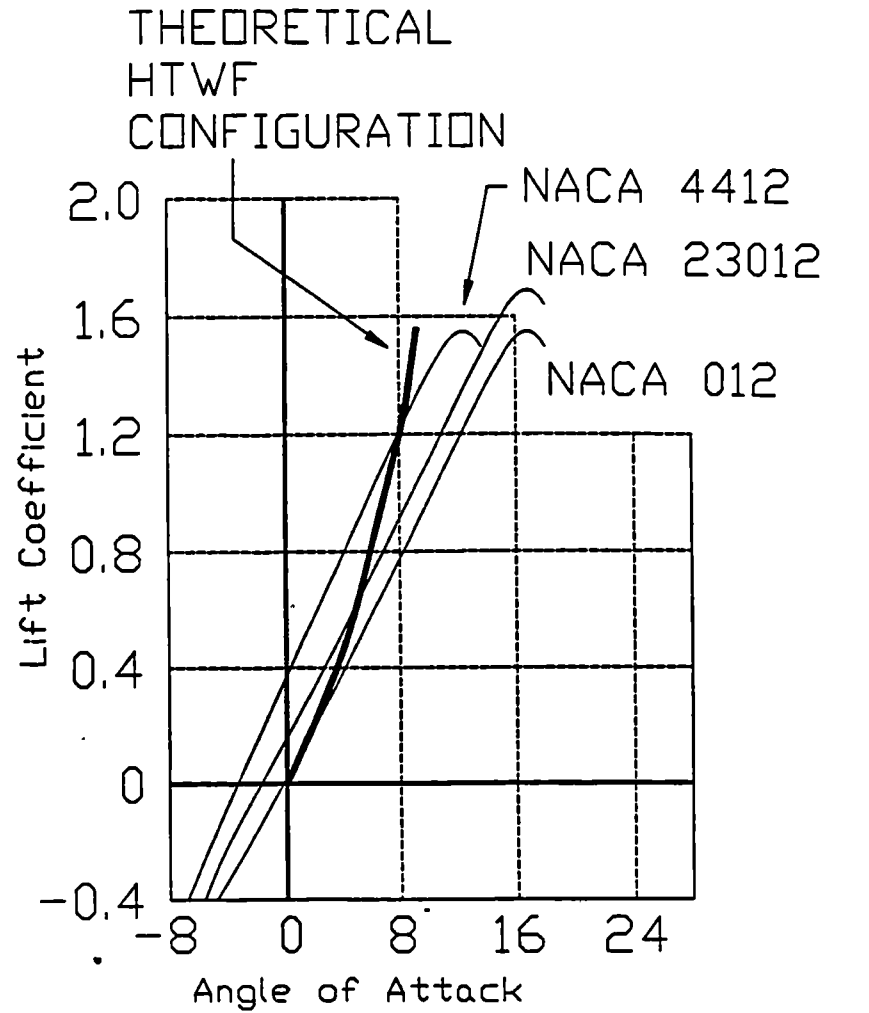
Figure 4.5   Lift Curve Slopes for NACA Sections (adapted from 'Theory of Wings Sections', Abbott and Doenhoff.)

THEORETICAL
HTWF
CONFIGURATION   NACA 012
                          NACA 23012
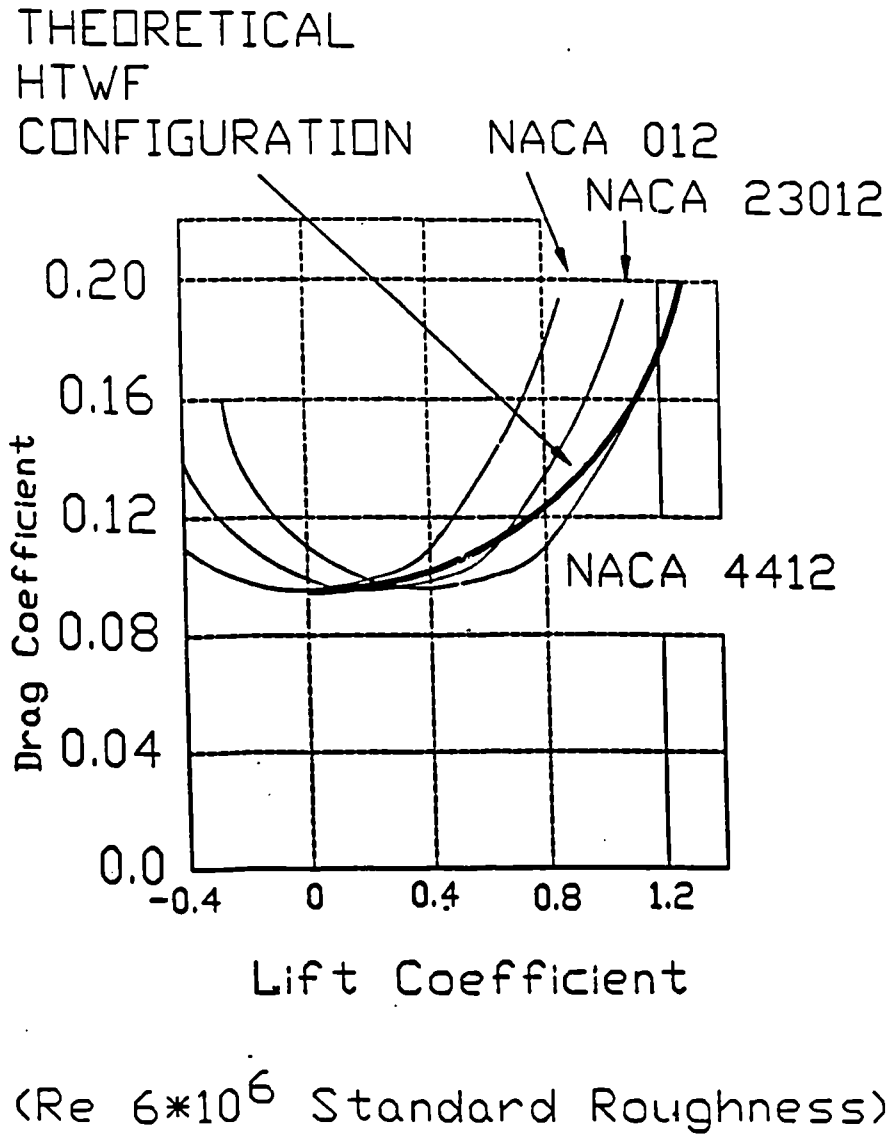
Figure 4.6   Drag Polars for NACA Sections (adapted from 'Theory of Wings Sections', Abbott and Doenhoff.)
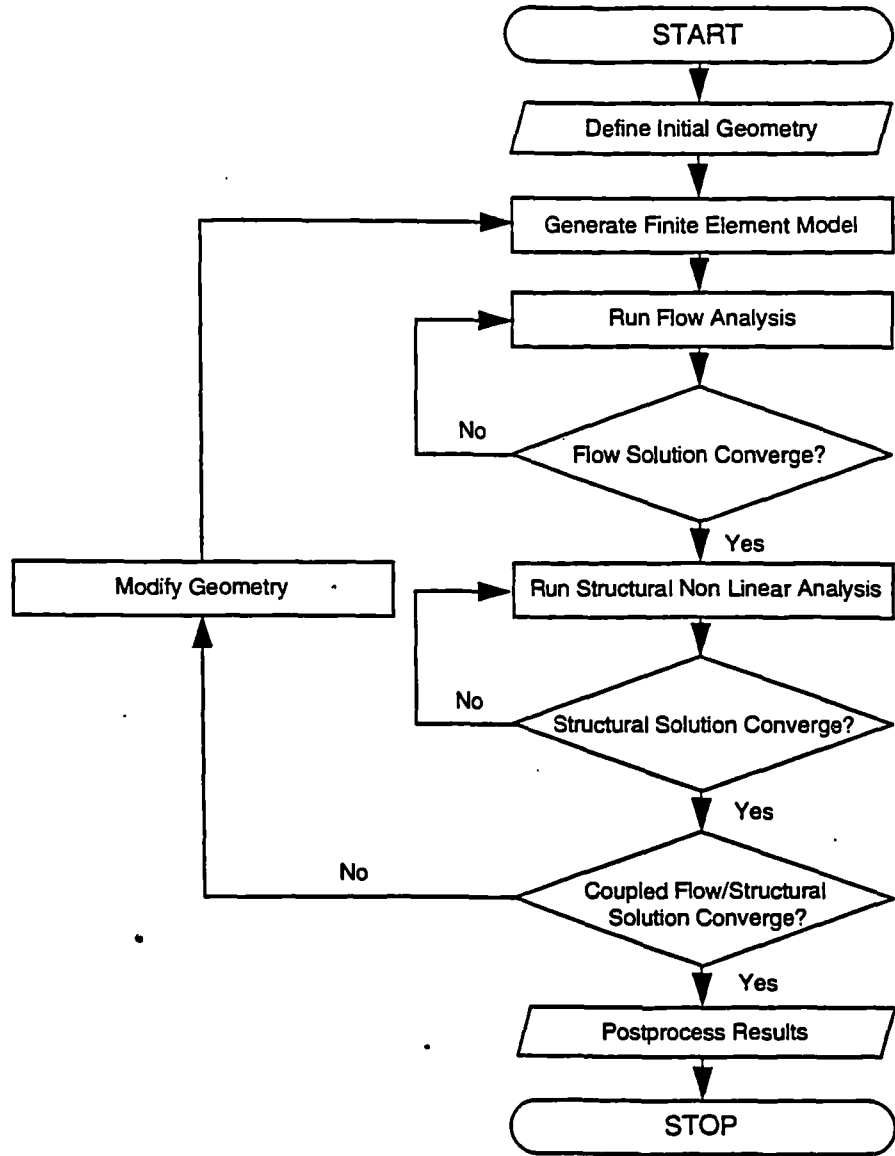
Figure 4.7   General Flowchart for Coupled Fluid Flow and Structural Analysis
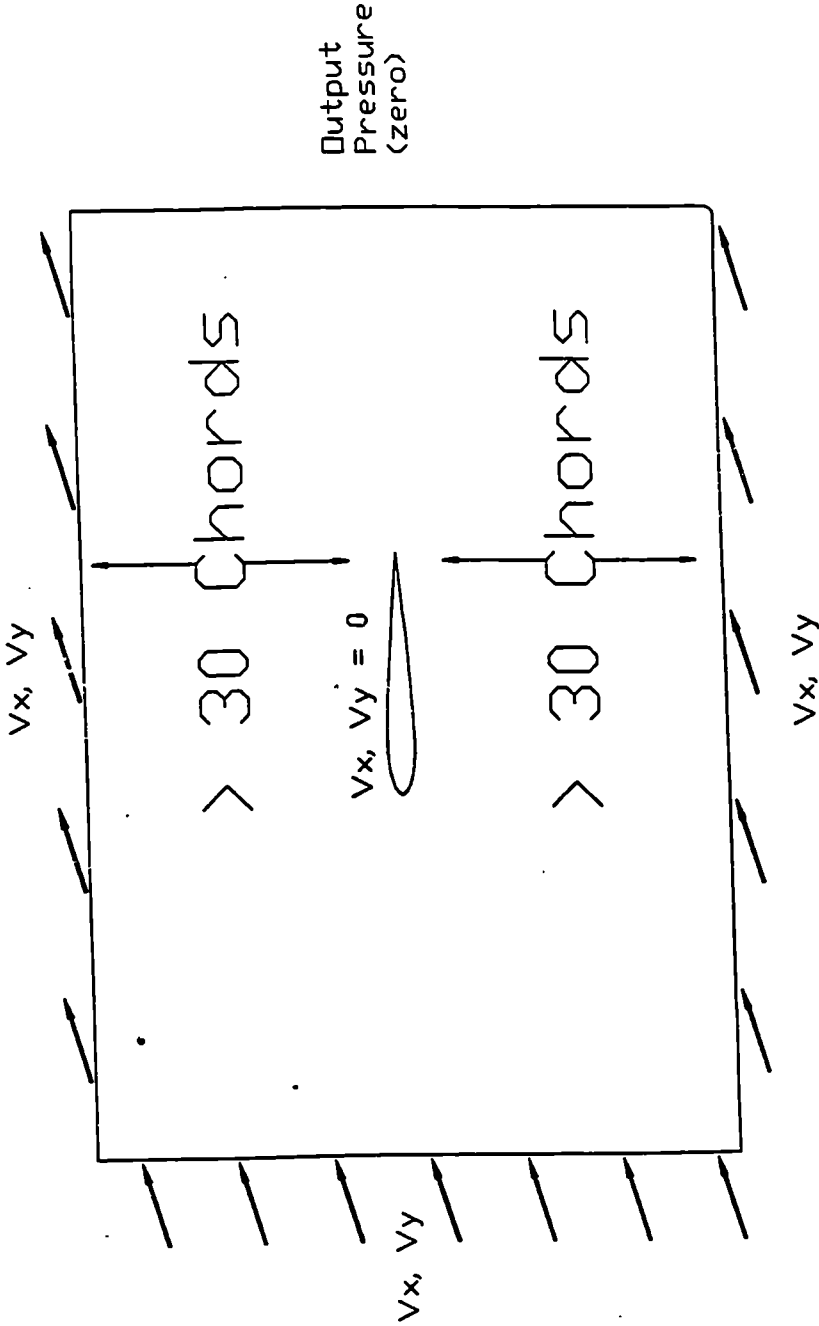
Figure 4.8   CFD Boundary Conditions
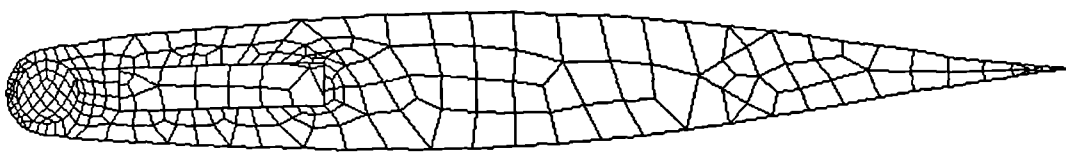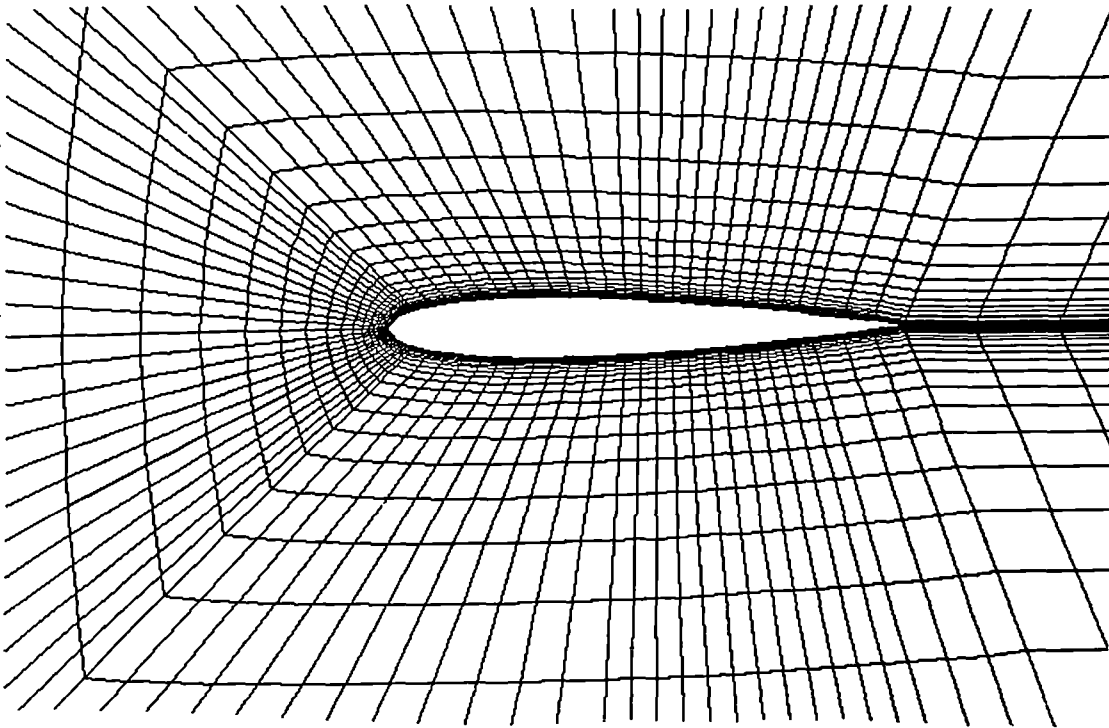
Figure 4.9 Mapped Mesh and Undeformed Cross Section Mesh
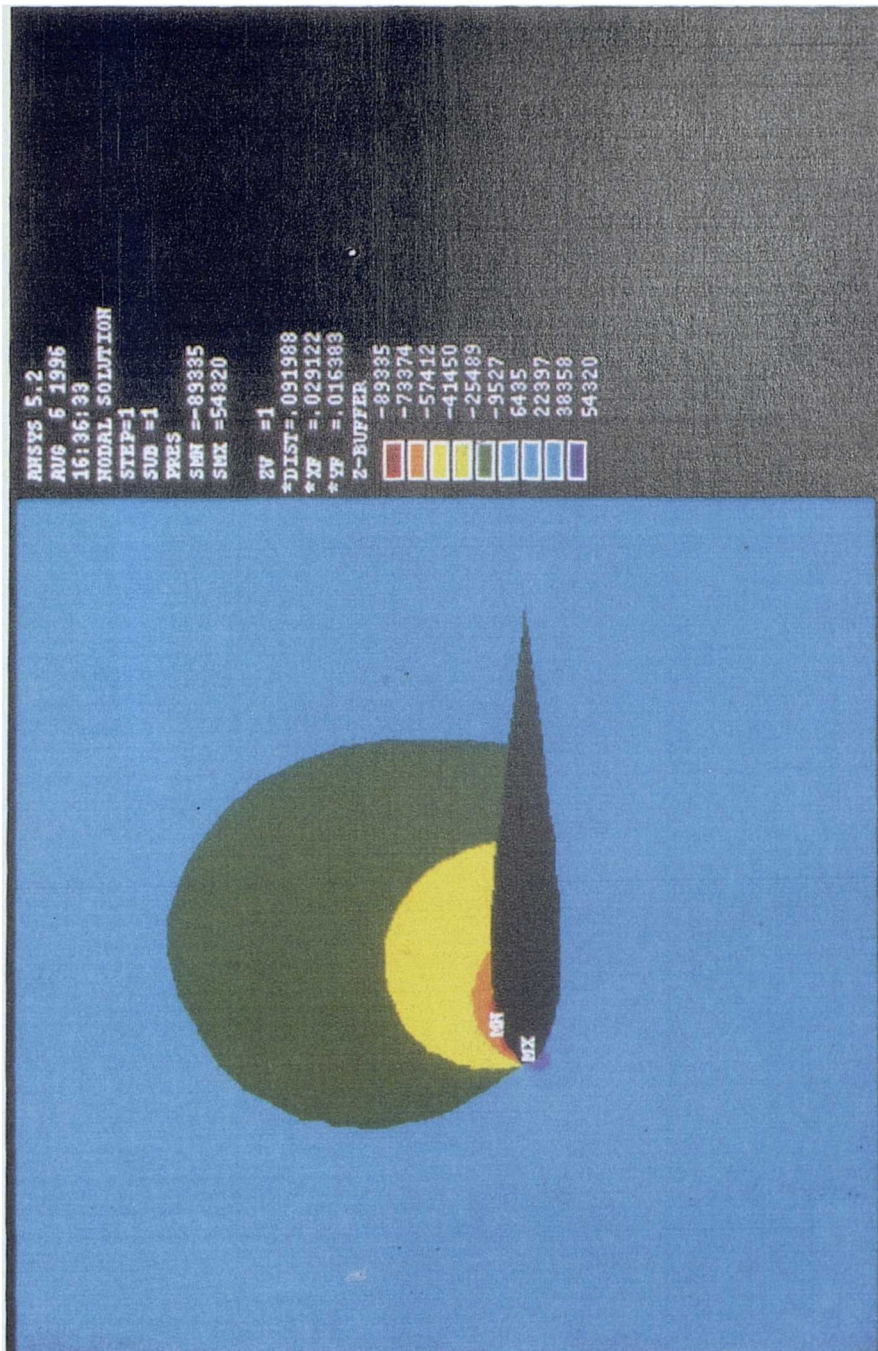
Figure 4.10 CFD Pressure Distribution

125
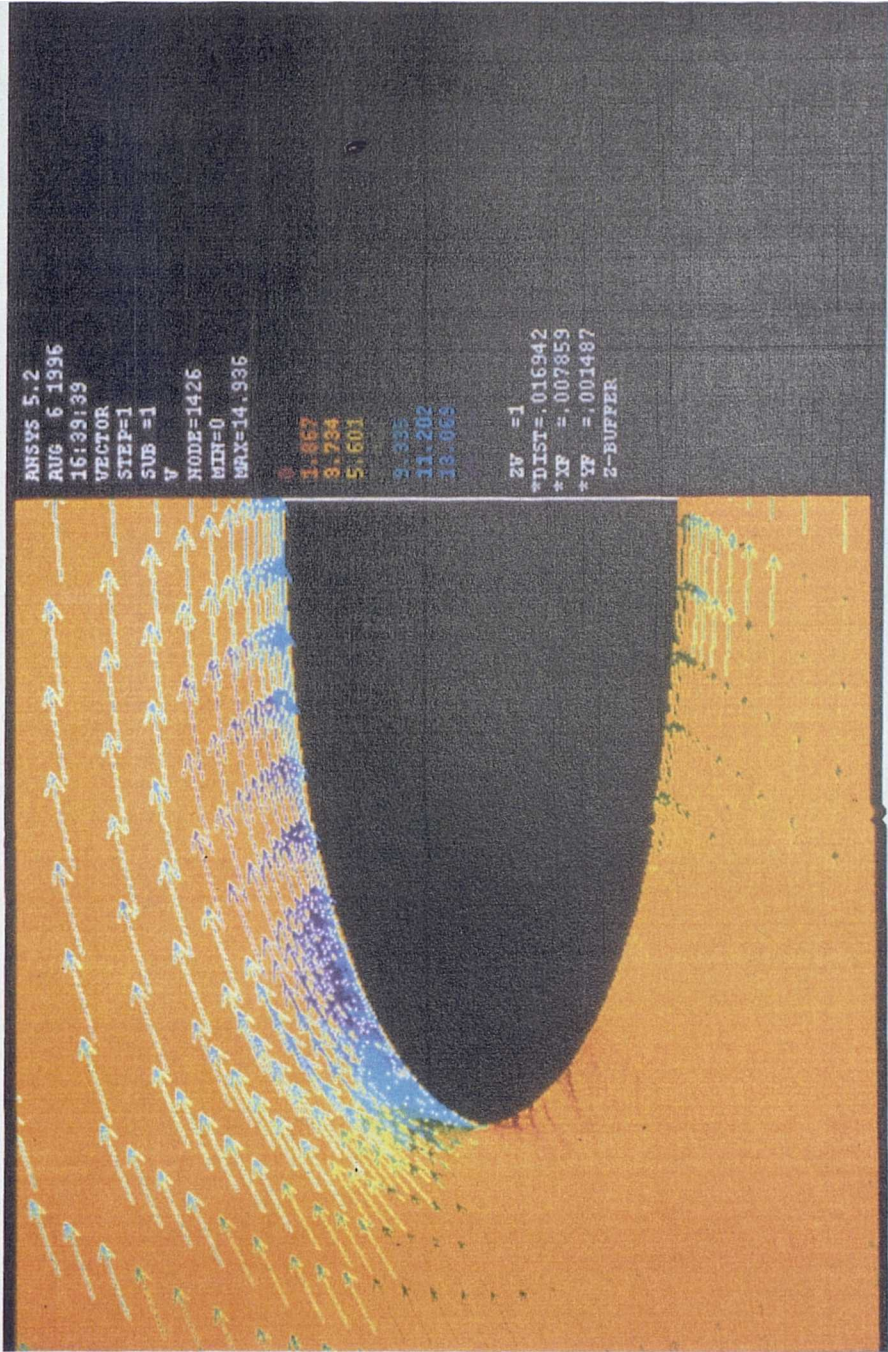
Figure 4.11   Computed Flow at Leading Edge

126

5.0   Experimental Procedure

5.1   Assessment of the Computed CFD and FEA Data

5.1.1   The CFD Method

The CFD component of the CFSAT was run independently to compare the predicted result data (lift and drag) with NACA experimental data [1].

The first analysis was with the NACA 0012 section. This was selected as it is representative of a typical windsurf fin cross-section. The Flotran tests were performed with the turbulence model switched on (because $R_e > 5 \times 10^5$) at a flow velocity of 10 ms^{-1} ($R_e = 8 \times 10^5$). The incidence angle was varied between 0° and 8°.

Figure 5.1 shows the lift curve slopes for the NACA 0012 wind tunnel test data, the Flotran computed 0012 data and the theoretical lift curve slope of the NACA 0012 based on the approximation;

$$C_l = 0.11\left(1+\frac{t}{c}\right)\alpha \tag{5.1}$$

Figure 5.2 shows the percentage difference between the NACA experimental data (R_e 6 × 10^6) and the Flotran computed lift data. The Flotran method demonstrates a reasonably consistent overestimation (7% to 9%) of the lift coefficient.

Figure 5.3 shows the drag polars for the NACA 0012 wind tunnel drag data and the Flotran computed drag data. The Flotran method consistently overestimates the drag coefficient.

Figure 5.4 shows the percentage difference between the NACA drag data (standard roughness) and the Flotran computed drag data. A reasonably consistent overestimation (nominally 15%) of the drag coefficient by the Flotran method is demonstrated. The

reason for this discrepancy can be directly attributed to the CFD method and the manner in which the boundary condition is modelled [113] (fully turbulent).

The total drag C_d associated with a streamlined body is described by Newman [10(2)] as being composed of the two components, skin friction and pressure drag.)

$$C_D(R_e) = C_f(R_e) + C_p \qquad (5.2)$$

The magnitudes of total drag C_d and frictional drag C_f are highly dependent on the Reynolds numbers (R_e). This is illustrated by Figure 5.5 which shows the variation in drag (C_D) for NACA foil sections over a similar range of Reynolds numbers. This figure illustrates that flow transition occurs between $R_e = 10^5$ and $R_e = 2 \times 10^6$ and that as a result of this it is problematic to accurately establish the magnitude of drag in this range. It is therefore unfortunate that this region of flow transition corresponds with the Reynolds numbers of interest in the current investigation.

In reality the NACA 0012 section could be expected to have regions of laminar and turbulent flows at a Reynolds number of 8×10^5. The Flotran CFD method however is only able to model the boundary layer as either fully turbulent or fully laminar. Based on the Reynolds number of the test ($> 5 \times 10^5$) the turbulence model must be switched on to converge the solution. Therefore the drag data predicted by the Flotran method will be (consistently) greater than expected.

For a second test the NACA 23012 profile was used (with the same flow conditions as specified for the NACA 0012). Figure 5.6 shows the NACA experimental and Flotran computed lift data. Figure 5.7 shows the percentage difference between the NACA experimental and Flotran computed data. The Flotran method demonstrates a reasonably consistent overestimation (1% to 3%) of the lift coefficient, leading to an underestimation (-2%) at an incidence angle of 8°.

Figure 5.8 shows the drag polars for the NACA 23012 wind tunnel drag data and the Flotran computed drag data. It is clear again that the Flotran method consistently overestimates the drag coefficient.

Figure 5.9 shows the percentage difference between the NACA drag data (standard roughness) and the Flotran computed drag data. A reasonably consistent overestimation (nominally 14%) of the drag coefficient by the Flotran method is demonstrated. The reason for this discrepancy can again be attributed to the manner in which the boundary condition is modelled as fully turbulent.

These tests have established that there is a consistent error associated with the CFD computed lift and drag data. Although this makes the data unreliable for direct comparisons with other sources of data, the consistency of the error does still enable the data to be used in a standalone sense. It is then possible to qualitatively assess the effects of changes in the configuration of the cross section, as '*It is more reliable to compare two different aerofoils by data obtained from the same computer program than by tests from different wind tunnels*' [44].

The modelling of a fully turbulent may also have implications in terms of the prediction of the deformed geometry in the FEA method. Following the CFD analysis the calculated pressure loads are used as the load set for the subsequent structural analysis. The drag data is applied as a tangential load and the lift data is applied as a normal load, to the surface of the cross section. It is the normal (lift) forces that have the greatest influence on the structural deformations, with the tangential forces having a minimal effect (because they act tangentially to the surface and that they are at least ten times less in magnitude than the lift forces).

Because the calculated normal forces (lift data) and hence load set for the structural analysis is overestimated by up to 10% the predicted elastomer deformations (in the FEA method) are also likely to be overestimated (by up to 10%).

The overestimation of the tangential forces are not considered to significantly affect the accuracy of the predicted elastomer deformations.

5.1.1.1 Iteration Values

To establish the optimum number of CFD program iterations (in terms of computing time versus satisfactory correlation of data) an investigation was performed to see the effect of the global iteration number on the lift and drag data for the Eppler E472 profile (with the same flow conditions as specified for the NACA 0012).

Figure 5.10 shows the C_l/C_d as a function of the iteration number. This indicates that approximately 400 program iterations (40 minutes computing time) are required to provide a consistent correlation of the data.

5.1.2   The FEA Method

To assess the accuracy of the FEA method a number of analyses were performed to compare the ANSYS predicted data with experimental and theoretical data. For these analyses a steady state or equilibrium is assumed opposed to a transient loading. Obviously this does not fully represent the anticipated unsteady loadings that the HTWF will experience in true sailing conditions, however this is believed to be sufficient for the current investigation.

To compare the FEA method data with experimental data a sample of cold cure elastomer was subjected to a tensile test, the plot of which is shown in Figure 5.11.

Based on the measured stress and strain values at a loading of 40N the Modulus of the elastomer was calculated to be 5.226×10^6 Nm^{-2} (quoted value is 5×10^6 Nm^{-2} at 0% elongation [114]).

The FEA model (to the same dimensions as tensile test piece) is shown in Figure 5.12. The bottom face of the test piece is constrained and the tensile loads (in the positive y direction) are applied evenly over the upper surface. The loadings on the finite element model were restricted to a maximum value of 50N.

Figure 5.13 shows the FEA predicted force extension data and the measured force extension data for the test piece. Good agreement is demonstrated between the two sets of data (shown in Table 5.1). The differences between the data can be attributed to the modelling of a linear force extension curve by the FEA method, whereas the tensile test demonstrates the non-linear characteristics of an elastomer. At the tensile load of 40 N (at which the elastomer modulus was derived) the difference between the computed data and the measured data is 0.5%. Ideally the tensile test data and the inherent non-linear force extension behaviour could be modelled in the structural analysis. However this was not implemented in the subsequent analysis work as the assumption of a linear force extension curve provides a sufficient representation for the envisaged range of deformations.

The accuracy of the ANSYS FEA method has similarly been demonstrated by Shareef et al [125] where good agreement between the predicted results data and experimentally measured data is shown.

FORCE (Newtons)	Measured Extension (mm)	Predicted Extension (mm)	Difference (mm)
10	0.717	0.962	0.245
20	1.627	1.924	0.297
30	2.657	2.886	0.229
40	3.827	3.848	0.021
50	5.177	4.809	0.368

TABLE 5.1. Comparison between measured and predicted extension data.

A second series of tests were performed with the FEA method to compare the results data with classical beam theory data.

Two scenarios were devised (as shown in Figure 5.14). The first is where the beam is fully constrained at both ends (Beam A) and the second is where the beam is constrained at one end and subjected to a point contact at the other end (Beam B). Based on the assumption of an even load across the span and a span to width ratio greater than 8, the maximum displacement of the beams can be predicted by the following beam theory formulae;

$$\text{For Beam A} \quad Y_b = \frac{PL^3}{384EI} \tag{5.3}$$

for Beam B at x = 0.4215

$$Y_b = \frac{PL^3}{185EI} \tag{5.4}$$

for Beam B at x = 3/8L

$$Y_b = \frac{PL^3}{187EI} \tag{5.5}$$

$$\text{where} \quad I = \frac{bh^3}{12} \tag{5.6}$$

P = Force over span

L = span length

The finite element model is shown in Figure 5.15 where the span (l) is set to 0.1m, the height (h) to 0.01m and the thickness (b) to 0.0025m. The modulus of the material is specified as 5.226×10^6 Nm^{-2} and the load across the span is 5N.

Figure 5.16 shows the predicted deformation of Beam A and Figure 5.17 shows the predicted deformation of Beam B. This data is collated with the theoretical calculations and shown in Table 5.2. Good agreement is demonstrated between the predicted data from the ANSYS program and the classical beam equations (difference of 1.2% to 5%).

In support of the ANSYS FEA method, Neto et al [106] have demonstrated good agreement between the calculated results data and the predictions from classical formulae.

	Displacement at x according to Beam Theory in mm	Displacement at x predicted by ANSYS in mm	DIFFERENCE in mm
BEAM A (x =0.5L)	11.96	12.56	0.60
BEAM B (x =0.4125L)	24.81	25.13	0.32
BEAM B (x =3/8L)	24.56	23.73	0.83

TABLE 5.2. Comparison of predicted deformations according to FEA method and beam theory.

5.1.3   The CFSAT Tool

As has already been established, the accuracy of the CFSAT tool is a function of the accuracy of its two constituent parts. To validate the program it was proposed to run the complete analysis with the elastomer region specified as having a very large value of Young's Modulus, such that the surface pressure loads would be insufficient to invoke structural deformations. In theory the CFSAT tool would converge on the first iteration and calculate C_l and C_d values corresponding with the undeformed initial outer profile geometry. However, a serious failure of the department's computing facility coupled with a loss of the system backup data resulted in a total loss of the CFSAT program. For this reason a prediction of the accuracy of CFSAT is made based on the known data output from the two constituent parts.

The CFD method has shown an error in the predicted lift data of up to 10% when compared with NACA experimental data. The FEA method has shown an error of up to 5% in comparison with classical beam theory. A worse case scenario is predicted in which the data from the analysis is subject to a cumulative 15% (single global iteration) margin of error. There is no further scope for cumulative errors in the analysis due to the program structure employed.

This potential error margin is significant and as such it precludes the direct comparison of the CFSAT computed results with other sources of data. However, because the margin of error is consistent for each analysis performed with the tool, it is concluded that the quantitative results data can be used in isolation to establish the effects of modifications to the HTWF configuration. From this trends can be established from which firm conclusions may be drawn. Similar work by Ulrich [139] demonstrated a good agreement between the predicted results data from a coupled fluid-structural analysis (using the same software) and the measured behaviour of a microvalve (for both static and transient load sets).

The correlation of the initial data from the preliminary experimental work with the CFSAT demonstrates a consistency which indicates that the analytical process is functioning in a satisfactory manner.

5.2   Two Dimensional Evaluation of HTWF Configurations

To assess the design variables of the HTWF a series of analyses were performed using the CFSAT.

To establish the reference lift and drag coefficients a series of standalone CFD analyses were performed on the rigid outer profile geometries (E472, NACA 0006, NACA 0008, NACA 0010 and NACA 0012). The calculated data for these initial outer profiles is then used as the reference by which the changes in the L/D ratio due to the hydroelastic tailoring techniques can be gauged.

The incidence angles for all the analysis work is restricted to the range between 0° and 10°, primarily because a conventional windsurf fin typically stalls at an incidence angle equal to 10°. Extending the range of incidence angles beyond this value would be pointless as it is not possible to determine the accuracy of the CFD code for predicting flow separation and stall. In support of this Thain [137] describes the difficulty in predicting the C_{Lmax} of high lift systems without physically tank testing them.

For each analysis the flow velocity was set to 10 ms^{-1} as this is representative of a moderate sailing speed for a planing windsurf board. Due to the limitations imposed by the CFD code the flow was defined as fully turbulent, even though in reality it could be expected to be partly laminar and partly turbulent.

So that a representative and practical solution to the HTWF configuration can be reached, realistic values were used to define the slot gap, elastomer modulus and outer profile geometry.

In terms of the slot gap the primary concern is to ensure that there is sufficient material in the supporting skeleton to retain the overall structural integrity of the fin. For this reason the slot gap width was restricted to a maximum value equal to 70% of the chord length. This is a nominal figure based on intuition and is not representative of a predetermined or derived value. Further work is required to establish the minimum material bulk required to provide satisfactory levels of structural integrity and support for a finite length fin.

The minimum thickness to chord (t/c) ratio was set at 6% due to the same concerns regarding structural integrity. A maximum value of 15% was chosen as beyond this the benefits of using camber become progressively ineffectual [1].

The range of modulus values for the elastomer material was between 6×10^6 Nm^{-2} and 16×10^6 Nm^{-2}. These values correspond with a range of cold cure elastomers suitable for fabricating test samples and prototypes [114].

The results data is presented as the percentage difference in performance of the HTWF configuration as compared with the corresponding rigid outer profile. This method of presentation enables the changes in performance due to the hydroelastic tailoring to be seen more clearly than with traditional lift curve and drag polar plots.

5.2.1 Nomenclature

The following nomenclature is used to designate the configuration of the hydroelastically tailored cross sections;

- First group of digits define outer profile shape.
- Second two digits designate modulus of elastomer covering.
- Final digit defines the value of the slot gap.

For example

n12_16_5   represents a NACA 0012 cross section with an elastomer of modulus $16 \times 10^6 \, \text{Nm}^{-2}$ and a slot gap of 50% chord.

e472_14_3   represents an Eppler e472 cross section with an elastomer of modulus $14 \times 10^6 \, \text{Nm}^{-2}$ and a slot gap of 30% chord.

5.2.2 Two Dimensional Analysis Results

The initial goal was to investigate the influence of the slot gap on the lift to drag ratio of a nominal foil section and so consideration was given to the work of Liebeck [94] into high lift single element airfoils.

These foil sections feature a maximum thickness and position of camber towards the leading edge. Additionally they feature a moderate nose radius to avoid flow separation at

off design incidence angles. Based on these single element high lift airfoils, the Eppler e472 foil was selected for the starting point for the investigation and analysis work as visually it features a 'base' thickness distribution and nose radius roughly in accordance with these high lift single element foils.

5.2.2.1 The Eppler e472 Profile

The first series of tests employed a configuration with an e472 outer profile, with fixed elastomer modulus (11×10^6 Nm^{-2}) and varying slot gap values (between 20% and 70% of the chord length).

Figure 5.18 shows the percentage difference in C_l for the e472 HTWF configurations as compared with the rigid e472 section data.

Figure 5.19 shows the percentage difference in C_d for the e472 HTWF configurations as compared with the rigid e472 section data.

Figure 5.20 shows the percentage difference in C_l/C_d for the e472 HTWF configurations as compared with the rigid e472 section data. The 70% slot gap configuration has inferior C_l/C_d characteristics at all incidence angles (as compared with the rigid section). The 60% slot gap configuration (e472_11_6) demonstrates a maximum improvement in performance of 4.5% at an incidence angle of 1.8°, but this rapidly changes to a reduction in C_l/C_d after 2.5°. The e472_11_5 configuration shows the largest increase in C_l/C_d of 5% at an incidence angle of 2°. This again changes to a reduction in performance after approximately 3.5°. The e472_11_4 configuration (40% slot gap) shows an increase in C_l/C_d at incidence angles up to 5°, with a maximum gain of 4% at 2°. The other two configurations with slot gaps of 20% and 30% perform less well than the 40% configuration at all incidence angles.

Due to the relative success of the 40% chord gap e472 configuration, a second series of tests were performed in which the slot gap was fixed and the elastomer modulus varied (between 6×10^6 Nm^{-2} and 12×10^6 Nm^{-2}).

Figure 5.21 which shows the percentage difference in C_l/C_d of the e472 hydroelastic sections as compared with the rigid reference model. This indicates that the HTWF configurations with an elastomer modulus of less than 9×10^6 Nm^{-2} perform the least well. A dependence between the elastomer modulus and the percentage gains in C_l/C_d is demonstrated. In terms of the percentage gain in C_l/C_d, the e472_12_4 configuration demonstrates an increase in lift to drag ratio up to an incidence angle of 5.5°, with a maximum gain of 4% at an incidence angle of 2.3°. After 5.5° none of the HTWF configurations perform as well as the rigid reference model.

The results from this initial work demonstrates that the C_l/C_d can be increased by the use of hydroelastic tailoring techniques. These increases are however limited to low incidence angles. Based on the fact that a conventional windsurf fin typically operates at an incidence angle of 6° these low incidence angle performance gains are of limited benefit.

The overall C_l/C_d performance at moderate to high incidence angles is disappointing. This indicates that even though the lift curve slope is being increased, the associated increases in drag are proportionally greater.

It is concluded that these increases in drag result from the 'blunt' nose shape of the e472 profile. This nose shape has been designed to operate over a wide range of incidence angles, for which a generous leading edge radius is employed to delay leading edge stall. This shape is however less efficient at 'splitting' the oncoming flow at low incidence angles. To realise the full benefits of the drooping nose a sharper nose shape is required because, *'The increment in lift due to camber is least for sections with relatively large radius leading edges and camber is more effective on thin sections than on thick sections'* [90]

5.2.2.2 Evaluation of NACA 0006, 0008, 0010 and 0012 Profiles

For the next series of tests the four sections NACA 0006, 0008, 0010 and 0012 were selected for the outer profile geometry as they feature a sharper nose radius. In addition, by selecting sections from the same family of foil shapes the effect of the thickness ratio could also be assessed. As with the previous work on the Eppler profiles the change in hydrodynamic performance resulting from the HTWF configuration is gauged by the percentage difference in the C_l and C_d data as compared with the calculated data for the rigid initial outer profile geometry.

Based on the results from the first series of tests on the e472 profile, the slot gap values for the NACA airfoils were restricted to 30%, 40% and 50% of the chord length and the elastomer modulus values were restricted to the range between $10 \times 10^6 \, \text{Nm}^{-2}$ and $16 \times 10^6 \, \text{Nm}^{-2}$.

5.2.2.2.1   Location of the Nose Pivot Point

It is desirable to move the mast rearwards as this allows its diameter to be increased, thereby improving structural integrity. However, by moving the mast rearwards a fundamental change will occur in the moment arms acting at this point.

Figure 5.22 shows the two moments acting at the nose. These moments result from the forces acting either side of the mast on the slot gap and the forward part of the nose. Three potential scenarios can be envisaged as a result of these moments;

1. The moment arm generated by the slot gap is greater than the moment arm generated by the nose. This will 'droop' the nose into the flow in the desired manner (Figure 5.22a).

2. The moment arm generated by the nose is greater than the moment arm generated by the slot gap. This will result in an upturned nose which is considered to be highly undesirable (Figure 5.22b).

3. The moment arms generated by the slot gap and the nose are equal and opposite. This situation of hydrodynamic equilibrium will result in a *stagnant nose* in which the elastomer is compressed in the negative pressure region immediately next to the mast and stretched on the positive pressure side of the mast (Figure 5.22c). This will raise the nose slightly and increase the curvature on the negative pressure leading edge surface. It is unclear as to the effect that this will have on the hydrodynamic performance of the section.

The magnitude of the moment arms is primarily a function of the position of the mast pivot point. To investigate this phenomenon a NACA 0012 outer profile with a constant slot gap of 30% and an elastomer modulus of 16×10^6 was used. The mast pivot point was varied between 4% and 9% of the chord length.

The effect on the lift to drag ratio as a function of the variations to the pivotal mast location is shown in Figure 5.23. This indicates an optimum location in the region of 5% of the chord length for this configuration.

In support of this Figure 5.24 and Figure 5.25 show the predicted deformation in the nose sections with the pivot point at 5% and 9% of the chord length. It is clear that for the 5% configuration the nose is drooped into the flow in the desired manner, whereas the 9% configuration has an upturned nose.

To maintain a realistic and practical configuration the position of the pivotal mast is specified at 5% of the chord for all configurations used in the subsequent analysis work.

5.2.2.2.2 Effect of Elastomer Modulus on NACA HTWF Configurations with a 50% of Chord Slot Gap

Figures 5.26 to 5.34 show the percentage change in C_l, C_d and C_l/C_d as a function of the elastomer modulus for NACA HTWF configurations with a slot gap equal to 50% of the chord length. It was not possible to derive solutions for all of the configurations due to excessive distortion in some of the finite element meshes.

Figures 5.26 to 5.28 show the performance characteristics of the HTWF configurations featuring a NACA 0012 outer profile. The percentage change in C_l is consistent for all configurations, indicating stability in the structures. A reduction in C_d is demonstrated, with the percentage reduction becoming progressively larger with increasing incidence angles. This indicates that the drooping nose is functioning in the desired manner, particularly at elevated incidence angles. The gain in C_l and reduction in C_d results in a significant overall gain in C_l/C_d for these configurations (typically a 15% gain at 6°). A dependence on the elastomer modulus is demonstrated with the best percentage gains in C_l/C_d corresponding with the highest modulus values (for this foil shape and slot gap).

Figures 5.29 to 5.31 show the performance characteristics of the HTWF configurations featuring a NACA 0010 outer profile. In comparison with the NACA 0012 configurations there is less consistency in the C_l and C_d data. Although there is a consistent (and comparatively larger) gain in the C_l for these configurations, the corresponding increases in C_d are greater, resulting in inferior C_l/C_d performance. The two configurations featuring the lowest values of elastomer modulus (n10_10_5 and n10_12_5) perform less well than a rigid section over a large range of incidence angles. A dependence on the elastomer modulus is shown with a continual increment in C_l/C_d associated with increasing modulus values. (for this foil shape and slot gap).

Figures 5.32 to 5.34 show the performance characteristics of the n08_16_5 HTWF configuration (featuring a NACA 0008 outer profile). There is a large gain in C_l for all

incidence angles (8% at 10°). However the corresponding increases in C_d are highly detrimental, resulting in inferior C_l/C_d performance most of the range of interest.

5.2.2.2.3   Effect of Elastomer Modulus on NACA HTWF Configurations with a 40% of Chord Slot Gap

Figures 5.35 to 5.46 show the percentage change in C_l, C_d and C_l/C_d as a function of the elastomer modulus for NACA HTWF configurations with a slot gap equal to 40% of the chord length. It was not possible to derive solutions for all of the configurations due to excessive distortion in some of the finite element meshes.

Figures 5.35 to 5.37 show the performance characteristics of the HTWF configurations featuring a NACA 0012 outer profile. The percentage change in C_l is similar for all of these configurations with a good correlation of the data shown. In comparison, the reduction in C_d is less consistent. The irregular C_d performance results in a fluctuating percentage change in the C_l/C_d. The most consistent percentage gain in C_l/C_d is achieved by the configuration with the highest elastomer modulus ($16 \times 10^6 \, Nm^{-2}$).

Figures 5.38 to 5.40 show the performance characteristics of the HTWF configurations featuring a NACA 0010 outer profile. The percentage change in C_l is similar for all of these configurations. The reduction in C_d is less consistent. The irregular C_d performance results in a fluctuating percentage change in the C_l/C_d. There is no obvious dependency between the elastomer modulus and the percentage change in C_l/C_d for these HTWF configurations.

Figures 5.41 to 5.43 show the performance characteristics of the HTWF configurations featuring a NACA 0008 outer profile. All configurations demonstrate similar percentage gains in C_l over the range of incidence angles. The percentage reduction in C_d is less consistent with the lowest modulus configuration (n08_10_4) showing the smallest reductions in drag. The C_l/C_d is increased by all of the configurations with the n08_14_4 showing the most consistent percentage gains. There is no obvious dependency between

the elastomer modulus and the percentage change in C_l/C_d, although the configuration with the lowest elastomer modulus (10×10^6 Nm^{-2}) performs the least well (even though it demonstrates a 28% gain in C_l/C_d at an incidence angle of 8°).

Figures 5.44 to 5.46 show the performance characteristics of the HTWF configurations featuring a NACA 0006 outer profile. The percentage gain in C_l for all of these configurations is reasonably consistent up to an incidence angle of 8°. At an incidence angle of 10° all of the configurations show a significant percentage gain in C_l. This indicates an increment in the magnitude of camber due to the increased surface pressure loads at this high incidence angle. In terms of the percentage change in C_d a clear dependency on the elastomer modulus is demonstrated, with the highest modulus values achieving the largest performance increments. This is reflected in the percentage change in C_l/C_d where a continual improvement in performance is associated with increasing elastomer modulus values.

5.2.2.2.4 Effect of Elastomer Modulus on NACA HTWF Configurations with a 30% of Chord Slot Gap

Figures 5.47 to 5.58 show the percentage change in C_l, C_d and C_l/C_d as a function of the elastomer modulus for NACA HTWF configurations with a slot gap equal to 30% of the chord length.

Figures 5.47 to 5.49 show the performance characteristics of the HTWF configurations featuring a NACA 0012 outer profile. The n12_10_3 configuration (lowest modulus value 10×10^6 Nm^{-2}) shows the highest (and most irregular) percentage gain in C_l for all incidence angles. This appears to be a result of an upturning of the nose which effectively increases the curvature of the upper surface, resulting in the unusual C_l gains. The percentage gain in C_l for the other configurations is consistent and correlated. The percentage change in C_d is dramatically inconsistent. The n12_10_3 shows an overall increase in C_d which again indicates a flow problem at the leading edge. All of the other configurations demonstrate a consistent reduction in C_d with the n12_16_3 showing the

143

greatest reductions overall. The configuration with the highest elastomer modulus (16×10^6 Nm^{-2}) shows the greatest gains in C_l/C_d whereas the configuration with the lowest elastomer modulus (10×10^6 Nm^{-2}) performs the least well. The performance of the other two configurations is not obviously dependent on the elastomer modulus.

Figures 5.50 to 5.52 show the performance characteristics of the HTWF configurations featuring a NACA 0010 outer profile. The two configurations with the highest elastomer modulus values perform similarly with a reasonably consistent gain in C_l at low to moderate incidence angles (3% to 4% up to an incidence angle of 8°). The two other configurations show irregular and large percentage gains in C_l with the lowest elastomer modulus (10×10^6 Nm^{-2}) achieving the greatest gains in C_l. These gains in C_l seem to indicate an upturning of the pivotal nose in the same manner as the n12_10_3 configuration. A reduction in C_d is shown by the two configurations with the highest modulus values. The other two configurations show a dramatic rise in drag over the range of incidence angles which again indicates a flow problem emanating from the leading edge region. The percentage change in C_l/C_d indicates that the n10_16_3 and n10_14_3 perform similarly and demonstrate a consistent gain in C_l/C_d at all incidence angles. The other two configurations generally perform less well than the rigid reference section. A dependence on the elastomer modulus is demonstrated with an increase in performance resulting from an increase in elastomer modulus. It can be hypothesised that the optimum elastomer modulus value for this configuration is between 14×10^6 Nm^{-2} and 16×10^6 Nm^{-2}.

Figures 5.53 to 5.55 show the performance characteristics of the HTWF configurations featuring a NACA 0008 outer profile. An increase in C_l is demonstrated by all configurations. There is no obvious dependency between the percentage gains in C_l and the elastomer modulus. Apart from the n08_16_3 configuration, a consistent and ever increasing reduction in C_d is demonstrated. This is once again reflected in the percentage changes in C_l/C_d where the configuration with the highest elastomer modulus (16×10^6 Nm^{-2}) performs consistently worse than the others. The percentage gains in C_l/C_d for the other configurations is highly correlated, with no apparent dependency on the elastomer

modulus. From this data it can be concluded that an elastomer modulus of 16×10^6 Nm^{-2} is too high for this combination of outer profile geometry and slot gap.

Figures 5.56 to 5.58 show the performance characteristics of the HTWF configurations featuring a NACA 0006 outer profile. The percentage gain in C_l for all of these configurations is irregular with no obvious dependency on elastomer modulus demonstrated. The two configurations with the highest elastomer modulus values show a consistent increase in C_d across the range of incidence angles. Only the n06_12_3 shows a reduction in C_d and gain in C_l/C_d for all incidence angles. This indicates an optimum elastomer modulus value of approximately 10×10^6 Nm^{-2} for this combination of outer profile geometry and slot gap.

5.2.2.2.5 Effect of Foil Thickness on NACA HTWF Configurations

Figures 5.59 to 5.70 show the percentage change in C_l/C_d as a function of the foil thickness for NACA HTWF configurations.

Figure 5.59 indicates that a thick foil (NACA 0012) is required for a HTWF configuration with a 50% slot gap and elastomer modulus of 10×10^6 Nm^{-2}.

Figure 5.60 shows that the NACA 0008 section has the most consistent gains C_l/C_d for a slot gap of 40% and an elastomer modulus 10×10^6 Nm^{-2}. Overall there is no obvious dependency between the foil thickness and the percentage gains in C_l/C_d.

Figure 5.61 shows the percentage change in C_l/C_d for HTWF configurations with a 30% slot gap and elastomer modulus of 10×10^6 Nm^{-2}. There is no obvious dependency between the foil thickness and the percentage gains in C_l/C_d. It can however be concluded that a NACA 0008 foil provides the optimum thickness for this combination of slot gap and elastomer modulus.

Figure 5.62 indicates that a thick foil (NACA 0012) is required for a HTWF configuration with a 50% slot gap and elastomer modulus of $12 \times 10^6 \, \text{Nm}^{-2}$.

Figure 5.63 shows the percentage change in C_l/C_d for HTWF configurations with a 40% slot gap and elastomer modulus of $12 \times 10^6 \, \text{Nm}^{-2}$. There is no obvious dependency between the foil thickness and the performance gains, although it can be concluded that a NACA 0008 section offers the optimum foil thickness for this combination of slot gap and elastomer modulus.

Figure 5.64 shows the percentage change in C_l/C_d for HTWF configurations with a 30% slot gap and elastomer modulus of $12 \times 10^6 \, \text{Nm}^{-2}$. The HTWF configuration with a NACA 0010 section shows the worst performance characteristics with the NACA 008 configuration demonstrating the most consistent percentage gains in C_l/C_d. There is no obvious dependency between the foil thickness and the percentage changes in C_l/C_d.

Figure 5.65 shows the percentage change in C_l/C_d for HTWF configurations with a 50% slot gap and elastomer modulus of $14 \times 10^6 \, \text{Nm}^{-2}$. Although both configurations demonstrate gains in C_l/C_d the plot indicates that a thicker profile (NACA 0012) is required for this combination of slot gap and elastomer modulus.

Figure 5.66 shows the percentage change in C_l/C_d for HTWF configurations with a 40% slot gap and elastomer modulus of $14 \times 10^6 \, \text{Nm}^{-2}$. There is no obvious dependency between the foil thickness and the percentage gains in C_l/C_d, although it is apparent that the NACA 0008 provides an optimum thickness for this combination of slot gap and elastomer modulus.

Figure 5.67 shows the percentage change in C_l/C_d for HTWF configurations with a 30% slot gap and elastomer modulus of $14 \times 10^6 \, \text{Nm}^{-2}$. It is shown that the NACA 0008 section provides an optimum thickness for this combination of slot gap and elastomer modulus and that any deviation from the NACA 0008 foil thickness is detrimental in terms of C_l/C_d performance.

Figure 5.68 shows the percentage change in C_l/C_d for HTWF configurations with a 50% slot gap and elastomer modulus of 16×10^6 Nm^{-2}. In the range of incidence angles between 4° and 8° a dependency between the foil thickness and percentage gain in C_l/C_d is shown. This indicates that a thicker foil profile achieves the greatest performance increments (for this combination of slot gap and elastomer modulus).

Figure 5.69 shows the percentage change in C_l/C_d for HTWF configurations with a 40% slot gap and elastomer modulus of 16×10^6 Nm^{-2}. Overall there is no obvious dependency between the foil thickness and the changes in C_l/C_d. It is apparent that the NACA 0012 and NACA 0008 configurations demonstrate the most consistent percentage gains in C_l/C_d.

Figure 5.70 shows the percentage change in C_l/C_d for HTWF configurations with a 30% slot gap and elastomer modulus of 16×10^6 Nm^{-2}. It is not possible to identify a relationship between the foil thickness and the percentage change in C_l/C_d, but it is clear that the two thicker sections perform similarly, with reasonably consistent percentage gains in C_l/C_d. The two thinner profiles demonstrate inferior performance characteristics at all incidence angles.

5.2.2.2.6 Effect of Slot Gap on NACA HTWF Configurations

Figures 5.71 to 5.85 show the percentage change in C_l/C_d as a function of the slot gap for NACA HTWF configurations.

Figure 5.71 shows the percentage change in C_l/C_d for HTWF configurations with a NACA 0012 outer profile and an elastomer modulus of 10×10^6 Nm^{-2}. This indicates an optimum slot gap of 40% for this combination of foil thickness and elastomer modulus.

Figure 5.72 shows the percentage change in C_l/C_d for HTWF configurations with a NACA 0012 outer profile and an elastomer modulus of 12×10^6 Nm^{-2}. There is a general correlation of the data up to an incidence angle of 6°, after which the 40% slot gap

configuration outperforms the others. There is no obvious relationship between the slot gap and the percentage changes in C_l/C_d. However, based on the post 8° performance characteristics, a 40% slot gap would seem to be an optimum for this combination of foil thickness and elastomer modulus.

Figure 5.73 shows the percentage change in C_l/C_d for HTWF configurations with a NACA 0012 outer profile and an elastomer modulus of 14×10^6 Nm^{-2}. Based on the pre 8° performance of these configurations, there is a clear dependency between the slot gap and the percentage change in C_l/C_d. This plot therefore demonstrates an increase in performance associated with an increase in the slot gap (for this combination of foil thickness and elastomer modulus).

Figure 5.74 shows the percentage change in C_l/C_d for HTWF configurations with a NACA 0012 outer profile and an elastomer modulus of 16×10^6 Nm^{-2}. Up to an incidence angle of 4° the percentage gains in C_l/C_d are shown to be a function of an increasing slot gap. After an incidence angle of 6° there is no obvious relationship between performance gains and the size of slot gap. Based on overall performance in the range 0° to 10° a slot gap of 40% seems to be an optimal value.

Figure 5.75 shows the percentage change in C_l/C_d for HTWF configurations with a NACA 0010 outer profile and an elastomer modulus of 10×10^6 Nm^{-2}. Only the configuration with a 40% slot gap demonstrates consistent gains in C_l/C_d. This therefore represents an optimal slot gap value for this combination of foil thickness and elastomer modulus.

Figure 5.76 shows the percentage change in C_l/C_d for HTWF configurations with a NACA 0010 outer profile and an elastomer modulus of 12×10^6 Nm^{-2}. All of these configurations perform inconsistently, with only the n10_12_4 (40% slot gap) demonstrating a gain in C_l/C_d for all incidence angles. This must therefore be considered as an optimum slot gap value for this combination of foil thickness and elastomer modulus.

Figure 5.77 shows the percentage change in C_l/C_d for HTWF configurations with a NACA 0010 outer profile and an elastomer modulus of 14×10^6 Nm^{-2}. A gain in C_l/C_d is demonstrated by all of these configurations, although the performance characteristics are highly irregular. There is no obvious dependency between the slot gap value and the percentage change in C_l/C_d. However, based on the consistency of percentage gain in C_l/C_d over the range of incidence angles, the 40% slot is considered to perform the best (for this combination of foil thickness and elastomer modulus).

Figure 5.78 shows the percentage change in C_l/C_d for HTWF configurations with a NACA 0010 outer profile and an elastomer modulus of 16×10^6 Nm^{-2}. The irregular nature of the data means that it is not possible to establish a relationship between the slot gap and the percentage change in C_l/C_d. The most consistent performance is demonstrated by the 30% slot gap configuration.

Figure 5.79 shows the percentage change in C_l/C_d for HTWF configurations with a NACA 0008 outer profile and an elastomer modulus of 10×10^6 Nm^{-2}. The data in this plot indicates that a 30% slot gap is preferable (to a 40% slot gap) for this combination of foil thickness and elastomer modulus.

Figure 5.80 shows the percentage change in C_l/C_d for HTWF configurations with a NACA 0008 outer profile and an elastomer modulus of 12×10^6 Nm^{-2}. Apart from the performance at 4°, the plot indicates that a 40% slot gap is preferable (to a 30% slot gap) for this combination of foil thickness and elastomer modulus. However, on the basis of overall consistency in the C_l/C_d gains, it could be argued that the 30% slot gap provides superior performance characteristics.

Figure 5.81 shows the percentage change in C_l/C_d for HTWF configurations with a NACA 0008 outer profile and an elastomer modulus of 14×10^6 Nm^{-2}. The 40% slot gap demonstrates the largest and most consistent gains in C_l/C_d, and hence offers an optimum value for this combination of foil thickness and elastomer modulus.

Figure 5.82 shows the percentage change in C_l/C_d for HTWF configurations with a NACA 0008 outer profile and an elastomer modulus of 16×10^6 Nm^{-2}. Only the 40% slot gap configuration demonstrates an overall gain in C_l/C_d. From this plot it is not possible to establish a dependency between the slot gap and the percentage gain in C_l/C_d. It is however possible to establish that a 40% slot gap is an optimum value for this combination of foil thickness and elastomer modulus.

Figure 5.83 shows the percentage change in C_l/C_d for HTWF configurations with a NACA 0006 outer profile and an elastomer modulus of 10×10^6 Nm^{-2} or 12×10^6 Nm^{-2}. This indicates an optimum configuration featuring a 30% slot gap and elastomer modulus of 12 $\times 10^6$ Nm^{-2} for this foil thickness.

Figure 5.84 shows the percentage change in C_l/C_d for HTWF configurations with a NACA 0006 outer profile and an elastomer modulus of 14×10^6 Nm^{-2}. This plot indicates that a 40% slot gap is preferable to a 30% slot gap. It is clear that these configurations demonstrate the greatest performance gains at high incidence angles (when a thin rigid foil is normally starting to stall) probably due to the beneficial effect of the drooping nose.

Figure 5.85 shows the percentage change in C_l/C_d for HTWF configurations with a NACA 0006 outer profile and an elastomer modulus of 16×10^6 Nm^{-2}. This plot indicates that a slot gap of 40% is preferable to a 30% slot gap for this combination of foil thickness and elastomer modulus.

5.3 Prototype Windsurf Fin Employing a HTWF Cross Section

The theory behind the HTWF has been outlined and investigated with the computer based analysis tool (CFSAT). In support of this theoretical work a full scale prototype fin was fabricated for applied testing.

The reasons for producing the prototype fin are threefold;

1. To establish a practical method of fabrication.

2. To ensure that suitable structural integrity could be achieved.

3. To subjectively determine the 'feel' and performance of the fin when used on an actual windsurf board.

5.3.1   The Design of the Fin

The prototype windsurf fin is designed to operate in light to moderate wind strengths (5 ms^{-1} to 8 ms^{-1}) based on the assumption that the sea state in these conditions would be slight and not too choppy. By avoiding the more extreme types of sailing conditions the sailor will be able to concentrate more on the characteristics and operational 'feel' of the fin.

Figure 5.86 and Figure 5.87 show third angle projections of the prototype HTWF windsurf fin. The span of this prototype is 0.29 m and the root chord is 0.1 m, giving a surface area of approximately 0.022 m^2 and an effective AR of 7.4. The span and hence surface area of this prototype is considerably less than would be normally used for these sailing conditions (normally a contemporary fin with span of at least 0.4 m would be employed for these conditions).

The prototype fin features an unusual planshape with a straight leading edge and elliptical trailing edge (the straight leading edge is used for structural reasons as it is easier to reinforce with a carbon rod).

The nominal cross section employed for the prototype fin is the Eppler E472. This again was selected for structural reasons opposed to purely hydrodynamic reasons. Although the provisional analysis work indicates that the NACA sections with the thinner nose geometries offer the best hydrodynamic performance, concerns about the structural integrity of the pivotal 'mast' region led to the selection of a section with more fullness at the leading edge

5.3.2 Fabrication Process

A two stage moulding process was developed to fabricate the prototype HTWF fins, in which;

1. The skeleton is fabricated.
2. The skeleton is covered with the elastomer.

For each of these steps a pair of matched moulds is required. These moulds were produced by generating a three dimensional computer model of the fin (outer geometry and skeleton geometry) on the SDRC I-deas Master Series package. This enabled a check to be made of the tolerances between the elastomer covering and the internal skeleton. Following this, the computer model data was sent to a tool maker for the fabrication of the matched moulds.

5.3.2.1 Fabricating the Skeleton

To fabricate the skeleton, glass and carbon fibre reinforcing cloths are laid up in the first mould with an epoxy resin matrix. This structure is further reinforced through the inclusion of stiffening carbon rods. Whilst the resin is still green, the two halves of the mould are assembled and compressed in a heated press. After cure, the skeleton is hand finished to remove the flash and then positioned in the second mould which defines the outer profile of the elastomer covering. To ensure that the drooping nose is achieved a release agent is applied to the pivotal mast of the skeleton to prevent the elastomer from bonding (to this region only).

5.3.2.2 Fabricating the Elastomer Covering

To fabricate the elastomer covering, a vacuum forming process is used to eliminate voids, thus ensuring a satisfactory surface finish. The second mould features inlet and outlet holes so that the elastomer can be introduced to the void mould. Once the skeleton has

been enclosed in this second mould, it is placed in the vacuum chamber and the elastomer is introduced via an inlet feed pipe. The curing time is approximately 30 minutes, after which the prototype fin can be released from the mould and the flash removed.

5.3.3 Sailing Performance

So that the performance of the prototype fin could be subjectively assessed, an additional solid composite prototype fin was fabricated with the same external geometric features (i.e. it was of a 'conventional' rigid and non-cambered configuration). Again, this is not as unusual as it may first seem, as it is common practice in the sailing world to gauge the performance differences between new design features and configurations by sailing the equipment against a known reference model (i.e. America's cup work [143]). By doing this it can be possible to determine the differences in performance, particularly pointing ability, control characteristics and general feel.

For the preliminary investigation, the author and a colleague sailed a prototype variable camber fin and solid reference model (shown in Figure 5.88) on a pair of identical Mistral Screamer II slalom boards with identical rigs of 6 m^2 in surface area. The wind speed in this first test was approximately 8 ms^{-1} (Beaufort Force 4). The variable camber fin featured a slot gap of 40% chord length and an elastomer modulus of 10×10^6 Nm^{-2}.

To assess the performance of the cambered fin in comparison with the rigid model, the boards were interchanged periodically. The first impressions from sailing the prototypes were that when a stall condition arose, it seemed to be more severe than would be expected with a conventional type design. Also, the drag of the two prototypes seemed to be higher than would be expected. This is likely to result from the 'blunt' cross section profile.

The increase in drag was particularly noticeable when sailing off the wind (i.e. the incidence angle of the fin is very low). Otherwise there were no apparent detrimental performance characteristics.

The variable camber fin felt 'solid' and provided sufficient lift to sail to windward at a good pointing angle. When sailing alongside the board with the rigid reference fin, the HTWF equipped board was able to point higher to windward.

One of the main successes of this test was to prove that the structural integrity of the HTWF could be maintained (even though 40% of the supporting structure had in effect been 'removed'). It also demonstrated that the configuration was stable and didn't seem to be experiencing flutter or a similar instability problems.

For an unbiased opinion on the performance of the prototype fins, they were dispatched to Ken Black and Nigel Howell for further testing (Ken Black is a professional sail designer, who produces his own brand of sails as well as designing for the UK's leading sail manufacturer, Tushingham Sails. Nigel Howell is a leading British windsurfer who has been competing internationally on the professional world tour for over ten years).

Due to a lack of wind in the timeframe in which these two sailors could test the fins, only one day of testing was performed. A transcribe of Ken Black's test report [131(6)] is provided on the following page.

It has not been possible to conduct further tests with the prototype fin due to severe damage resulting from a collision with a submerged object.

To: Roger Tushingham

From: Ken Black

24th June 1996

Re: Asymmetric Foil Fins from Simon Fagg

Not much wind of late but managed to try the softest of the three 29 cm fins in comparison to a 40 cm Concrete Wave G10 race fin that I know is fast.

Conditions: 12-18 knots (est) slight chop. Using Nigel Howell on 295 course/slalom with 1997 7.9 proto sail to test against.

My board: Critical Section 280 course/slalom. Sail 1997 7.4 course.

With Concrete Wave Fin. *Upwind on both tacks, in gust I was similar in speed and pointing to Nigel but lost out if the wind dropped at all.*
Off wind speed was almost identical unless wind dropped, when I dropped back.

With Asymmetric Test Fin. *Upwind on starboard tack performance almost as good as 40 cm Concrete Wave Fin, but did not point quite as high. Felt very solid. Able to put all my weight on back foot. Off wind on starboard felt good, but comparison with Nigel was not possible at the time. On port tack the fin did not have nearly as much bite. It gripped then slid a little then gripped etc. Didn't have anything like the speed or pointing ability that it had on starboard. Off wind on port tack there was serious turbulence slowing the board severely.*

The wind dropped before I was able to try the other models. I'll try them as soon is there is more wind.

Ken Black.

Comparison of Lift Curve Slopes

Figure 5.1

% Difference in Lift Data
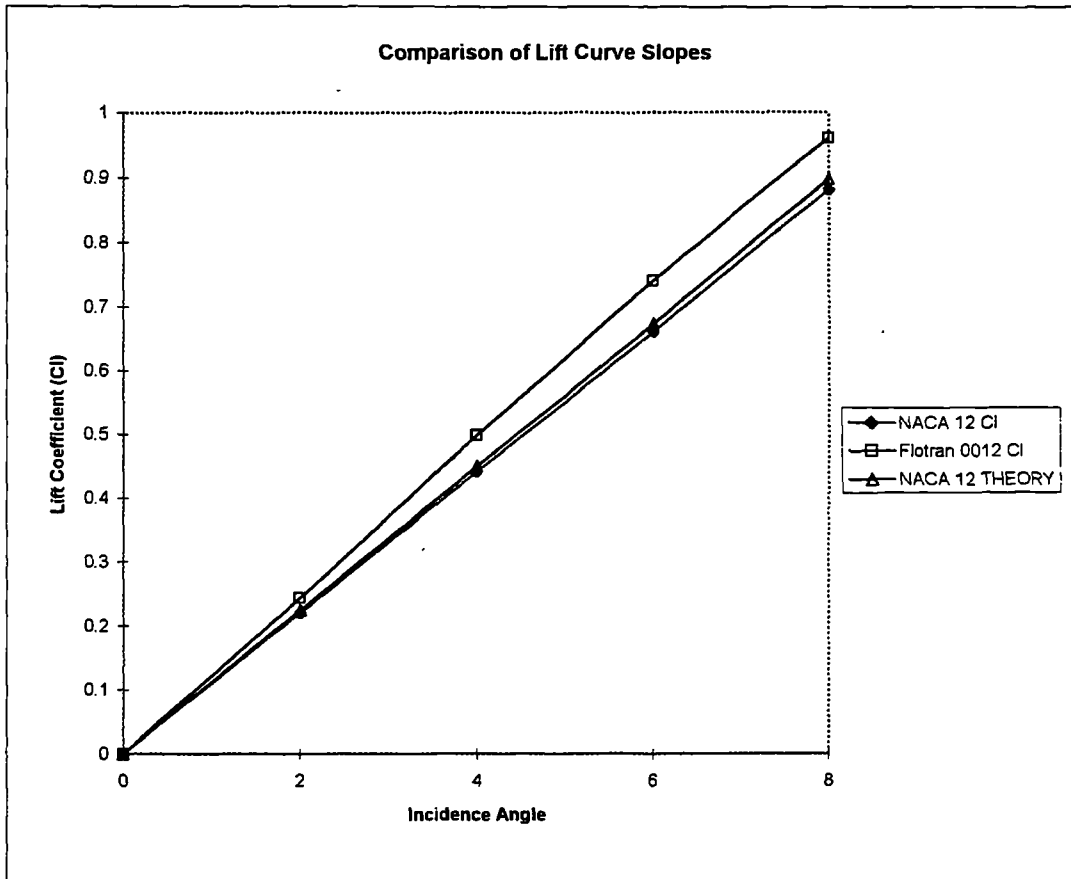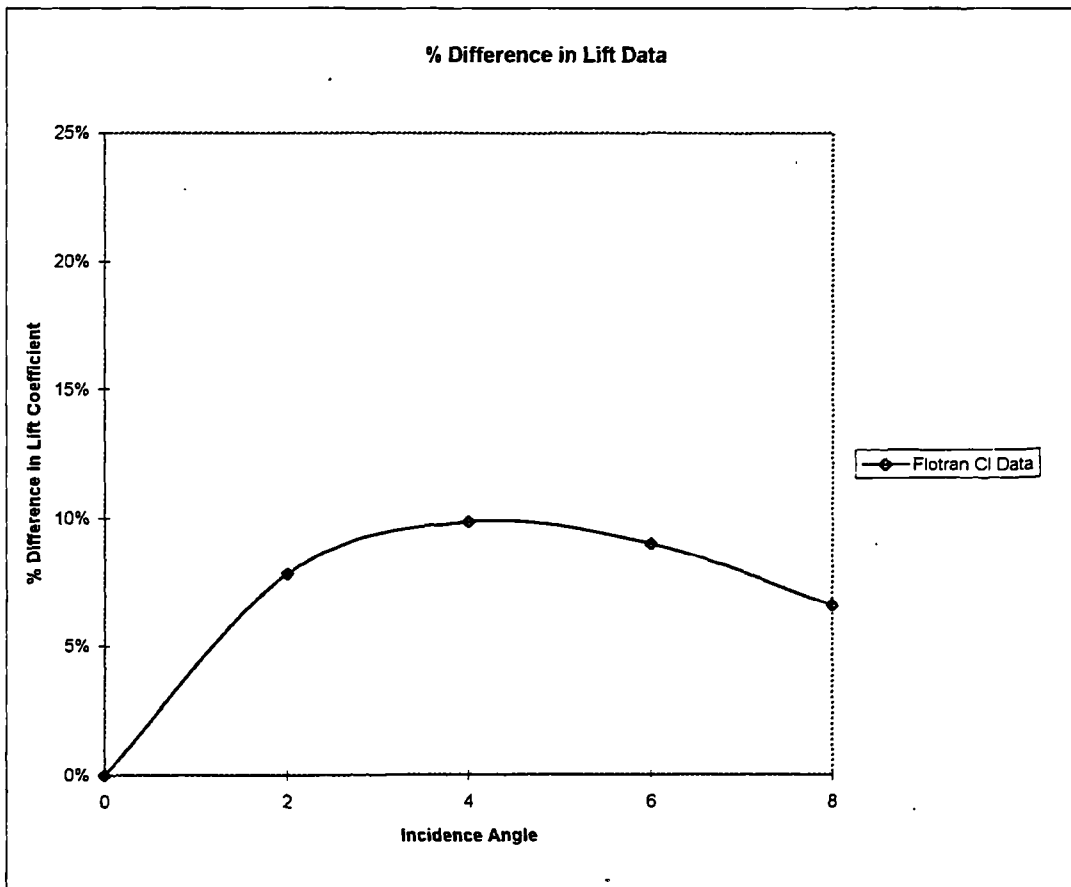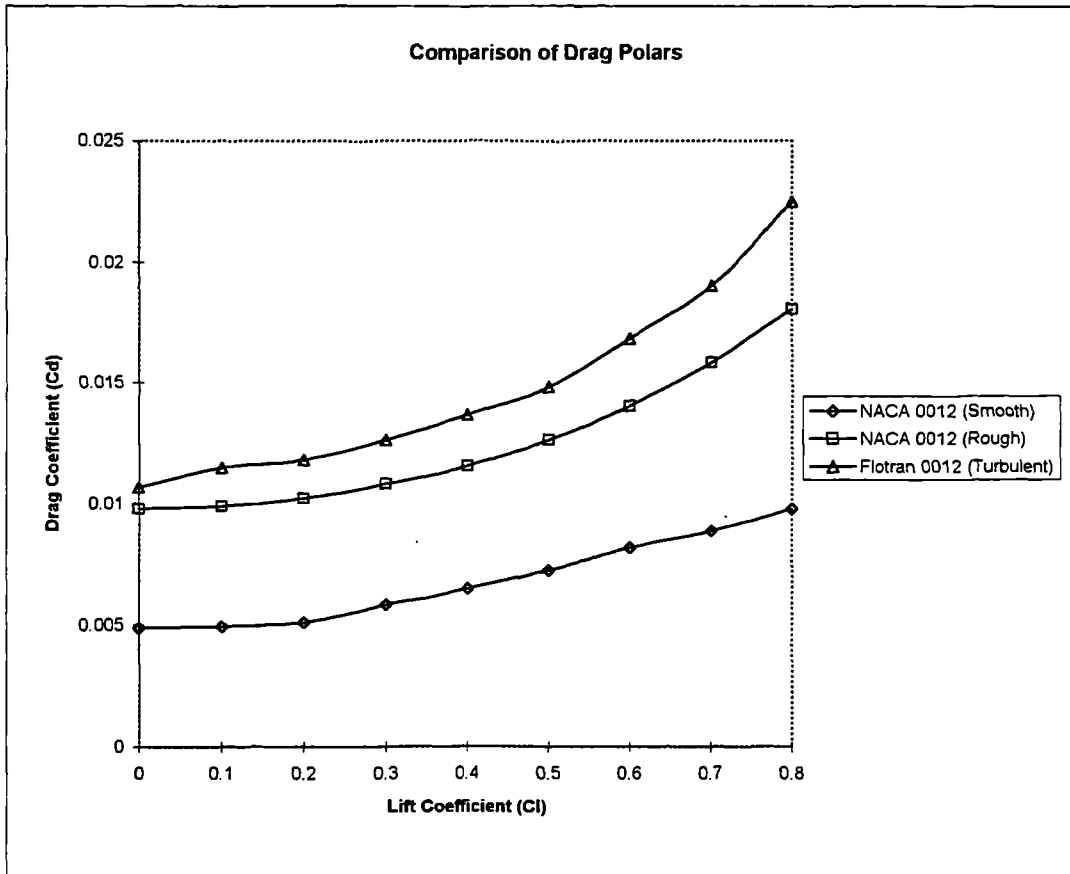
Figure 5.2

Figure 5.3

Figure 5.4

157
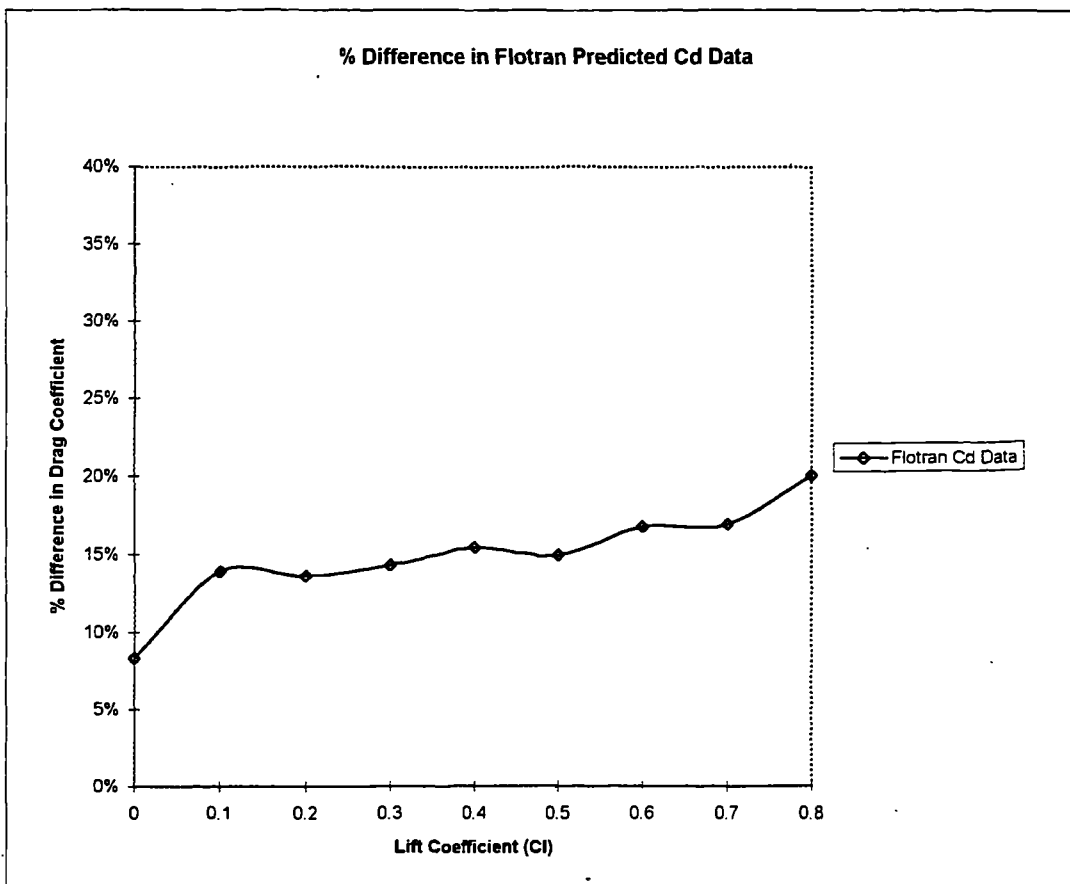
Figure 5.5   Effect of Reynolds Number on Drag of NACA Sections

158

Figure 5.6

Figure 5.7
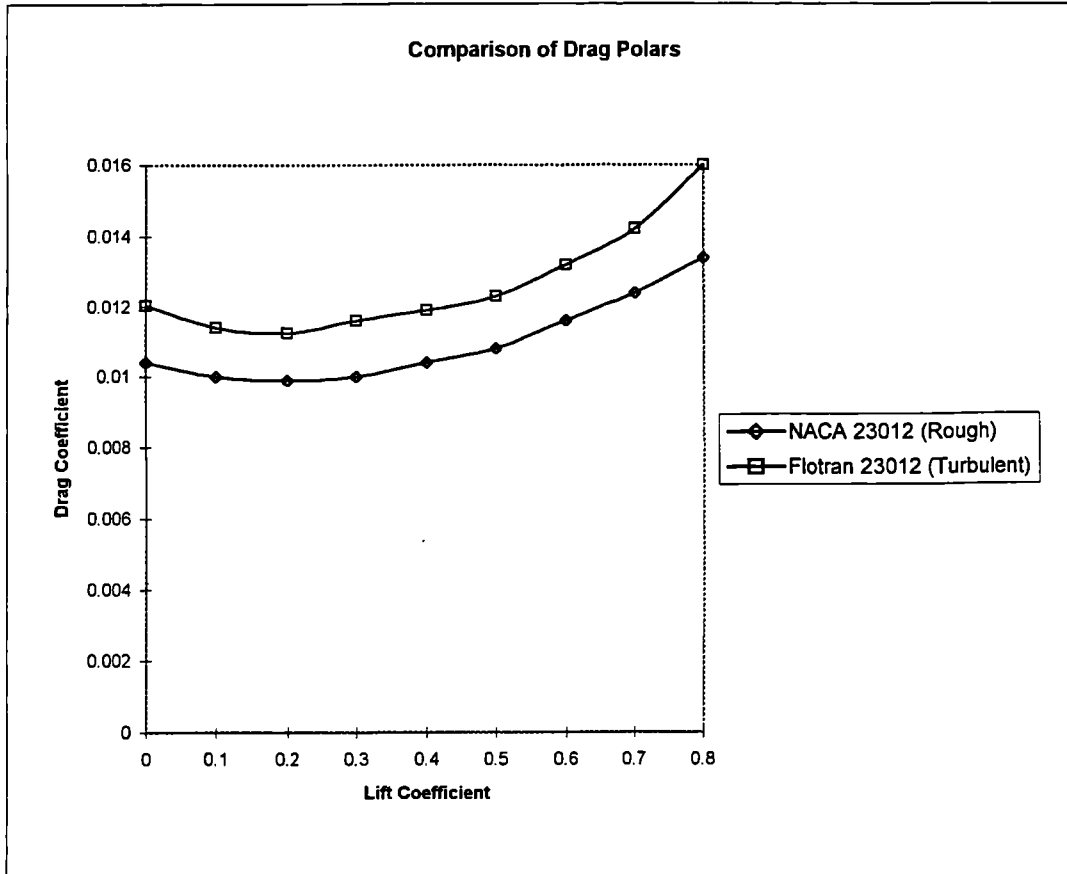
Figure 5.8
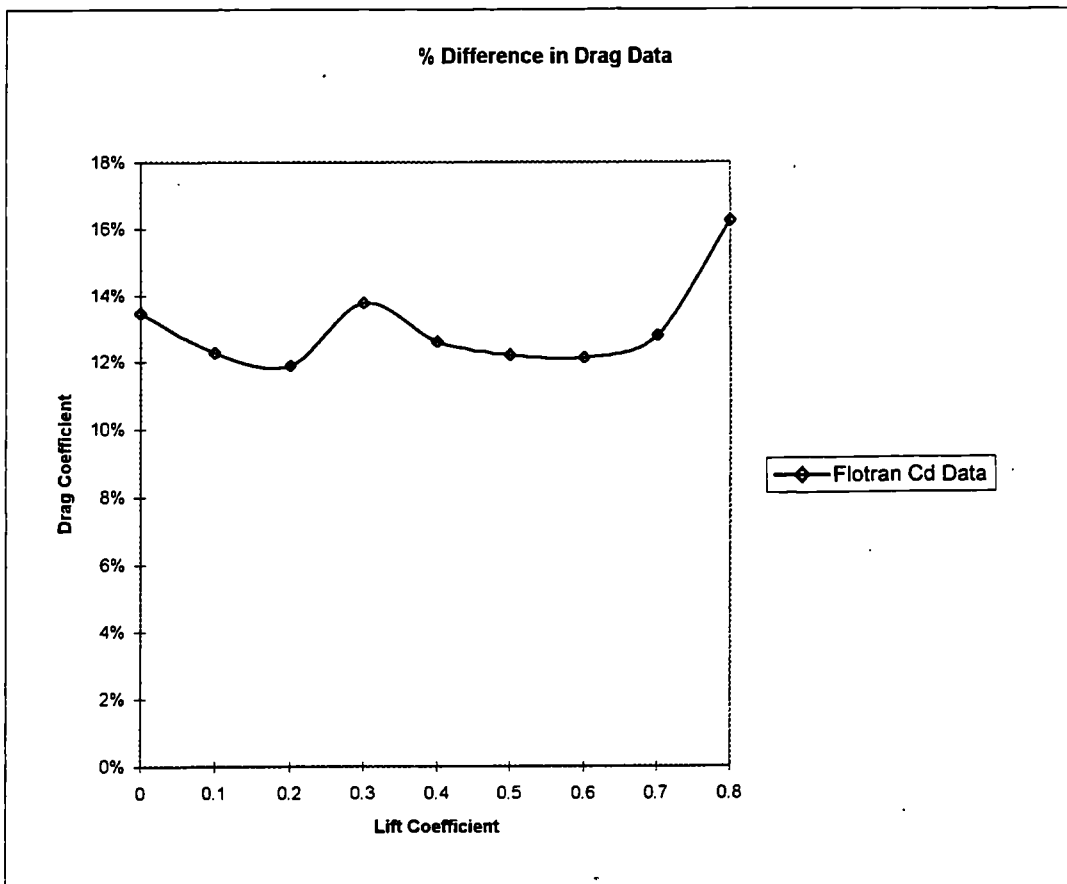
Figure 5.9

Figure 5.10

Figure 5.11

161
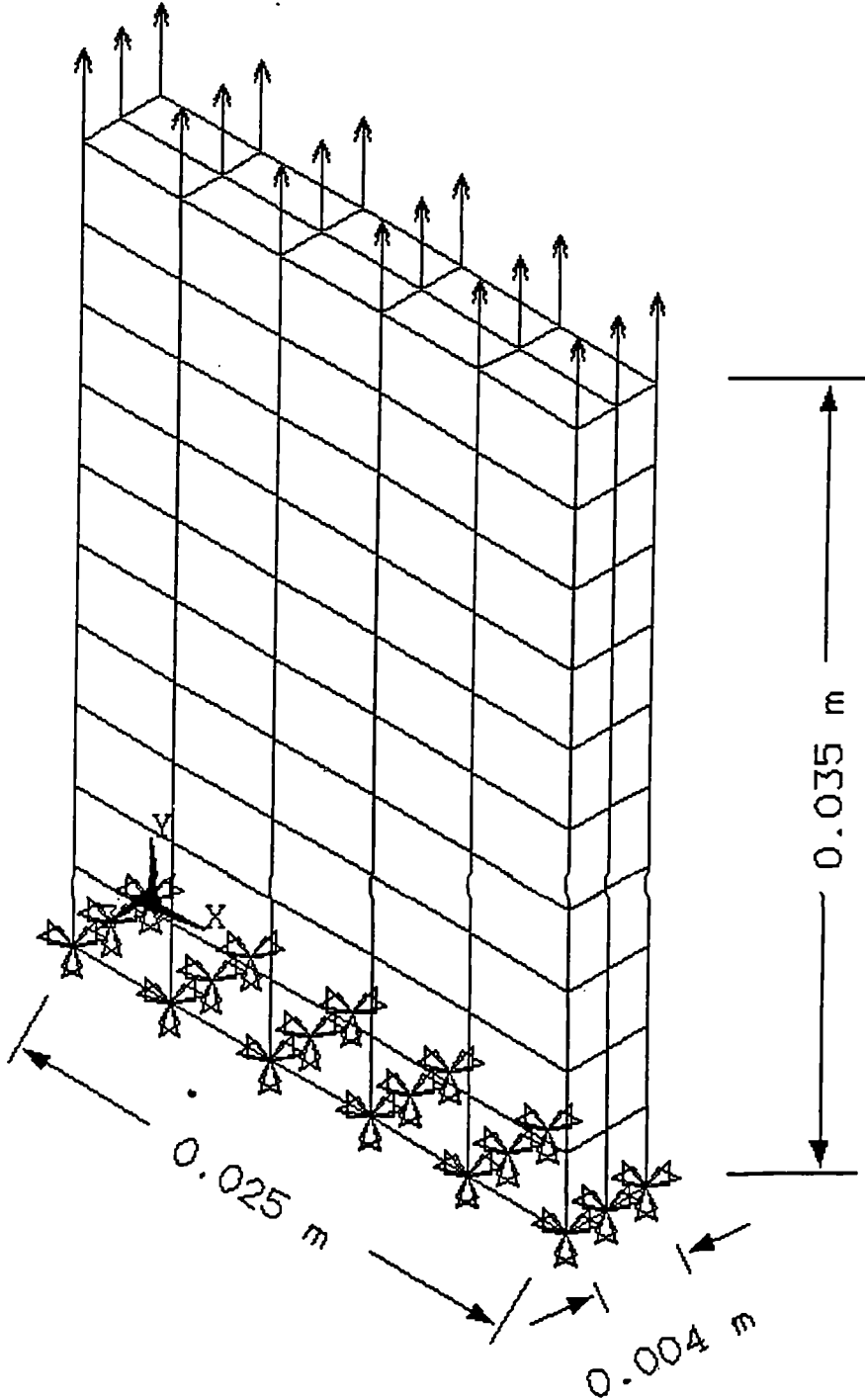
Figure 5.12   FEA Model of Elastomer Test Piece

162

Figure 5.13

FORCE (P)

$$Y_b = \frac{PL^3}{384\,EI}$$

BEAM A

$$I = \frac{bh^3}{12}$$

FORCE (P)

BEAM B

$$Y_b = \frac{PL^3}{185\,EI}$$
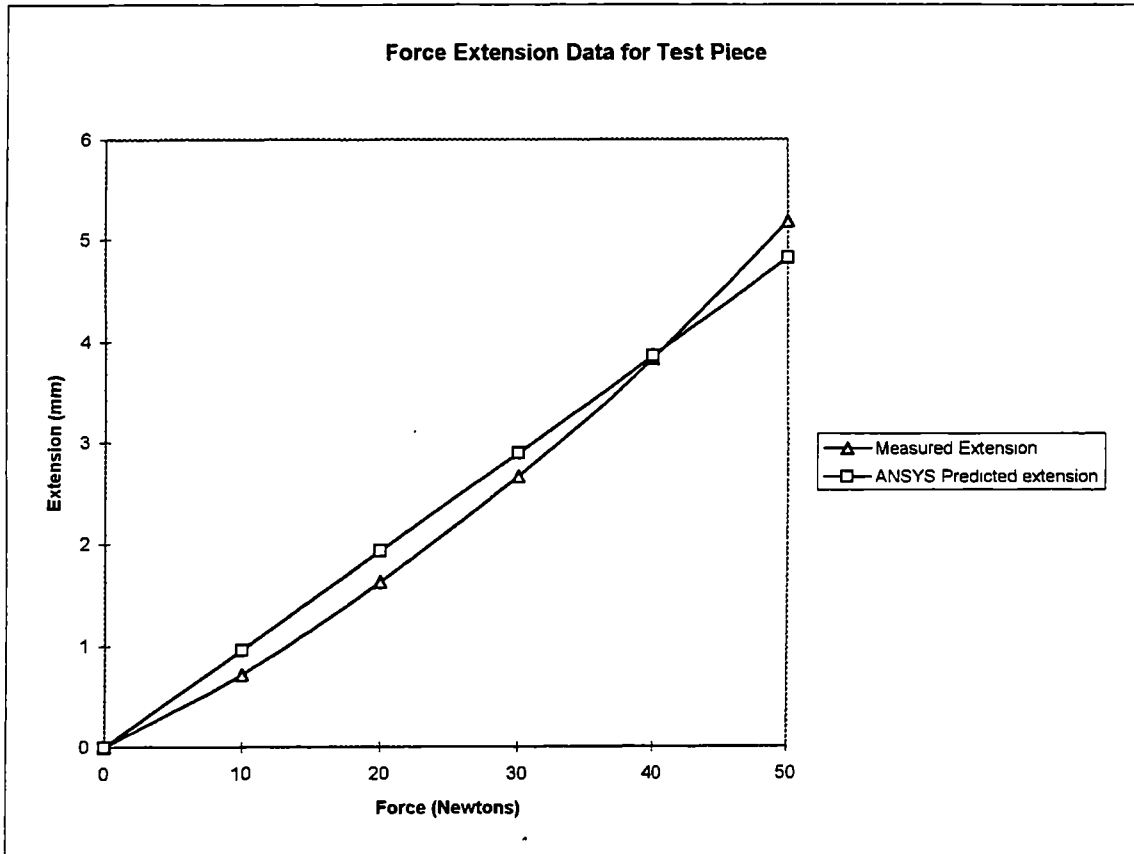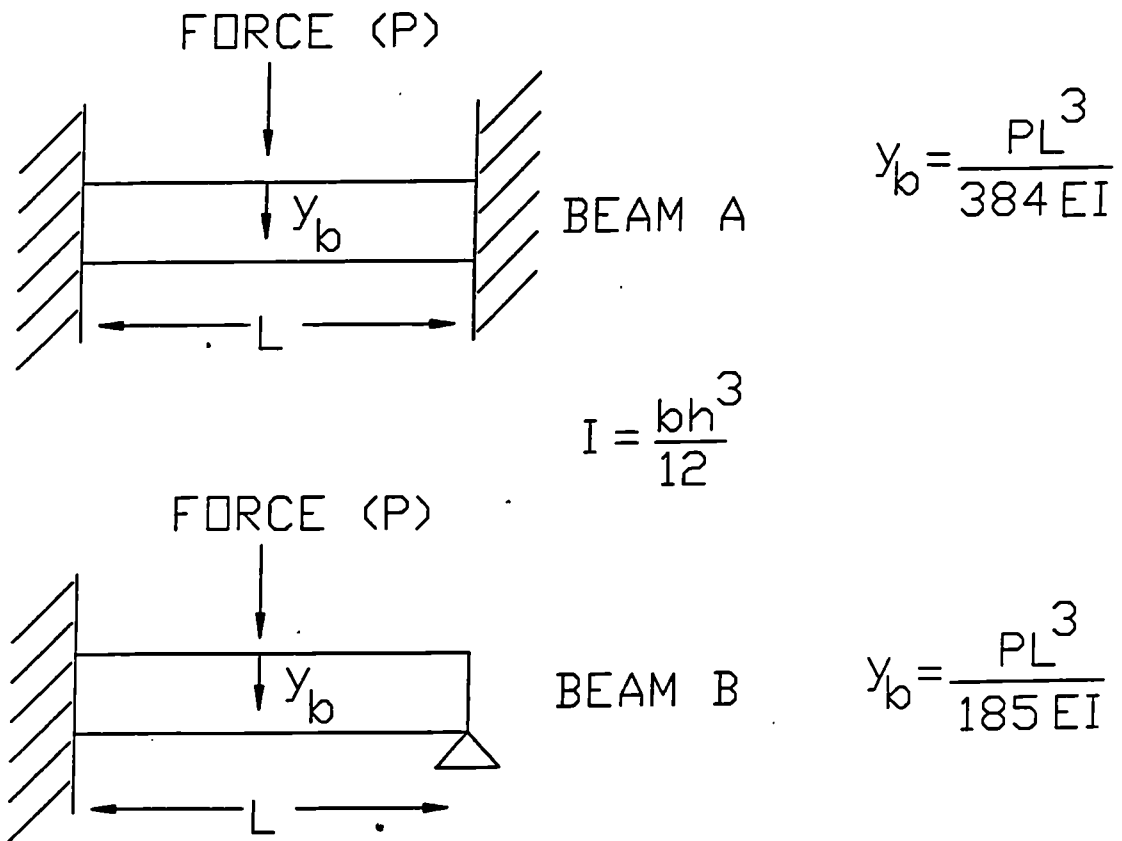
Figure 5.14   Classical Beam Theory
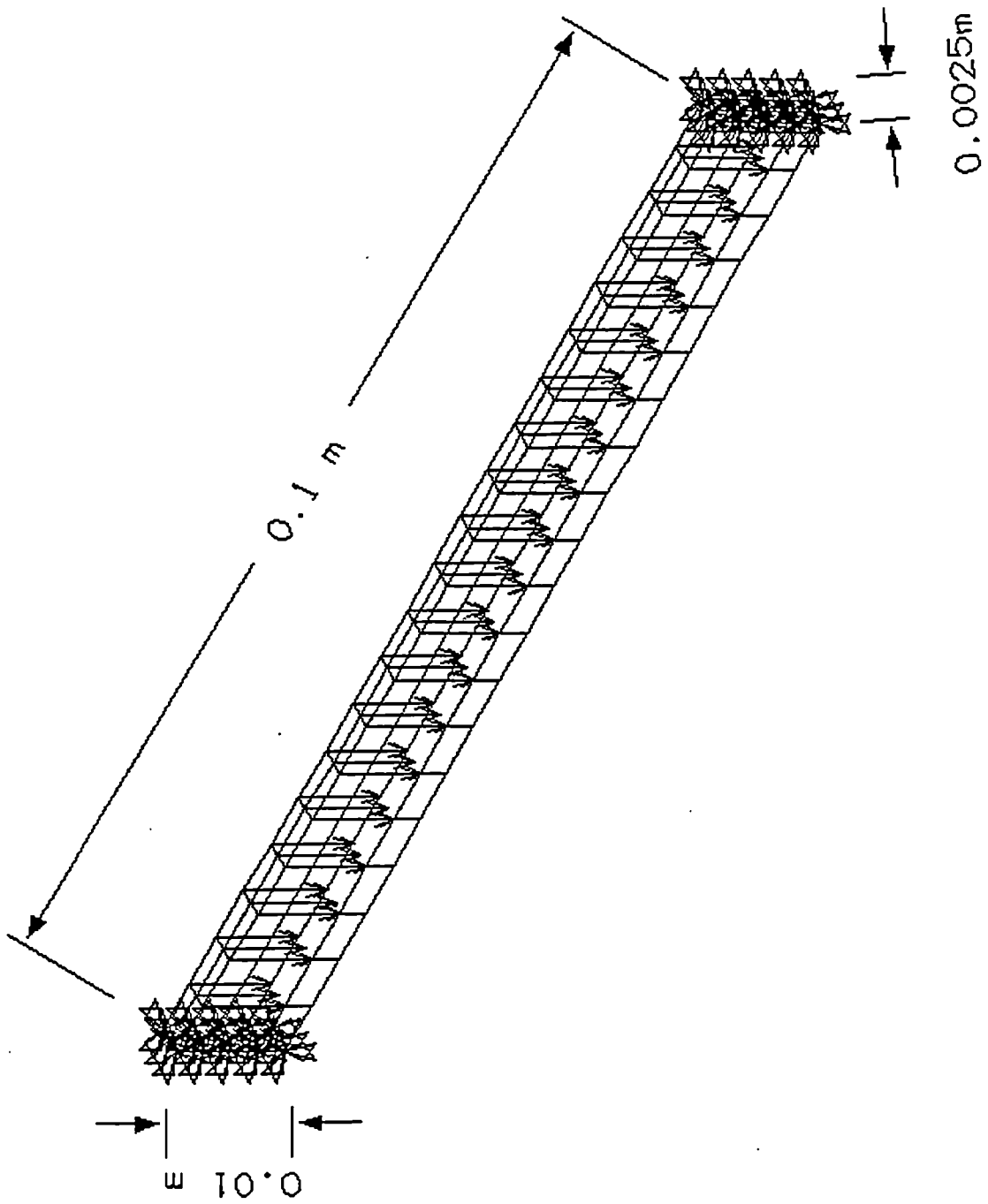
Figure 5.15 FEA Model of Beam
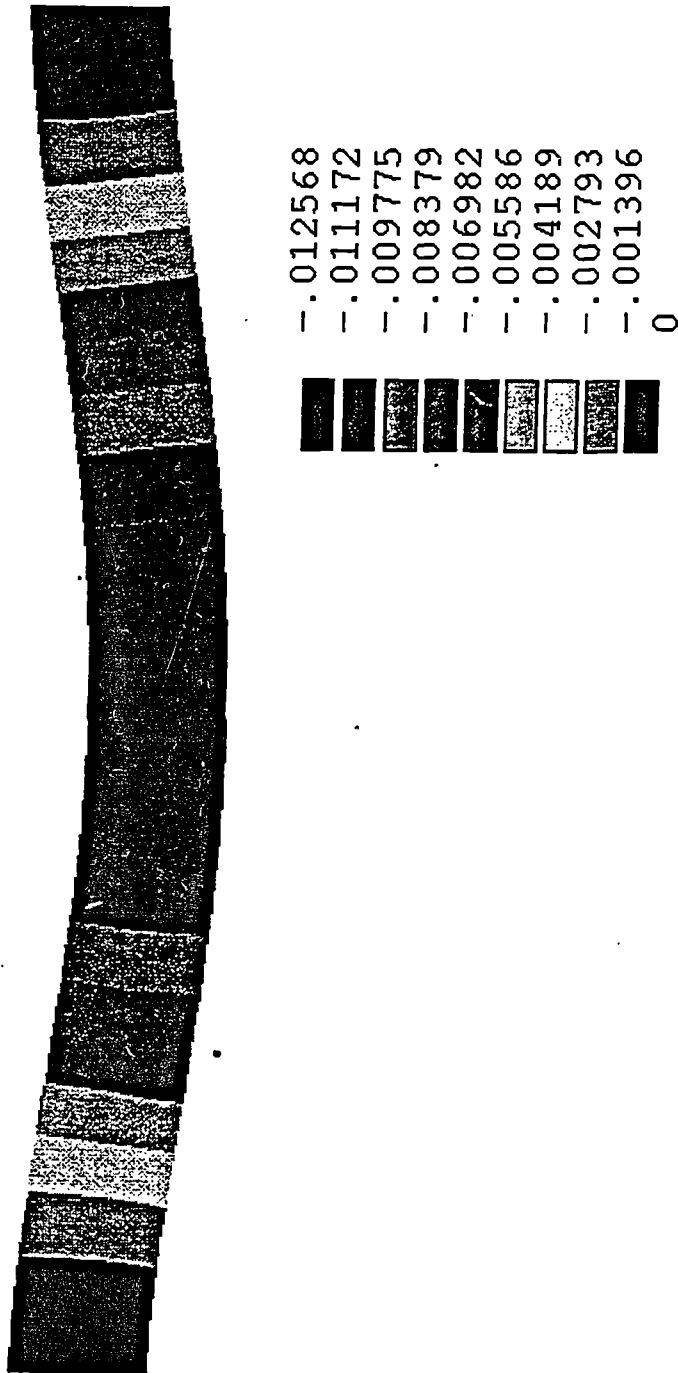
Figure 5.16   Beam A Predicted Deformation
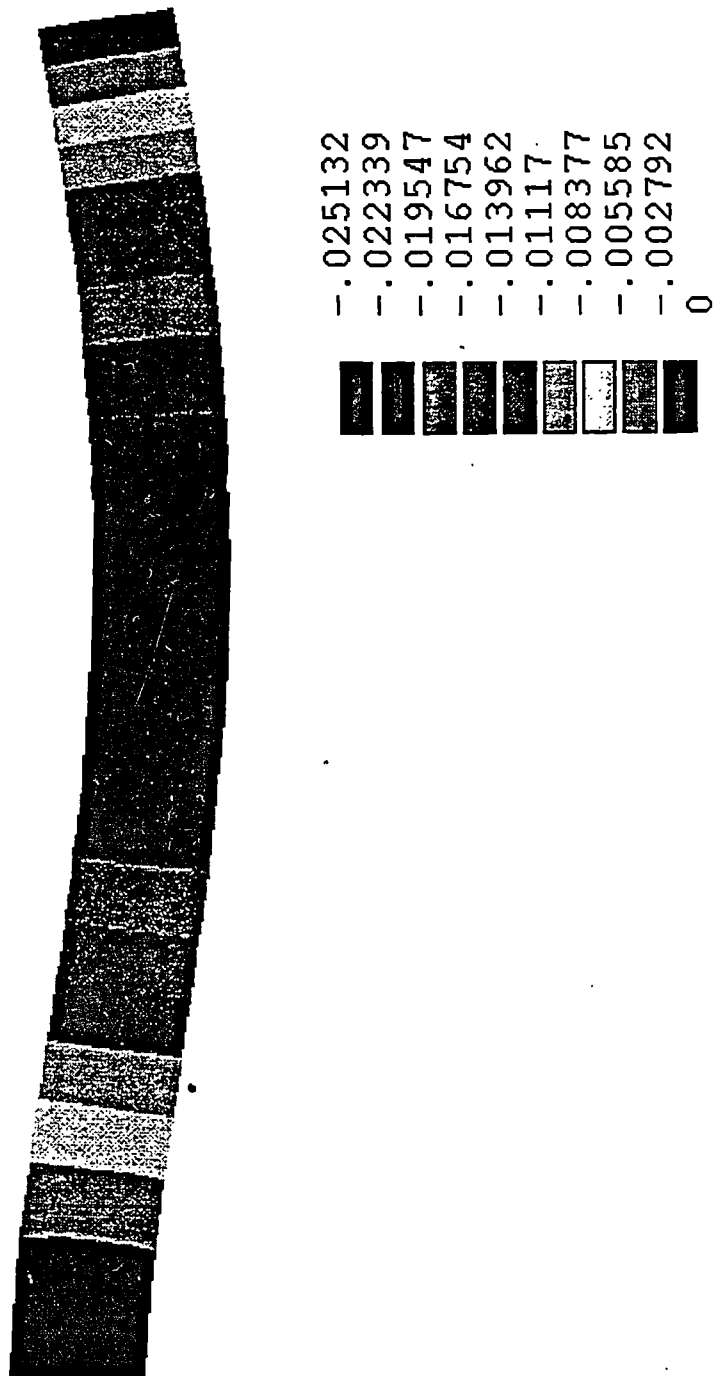
Figure 5.17   Beam B Predicted Deformation
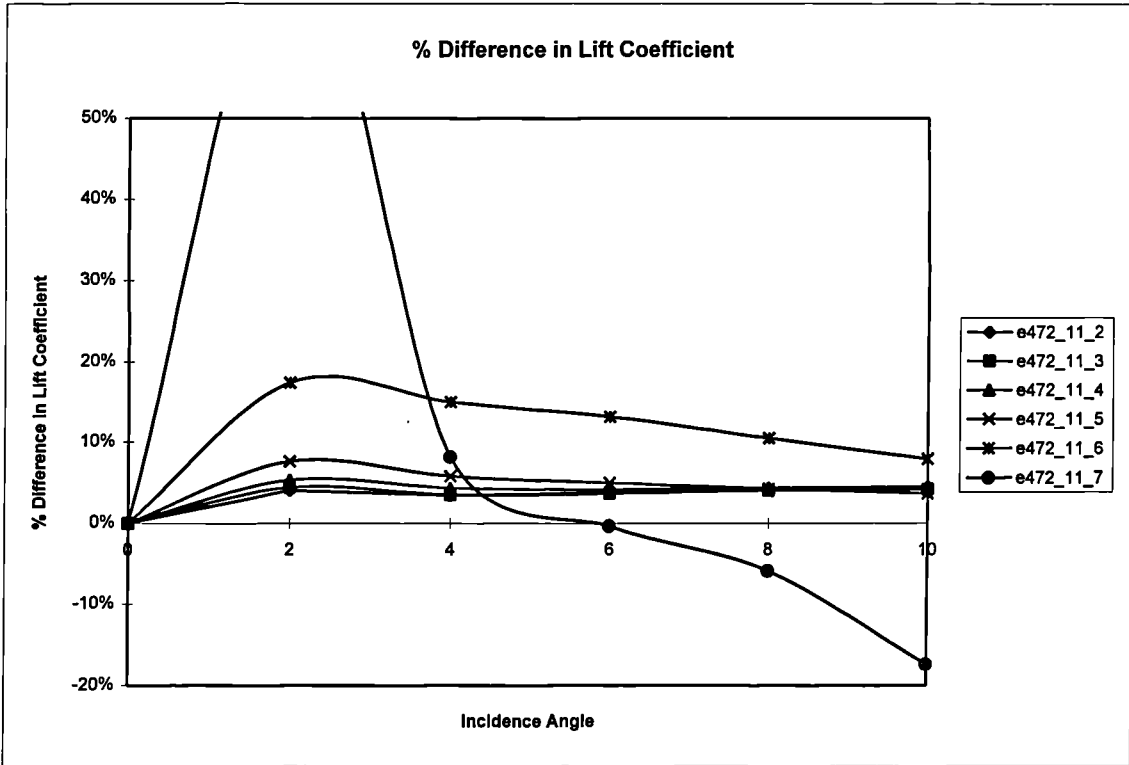
Figure 5.18
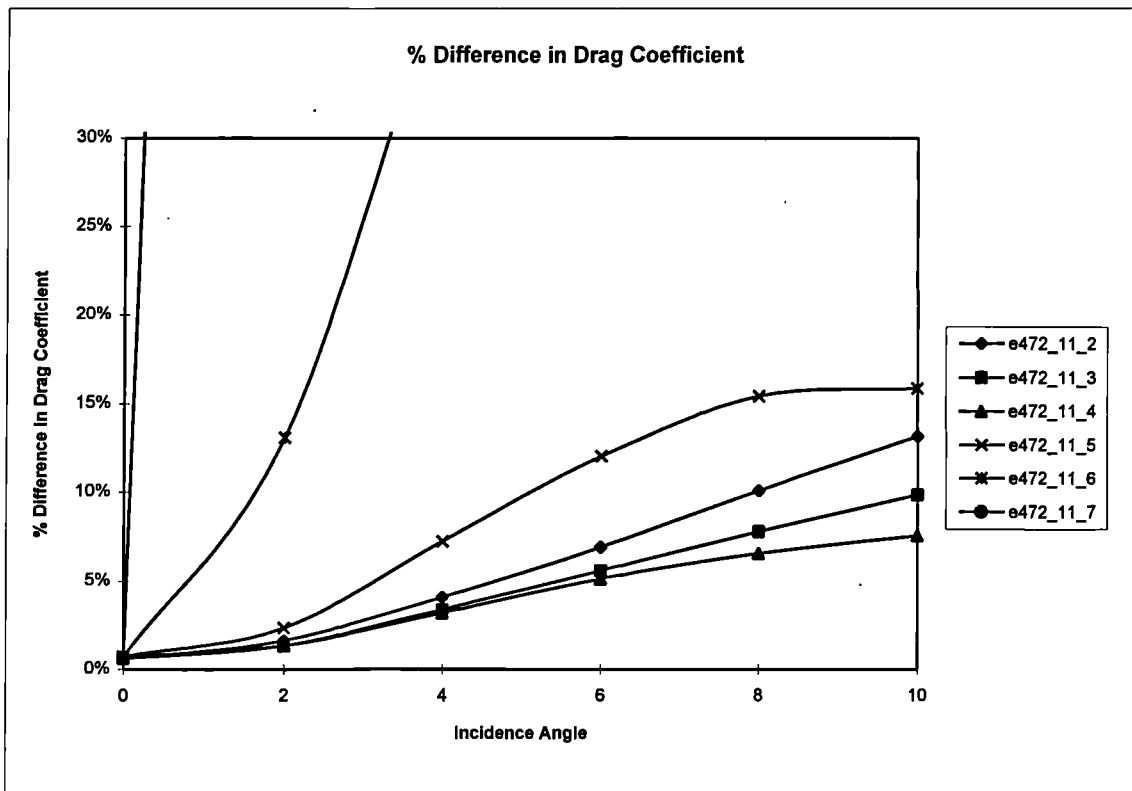
Figure 5.19

Figure 5.20

Figure 5.21

DROOP NOSE

UPTURNED NOSE

STAGNANT NOSE

(A) NOSE MOMENT ARM < SLOT GAP MOMENT ARM

(B) NOSE MOMENT ARM > SLOT GAP MOMENT ARM

(C) NOSE MOMENT ARM = SLOT GAP MOMENT ARM
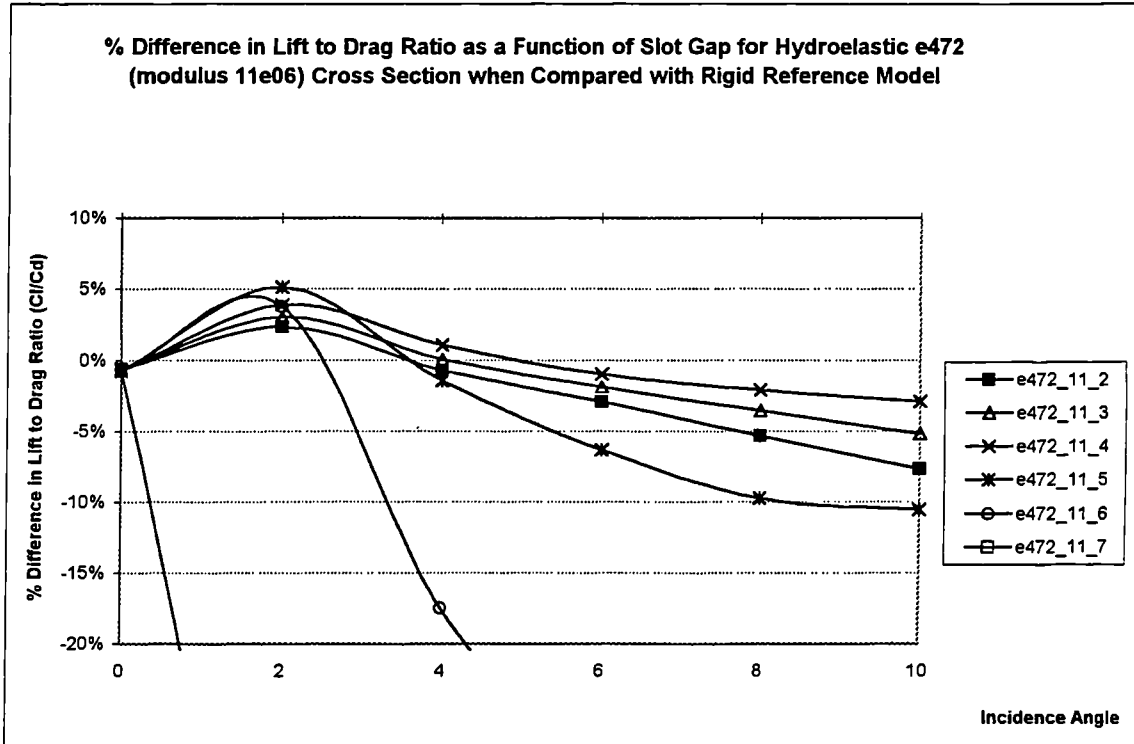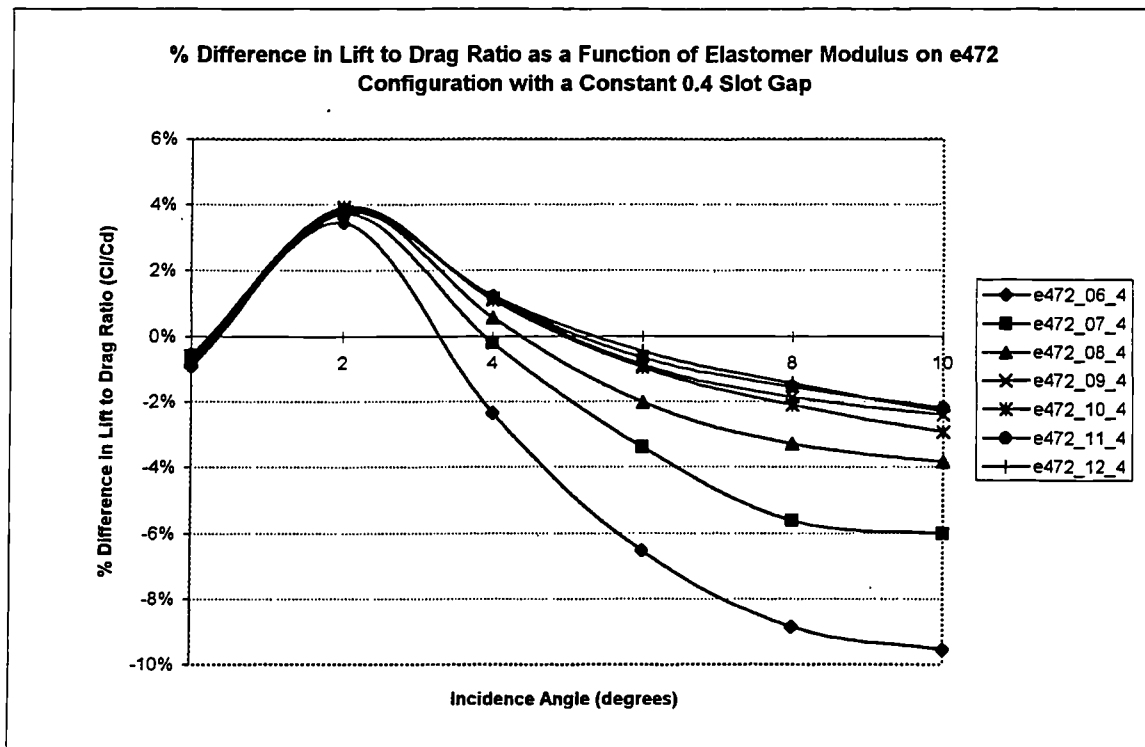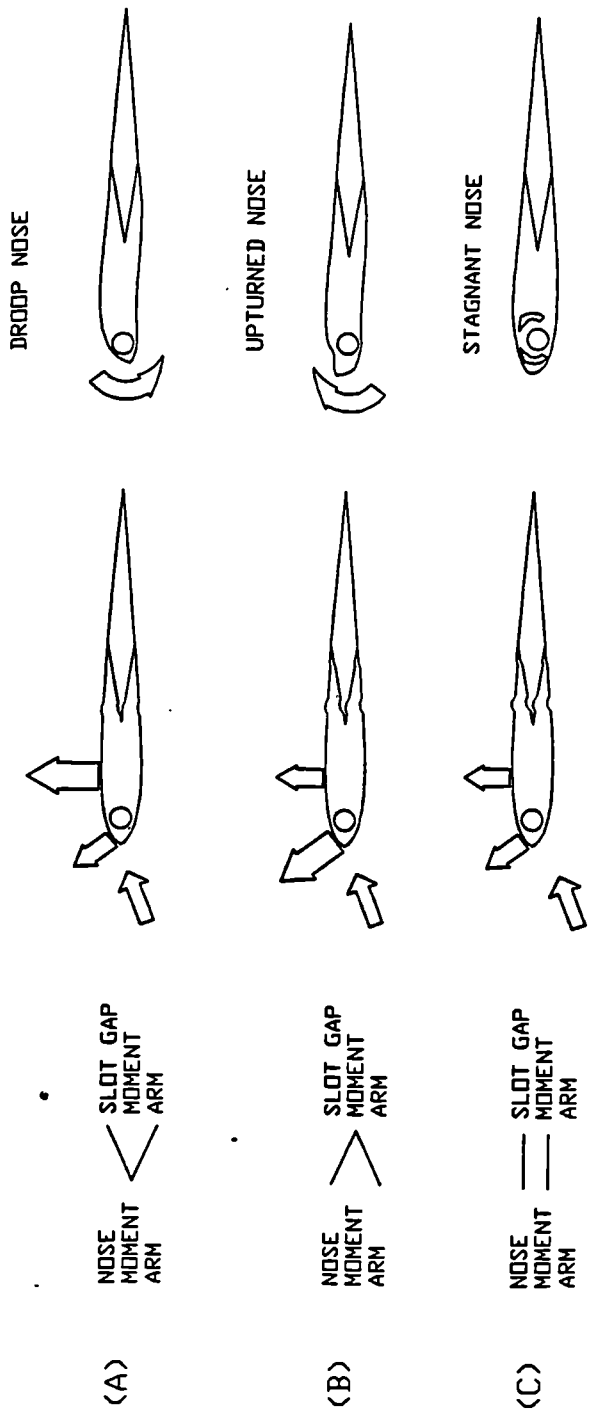
Figure 5.22 Behavior of Pivotal Nose

170
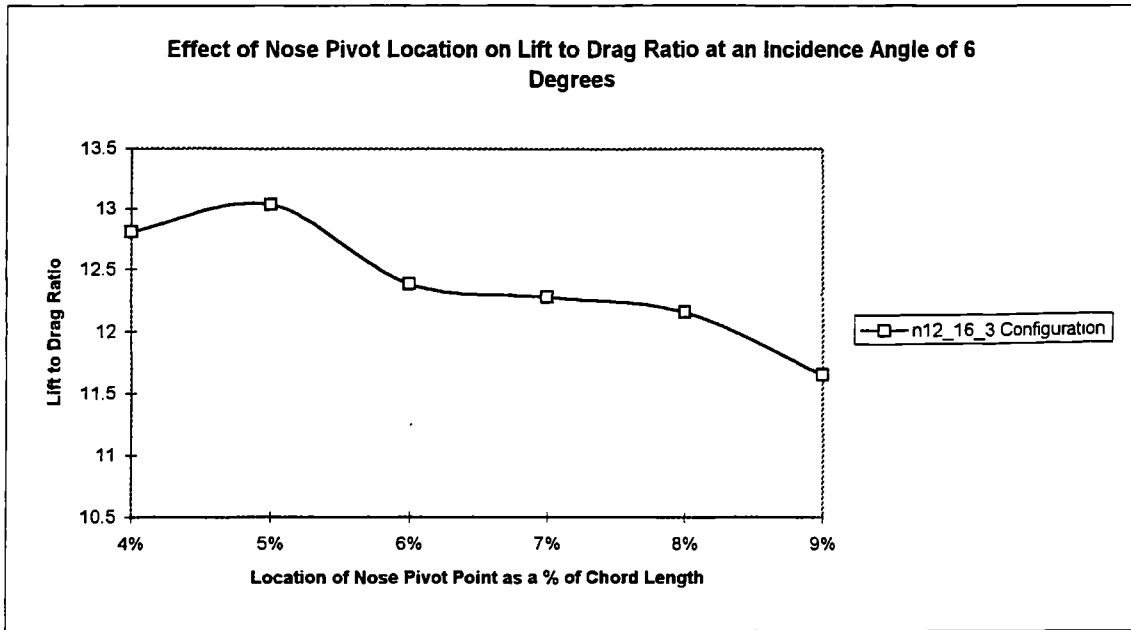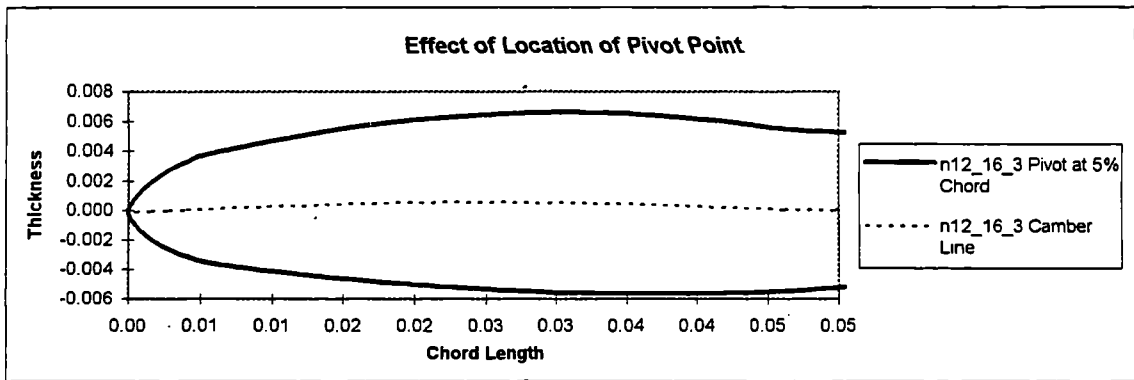
Figure 5.23

Figure 5.24

Figure 5.25

171
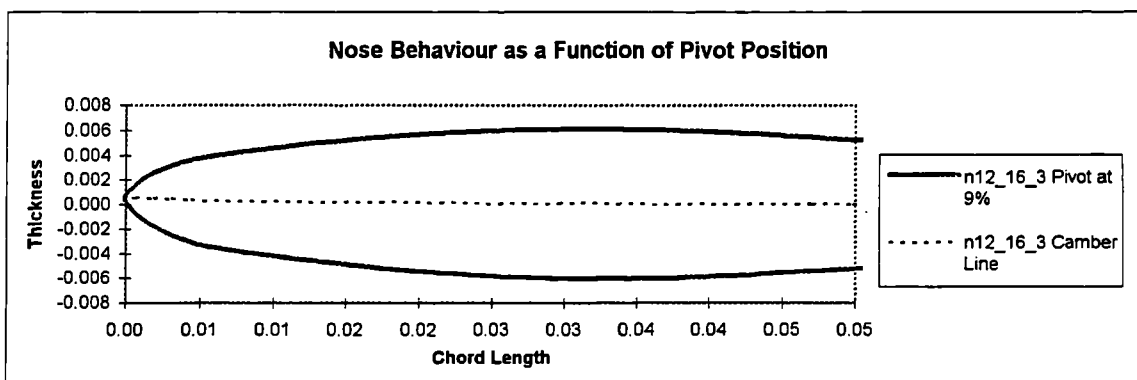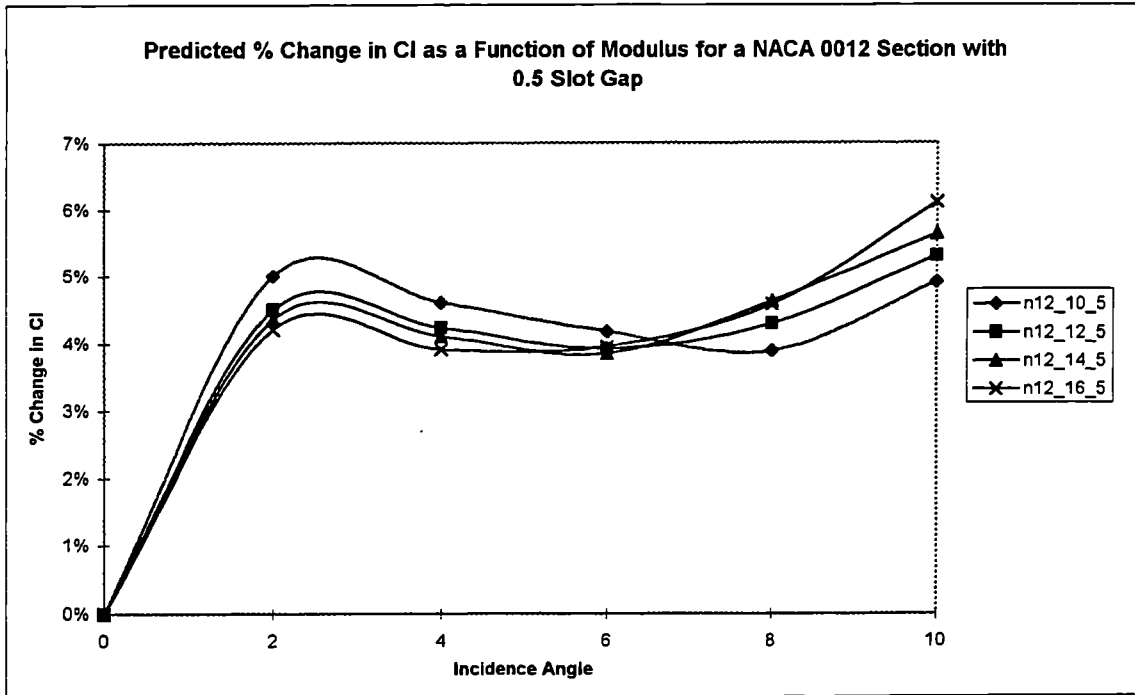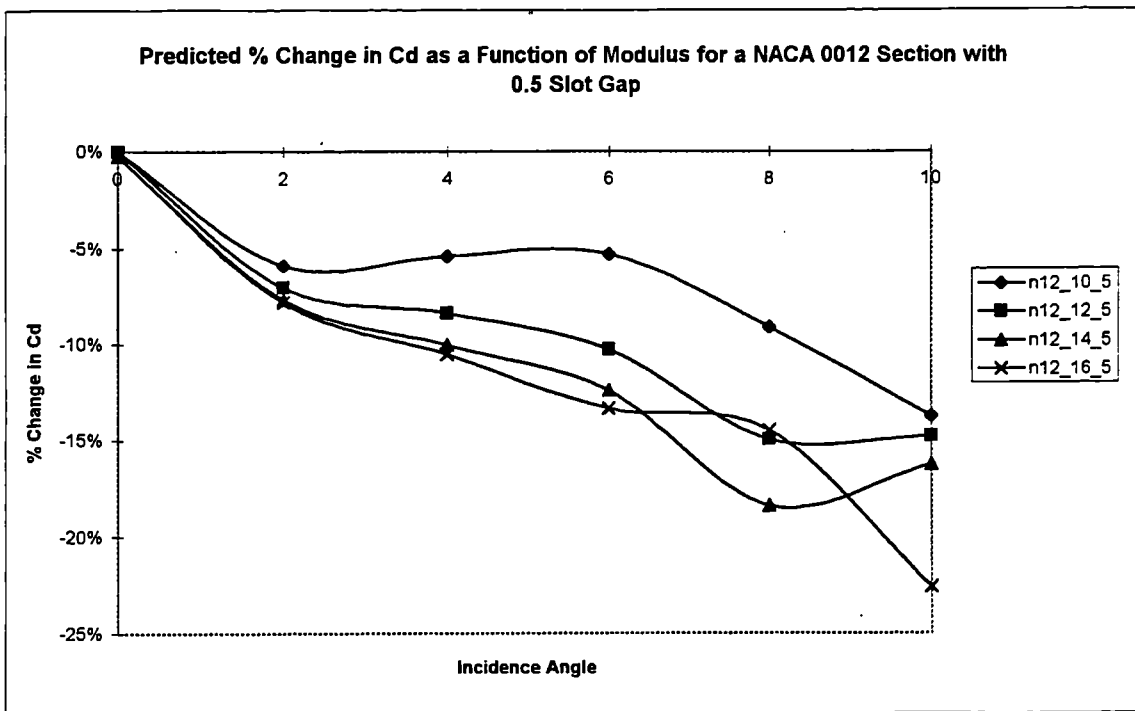
Figure 5.26

Figure 5.27
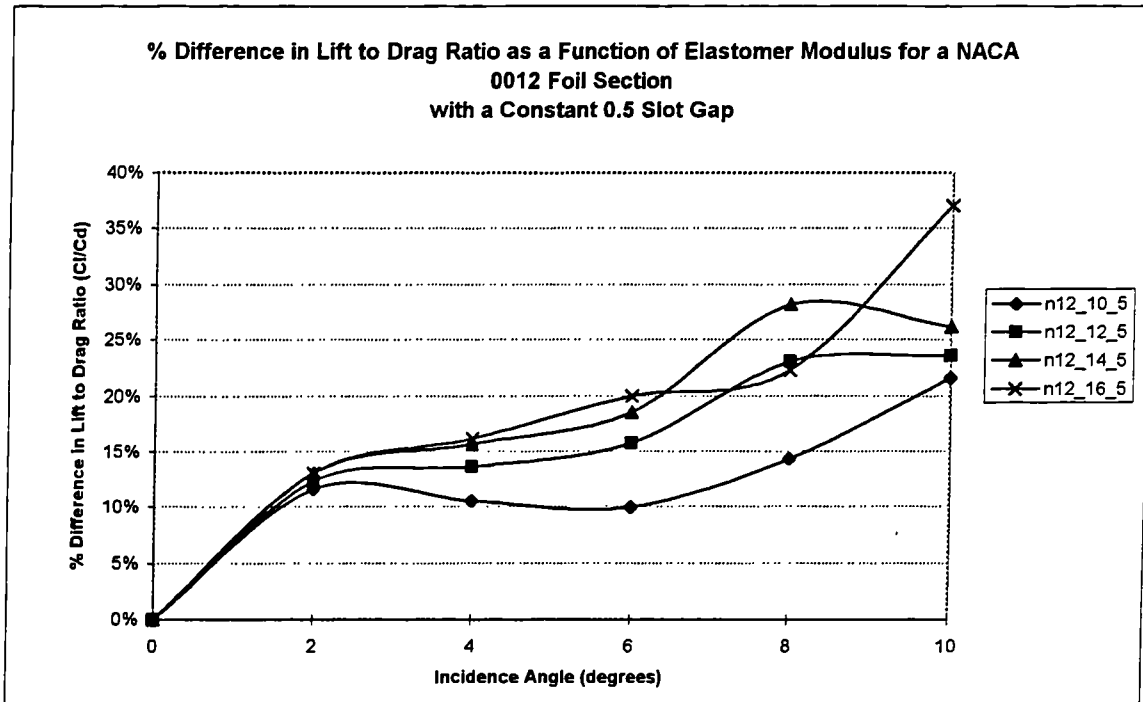
Figure 5.28

Figure 5.29

173
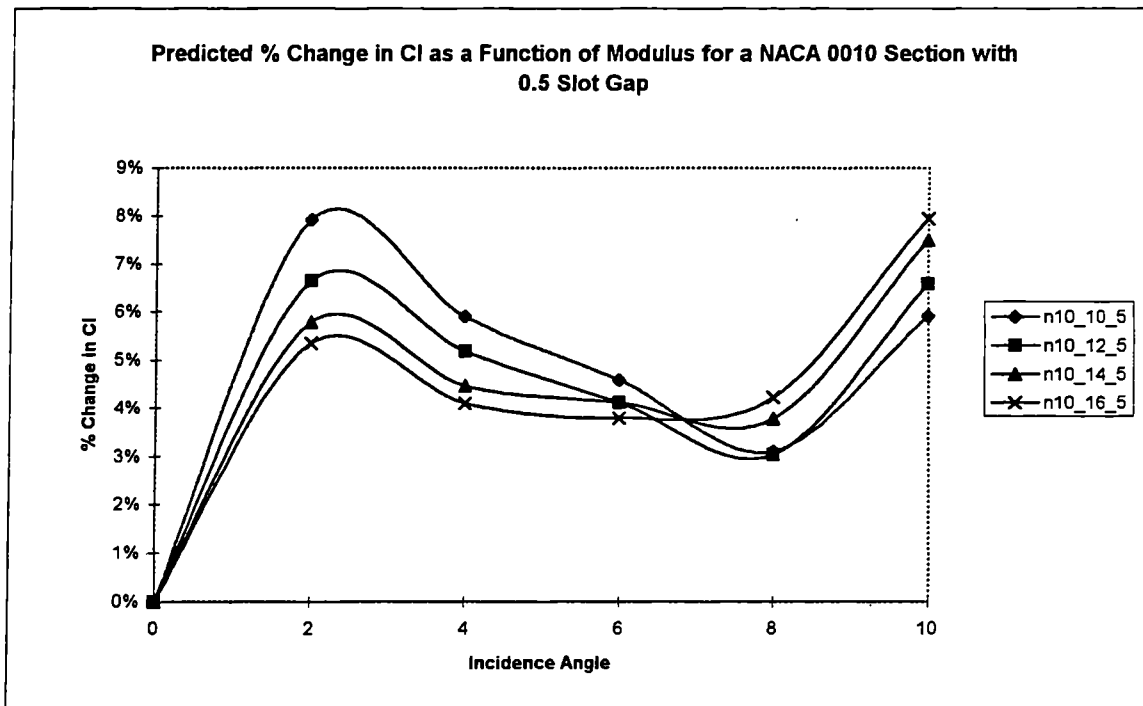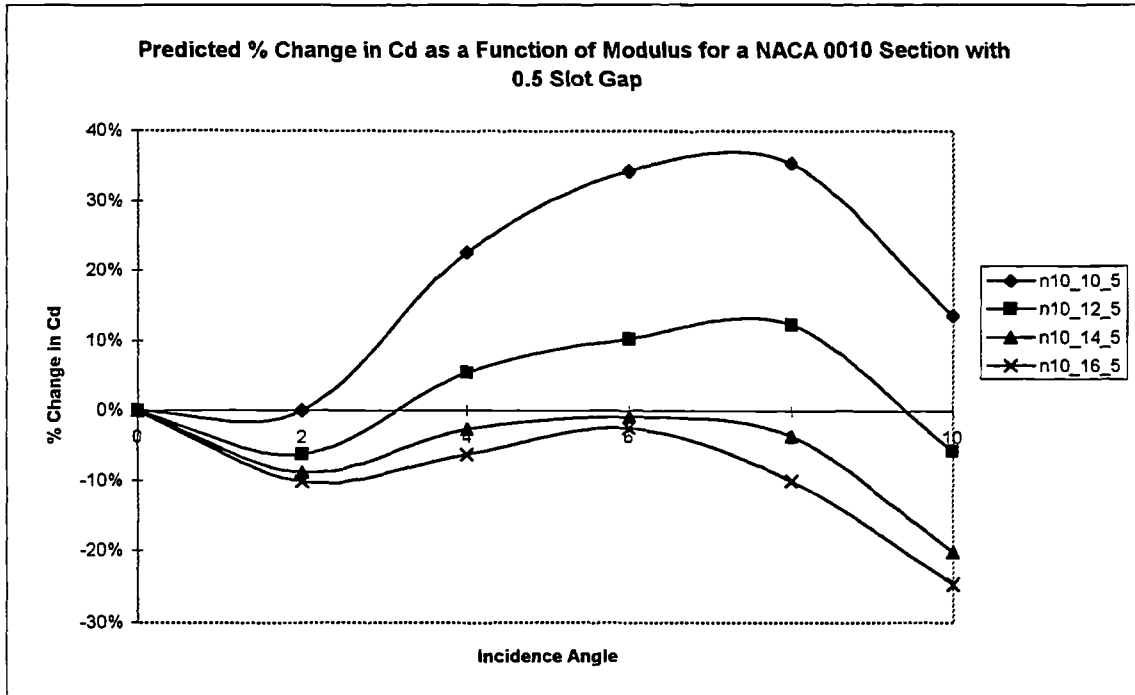
Figure 5.30

Figure 5.31

174

Figure 5.32

Figure 5.33

% Difference in Lift to Drag Ratio as a Function of Elastomer Modulus for a NACA 008 Foil Section with a Constant 0.5 Slot Gap

Figure 5.34

Predicted % Change in Cl as a Function of Modulus for a NACA 0012 Section with 0.4 Slot Gap

Figure 5.35

176
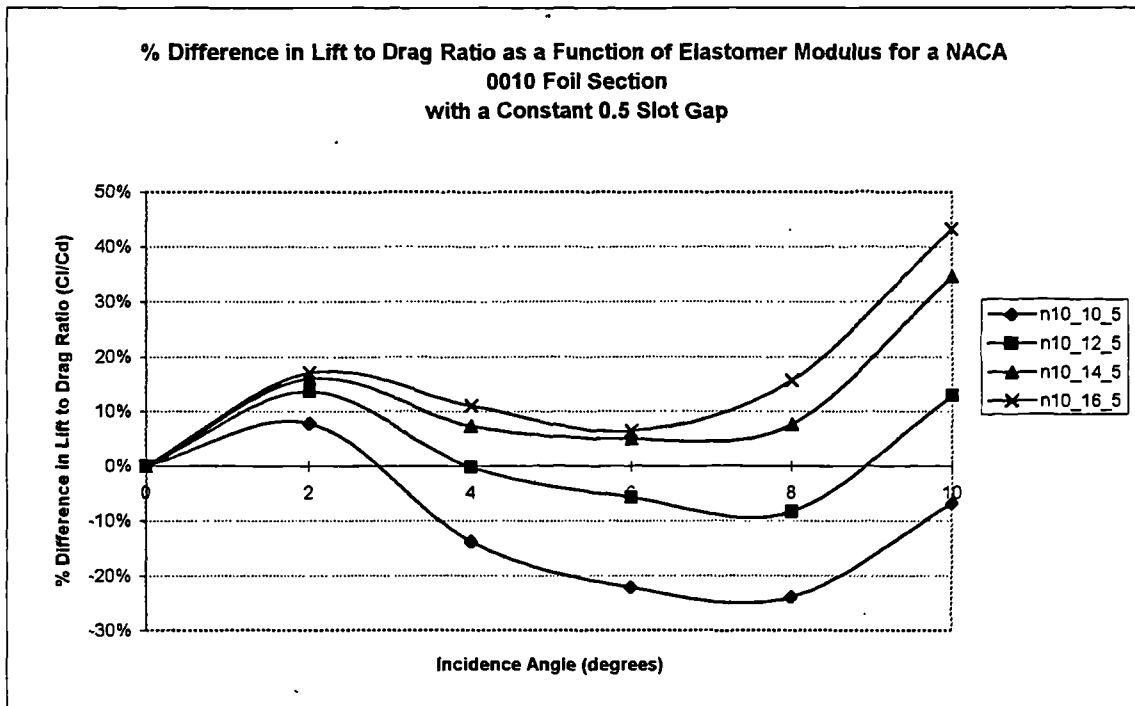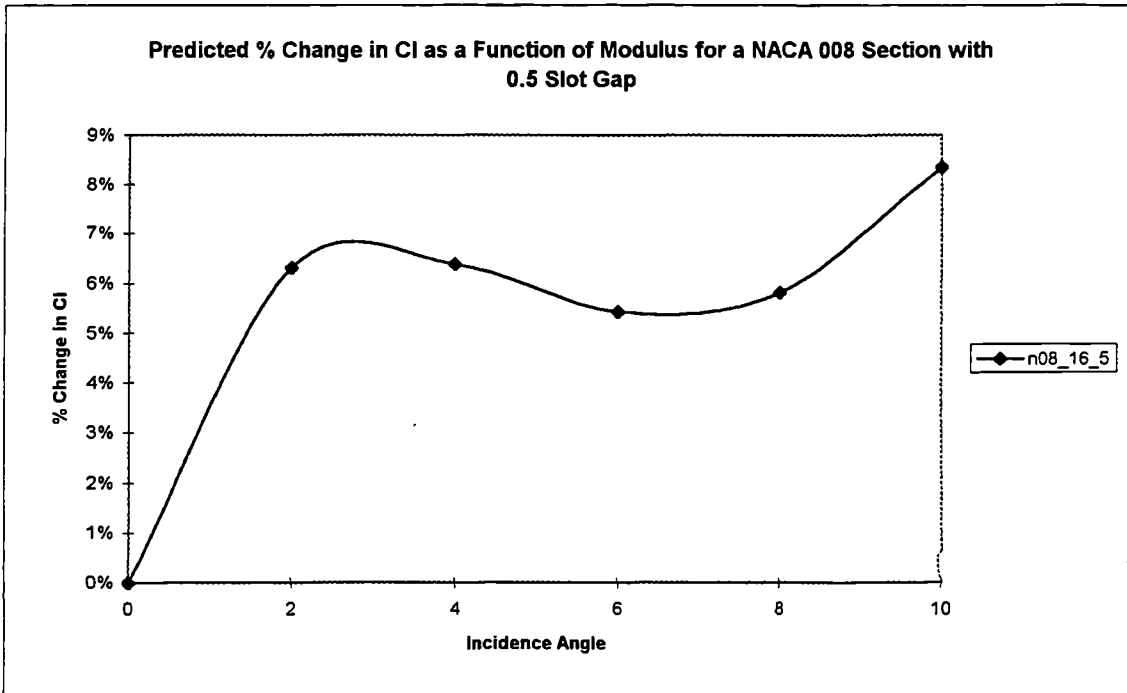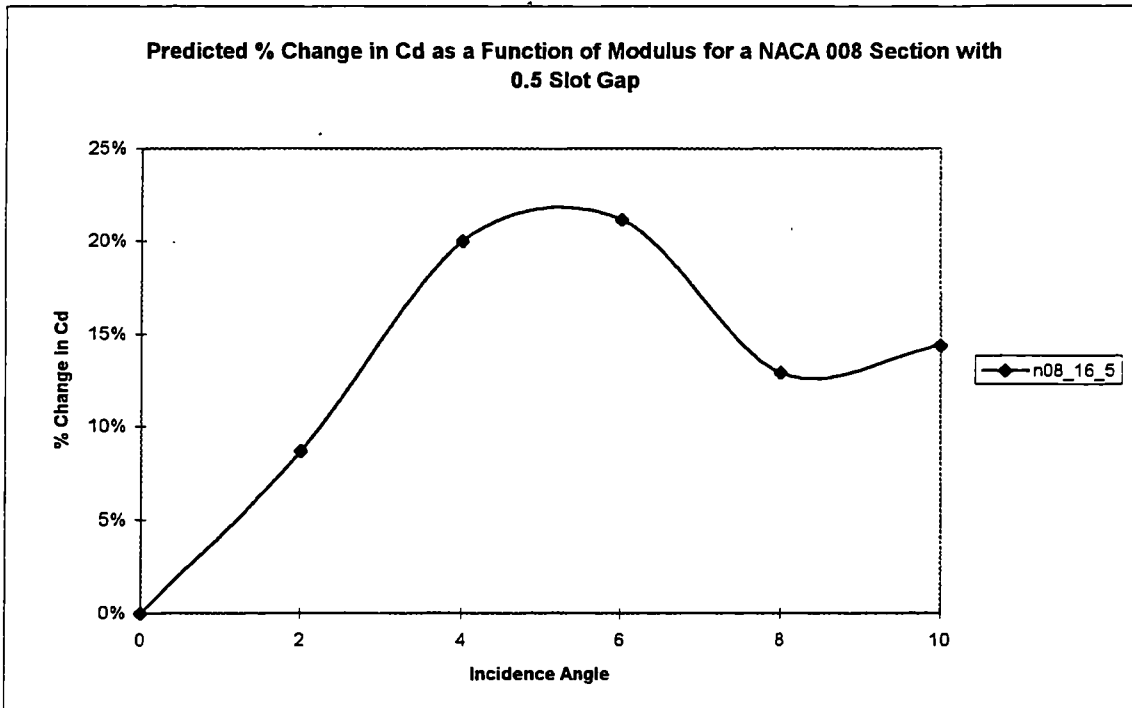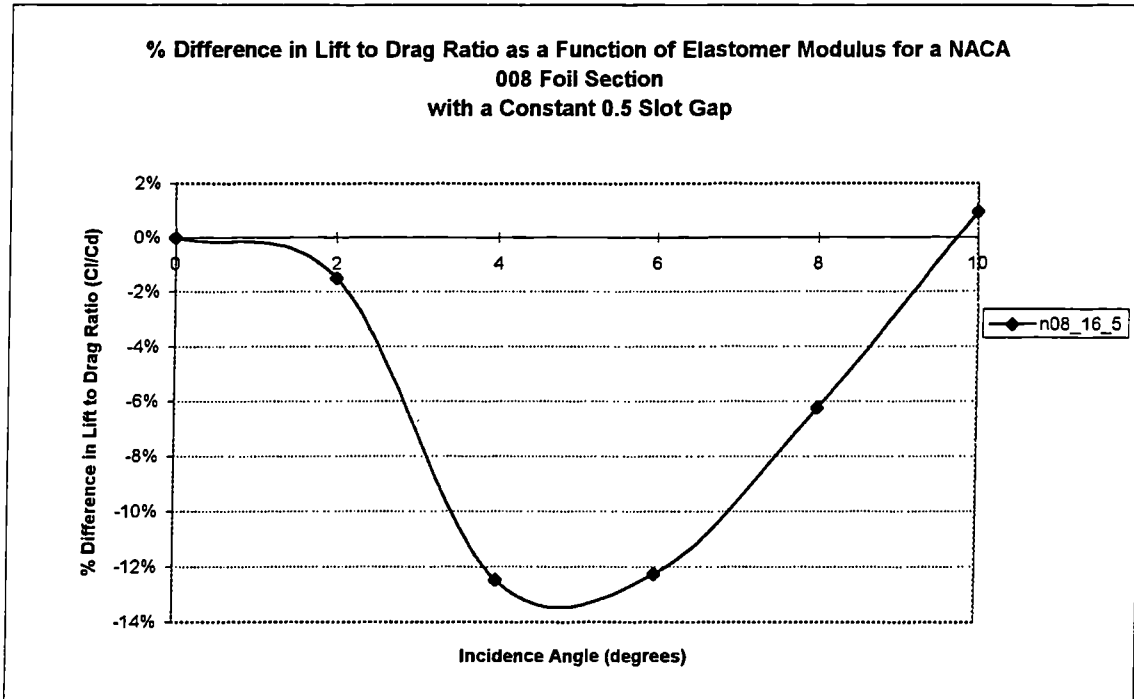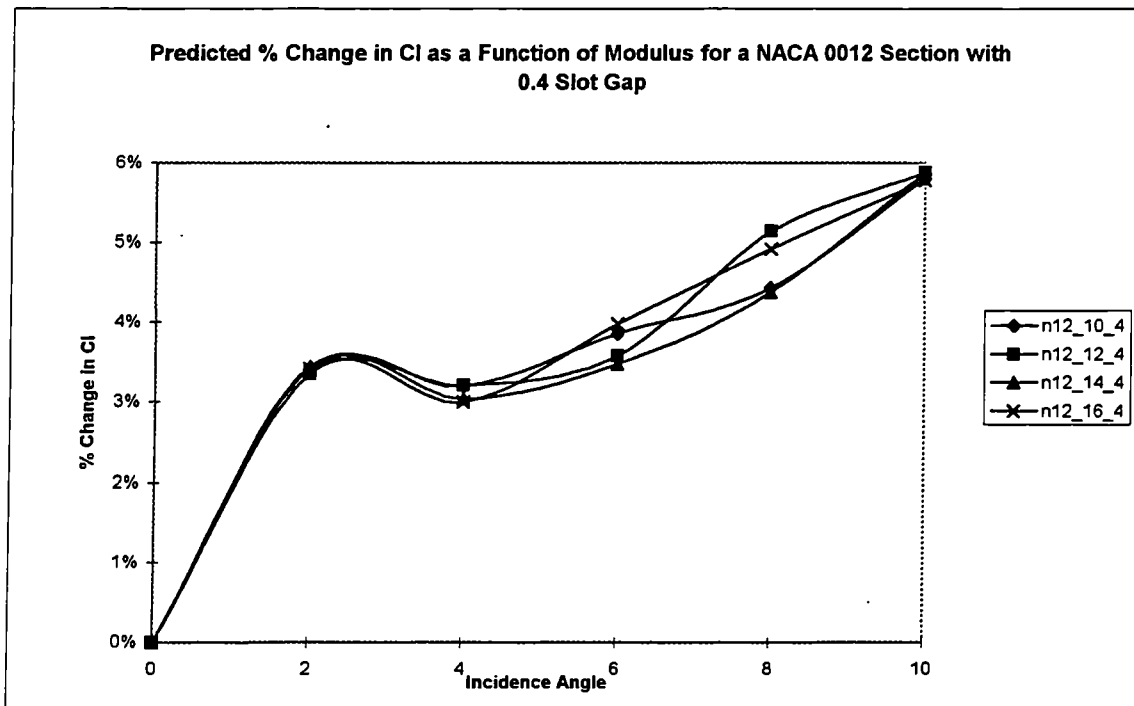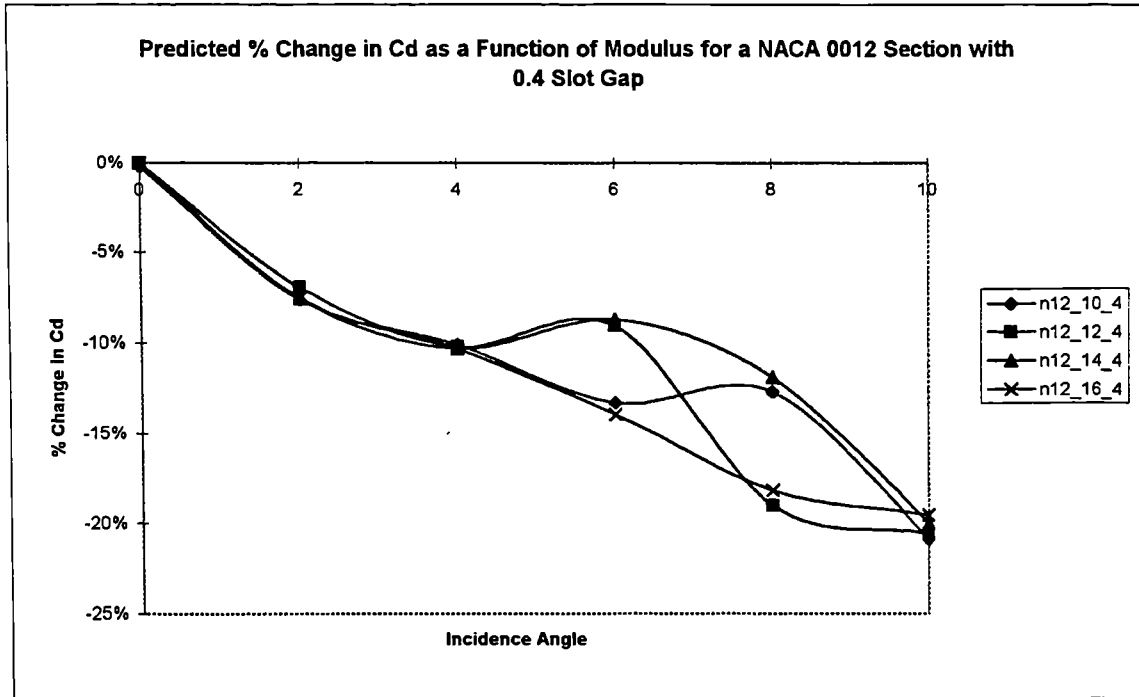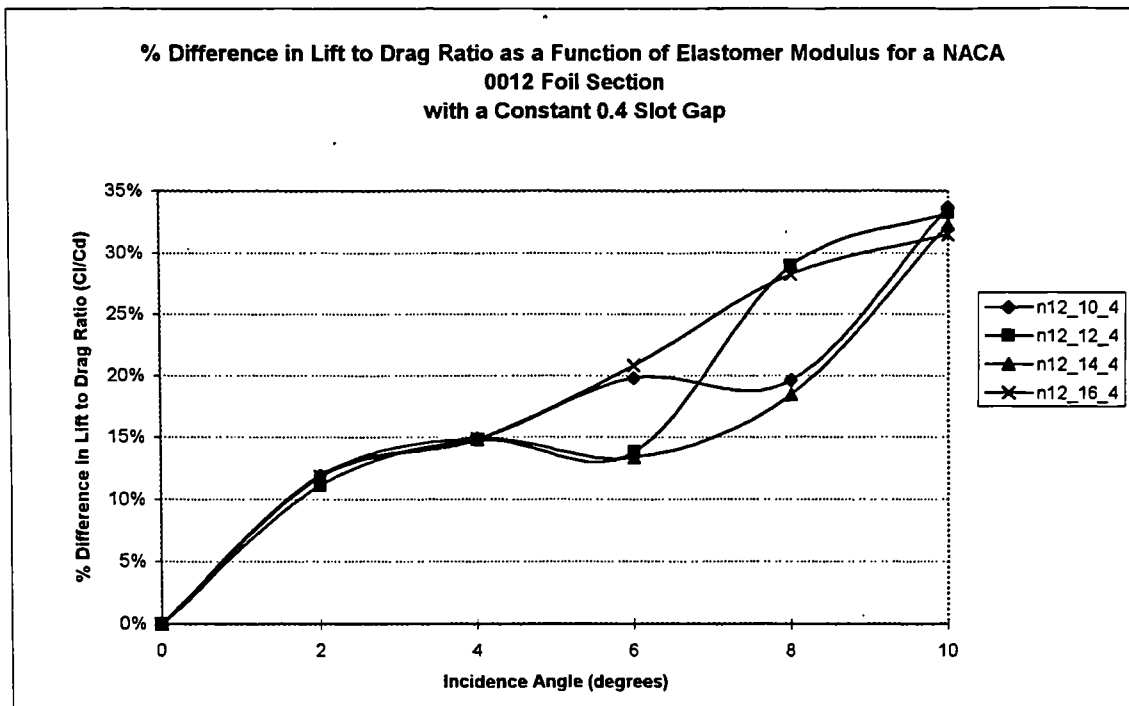
Figure 5.36
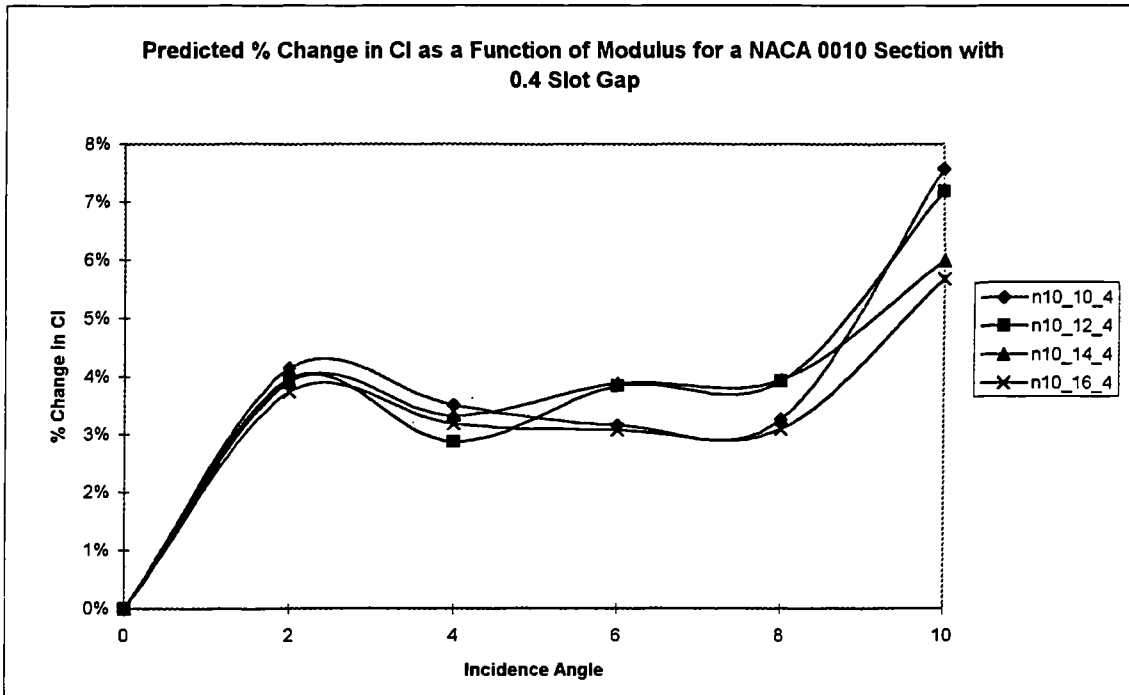
Figure 5.37

Figure 5.38
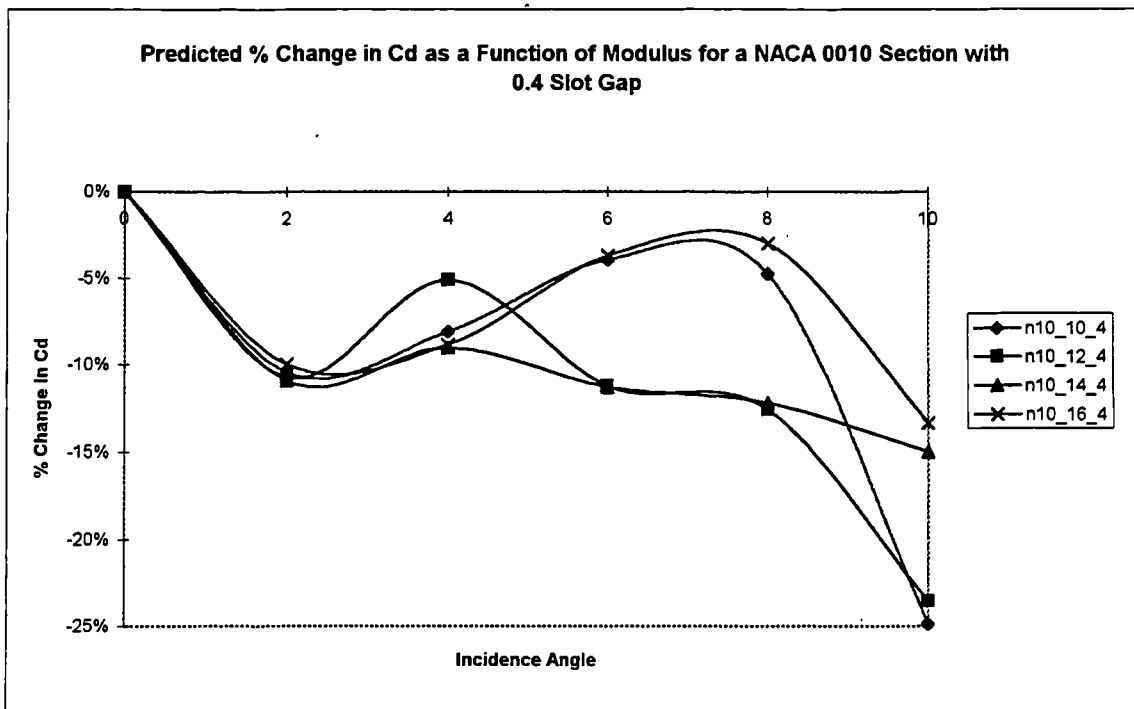
Figure 5.39
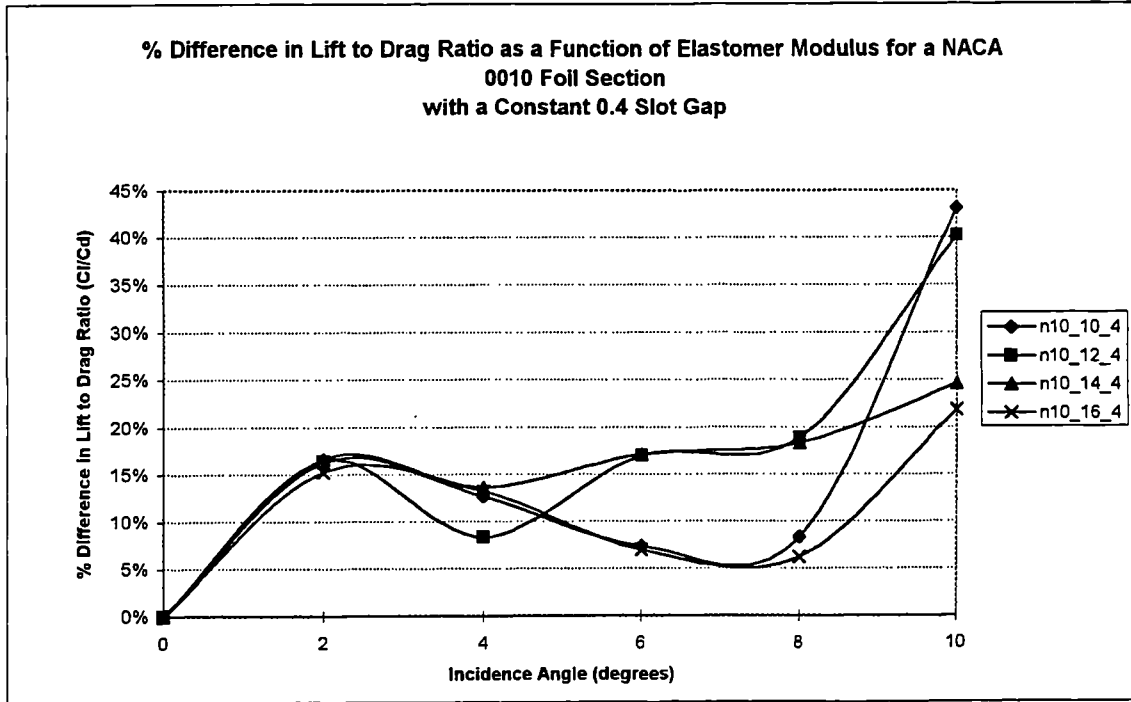
Figure 5.40

Figure 5.41

179
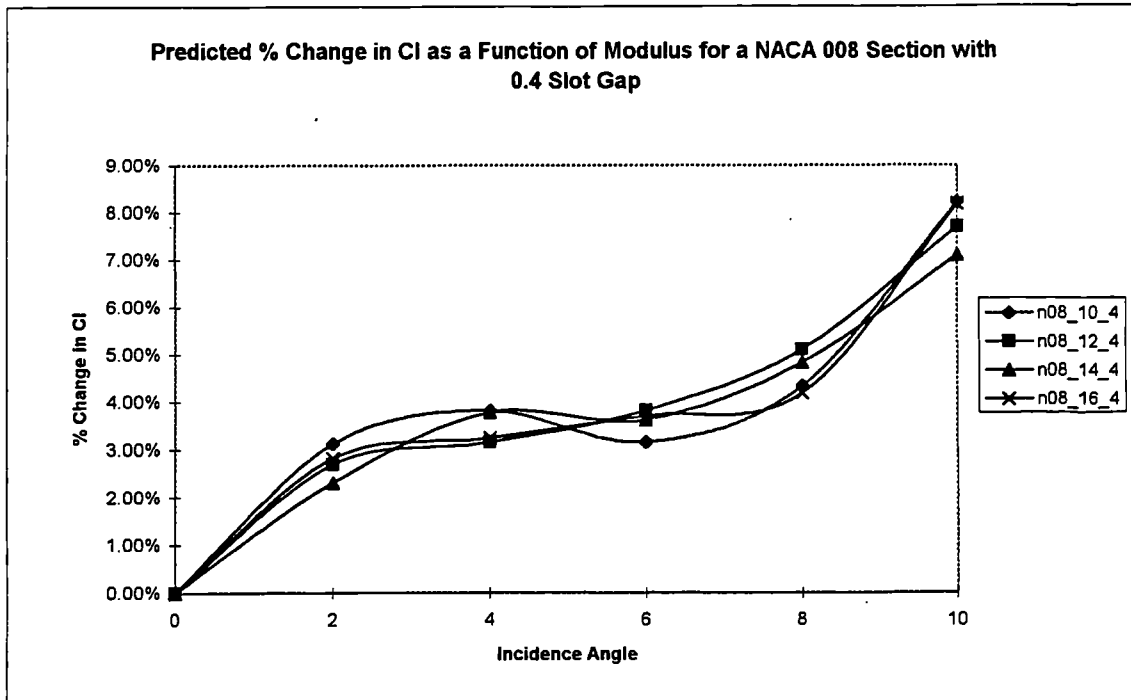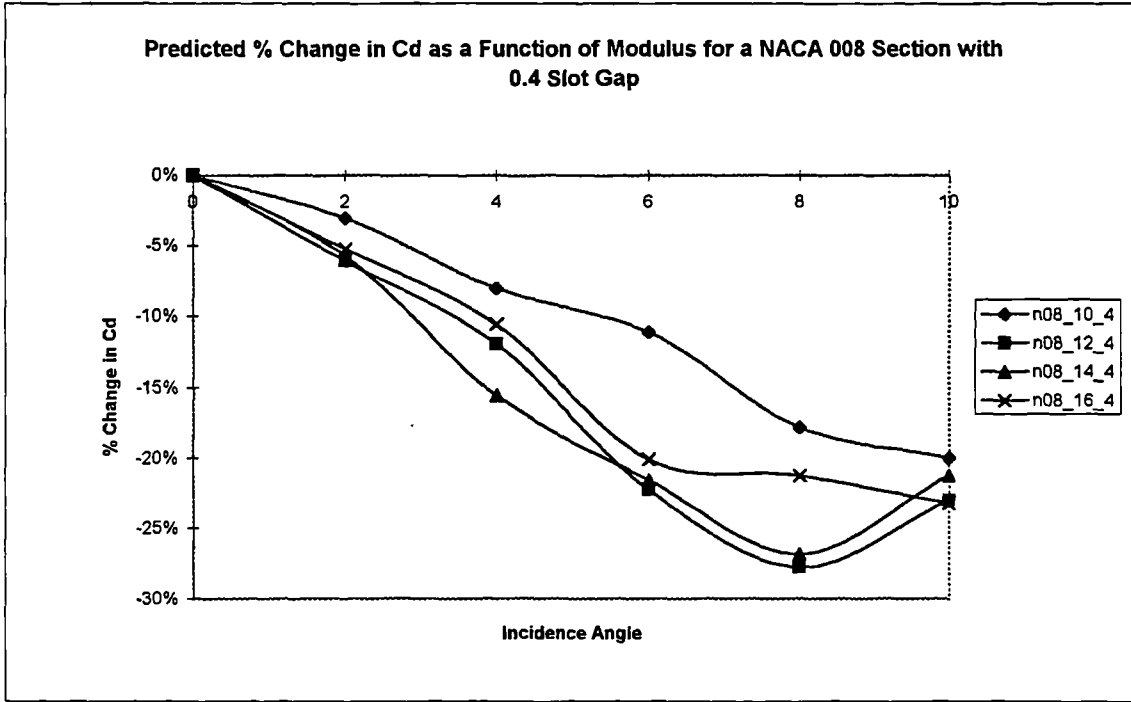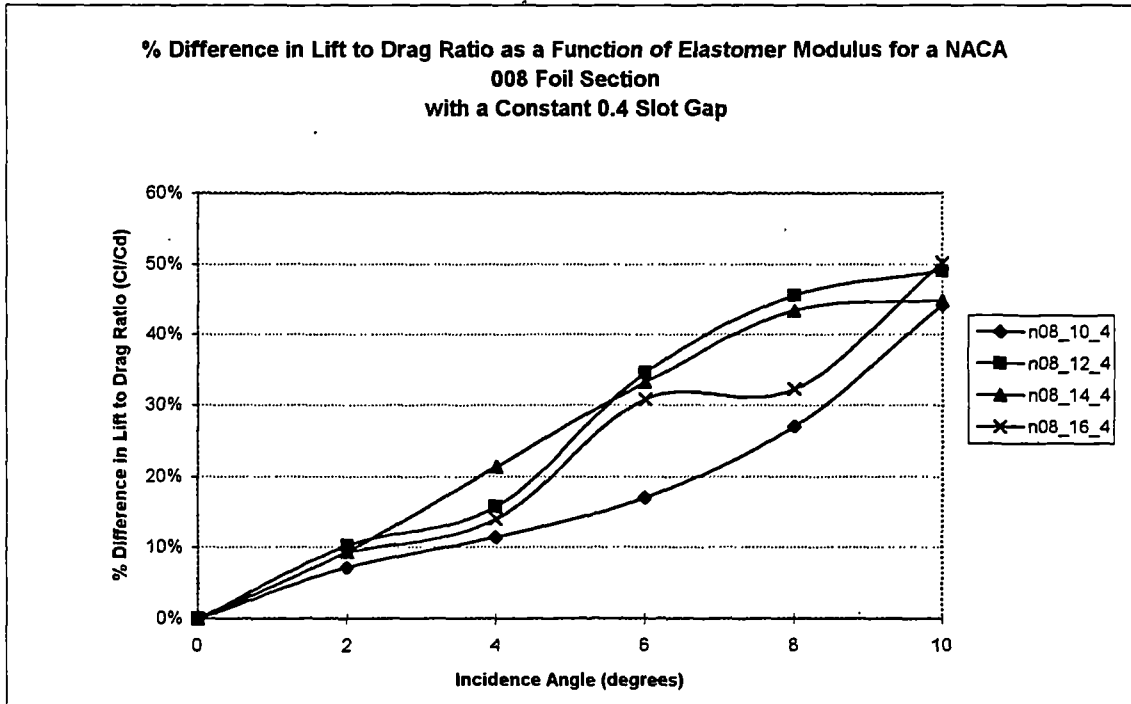
Figure 5.42

Figure 5.43
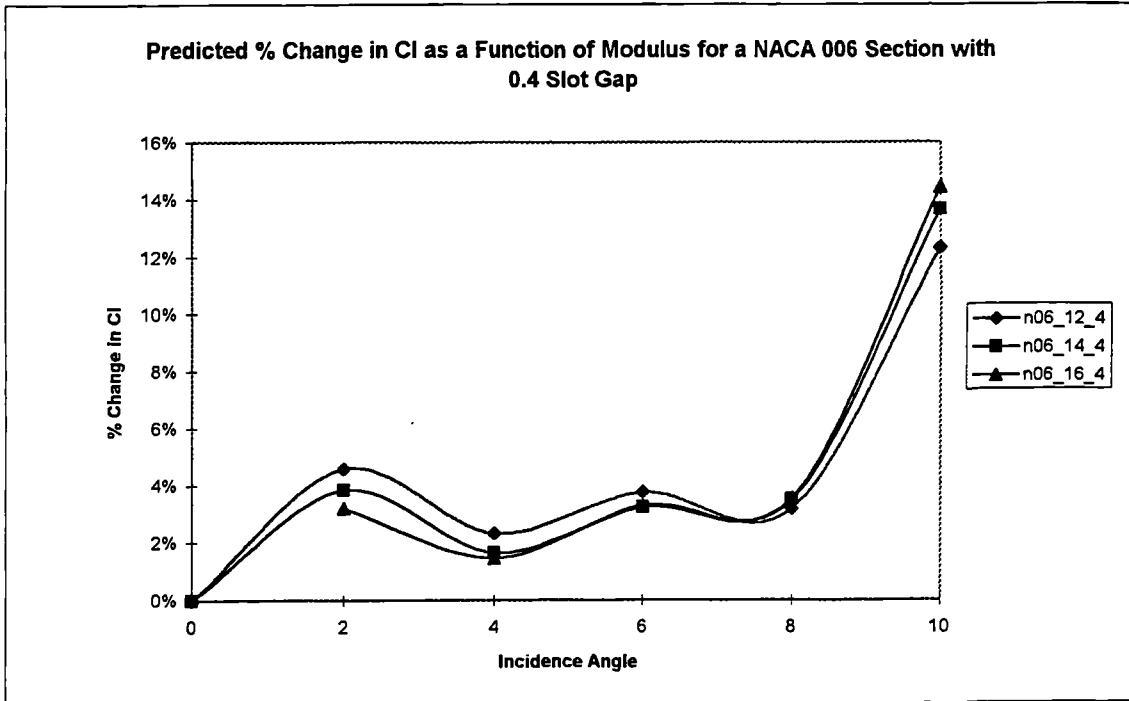
Figure 5.44

Figure 5.45

181
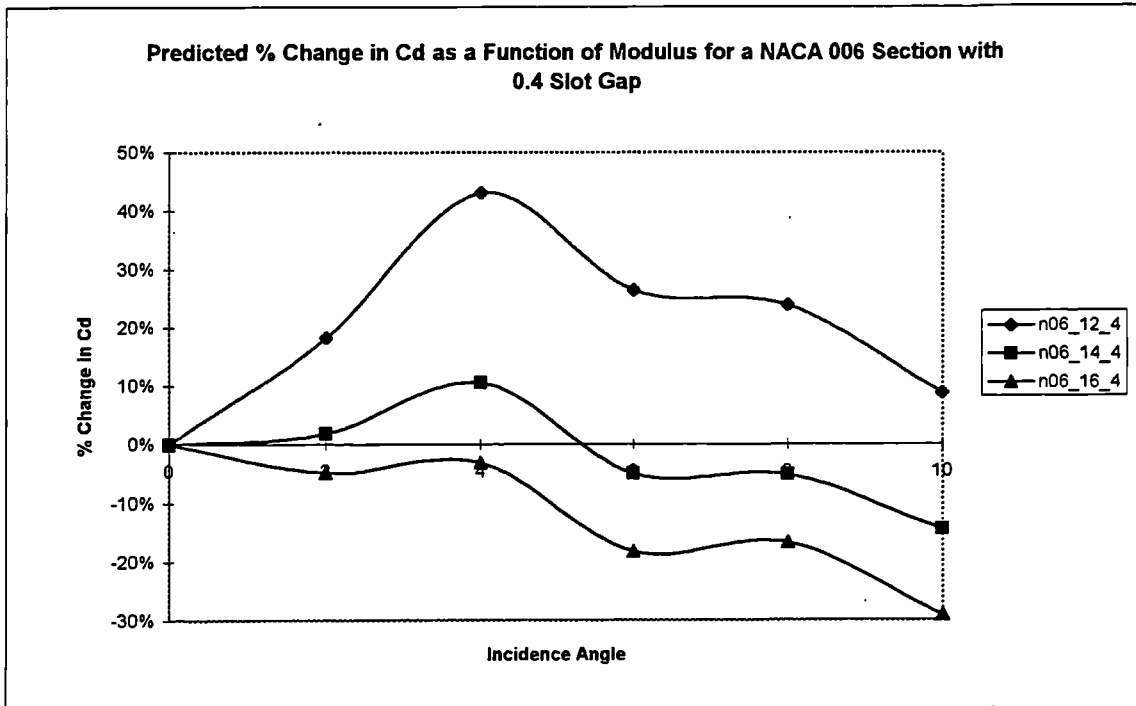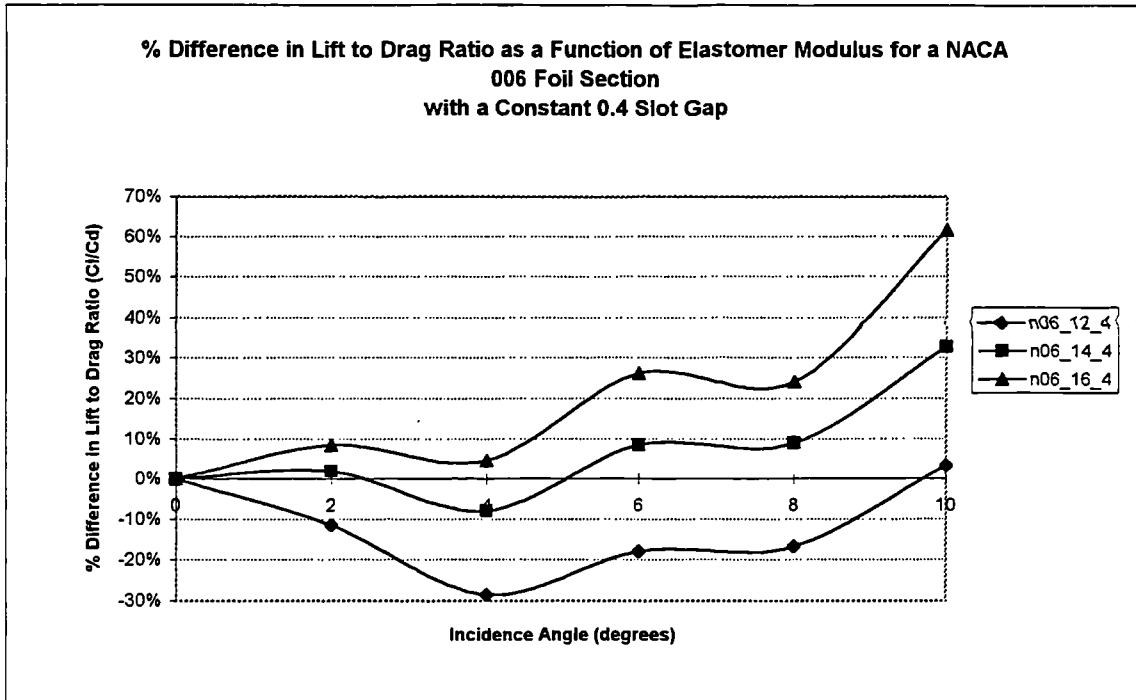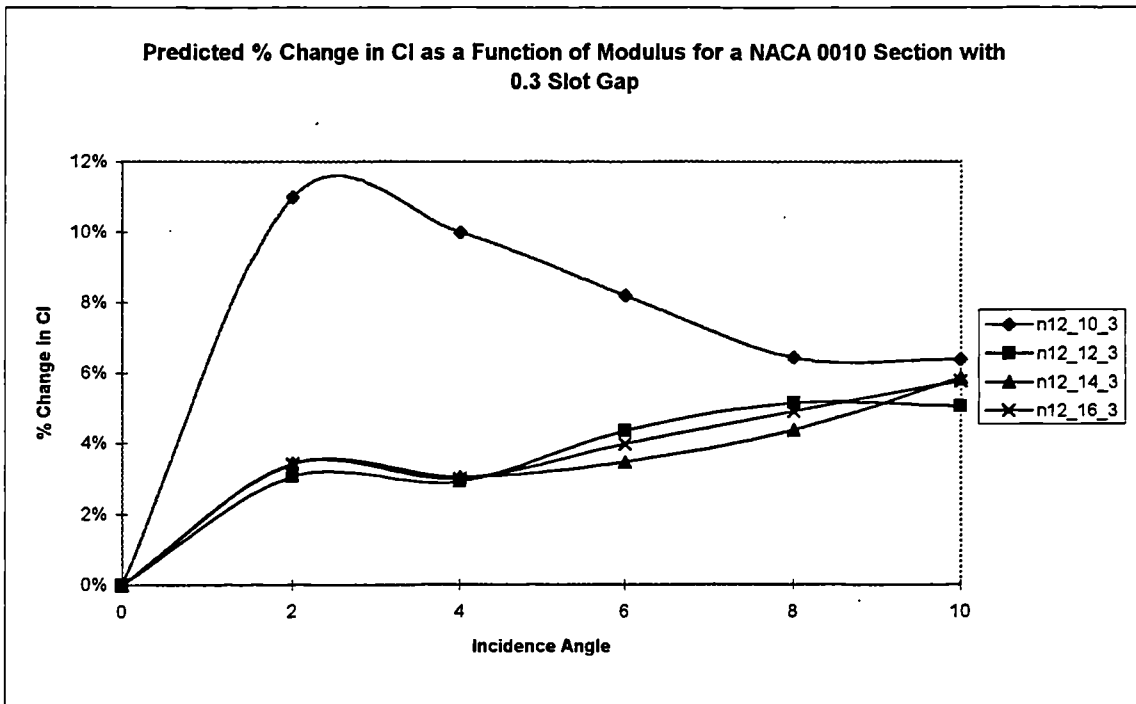
Figure 5.46

Figure 5.47
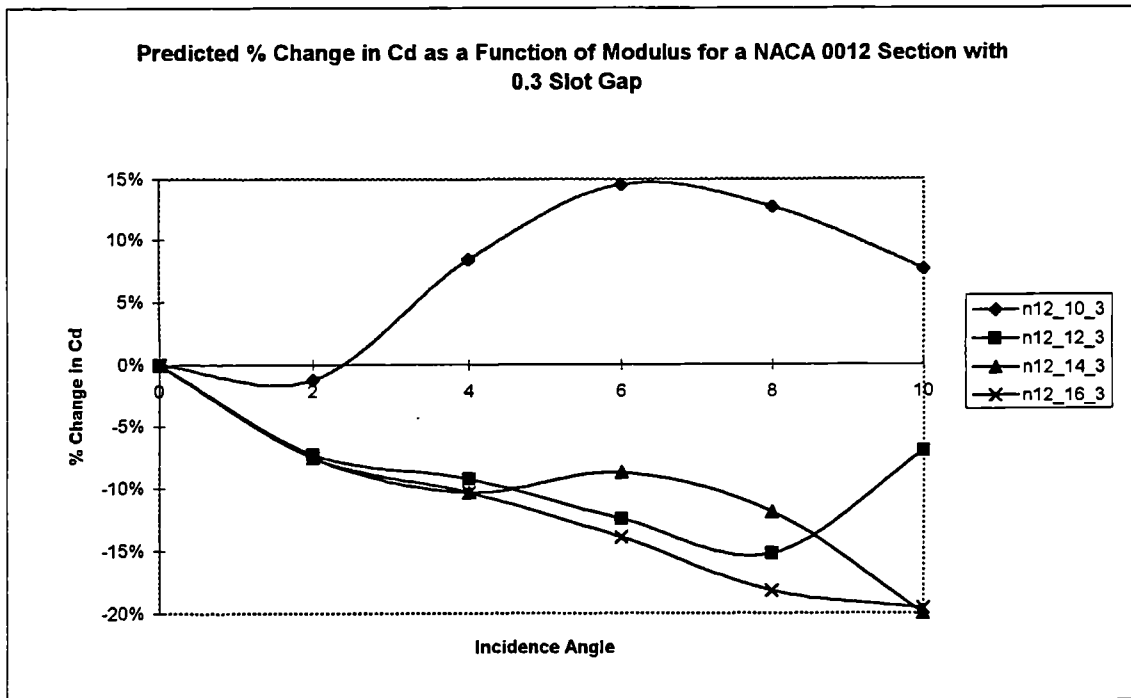
Figure 5.48
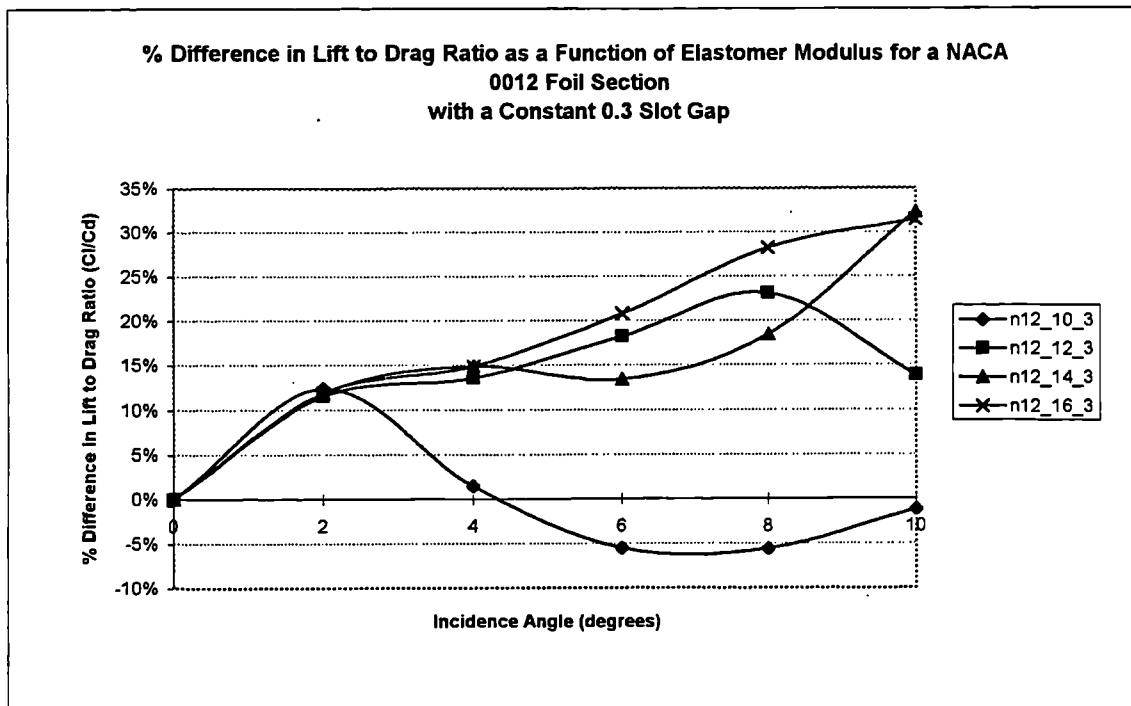
Figure 5.49
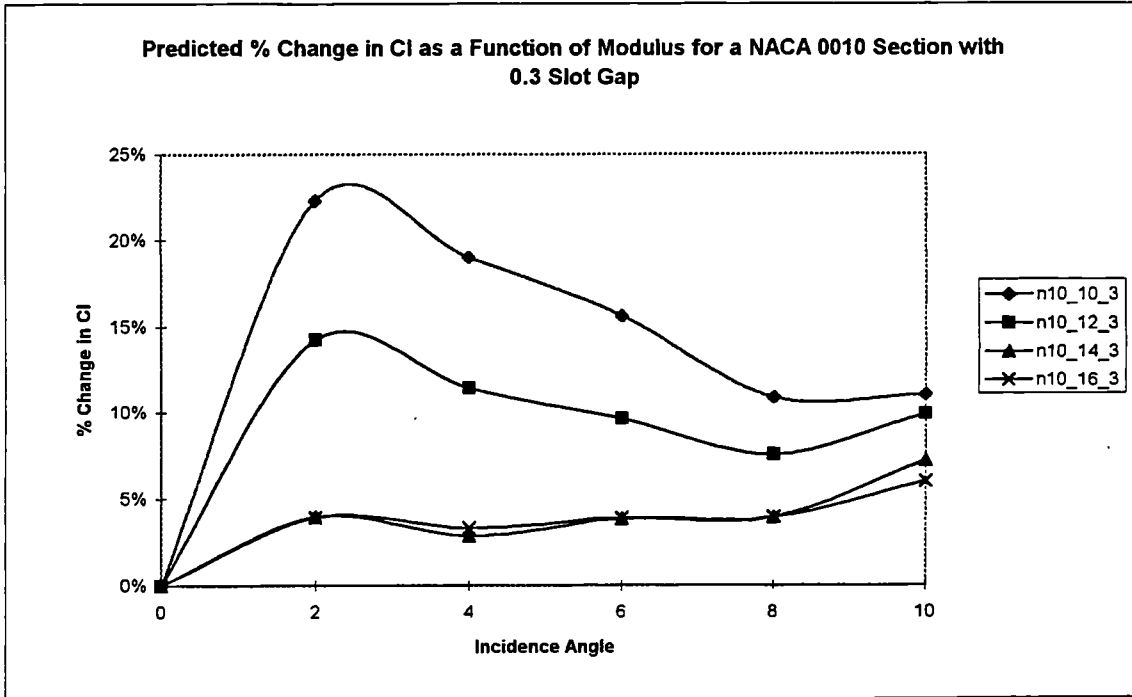
Figure 5.50
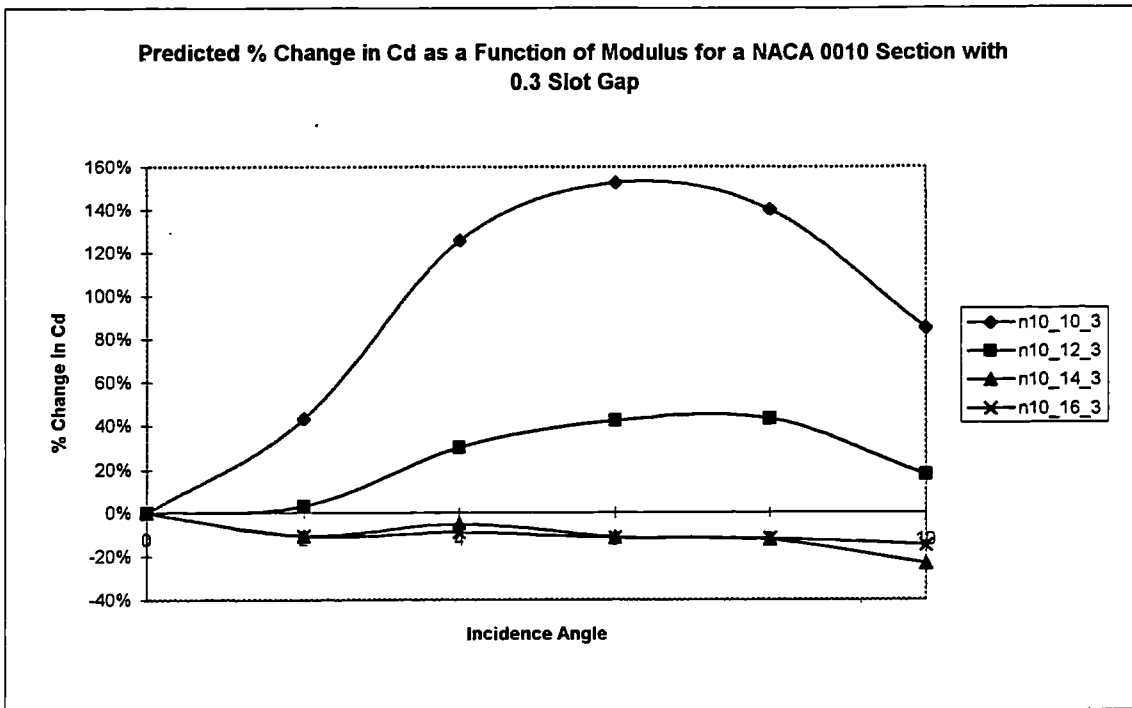
Figure 5.51
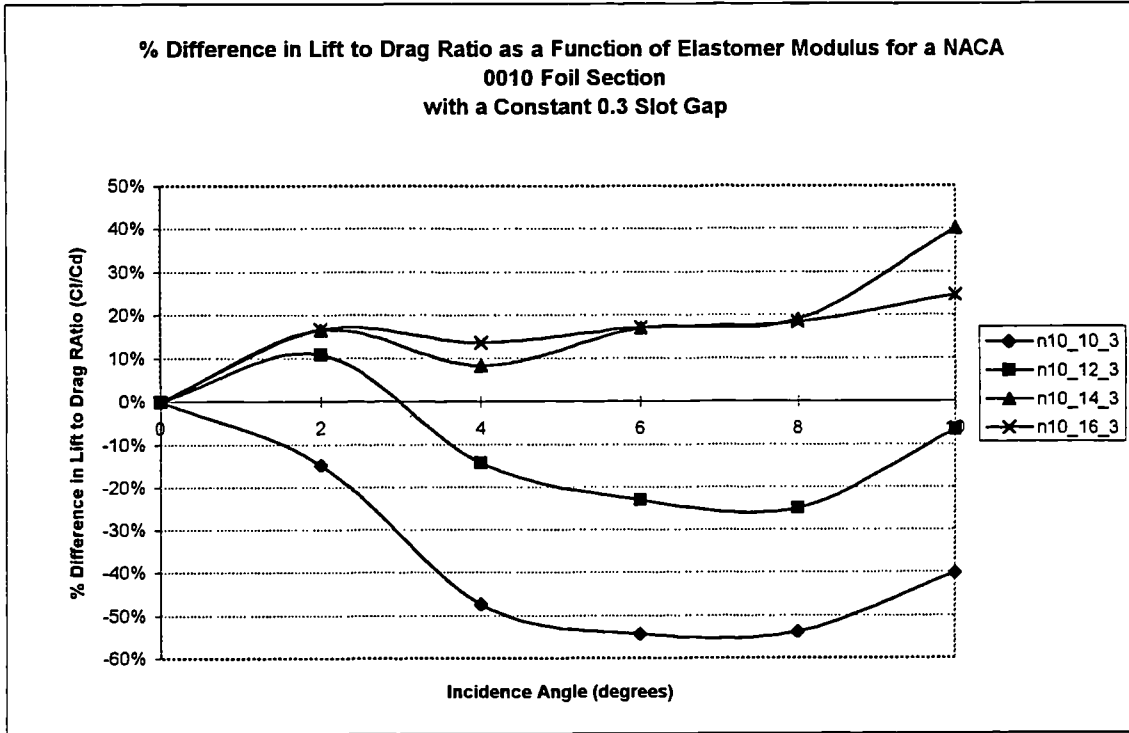
Figure 5.52
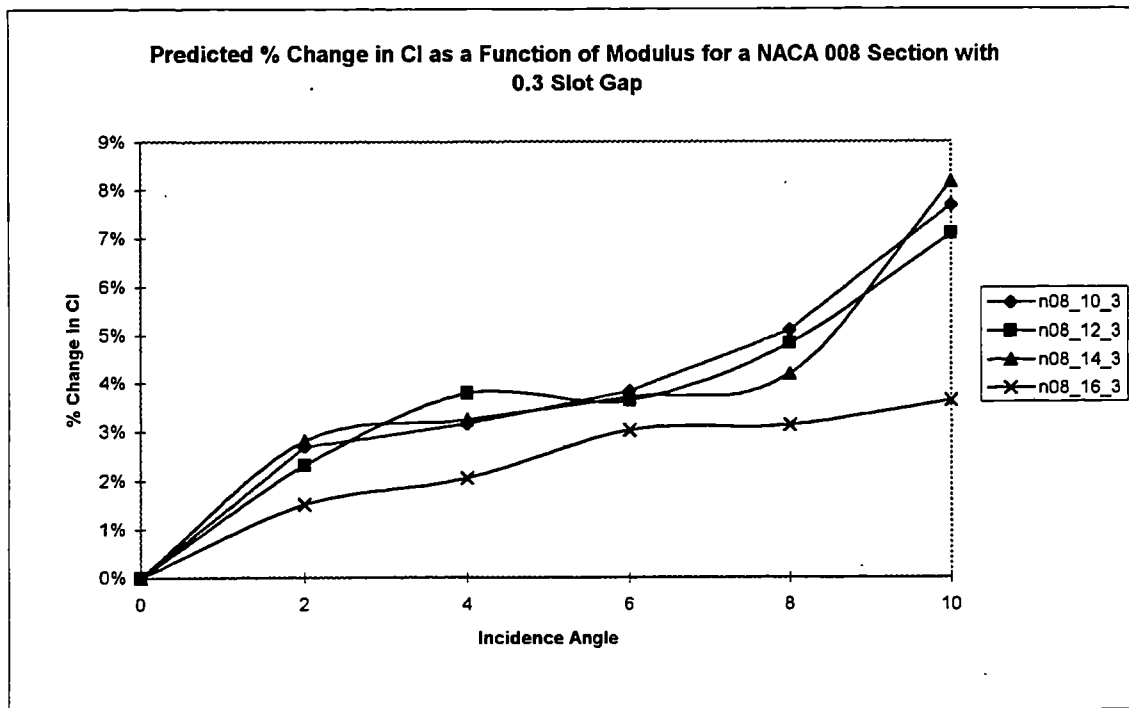
Figure 5.53

185

Figure 5.54

Figure 5.55

186

Predicted % Change in Cl as a Function of Modulus for a NACA 006 Section with 0.3 Slot Gap

Figure 5.56

Predicted % Change in Cd as a Function of Modulus for a NACA 006 Section with 0.3 Slot Gap

Figure 5.57

187

Figure 5.58

% Difference in Lift to Drag Ratio for Varying Thickness NACA Sections of Elastomer Modulus 10e06 and Slot Gap 0.5

Figure 5.59

% Difference in Lift to Drag Ratio for Varying Thickness NACA Sections of Elastomer Modulus 10e06 and Slot Gap 0.4
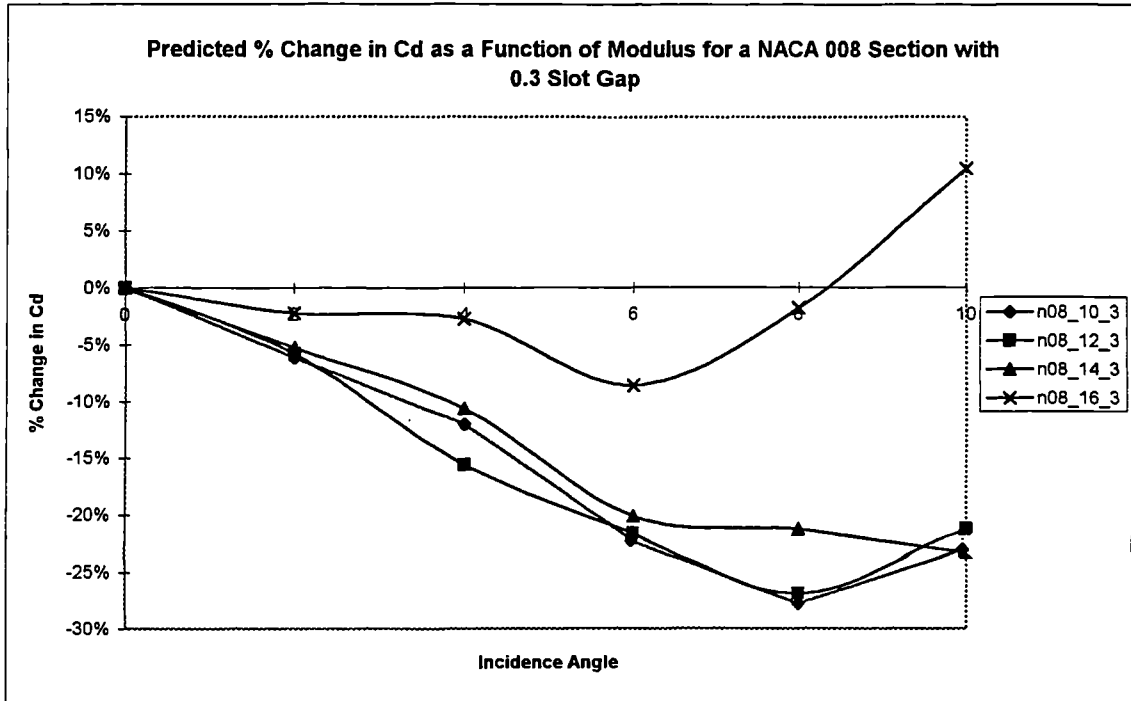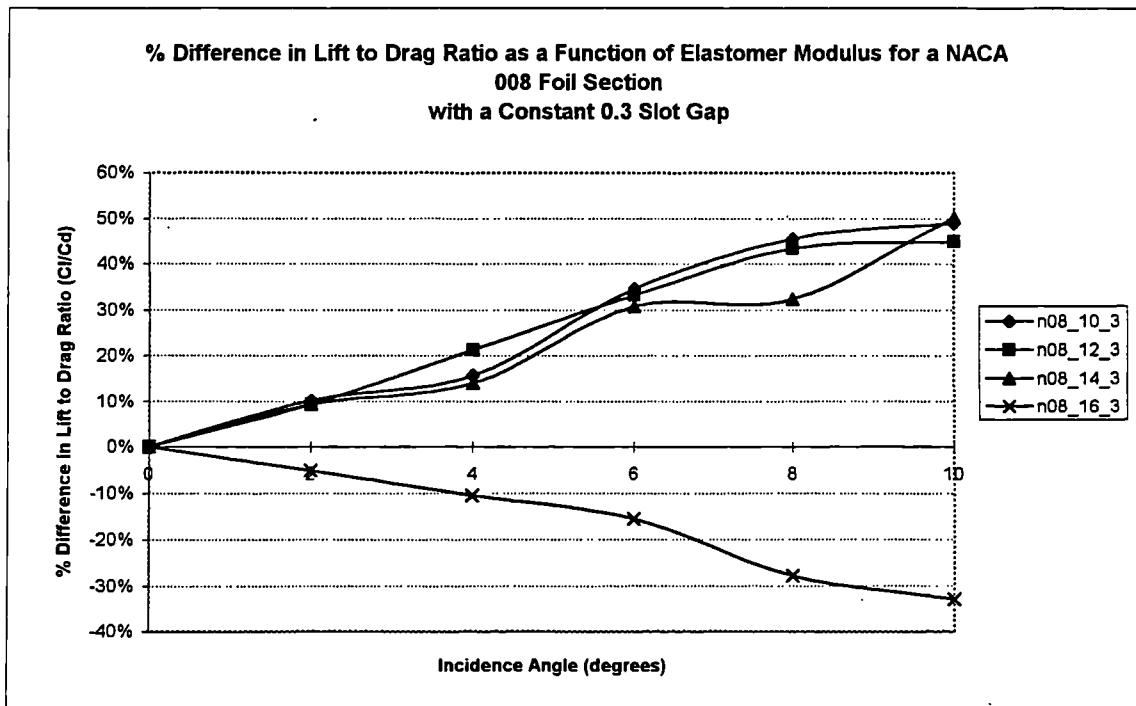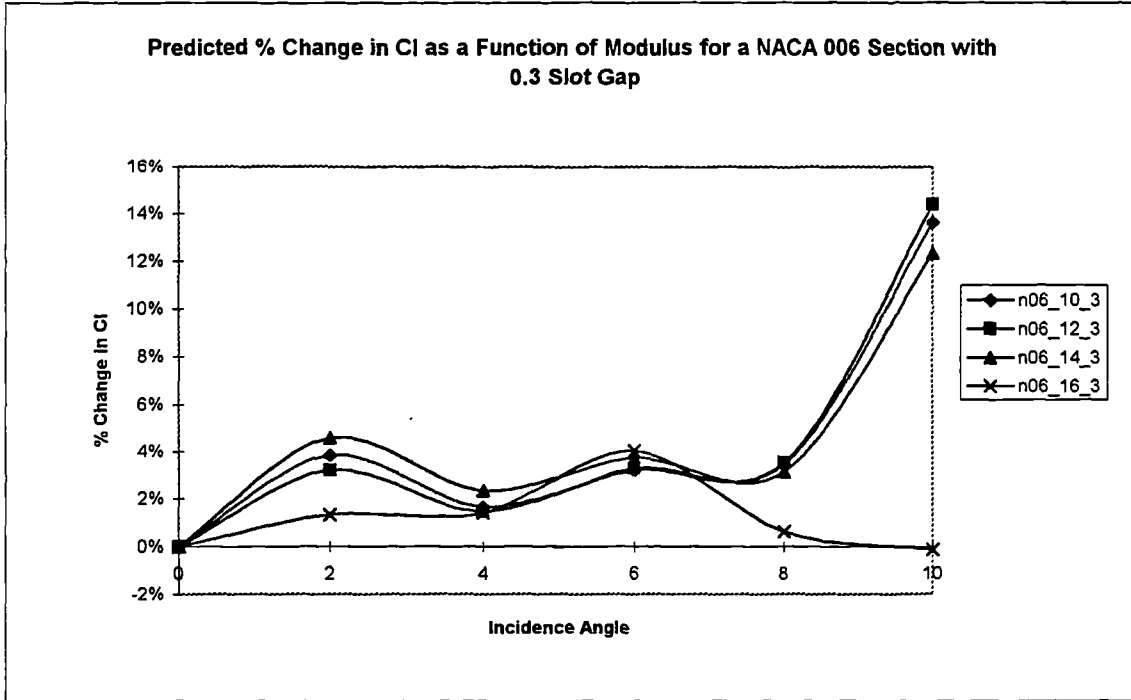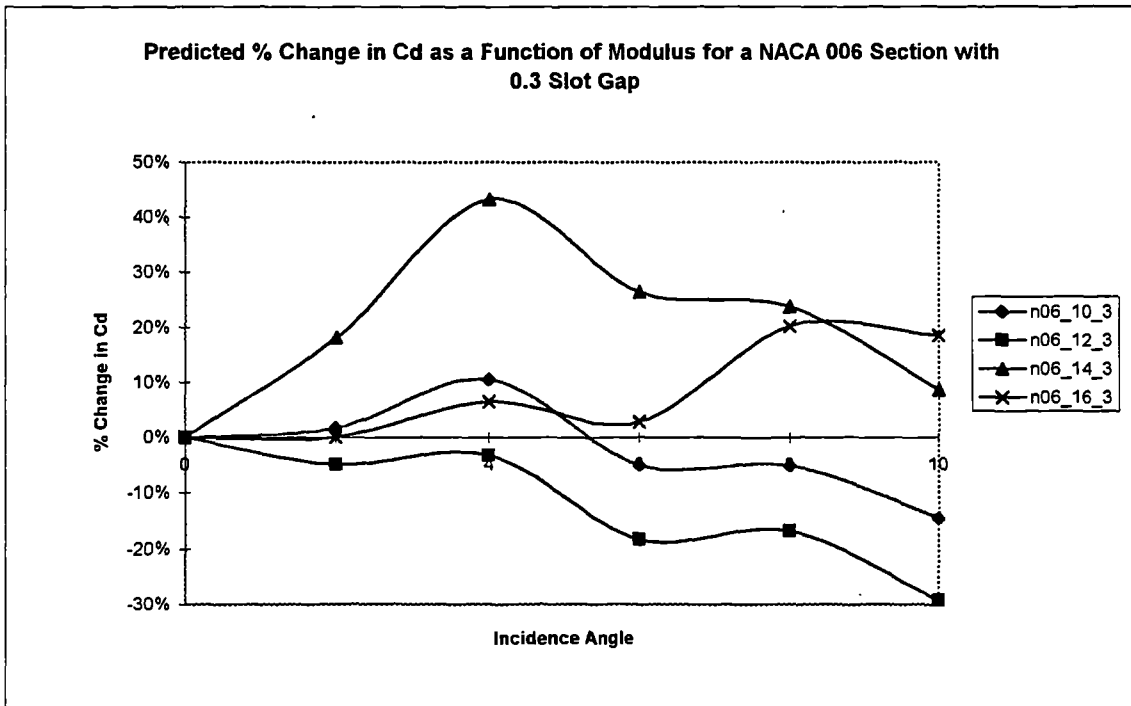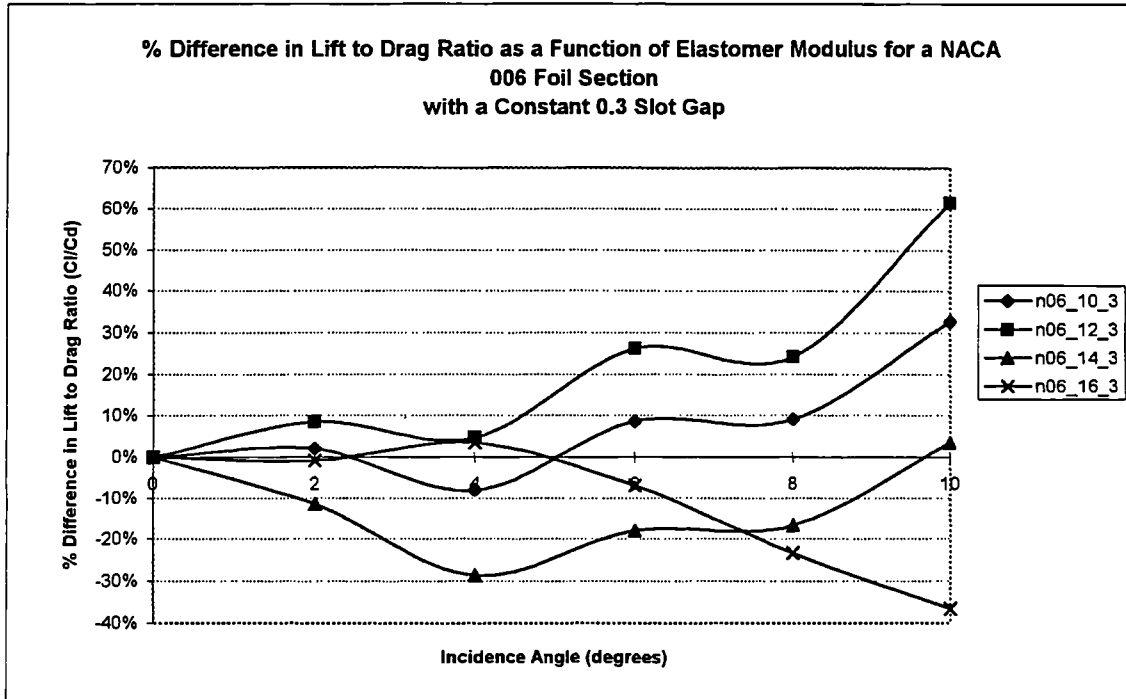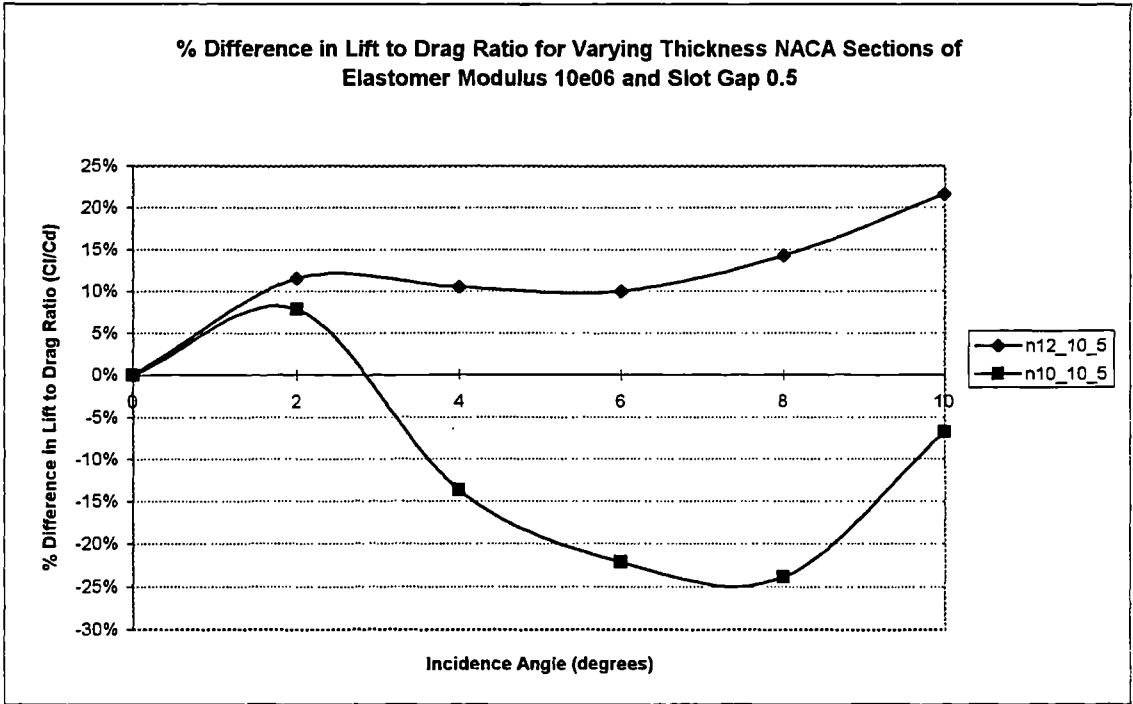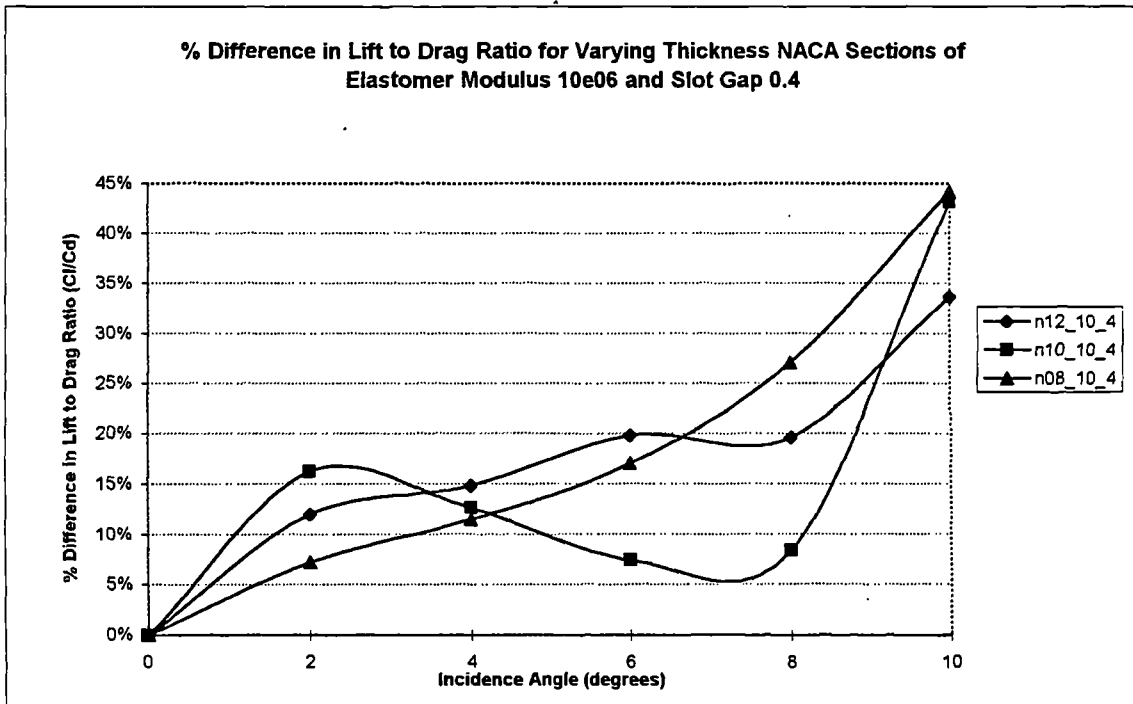
Figure 5.60

Figure 5.61

Figure 5.62

% Difference in Lift to Drag Ratio for Varying Thickness NACA Sections of Elastomer Modulus 12e06 and Slot Gap 0.4

Figure 5.63

% Difference in Lift to Drag Ratio for Varying Thickness NACA Sections of Elastomer Modulus 12e06 and Slot Gap 0.3
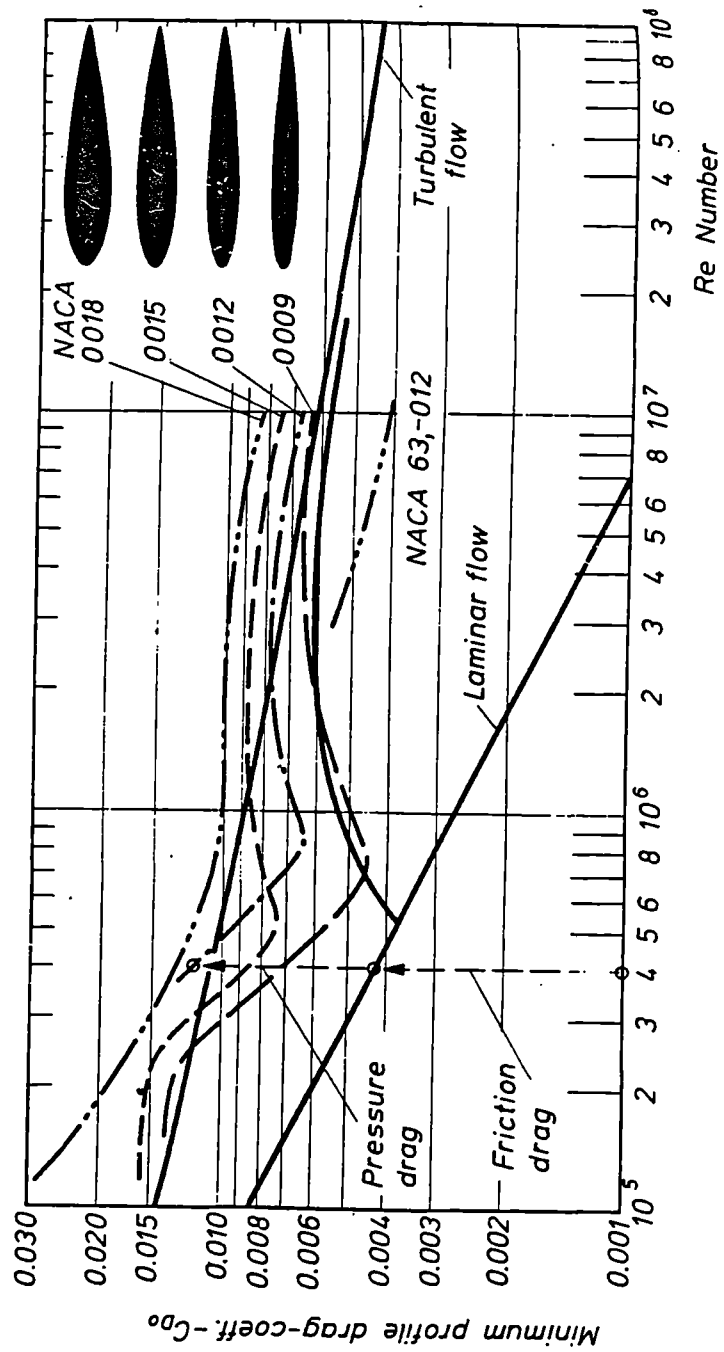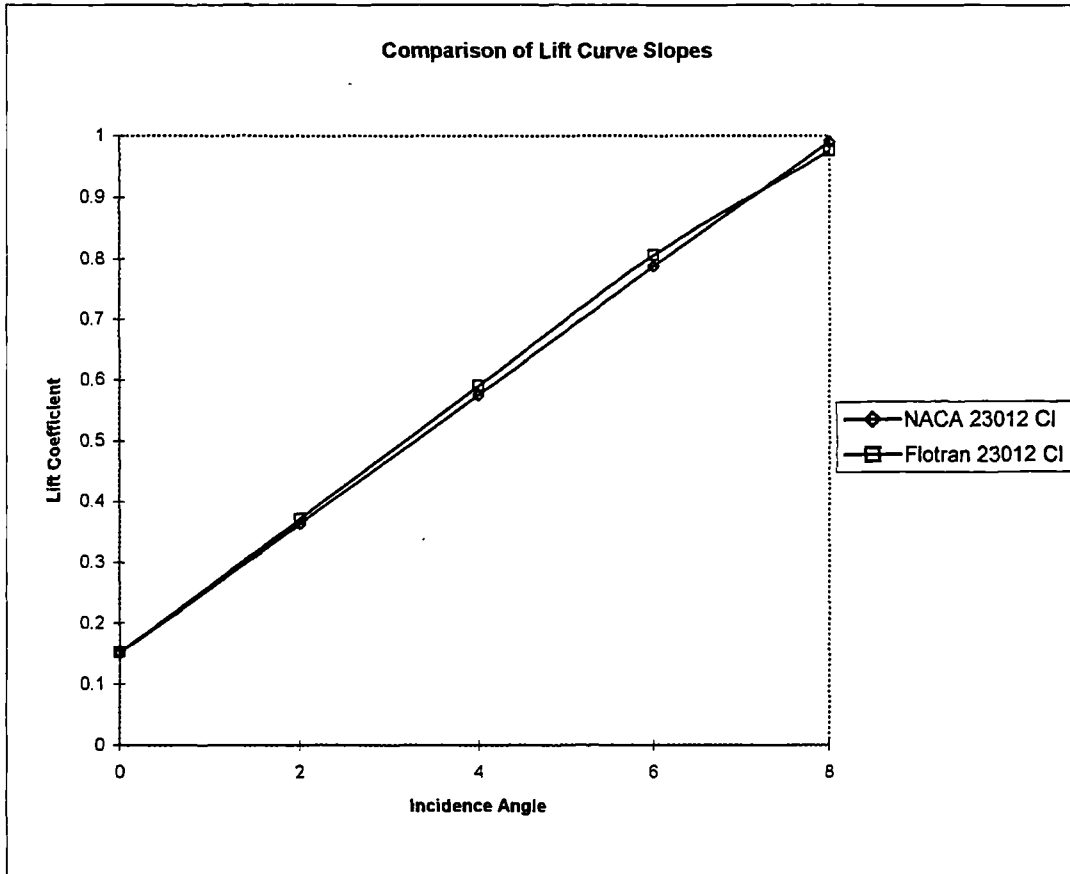
Figure 5.64

191
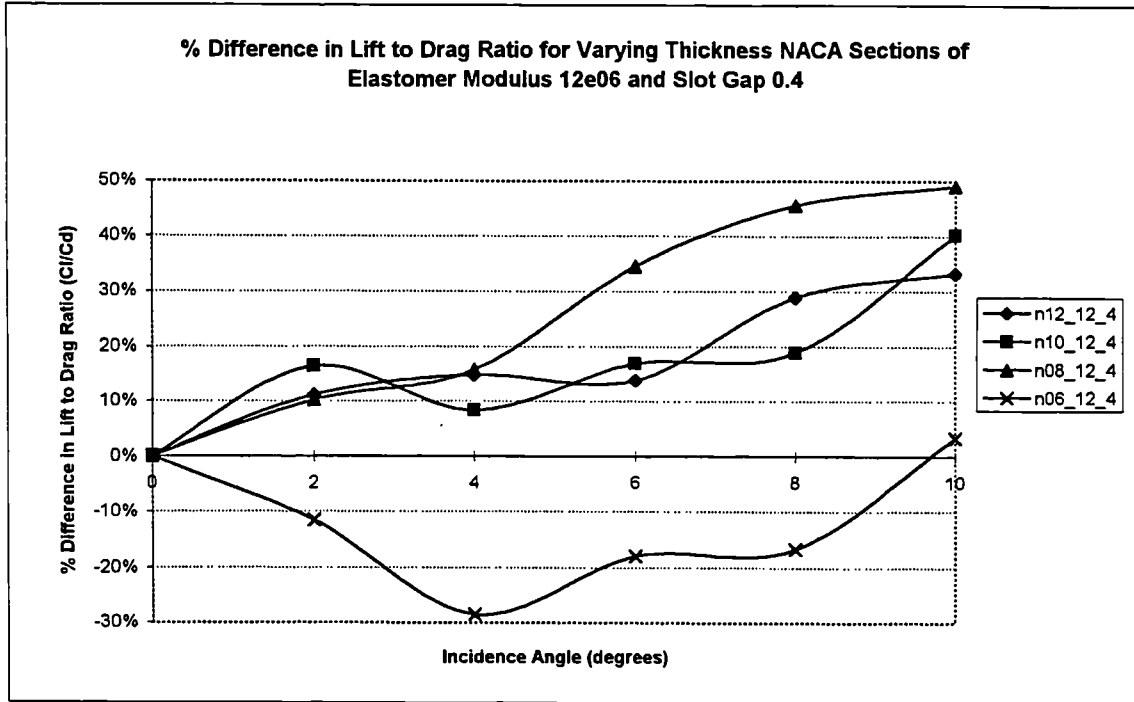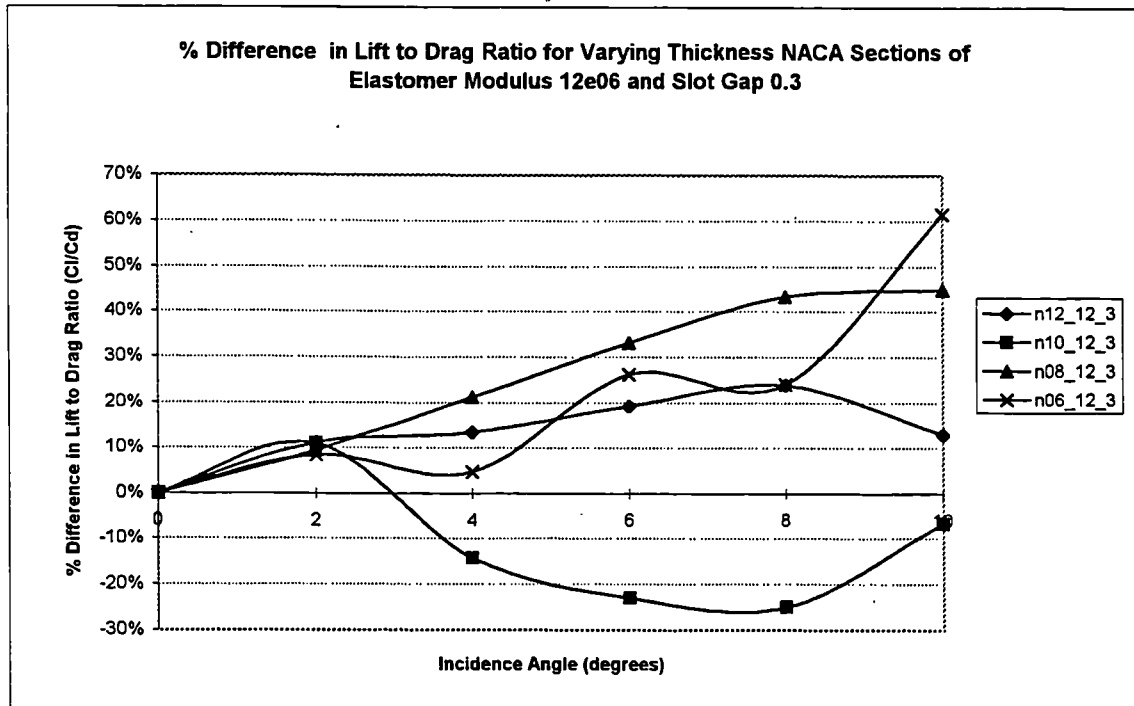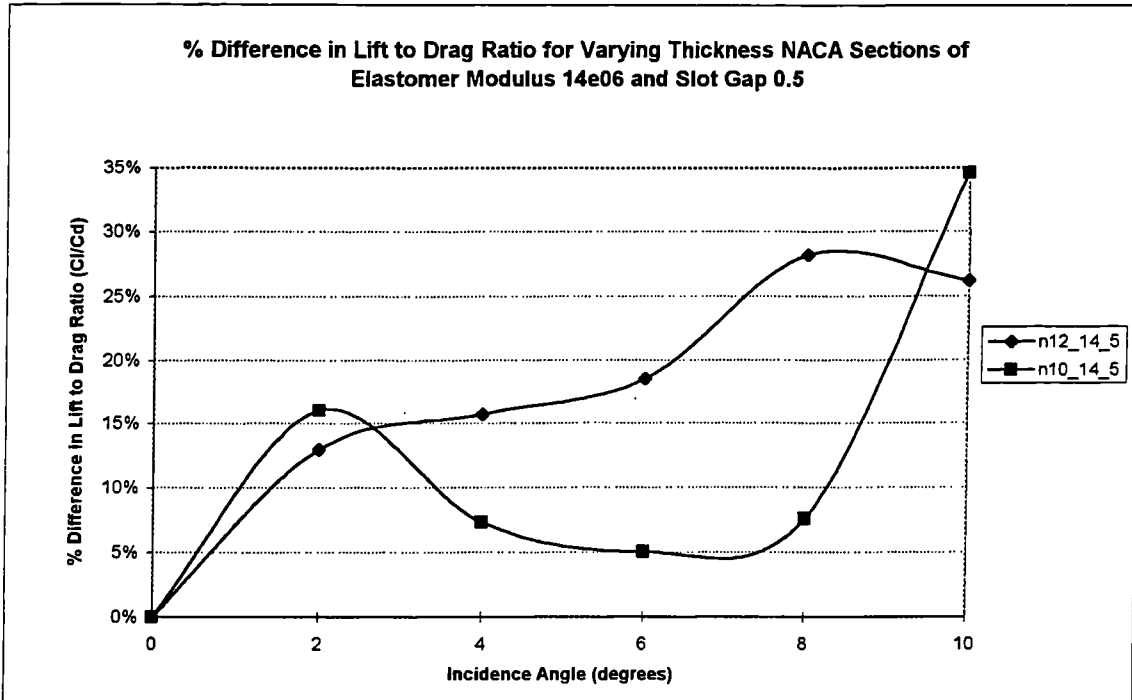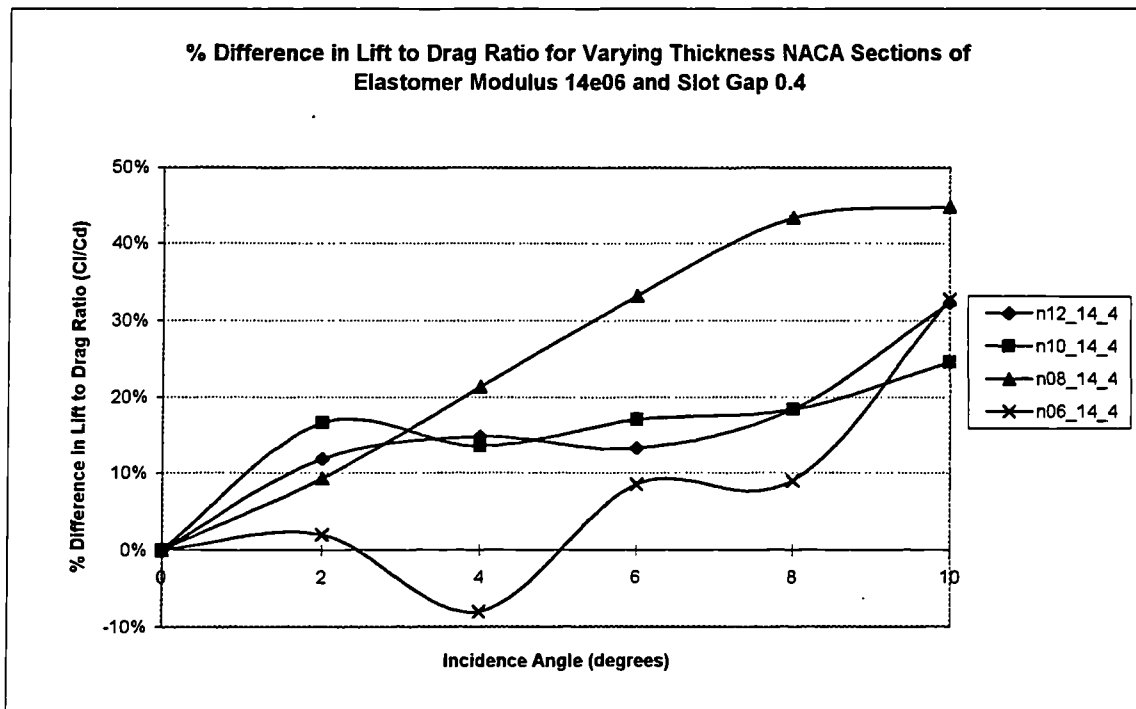
Figure 5.65
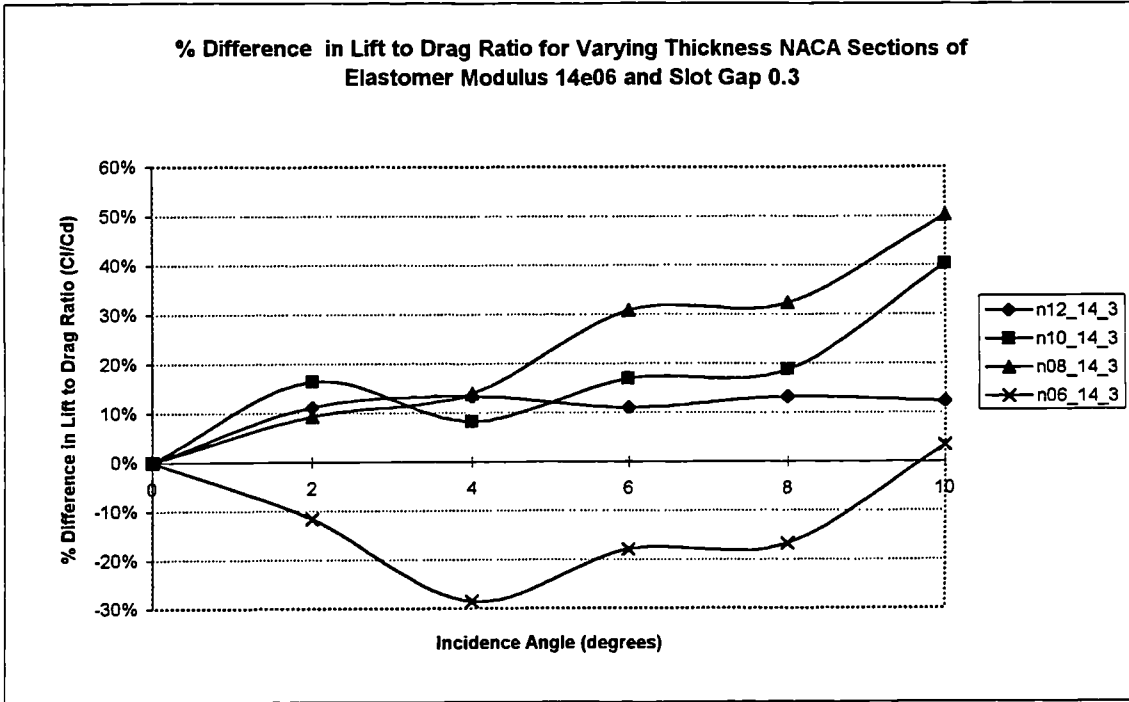
Figure 5.66
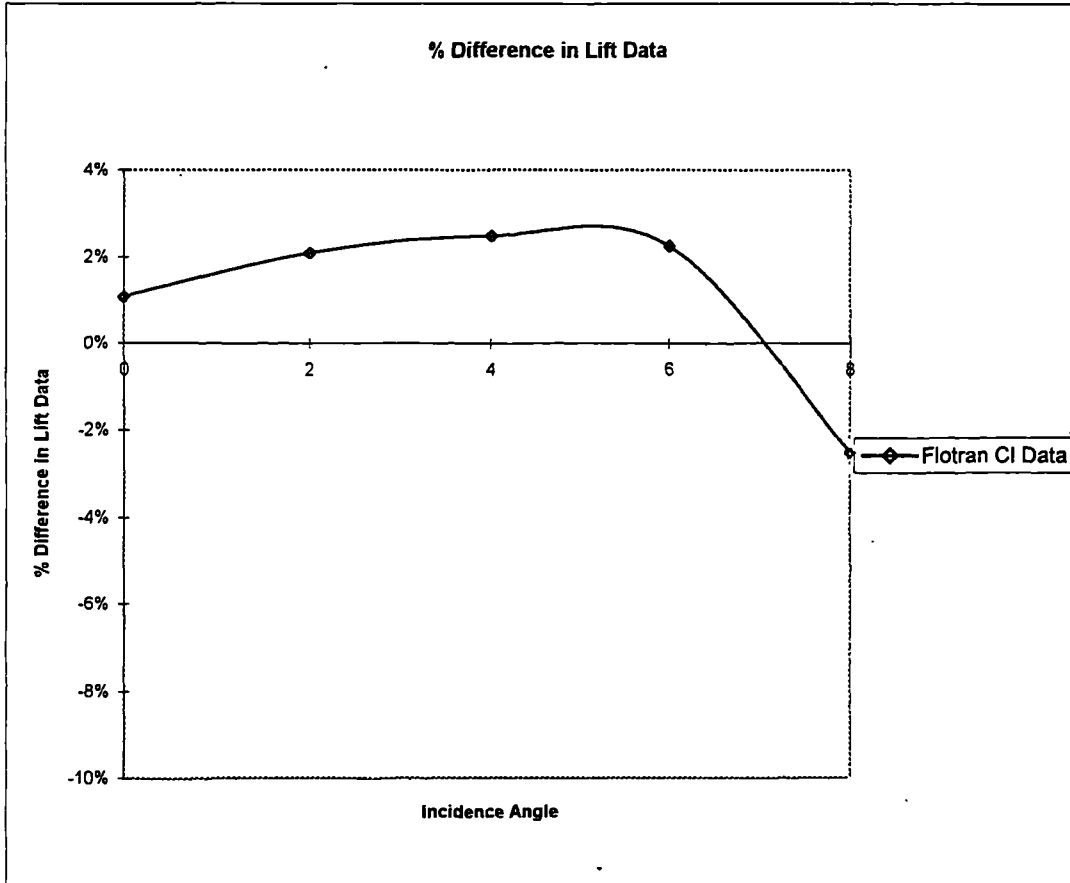
Figure 5.67

Figure 5.68

193
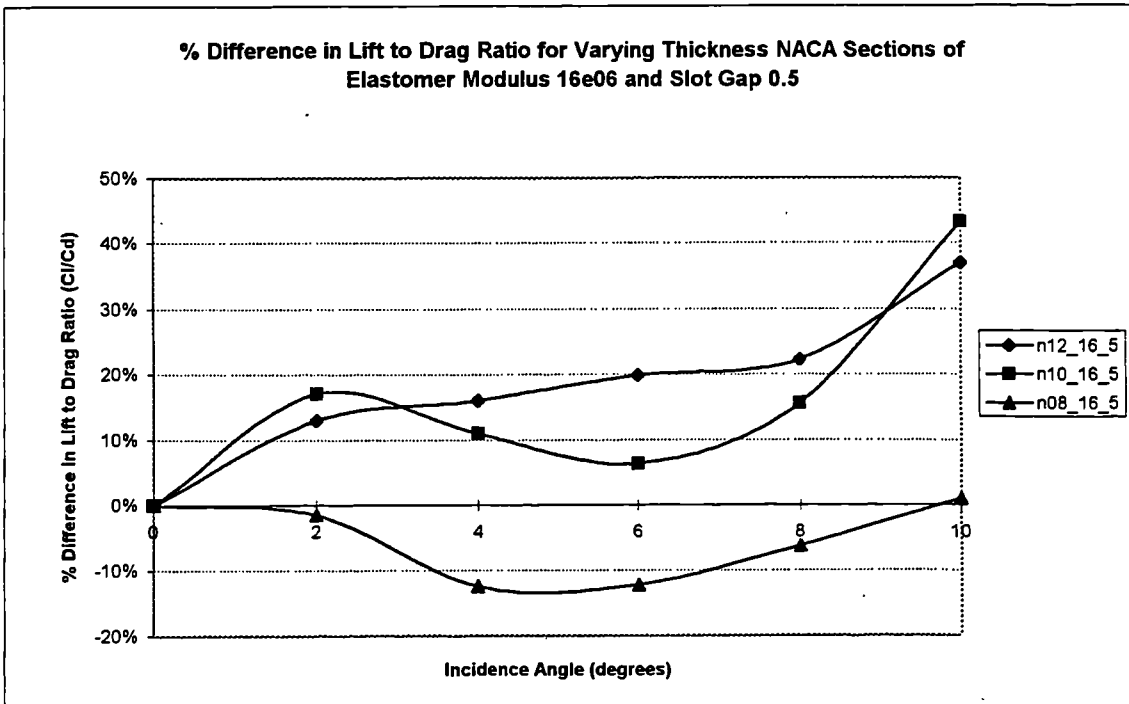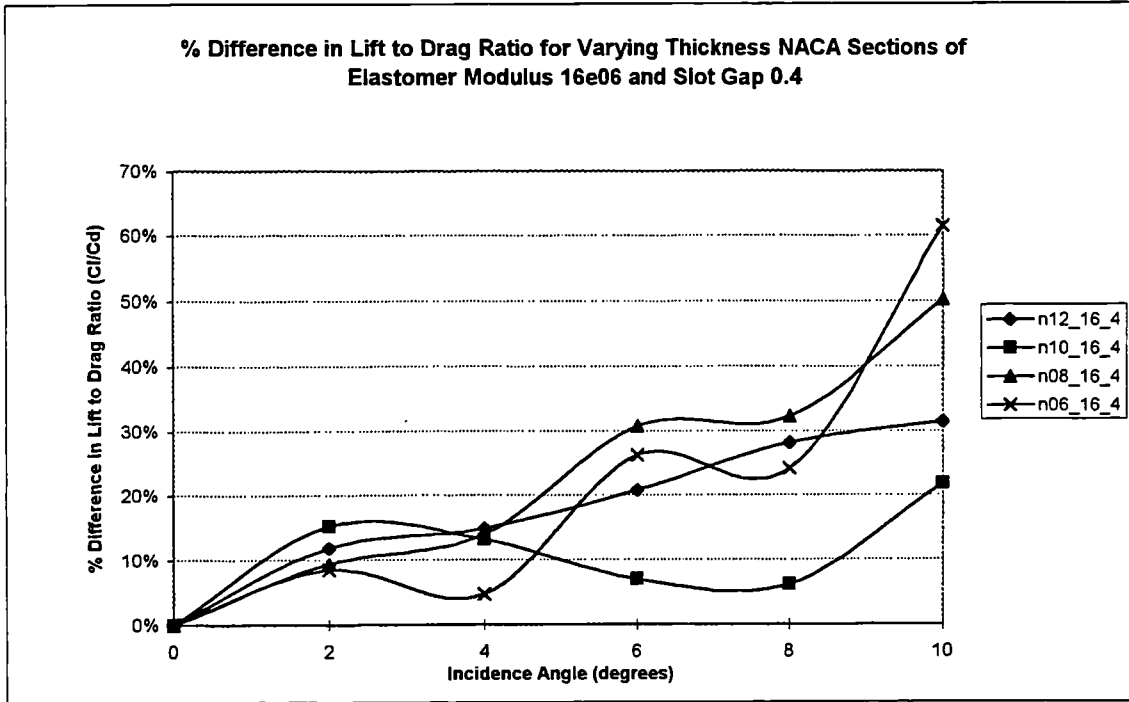
Figure 5.69

Figure 5.70

194
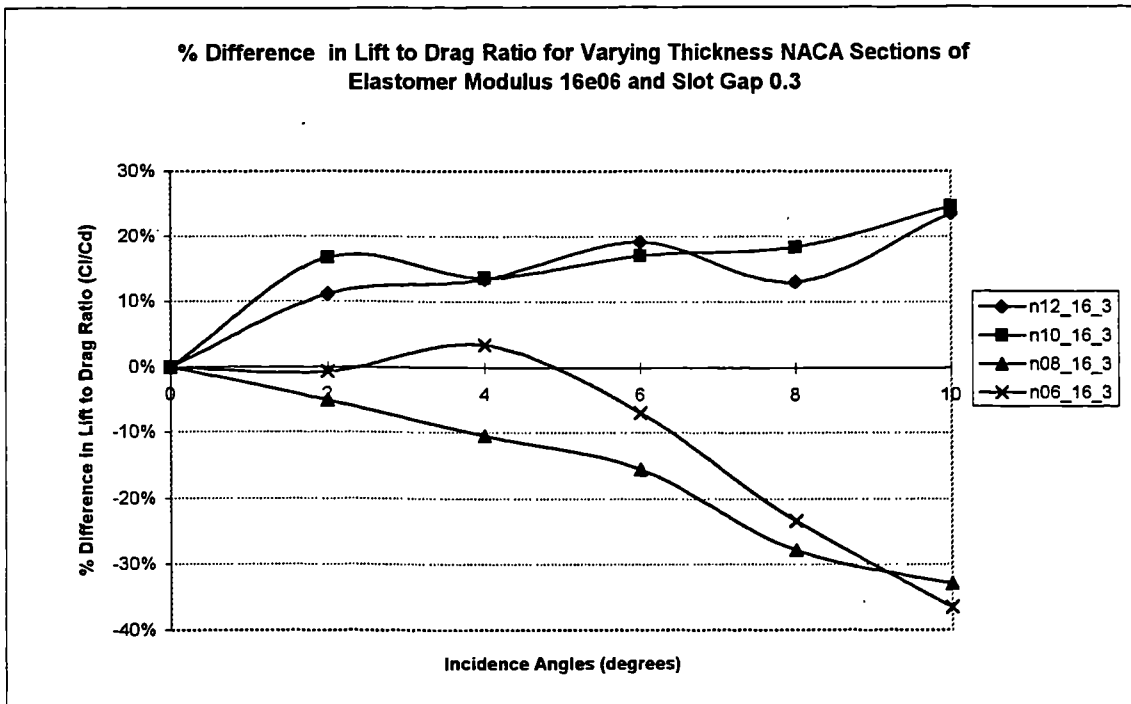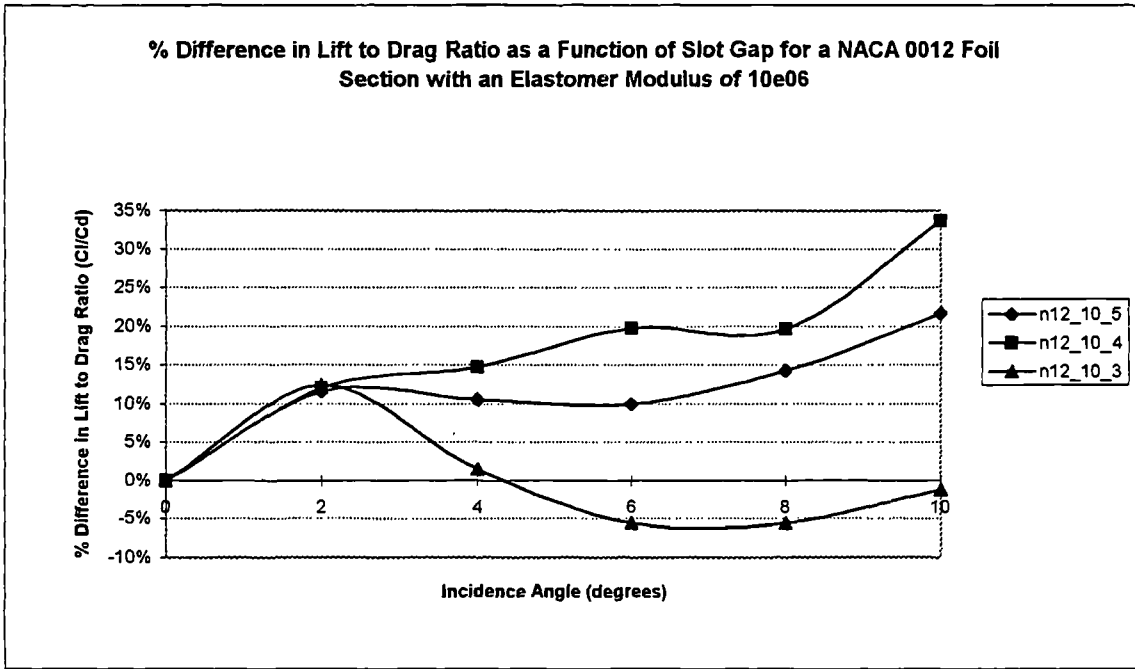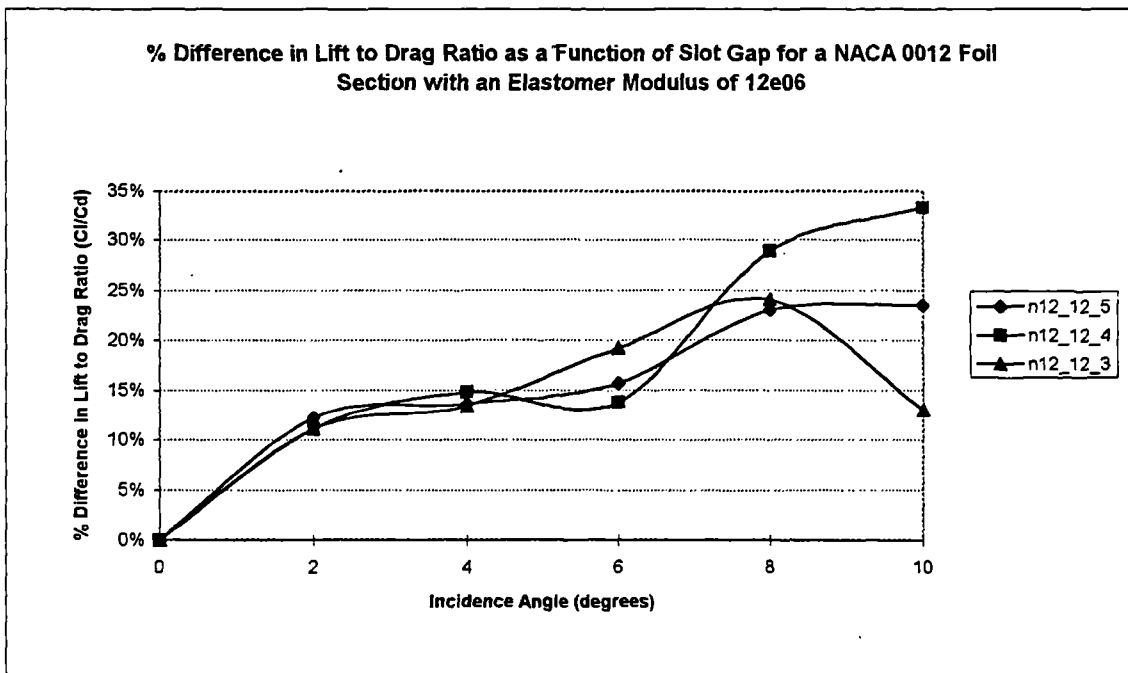
Figure 5.71

Figure 5.72

Figure 5.73

Figure 5.74

% Difference in Lift to Drag Ratio as a Function of Slot Gap for a NACA 0010 Foil Section with an Elastomer Modulus of 10e06

Figure 5.75

**% Difference in Lift to Drag Ratio as a Function of Slot Gap for a NACA 0010 Foil Section with an Elastomer Modulus of 12e06**
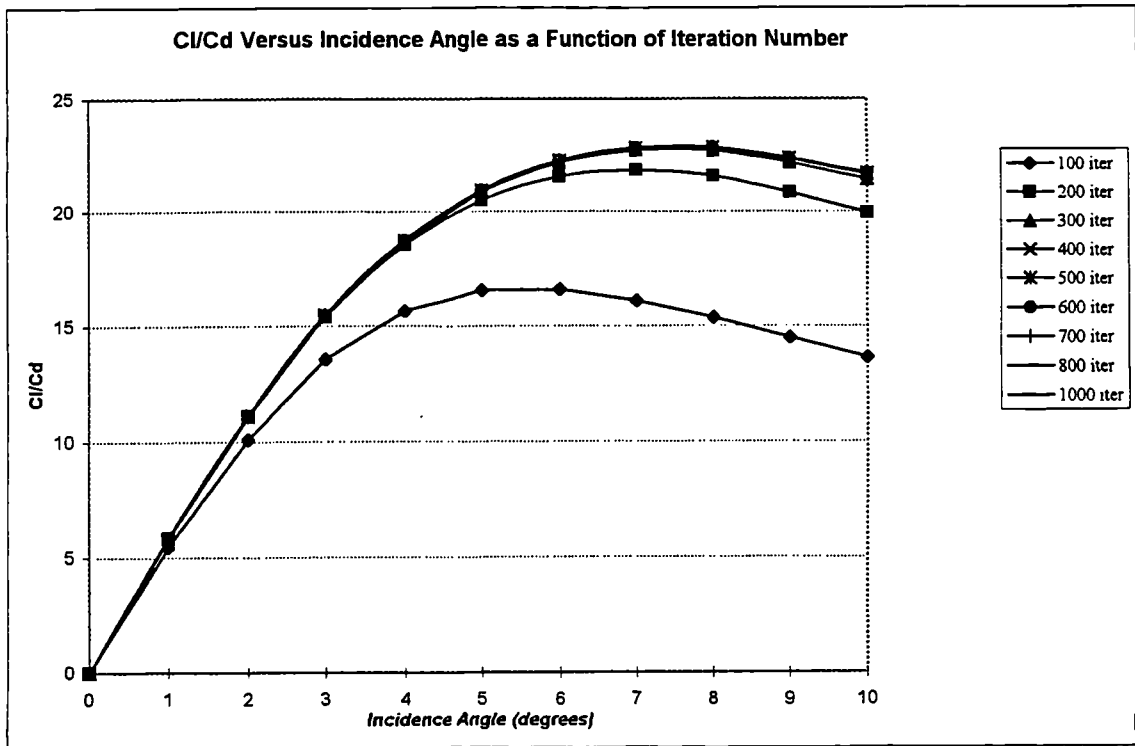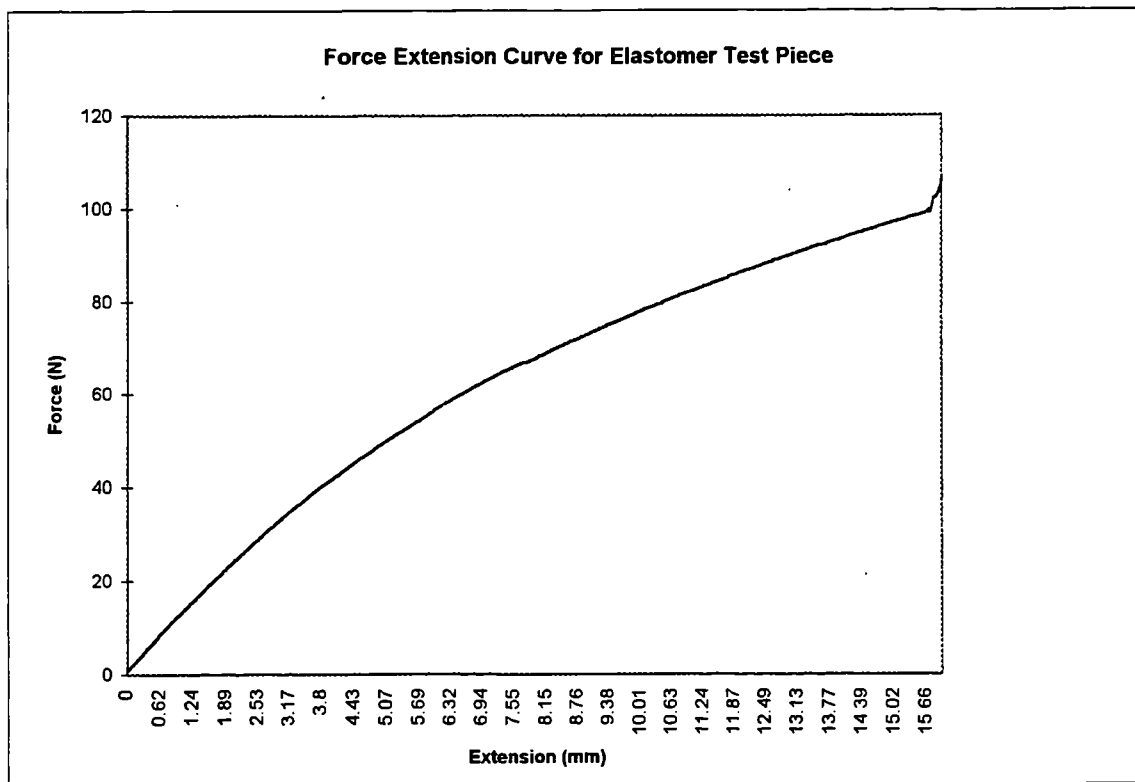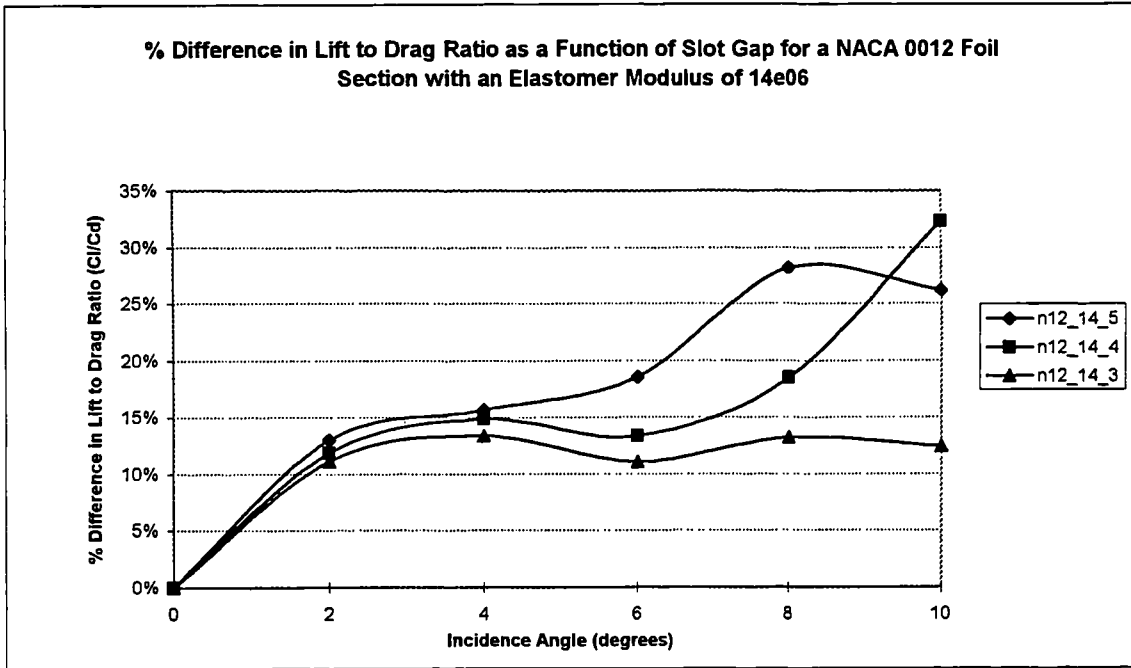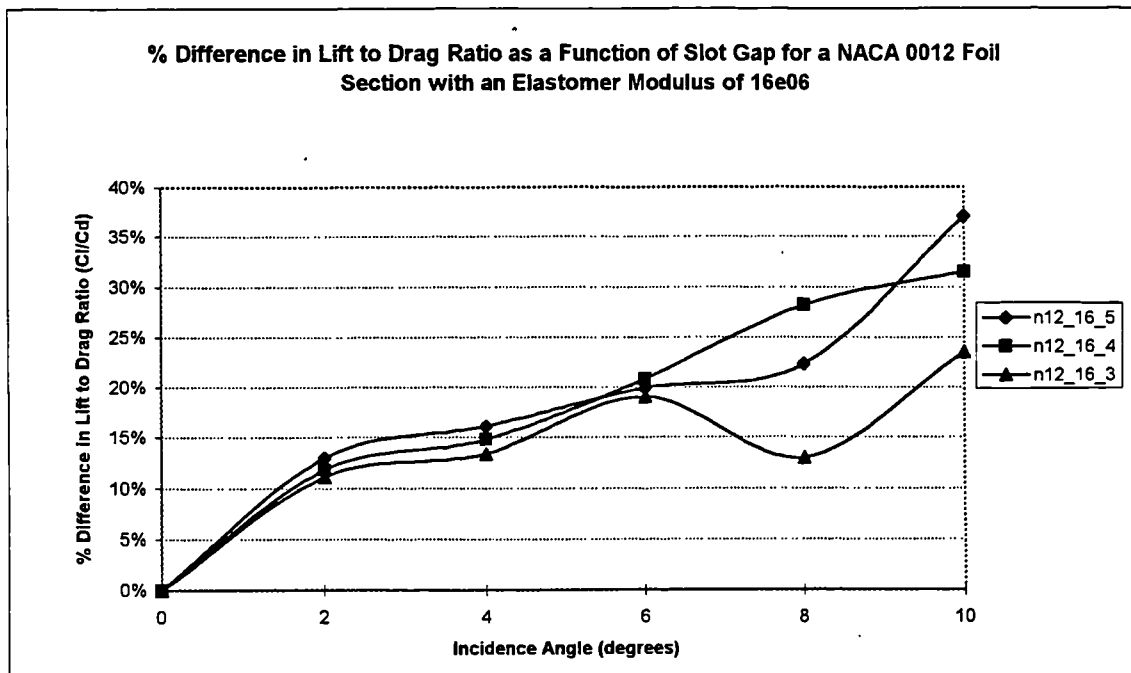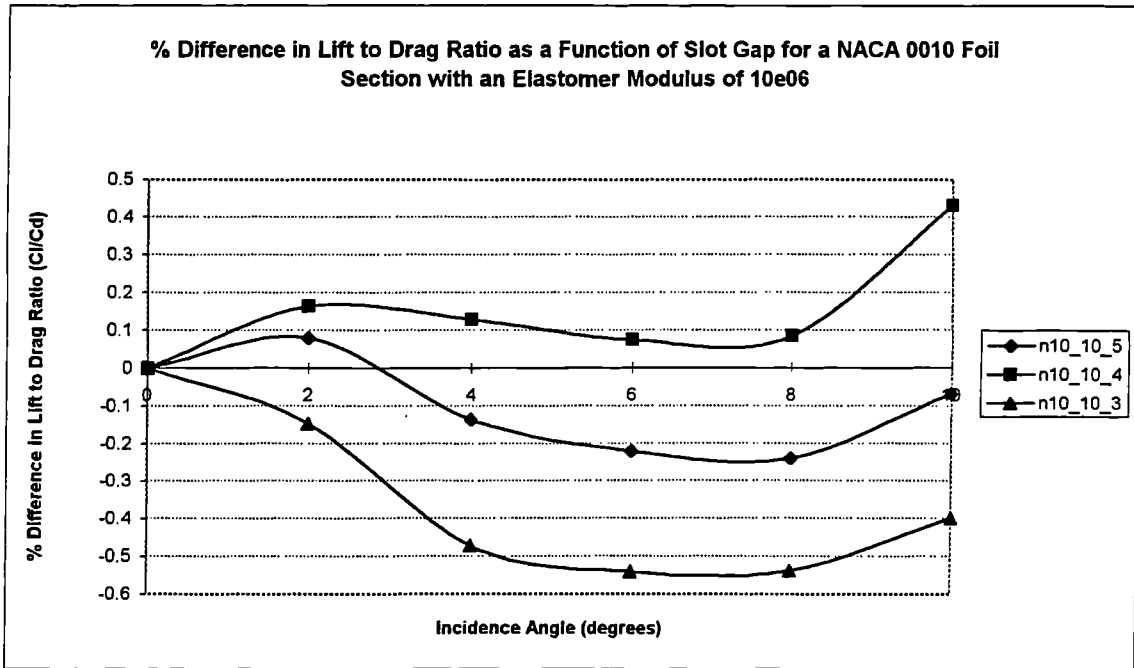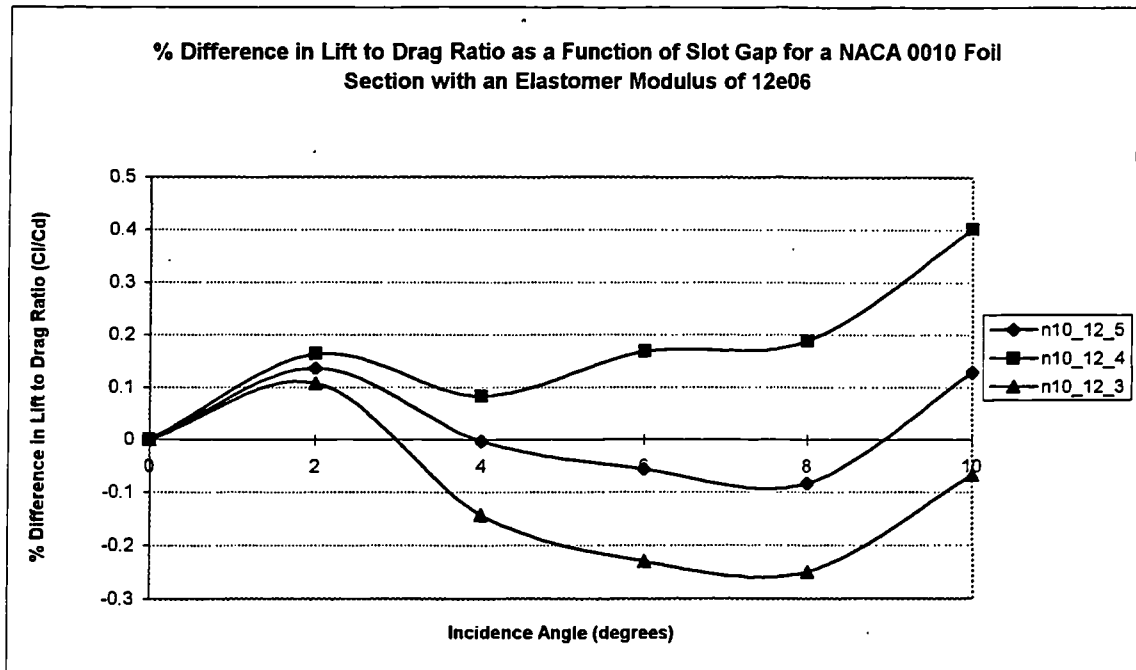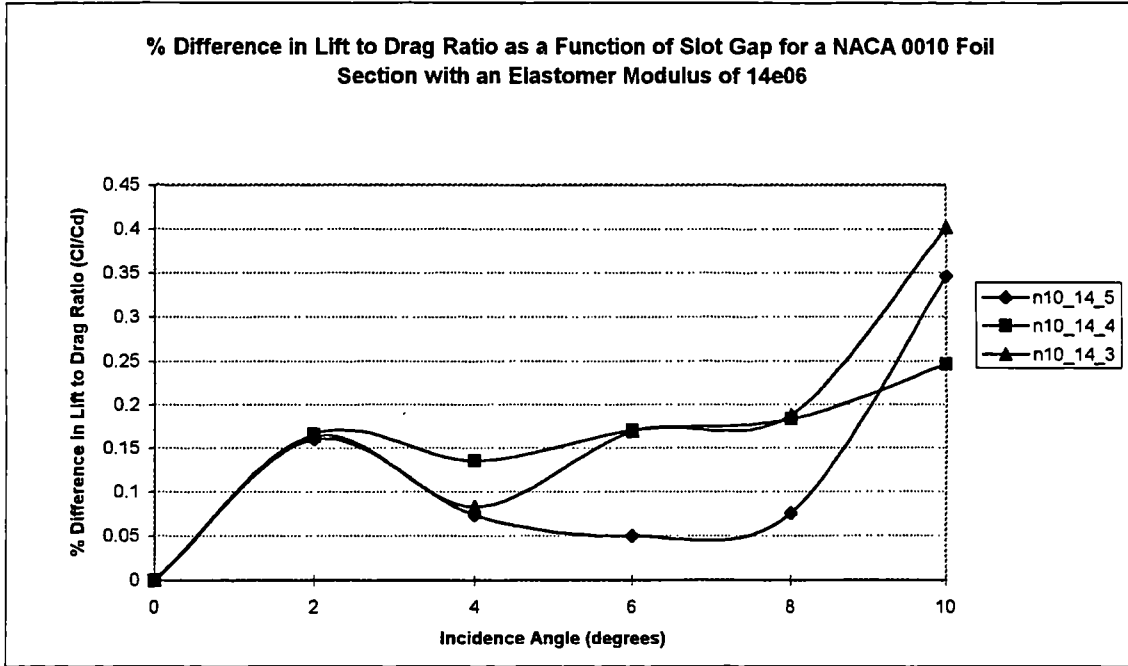
Figure 5.76
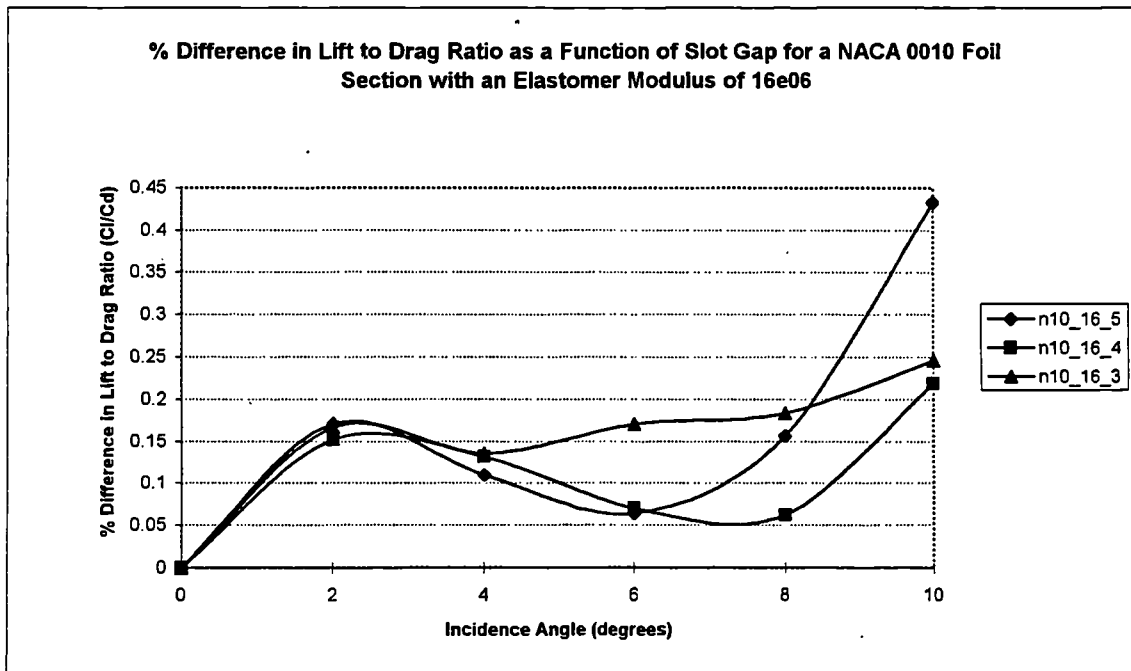
Figure 5.77

Figure 5.78
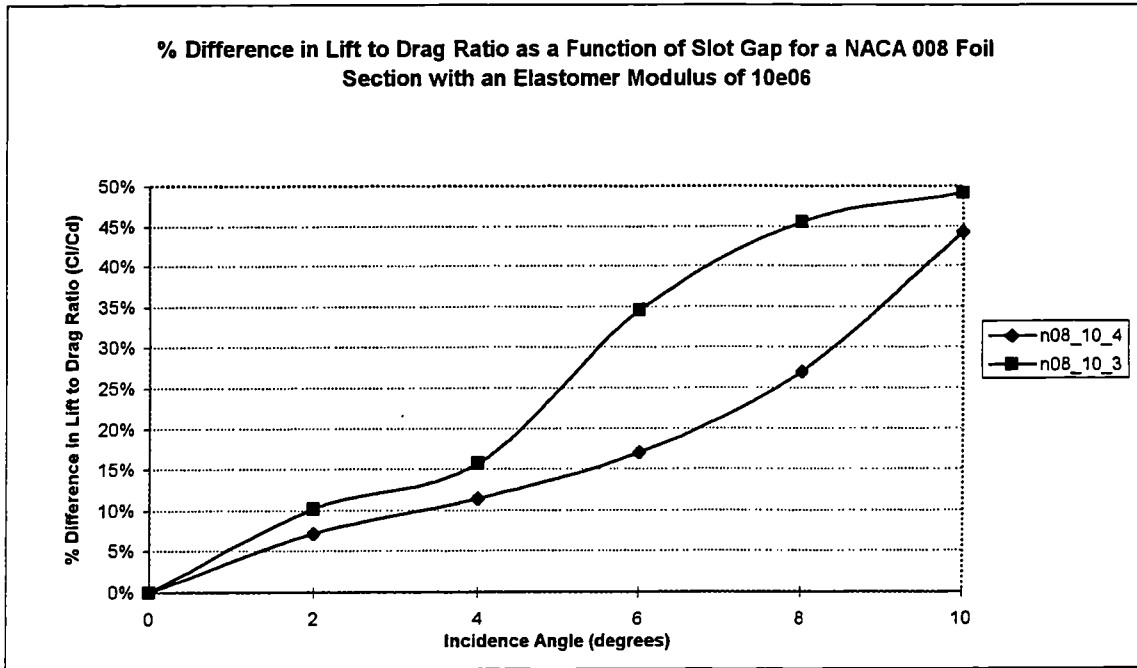
Figure 5.79

Figure 5.80

199
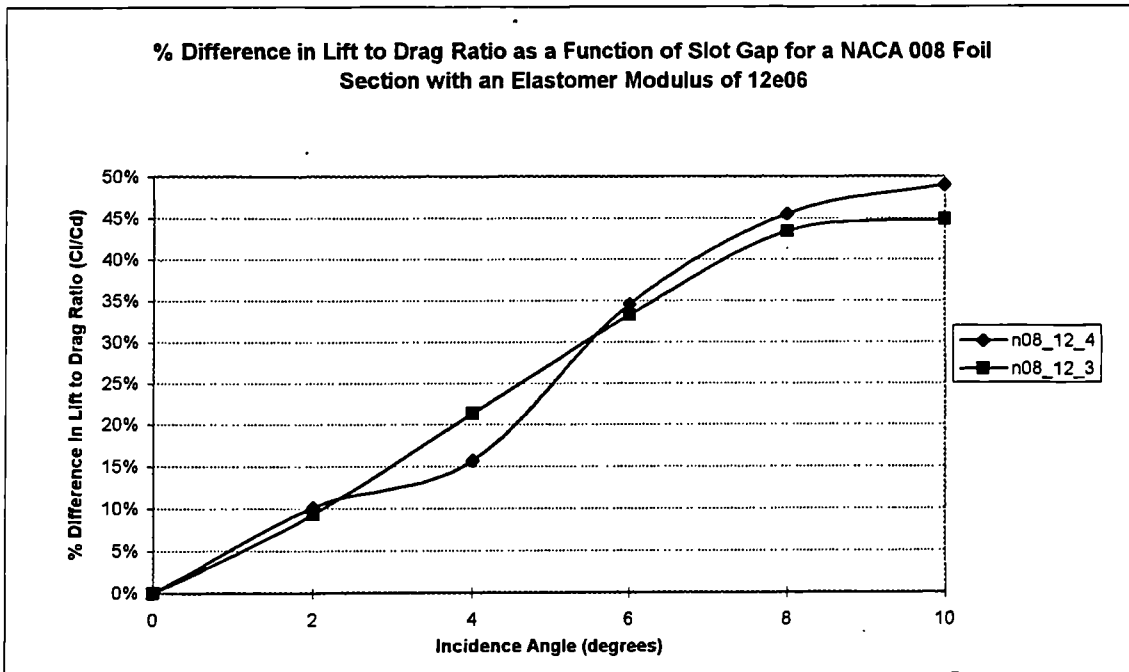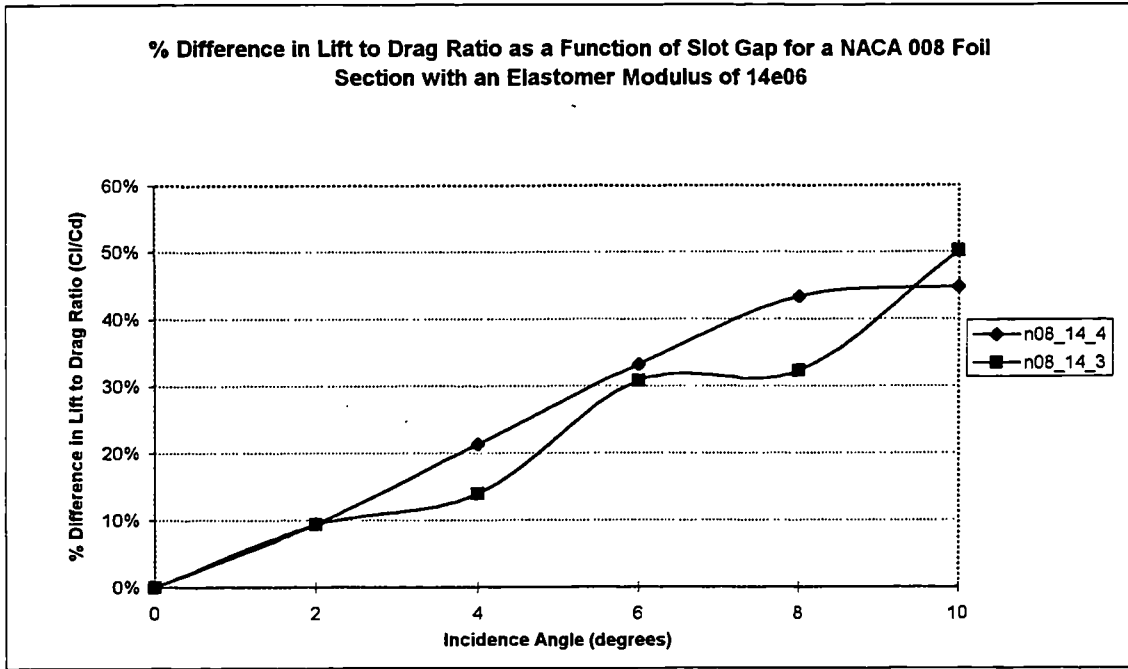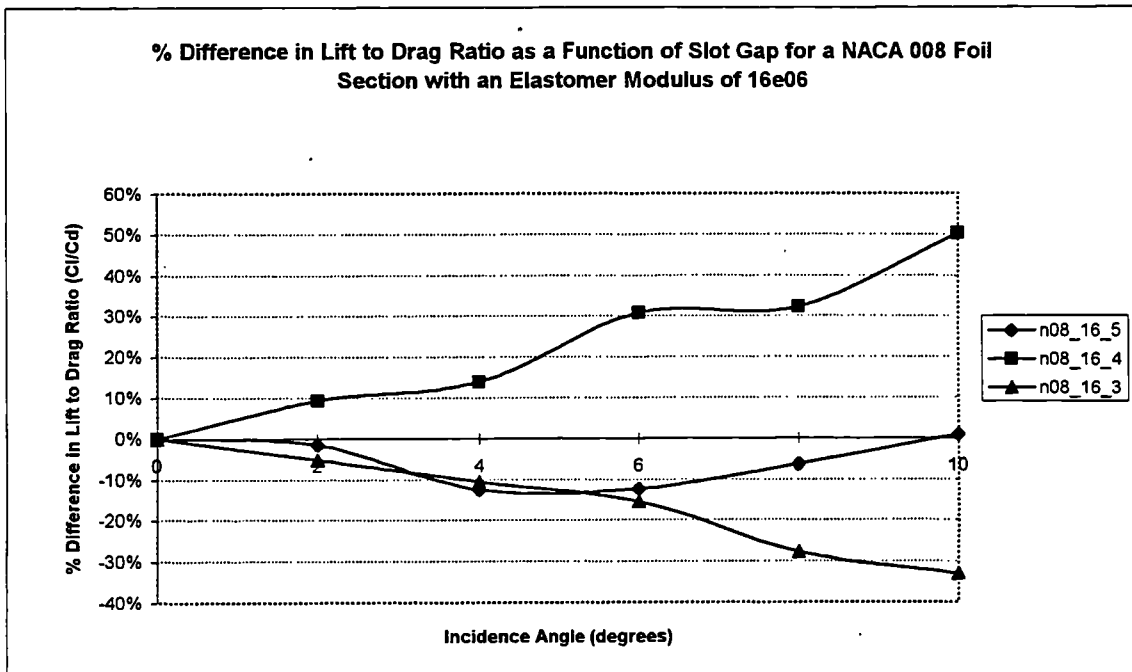
Figure 5.81

Figure 5.82

Figure 5.83

Figure 5.84

201

% Difference in Lift to Drag Ratio as a Function of Slot Gap for a NACA 006 Foil Section with an Elastomer Modulus of 16e06

Figure 5.85

202
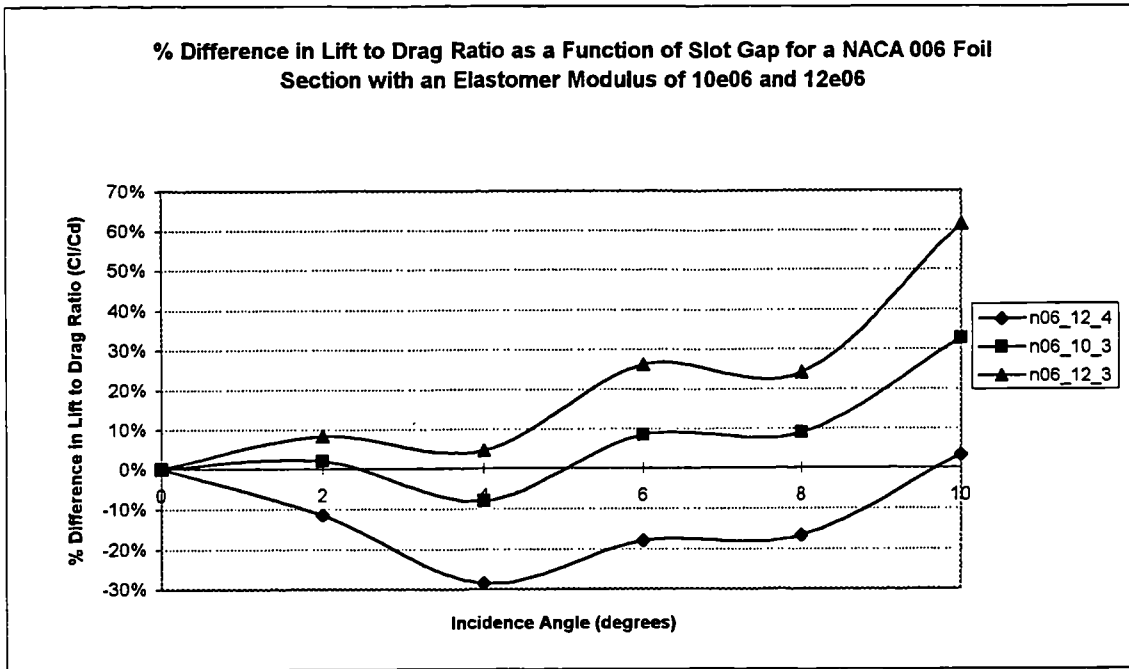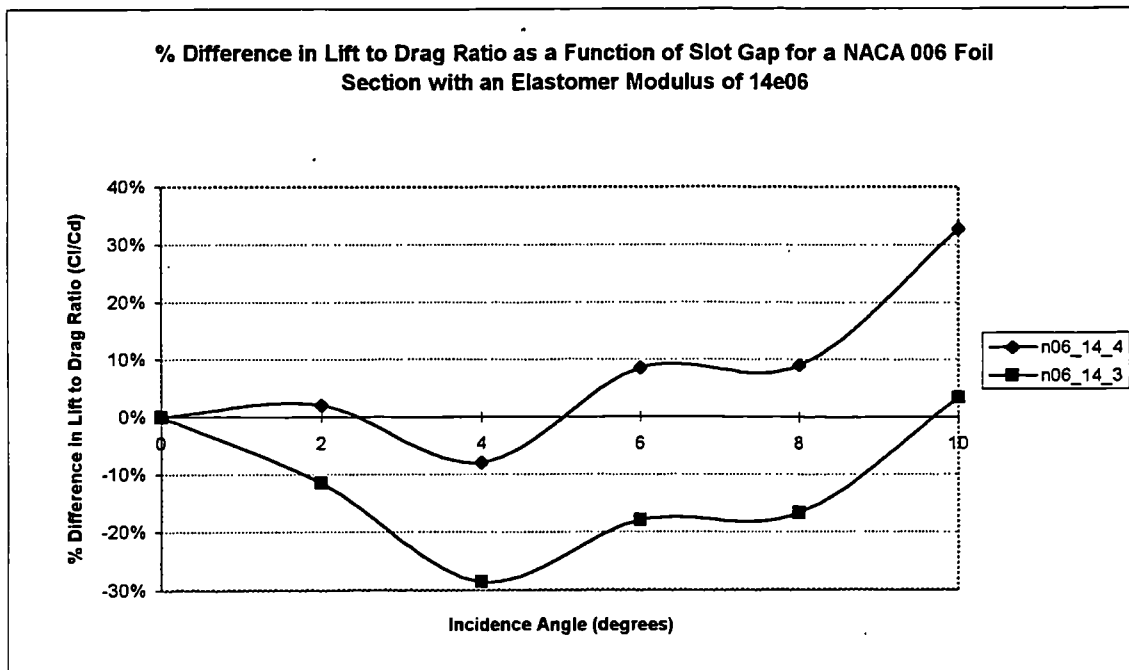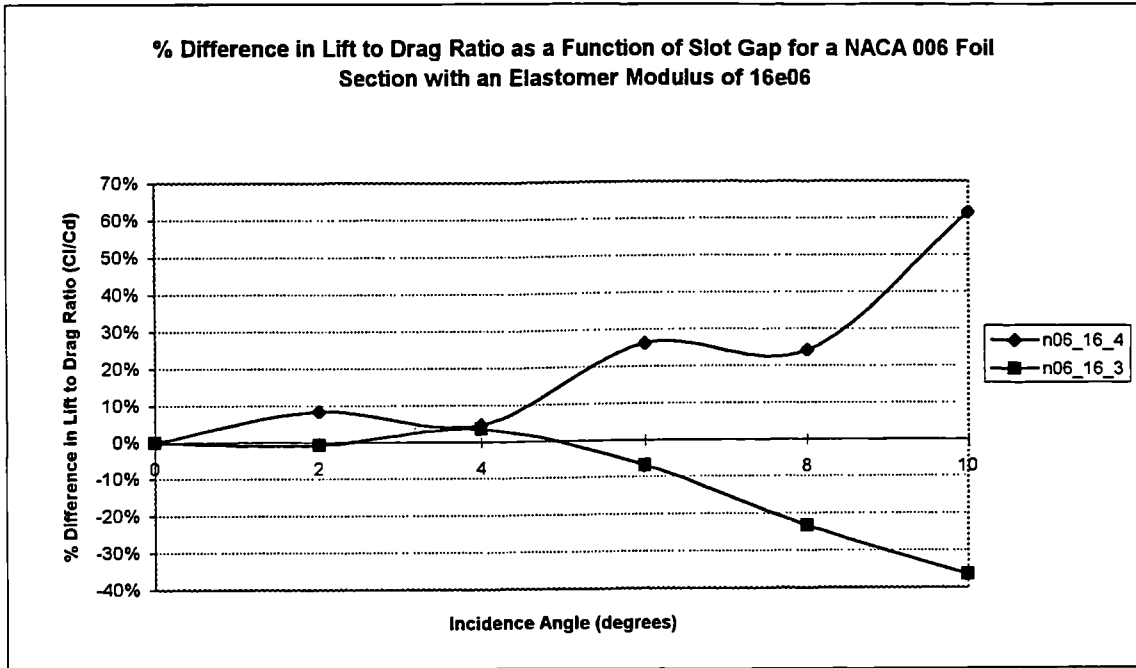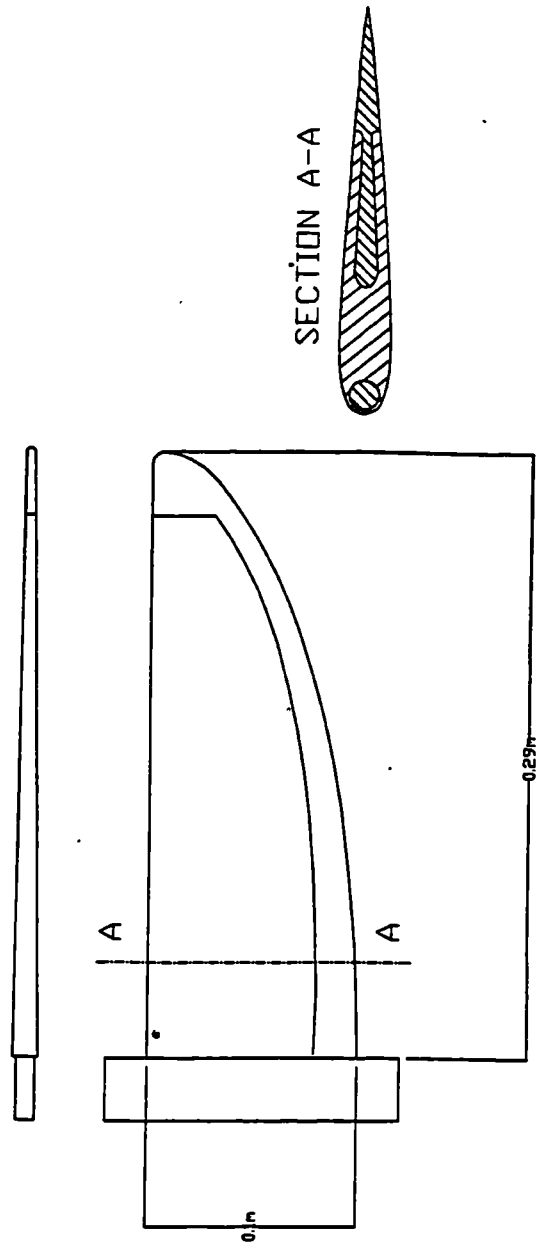
Figure 5.86 The General Assembly of the Prototype HTWF
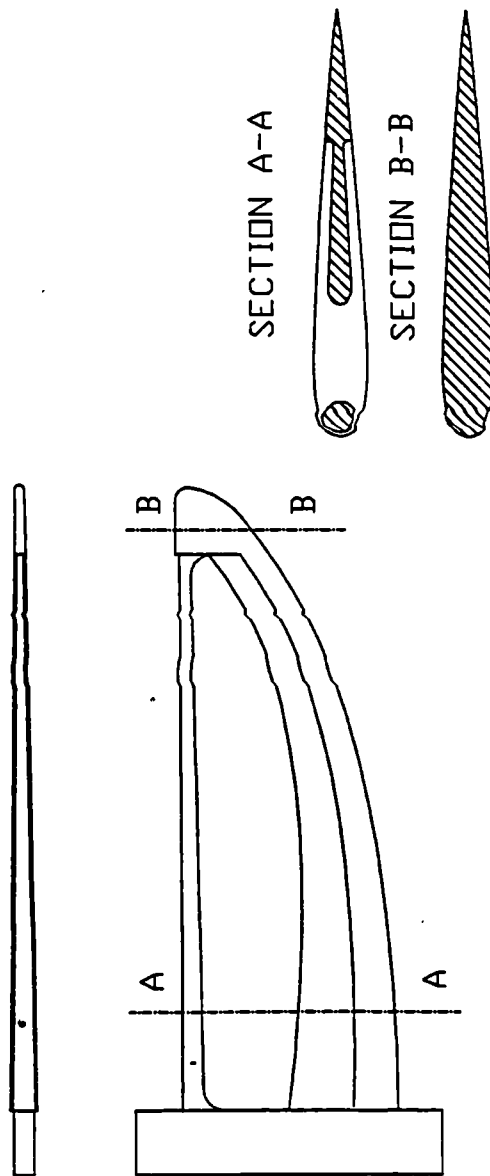
Figure 5.87   Skeleton Detail for Prototype HTWF
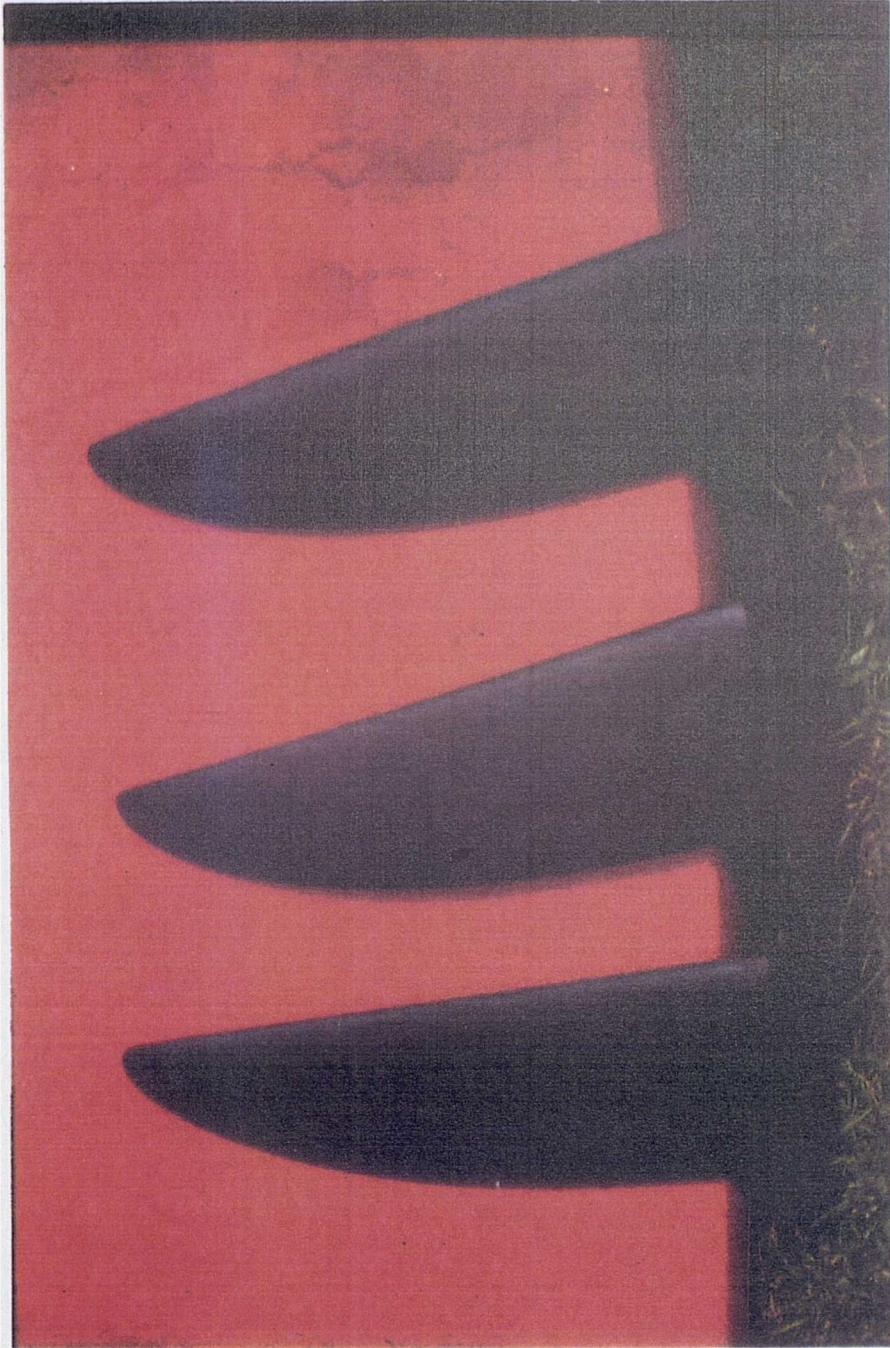
Figure 5.88   The Prototype Windsurf Fins

6.0   Discussion

This chapter attempts to draw together the various ideas and results found to date and to suggest the direction in which future work should be directed.

6.1   Summary of Test Results

6.1.1   Lift Data

A consistent increment in the C_l was demonstrated at all incidence angles for the HTWF configurations (with the exception of the n06_16_3) when compared with the rigid reference sections. This is as anticipated and is a direct result of the hydroelastic tailoring techniques employed to develop camber in a (normally) symmetrical cross section.

The increments in C_l are seen to be dependent on the initial outer profile geometry (t/c) and the magnitude of camber in the section. These in turn are a function of the flow characteristics, the geometric features of the HTWF section and the material usage.

The largest increments in C_l are demonstrated by what may be considered the most 'flexible' configurations. The 'flexibility' of the configurations can be seen to increase with larger slot gaps, thinner outer profiles and lower elastomer modulus values. Conversely, the 'flexibility' is reduced by smaller slot gaps, thicker profiles and higher elastomer modulus values.

In general the more 'flexible' configurations (NACA 0006 with 40% slot gap) demonstrate irregular percentage gains in C_l. This indicates that the configuration is somewhat unstable and 'sensitive' to the boundary conditions. It is considered that the more flexible configurations will be able to operate satisfactorily over a very limited range of Reynolds numbers and hence would not be suited to the unsteady loadings experienced in an open sea environment.

In comparison, the more 'rigid' or stable configurations (NACA 0012 with a 40% slot gap) show a consistent and almost linear percentage increase in C_l with increasing incidence angle. The extra material bulk and hence structural integrity associated with these thicker sections results in a more 'tolerant' design. The 'tolerance' of the thicker sections is demonstrated by the similar performance characteristics exhibited for varying slot gaps and elastomer modulus values. The thicker foils can therefore be considered to be more robust and able to tolerate a wider range of Reynolds numbers.

Some erroneous C_l increments are demonstrated by the configurations employing thick foil sections, low elastomer values and small slot gaps (n12_10_3, n10_10_3 and n10_12_3). This unusual rise in C_l results from the 'upturning' of the pivotal nose, which effectively increases the curvature on the upper surface. This is confirmed by considering the corresponding (substantial) increases in drag for these configurations.

Some of the largest percentage gains in C_l occur at low incidence angles (although this is slightly exaggerated by the smoothing of the graph curves). This behaviour is similar to the performance of sailwings and double surface sails and is likely to be the result of the significant contribution to the C_l resulting from the initial deformation of the section.

Most of the HTWF configurations demonstrate a large percentage gain in C_l at high incidence angles. This indicates that the drooping nose is operating in the prescribed manner, thereby delaying the onset of leading edge flow instabilities through the introduction of a suitable camber shape over the front of the section. Additionally, the percentage gains in C_l at these high incidence angles indicates that the camber in the HTWF configuration is still increasing in response to the surface pressure loads.

The effect of the camber system on the C_{Lmax} was not determined although it can be assumed that the drooping nose will have a beneficial effect in delaying the onset of leading edge stall (a thorough investigation of the stalling characteristics of the HTWF configuration would need to be performed in a flow tank at representative Reynolds numbers).

6.1.2   Drag Data

The percentage reductions in C_d for many of the HTWF configurations is significant (typically 20% at high incidence angles) and can be attributed to the successful operation of the drooping nose (the e472 configurations with the 'blunt' nose realised no performance benefits from this feature). By successfully drooping the nose, the following benefits are realised;

1. A more efficient splitting of the freestream at moderate to high incidence angles (when compared with a rigid symmetrical section).
2. A reduction in the negative pressure peak towards the nose region.
3. A rearward movement of the negative pressure peak.
4. A delay in the onset of leading edge stall.
5. A smoother upper surface curvature.

However it is also possible to over-rotate the nose by employing geometries and elastomer values which are too 'flexible'.

As with the gains in C_l, the reductions in C_d are a function of the camber shape, which again is principally governed by the 'flexibility' of the HTWF configuration (and the successful operation of the drooping nose).

It is possible to see that 'any' amount of camber will have a beneficial effect on C_l, whereas the opposite may be true in terms of drag reduction. This is because any modification to the outer geometry of a foil section can have a fundamental effect on the flow pattern and hence the C_d.

In general the least successful HTWF configurations, in terms of percentage reductions in C_d, are the most flexible (or unstable) ones (low elastomer modulus values, thin foil

sections and/or a large slot gap). A dependence between the elastomer deformation and the percentage change in C_d is therefore shown.

The greatest reductions in C_d at high incidence angles are associated with the thinnest sections, thereby indicating a relationship between the foil thickness and the percentage reduction in C_d (at high incidence angles). The pivotal nose can be seen to be having the greatest effect on the thinner sections (which inherently have a sharper nose radius) and the least effect on the thicker sections (with a 'blunter' nose radius). This is expected and is in agreement with theory.

It is also shown that the thinner sections are less stable than the thicker sections and are highly sensitive to the combination of slot gap and elastomer modulus. The thicker sections on the otherhand seem to be more 'tolerant' to changes in the elastomer modulus and slot gap.

The sudden improvements in C_l/C_d performance at high incidence angles for a number of the thinner configurations suggests that the nose is over-rotated for low and moderate incidence angles.

In terms of a consistent percentage reduction in C_d it is preferable to employ a configuration in which there is sufficient elastomer 'bulk' to resist excessively large deformations. Furthermore it is demonstrated that there is an optimum combination of elastomer modulus and slot gap for a maximum 'allowable' value of camber for each foil thickness and slot gap.

A number of summary points can be made about the C_d characteristics of the HTWF configurations.

1. At an incidence angle of zero degrees the HTWF configurations had nominally the same C_d as the corresponding rigid reference sections.

2. The magnitudes of C_d reduction (for the successful configurations) increased with increasing incidence angle, thereby indicating that the drooping nose is most effective at high incidence angles.

3. The drooping nose is least effective on 'blunt' nose profiles (large nose radius) and is most effective on 'sharper' nose profiles.

4. If the nose does not droop into the flow the detrimental effect on drag is considerable.

5. It is possible to over rotate the nose region which is detrimental.

6.1.3 Lift to Drag Ratio (C_l/C_d)

The overall percentage change in C_l/C_d is primarily a function of the C_d characteristics. This is because the percentage gains in C_l are considerably less than the corresponding percentage reductions in C_d.

It is demonstrated that there are optimum combinations of slot gap and elastomer modulus for a nominal foil thickness. Due to this it is not possible to establish general rules such as *'an increasing elastomer modulus and slot gap of 40% is optimal for all foil thicknesses'*. Predetermining the optimum values of slot gap and elastomer modulus for a nominal foil section is therefore not possible at the present time.

In general the thicker profiles exhibit the most consistent overall gains in C_l/C_d. They are also less likely to demonstrate a reduction in performance (when compared with the corresponding rigid section).

For the largest slot gap value (50%) the NACA 0012 configurations performed consistently well and achieved significant percentage gains in C_l/C_d (typically between 10% and 20% at 6°). In comparison, the NACA 0010 configurations did not perform as well (or as consistently) for this value of slot gap (-22% to 7% change in C_l/C_d at 6°). Excessive distortion in the finite element meshes precludes a comparison with the NACA 0006 and 0008 configurations.

For a slot gap of 40%, all of the configurations (apart from n06_12_4 and n06_14_4) demonstrated significant percentage increases in C_l/C_d. This indicates that the 40% slot gap is able to perform well with (and is tolerant of) a wide variety of foil thicknesses and elastomer modulus values.

The 30% slot gap will obviously be more restrictive in terms of the magnitudes of camber that can be induced in the section. This slot gap will also restrict the position of maximum camber to the leading edge region of the configuration. The effect of this demonstrated by the limited average percentage gains in C_l of approximately 4% (for the configurations which show an overall gain in C_l/C_d). A dependency between the percentage gain C_l/C_d and the foil thickness is demonstrated, with the thinner foils achieving the largest increments.

6.1.4 Converged HTWF Outer Profile Geometries

For a number of the more notable HTWF configurations, the converged outer profile geometries at an incidence angle of 6° are presented in Figures 6.1 to 6.7. The mean camber line is shown as the mid-point between the two surfaces. For all of these configurations the flow is emerging from the lower left corner of the page and travelling towards the upper right corner of the page.

Figure 6.1 shows the hydroelastically tailored n12_16_5 configuration, which exhibits the best percentage gains in C_l/C_d at an incidence angle of 6°. The effects of the hydroelastic tailoring of this section are shown by the induced camber and the drooping pivotal nose. These changes in geometry are subtle and yet significantly improve the C_l/C_d performance over the range of incidence angles.

Figure 6.2 shows the hydroelastically tailored n10_10_5 configuration, which exhibits a substantial reduction in C_l/C_d performance at an incidence angle of 6°. It is clear that the configuration is experiencing excessive distortions in the elastomer region. The result of this is the formation of a concave region on the pressure surface, an over-rotation of the pivotal nose and a the generation of discontinuities on both surfaces. This causes a substantial rise in C_d and hence reduction in C_l/C_d performance.

Figure 6.3 shows the hydroelastically tailored NACA 0008 sections with slot gaps of 40%. The dependence between the magnitudes of camber and the elastomer modulus is shown (larger magnitudes of camber with decreasing elastomer modulus).

Figure 6.4 shows the hydroelastically tailored n06_10_3 configuration. This illustrates that even though the pivotal nose has upturned (opposed to drooping) the resulting effect on C_l/C_d is beneficial. It is shown that the deformations in the elastomer result in an increase in the curvature of the upper surface and nose region. The increased radius reduces the local flow velocities and hence reduces C_d. The induced camber is shown to extend to 40% of the chord length. This is due to the tapering of the rear support and the extension and compression of the elastomer in these regions. Figure 6.8 shows the deformed mesh corresponding to similar initial configuration as Figure 6.2.

6.2   The Design Variables

From the analysis data it is clear that the operation of the HTWF configuration is dependent on the interaction of the separate design variables and not on one design feature alone. This suggests that for a given outer profile shape there will be an optimum combination of slot gap, elastomer modulus and pivotal mast location.

The successful configurations demonstrated the ability to raise the C_l and lower the C_d, thereby increasing the overall C_l/C_d.

An increase in the C_l was seen for all configurations in which the elastomer region was deformed. The increase in C_l is therefore a function of the deformation in the elastomer (induced camber).

The magnitudes of C_d are also a function of the elastomer deformation, with excessive geometry changes resulting in an increase in C_d. An optimum 'allowable' deformation in terms of increases in lift without an excessive increase in drag for a nominal foil thickness has not been established.

The analysis data shows that there is a requirement for a minimum slot gap to ensure that the HTWF configurations (in this format) operate in the desired manner and droop the nose into the flow. Currently this minimum slot gap would seem to be between 30% and 40% of the chord length.

The determining of this minim slot gap value is based on the limitations of a static analysis in which the assumption of an instantaneous loading of the foil section at an incidence angle of 6° and flow velocity of 10 ms^{-1} is made. In reality this loading would be transient and would develop gradually as a result of increasing sailing speed and incidence angle. The negative pressure peak calculated by the method at the leading edge is therefore unlikely to be so intense and is hence less likely to generate a moment arm of sufficient strength to stop the nose drooping into the flow. To suppress this phenomenon (in the

analysis) it may be necessary to artificially modify the load data in the first global loop so that the method is able to initiate the drooping movement of the nose.

Further work is required to establish the interaction of the design variables and how they can be tailored to arrive at an 'optimum configuration'.

6.3   Theoretical Three Dimensional Performance Gains

The data from the two dimensional analysis work is used to determine the theoretical effectiveness of the hydroelastically tailored variable camber system on a finite length windsurf fin. To simulate typical sailing conditions an incidence angle of 6° and a flow velocity of 10 ms^{-1} is assumed.

A benchmark finite length fin (Reference Fin) is specified as having a semi-elliptical planform of span 0.35m and root chord 0.08m with a rigid NACA 0012 cross section. This equates to a surface area of 2.199 × 10^{-2} m^2 and a geometric aspect ratio of 5.57 (AR$_{ef}$ = 11.14). The rake angle is 0° and there is no geometric twist such that a constant downwash is anticipated across the span in accordance with Prandtl's theory for elliptical wings (K = 1).

For comparative purposes a second fin (HTWF Fin) is specified as having an identical semi-elliptical planform, but employing a cross section featuring the n12_16_4 HTWF configuration. It is assumed that this hydroelastic cross section is incorporated across the entire span, although this may not be possible in reality.

6.3.1   Effective Incidence Angles of the Two Windsurf Fins

Due to the downwash the effective incidence angle of the two finite length fins will be less than the geometric angle of incidence where;

$$\alpha_{ef} = \alpha_g - \alpha_i \qquad (6.1)$$

where

$$\alpha_i = \frac{C_l}{\pi \cdot AR} \qquad (6.2)$$

At an incidence angle of 6°;

$C_l = 0.6862$ (reference fin)

$C_l = 0.7137$ (HTWF fin)

$AR_{ef} = 11.14$

giving effective incidence angles of;

$\alpha_{ef} = 4.88°$ (reference fin)

$\alpha_{ef} = 4.83°$ (HTWF fin)

and new effective wing coefficient of lift values C_L;

$C_L = 0.5577$ (reference fin)

$C_L = 0.5740$ (HTWF fin)

This represents a 2.7% increase in the section lift coefficient for the HTWF configuration as compared with the rigid reference fin.

The effect of this on total lift is given by;

$$Lift = \frac{1}{2}\rho v^2 S C_L \qquad (6.3)$$

giving

Lift = 628.01 N (reference fin)

Lift = 646.36 N (HTWF fin)

6.3.2   Total Drag for the Two Windsurf Fins

The total drag for a finite length lifting surface is defined as;

$$C_D = C_d + C_{Di} \qquad (6.4)$$

$$C_{Di} \doteq \frac{C_L^2}{\pi AR}(inRadians) \qquad (6.5)$$

where

$C_d = 0.0315$ (reference fin)

$C_d = 0.0271$ (HTWF)

giving

$C_D = 0.0409$ (reference fin)

$C_D = 0.0359$ (HTWF fin)

Applying these figures to the equation for total drag;

$$DRAG = \frac{1}{2}\rho v^2 S C_D \qquad (6.6)$$

giving

Drag = 46.05 N (reference fin)

Drag = 40.42 N (HTWF fin)

This represents a 12.22 % reduction in the drag for the HTWF as compared with the rigid reference fin.

6.3.3 Lift to Drag Ratio (L/D)

The L/D ratios of the two fins at an incidence angle of 6° are 13.64 for the Reference Fin and 15.99 for the HTWF fin.

These figures represent an increase in the lift to drag ratio of approximately 17.23 % for the HTWF configuration fin when compared with the rigid reference model.

6.3.4 Optimising the Windsurf Fin for Varying Parameters

Two approaches can be adopted for the reversible and variable camber system.

The first of these is to produce a fin with nominally the same surface area as a comparable conventional design. By employing the HTWF concept however, the lift produced at all incidence angles will be greater and the drag will be lower. The sailor will therefore be able to sail the fin at lower incidence angles, than with a conventional fin, to achieve the same magnitudes of lift. By sailing at a lower incidence angle further reductions in the magnitudes of drag (particularly induced due to the dependence on C_l^2) will be realised. Additionally it can be assumed that the stalling incidence angle will be increased thereby increasing the C_{Lmax}.

Alternatively, if the assumption is made that the same magnitudes of lift are required at a nominal incidence angle, a reduction in the surface area of the HTWF fin can be made due to the corresponding increase in the section lift coefficient. A 2.7% gain in the C_L at an incidence angle of 6°, will allow for a corresponding 2.7% reduction in the surface area.

6.4 Applicability of Data to Other Reynolds Numbers

The series of two dimensional tests were performed at a representative Reynolds number of 8.4×10^5 based on a sailing speed of 10 ms^{-1} and a fin chord length of 0.1m. Assuming a doubling of the sailing speed the Reynolds number will increase to 1.68×10^6 (although this is unrealistic because a smaller fin with a shorter chord length would be used for these sailing speeds, thus reducing the Reynolds number).

In terms of the flow characteristics, this magnitude of change in Reynolds number is unlikely to have any noticeable effects apart from a modification to the transition point. Baubeau and Latorre [8] observe the trend whereby for a constant angle of attack, the position of the boundary layer moves forward with increasing Reynolds number for two dimensional hydrofoil sections. They also conclude that at a constant Reynolds number,

the changing angle of incidence can result in a large shift of the location of seperation and transition. It can therefore be concluded that the transition point will move further forwards with an increasing Reynolds number. The effect of this on the C_l and C_d would need to be investigated experimentally.

In terms of the behaviour of the elastomer, this change in Reynolds number will have a profound effect due to the dependence of the surface pressure forces on the velocity squared (v^2). A doubling of the Reynolds number will result in a fourfold increase in the surface pressure loading. This is highly significant as any change in the surface pressure loads has the potential to significantly alter the profile of the cross section.

It is however reasonable to expect that footsteering techniques will be used to moderate or 'tune' these forces through changes to the incidence angle as there is a finite limit to the fin generated moment arm that the sailor can resist.

To deal with the varying surface loads at different flow speeds, three approaches for the flexible elastomer are envisaged;

1. Optimise the HTWF concept for a specific or limited range of Reynolds number.
2. Investigate methods for making the stiffness of the elastomer adaptive over a range of Reynolds numbers.
3. Incorporate some form of 'limiter' (mechanical or otherwise) to restrict the deformations in the elastomer to an 'allowable' or finite value.

6.5   Structural and Mechanical Design Considerations

Although a detailed structural design was not carried out, the development of the prototype windsurf fin (Section 5.3) has established that the concept can be fabricated and operated successfully. Further work is required to investigate the limits of the HTWF geometries and material properties.

6.6   Summary of HTWF Investigation

This preliminary investigation into a variable and reversible camber system for the windsurf fin has established the following points.

- Hydroelastic tailoring techniques can be used to develop a functioning reversible and finitely variable cambered fin for the sport of windsurfing.

- It is possible to increase the C_l and reduce the C_d (thereby achieving a gain in C_l/C_d) at all of the incidence angles considered.

- The pivotal mast design droops the nose into the flow. This is more efficient at splitting the flow at moderate to high incidence angles (in comparison with a rigid symmetrical section) resulting in a reduction in C_d. The drooping nose will also delay the onset of stall thereby increasing the potential C_{Lmax} (although this has not been investigated in the current study).

- The hydroelastically tailored windsurf fin has superior C_l/C_d performance characteristics at a nominal incidence angle than comparable rigid cross section windsurf fin.
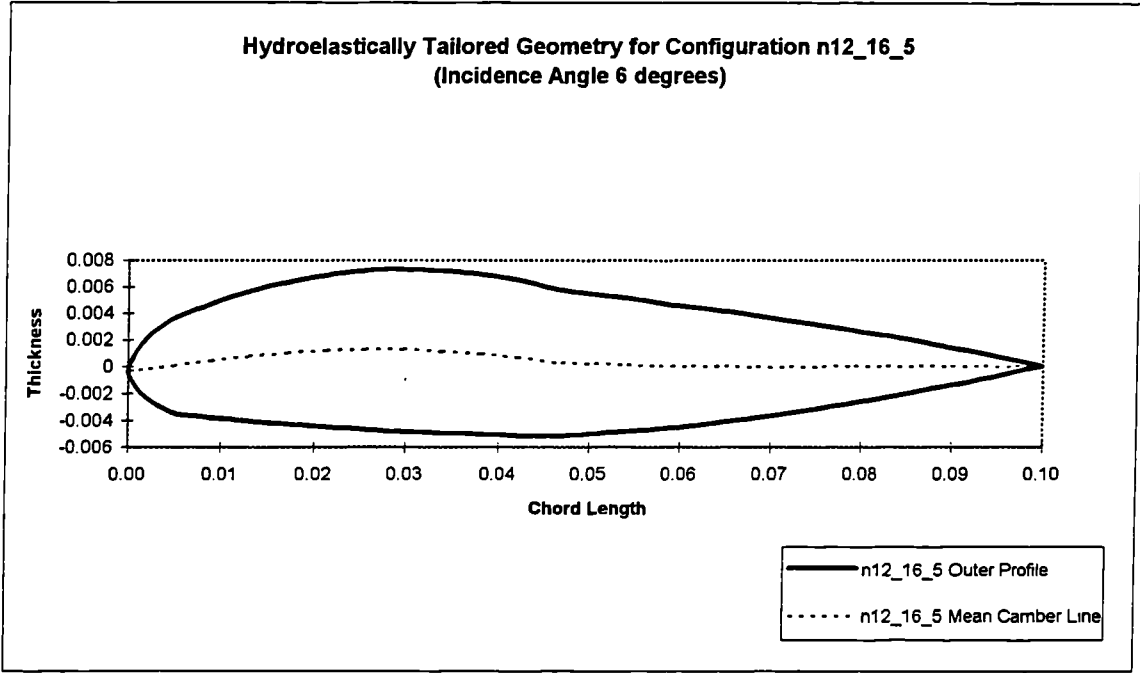
Figure 6.1
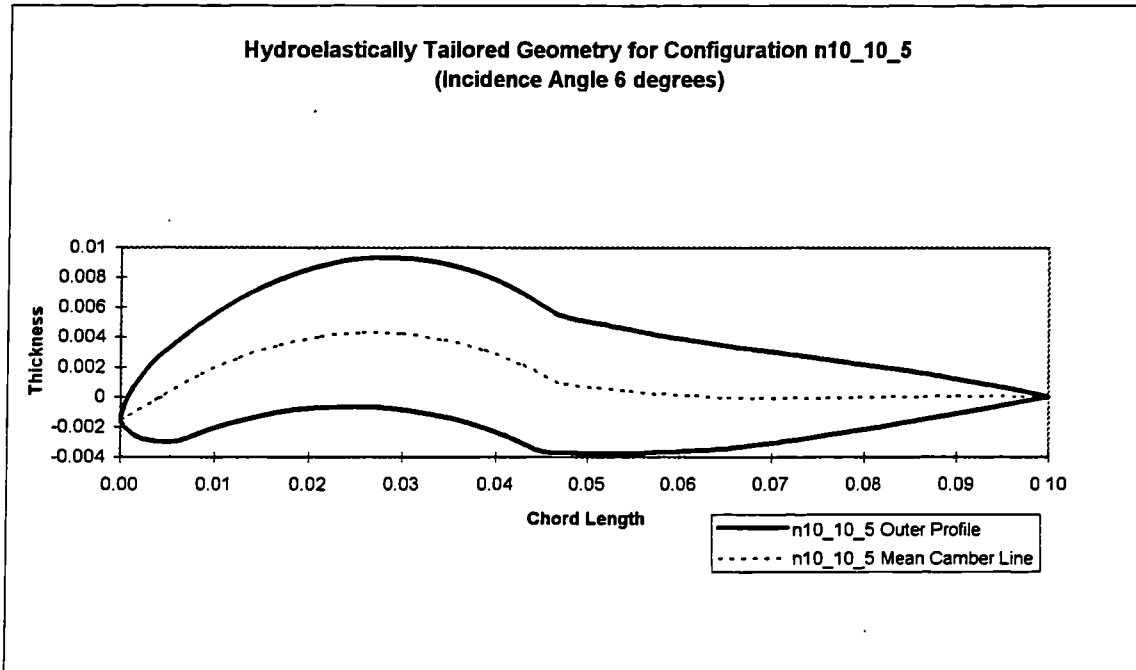
Figure 6.2

Figure 6.3

Figure 6.4

**Hydroelastically Tailored Geometry for Configuration n08_12_4
(Incidence Angle 6 degrees)**

Figure 6.5

**Hydroelastically Tailored Geometry for Configuration n08_10_4
(Incidence Angle 6 degrees)**
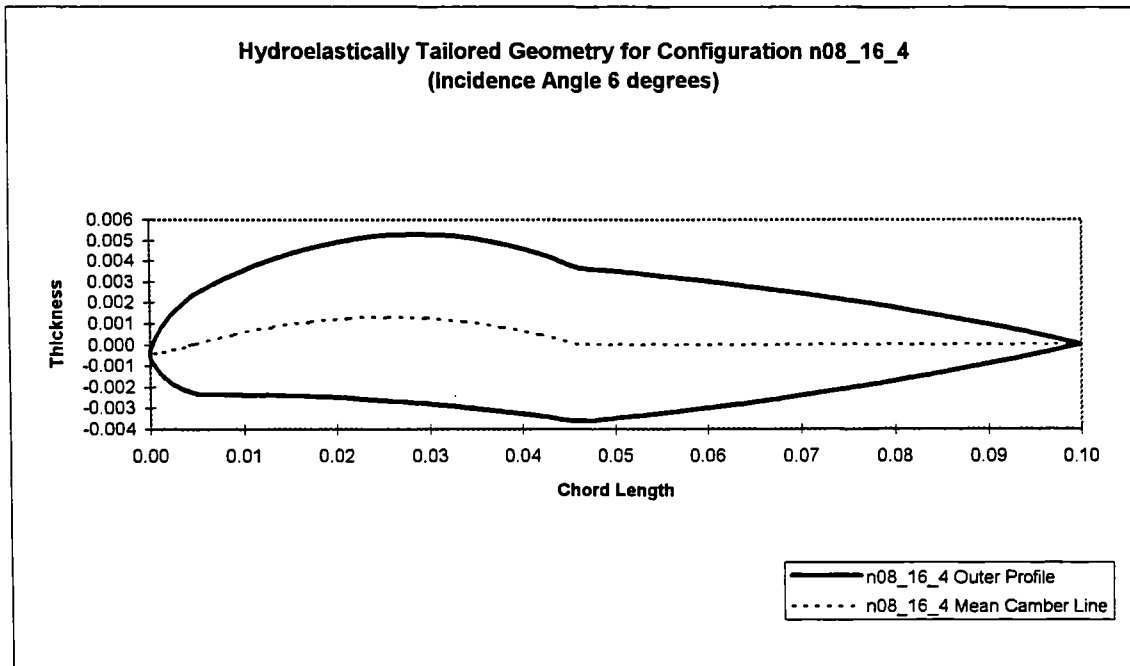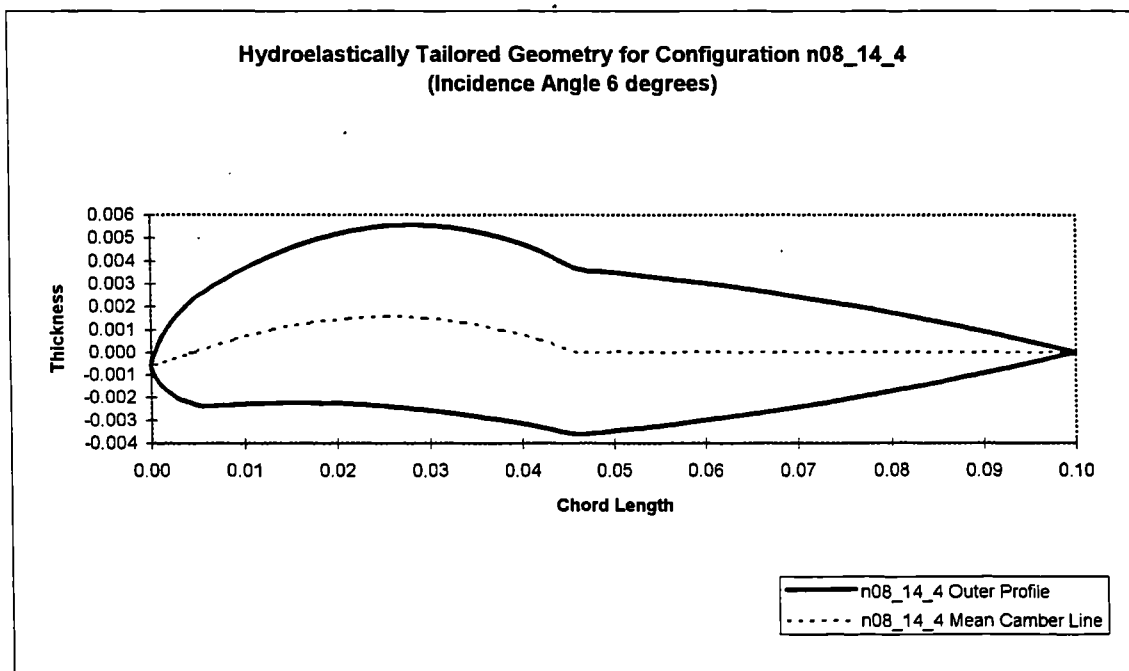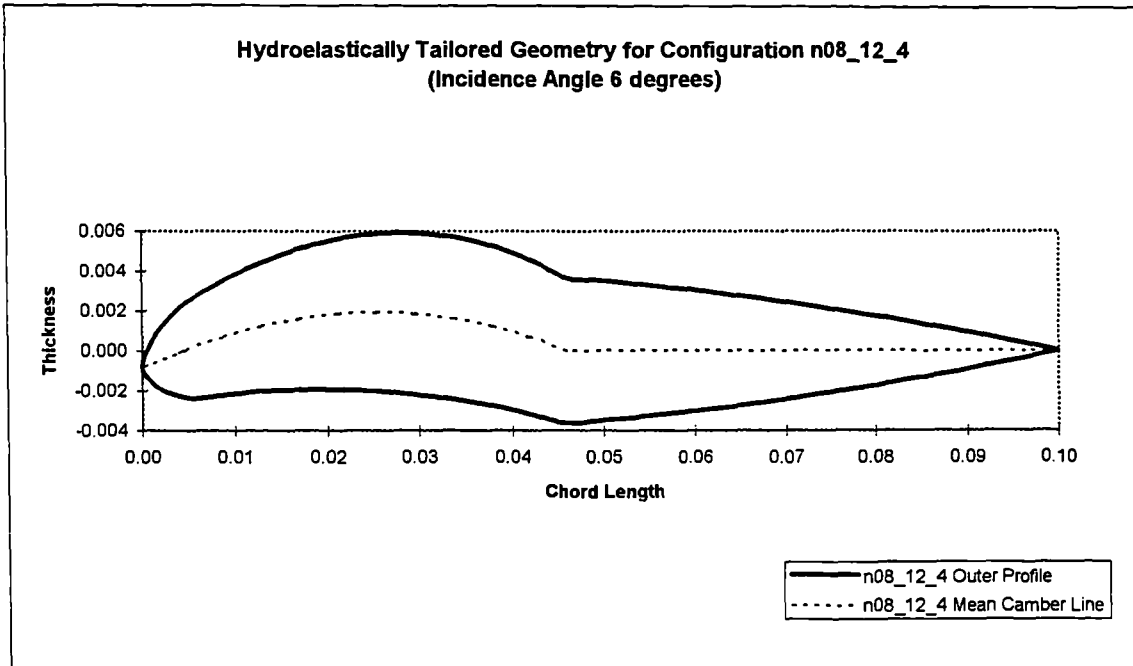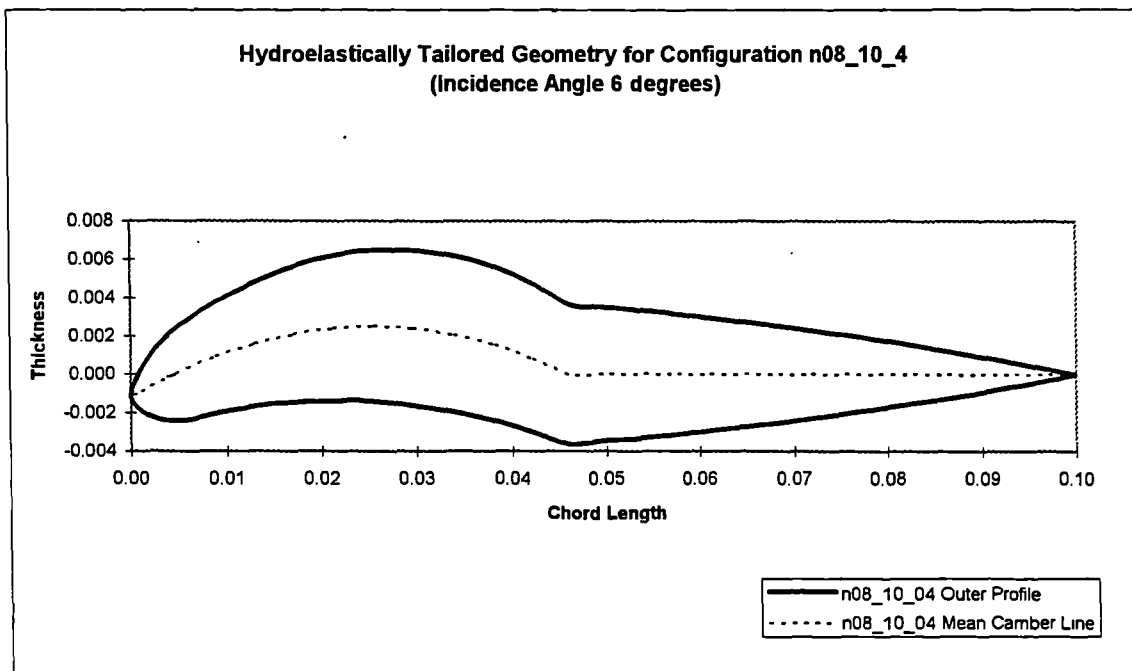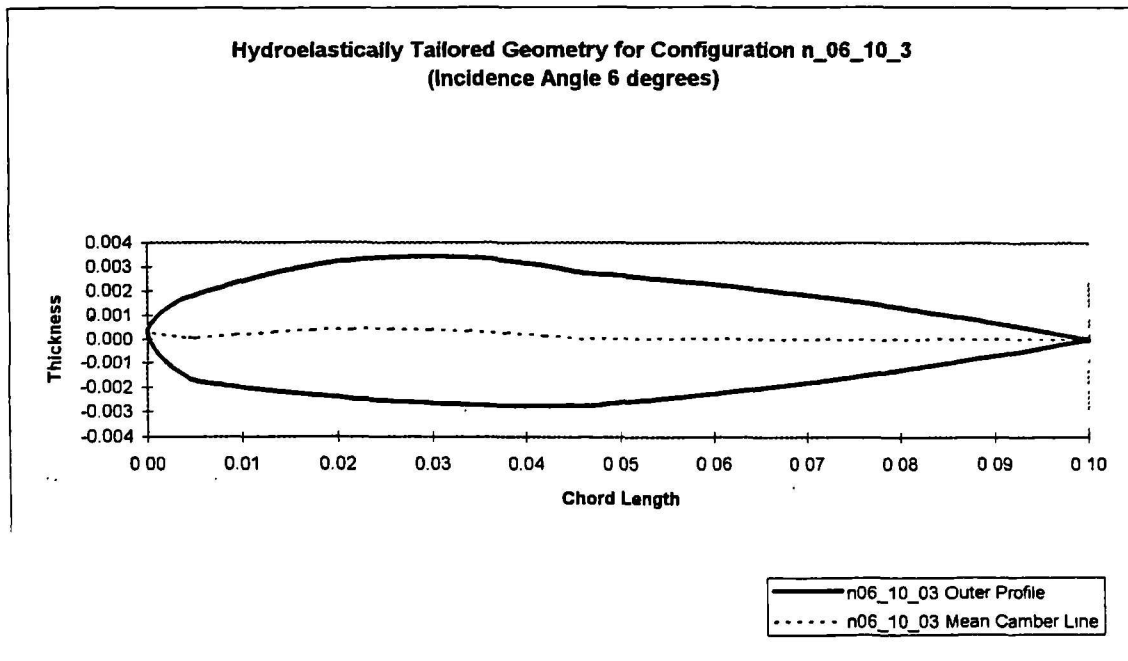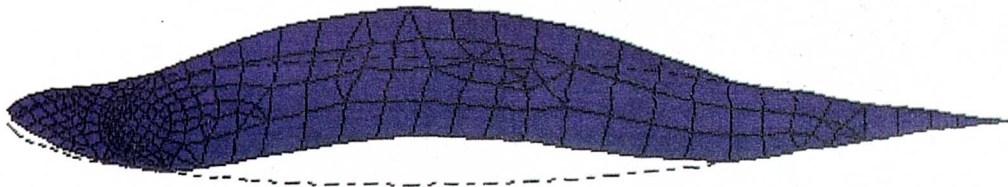
Figure 6.6

Figure 6.7

Figure 6.8 Deformed Cross Section Mesh

7.0   Conclusions and Recommended Areas for Further Work

7.1   Conclusions

1. Limited gains in the operational efficiency of the conventional windsurf fin are likely to result from further refinements to the planshape, cross section, surface finish and material usage.

2. A radical reworking of the design of conventional windsurf fin is required to realise significant operational performance gains.

3. Although variable geometry technologies offer the potential for significant performance gains to the windsurf fin, there has only been limited development work in this area.

4. Conventional mechanical flaps are not suitable for developing a variable camber section for the sport of windsurfing.

5. Hydroelastic tailoring techniques offer a method for developing a reversible and finitely variable cambered windsurf fin. The proposed hydroelastically tailored windsurf fin concept features a supporting skeleton structure and a flexible elastomer material which is able to deform under the influence of the surface pressure forces, thereby creating camber in the cross-section. This technique may also lead to the development of reversible supercritical type fins for the boards operating at the cavitational limits of conventional windsurf fins.

6. Test results (assuming a 2D flow) indicate that, for the successful configurations, the lift coefficient at all incidence angles is increased and the drag coefficient at all incidence angles is decreased. This results in a higher lift to drag ratio at all incidence angles.

7. The preliminary investigation indicates that the use of a pivotal nose is more efficient at splitting the flow and hence reducing the section drag coefficient. It can be tentatively

concluded that this feature will also be successful at delaying the onset of leading edge stall and hence elevating the value of C_{Lmax}.

8. The pivotal nose is least effective on blunt nose shapes and most effective on the thinner profiles with a sharper nose radius.

9. The introduction of camber can allow the nominal surface area of the fins to be reduced whilst still producing the same magnitudes of lift for less drag. Perhaps more importantly, the use of a variable and reversible cambered section with a drooping nose will allow a wider range of performance possibilities within the existing envelope of fin design. The hydroelastic tailoring thereby provides a means for optimising the performance of the fin for multipoint operation.

10. The manner in which the slot gap, foil thickness, elastomer modulus and mast pivot point interact is complex.

11. The production of a prototype fin has established that it is feasible to fabricate and operate a functioning finite length windsurf fin featuring a hydroelastically tailored cross section.

12. The hydroelastically tailored cross section evaluated in this study was deliberately kept simple. More advanced approaches are envisaged to regulate the deformations in the adaptive structure. This could be through the inclusion of additional materials and stiffening structures to precisely regulate and limit the nature of the elastomer deformations.

7.2   Recommended Areas for Further Work

The current investigation has demonstrated the potential for producing a very effective variable camber cross section for the fins used in the sport of windsurfing. There are however many areas where further work is required.

1. The accuracy of the CFSAT (particularly the CFD method) and the results data needs to be fully investigated. For this a series of comparative two dimensional model flow tests at representative Reynolds numbers is recommended. Following on from this three dimensional tank tests of finite length windsurf fins are required.

2. An investigation into alternative CFD methods is required. By using other methods it may be possible to model the behaviour of the boundary layer more accurately (than with the present method).

3. The dynamic performance, flutter and stability characteristics of the configuration needs to be investigated. These phenomena are again likely to be revealed through the use of tank testing techniques on both two dimensional and three dimensional models.

4. The effect of the variable camber system and particularly the pivotal nose on the stalling angle and hence the C_{Lmax} needs to be investigated with tank testing techniques.

5. An investigation over a range of Reynolds numbers is required due to the dependence of the surface pressure loads, and hence the elastomer deformations, on the velocity squared.

6. Further work is required to establish the optimum position of the pivotal mast and to determine the minimum allowable slot gap to ensure that the nose rotates properly into the freestream.

7. A detailed structural and mechanical design investigation is required. This investigation will establish the weight penalties (if any) associated with the system, as well as establishing the limits to which the geometries of the skeleton can be taken and yet still be able to provide sufficient structural integrity.

8. The gains resulting from the use of the variable camber system on a finite length windsurf fin need to be carefully evaluated. An example of this is the trade off in terms of reducing the surface area with the resulting increase in induced drag.

9. An investigation into the use of additional materials, geometries or devices to stabilise, regulate or limit the nature of the elastomer deformations is required. In the current system the elastomer is pretty much 'free to find' its own final deformed shape. It may therefore be beneficial to control or regulate the elastomer deformations, particularly in the pressure recovery region, so that the location and nature of the camber is predetermined. This could lead to a reduction in the drag associated with some of the more deformed configurations.

10. An investigation into how the configuration of the HTWF cross section might need to be adapted or modified for the different disciplines and ability levels in the sport. This problem exists with other equipment components whereby the more efficient articles of equipment tend to require a certain ability level to be used effectively (for example a fully battened race sail is not suitable for a beginner).

11. An investigation into the most suitable candidate materials and fabrication processes needs to be performed. The prototype fin was fabricated using materials, technologies and techniques that were readily available to the author. It is acknowledged that there are likely to be more suitable materials and fabrication processes for both the elastomer and the skeleton.

12. An investigation into the 'feedback' loop between the sailor and the hydroelastically tailored windsurf fin needs to be performed.

13. An investigation into the use of this technology to develop reversible lifting surfaces for supercritical or cavitating flow conditions.

14. An investigation into an inverse method whereby the required final outer profile geometry is specified first, from which the required geometries and material properties (in the symmetrical shape) to achieve the shape are derived.

15. An investigation into the application of the concept to other lifting and control surfaces such as the keels, fins and rudders on other marine vehicles, and wings and spoilers on aircraft and land based vehicles.

8.0   REFERENCES

[1] **Abbott, I. H. and von Doenhoff, A. E.** (1949). Theory of Wing Sections. Dover Publications. ISBN 0-486-60586-8.

[2] **Acosta, A.J., Akbar, R. and Green, S.I.** (1988). The Influence of Tip Geometry on Trailing Vortex Rollup and Cavitation. Cavitation and Multiphase Flow Forum. pp76-80.

[3] **Alfredsson, P.H. and Johansson, A.V.** (1985). Recent Developments of Drag Reduction Methods for Ships. Second International Symposium on Ship Viscous Resistance. Goteborg, March 18 - 20, 1985.

[4] **Anderson, J.D.** (1995). Computational Fluid Dynamics - The Basics with Applications. McGraw-Hill. ISBN 0-07-001685-2.

[5] **Ashenberg, J. and Weihs, D.** (1984). Minimum Induced Drag of Wings with Curved Planforms. Journal of Aircraft. 21, pp89-91

[6] **Baker, R.M.L.** (1968). Science. Hydrofoils: Optimum Lift Off Speed for Sailboats. 162, pp1273-1275

[7] **Bathe, K-J.** (1996). Finite Element Proceedures. Prentice-Hall. ISBN 0-13-301458-4.

[8] **Baubeau, R. and Latorre, R.** (1986). Numerical Study of the Boundary Layer Transition for 2-Dimensional NACA 16-012 and 4412 Hydrofoil Sections. Journal of Ship Research. 30(1), pp43-50.

[9] **Benjamin, B.T.** (1960). Effects of a Flexible Boundary on Hydrodynamic Stability. Journal of Fluid Mechanics. Part 9, pp513-532.

[10] **Berry, A.** (1994). Invisible Force Field Cuts Drag. Eureka Magazine. pp11.

[11] **Blick, E.F. and Walters, R.R.** (1968). Turbulent Boundary Layer Characteristics of Compliant Surfaces. Journal of Aircraft. 5(1), pp11-16.

[12] **Bradfield, R.G. and Harris, R. G.** (1920). Model Experiments with Variable Camber Wings. Aeronautical Research Committee Reports and Memoranda No. 677.

[13] **Bragg, R., Lee, Y.T., Long, R.F. and Thew, M.T.** (1977). Experiments with Soluble Polymeric Drag Reducing Coatings. 2nd International Conference on Drag Reduction Aug 31st - Sept 2nd, 1977. ppG2-23 - G2-40.

[14] **Brahney, J. H.** (1985). Optimum Wing for All Conditions? Aerospace Engineering, vol5, pp36-40.

[15] **Bresina, J. J., Fullerton, C. G., Kempel, R. W. and Phillips, P. W.** (1989). AFTI/F-111 Airplane Mission Adpative Wing Operational Flight Evaluation Technique Using Uplinked Pilot Command Cues. NASA DFRG H-1585, pp3.6-1 - 3.6-19.

[16] **Broers, C.A.M. and Buckingham, D.J. and Chiu, T.W. and Pourzanji, M.M.A.** (1992). Effects of Fin Geometry and Surface Finish on Sailboard Performance and Maneouvreability. Maneouvring and Control of Marine Craft. Computational Mechanics Publications. Edited Wilson, P.A.

[17] **Broers, C.A.M. and Chiu, T.W. and Walker, A.H.C.** (1993). An Experimental Study of the Effects of Deformable Tip on the Performance of Fins and Finite Wings. AIAA 93-3000.

[18] **Brown, D.K.** (1980). Hydrofoils: A Review of Their History, Capability and Potential. NASA TP 1427.

[19] **Burkett, C.W.** (1989). Reductions in Induced Drag by the Use of Aft Swept Wing Tips. Aeronautical Journal. December 1989, pp400-405.

[20] **Burns, B. R. A.** (1979). Whys and Wherefores of Wings. Air International. 16, pp81 - 85.

[21] **Butter, D.J.** (1984). Recent Progress on Development and Understanding of High Lift Devices. In AGARD Conference Proceedings No. 365, Brussels, 21-23 May 1984. pp1-1 - 1-26.

[22] **Buttrill, C.S., Bacon, B.J., Houck, J.A., Heeg, J. and Wood, D.V.** (1996). Aeroservoelastic Simulation of an Active Flexible Wing Wind Tunnel Model. NASA Technical Paper 3510.

[23] **Callaghan, J. G.** (1974). Aerodynamic Prediction Methods for Aircraft at Low Speeds with Mechanical High Lift Devices. AGARD Lecture Series no. 67. pp2-1 - 2-52. Von Karman Institute, Brussels, 1974

[24] **Carter, M.** (1989). Fin Theory and Design. Windsurf Magazine. 88, pp62-63.

[25] **Chen, Z.L. and Vakili, A. and Wu, J.M.** (1982). Wing Tip Jets Aerodynamic Performance. International Council of the Aeronautical Society. (2) pp1115-1121.

[26] **Chiu, T.W. and Van Den Bersselaar, T.** (1993). The Effects of Tip Flexibility on the Performance of a Blade Type Windsurf Fin. Exetr University, England.

[27] **Clayton, B.R. and Bishop R. E. D.** (1982). Mechanics of Marine Vehicles. J. W. Arrowsmith Ltd., Bristol. ISBN 0-419-12660.

[28] **Cole, S. R., Boyd, P. and Miller, G.** (1990). An Overview of the Active Flexible Wing (AFW) Program. Fourth Workshop on Computational Control of Flexible Aerospace Systems, Williamsburg, VA. July 11-13, 1990.

[29] **Colling, J. D.** (1995). Sailplane Glide Performance and Control with Fixed and Articulating Winglets. M. S. Thesis, Texas A and M University. NASA-CR-198579.

[30] **Cook, M.V.** (1988). To Fly Like a Bird. Physics in Technology. 19, pp84-96.

[31] **Cook, S.** (1994). Cutting Edge. Windsurf Magazine. 136, pp40-44.

[32] **Crimi, P.** (1970). Experimental Study of the Effects of Sweep on Hydrofoil Loading and Cavitation. Journal of Hydronautics. 4(1), pp3-9.

[33] **Crossley, G.** (1992). Findestructibility. Boards Magazine. 85, pp86-88.

[34] **Cuche, D.E. and Nagamatsu, H.T.** (1981). Low Reynolds Number Aerodynamic Characteristics of Low Drag NACA 63-208 Airfoil. Journal of Aircraft. 18(10), pp833-837.

[35] **Dawes, B., Bornhoft, S. and Leonard, I.** (1988). Technical Test: Sea Slide. Boards Magazine. 54, pp 88.

[36] **Deschamps, A.** (1995). Voici Le Matos Du XXIe Siecle. Planchemag. 170, pp44-51.

[37] **Dillner, B. and May, F.W. and McMasters, J.H.** (1984). Aerodynamic Issues in the Design of High Lift Systems for Transport Aircraft. AGARD, pp9-1 - 9-22.

[38] **Dimotakis, S. and Shen, Y.T.** (1989). Viscous and Nuclei Effects on Hydrodynamic Loadings and Cavitation of a NACA 66(mod) Foil Section. Journal of Fluids Engineering. 89(111), pp306-316.

[39] **Dovey, A.** (1987). Shaping Up For Speed. Windsurf and Boardsailing Magazine.

[40] **Duan, S.Z., Acosta, A.J. and and Green, S.I.** (1992). Lift/Drag Performance of Conventional and Ducted Wing Tips. Cavitation and Multiphase Flow Forum. 135, pp189-194.

[41] **Dunham, R.E.** (1977). Unsuccessful Concepts for Aircraft Wake Vortex Minimisation. NASA Report SP-409, pp221-249.

[42] **Ehlers, S. M.** (1991). Aeroelastic Behaviour of an Adaptive Lifting Surface. Ph.D. Thesis, Purdue University, USA.

[43] **Ellsworth, W.M.** (1974). Hydrofoil Development: Issues and Answers. AIAA Paper 74-306. pp1-12

[44] **Eppler, R.** (1990). Airfoil Design and Data. Springer Verlag. ISBN 0-387-52505-X (US).

[45] **Eppler, R. and Shen, Y. T.** (1978). Section Design for Hydrofoil Wings with Flaps. AIAA Paper 78-726, 11p.

[46] **Eppler, R. and Shen, Y.T.** (1979). Wing Sections for Hydrofoils - Part 1: Symmetrical Profiles. Journal of Ship Research. 23(3), pp209-217.

[47] **Evans, J.** (1990). Fins We Would Choose. Boards Magazine. 64, pp71-74.

[48] **Fagan, M. J.** (1992). Finite Element Analysis. Longman Scientific and Technical. ISBN 0-582-02247-9.

[49] **Fagg, S. B.** (1996). Reversible and Finitely Variable Cambered Lifting Section. United Kingdom Patent Application GB 9600137.5 A.

[50] **Fagg, S. B. and Velay, X.** (1996). Simulating the Operation of a Novel Variable Camber Hydrofoil. Conference Proceedings IEEE 96 Aerospace Applications, Aspen, February 1996. (3), pp261-271.

[51] **Fagg, S. B. and Velay, X.** (1996). Coupled Fluid Flow and Non-Linear Analysis of an Advanced Hydrofoil. In Conference Proceedings. The Future of Simulation Tools: Computer Aided Design in the 21st Century. Pittsburgh, May 1996. (2), pp2.341 - 2.352.

[52] **Fagg, S. B. and Velay, X.** (1996). The Development of a Coupled Fluid Flow and Structural Analysis Tool. Advances in Fluids Mechanics AFM 96, New Orleans, June 1996. pp123-133.

[53] **Fagg, S. B. and Velay, X.** (1996). The Development of a Novel Composite Material Hydrofoil through Advanced Computational Techniques. Conference Proceedings, CADCOMP 96, Udine, July 1996. pp167-177.

[54] **Ferris, J. C.** (1977). Wind Tunnel Investigation of a Vraiable Camber and Twisting Wing. NASA TN-D-8475.

[55] **Fink, M. P.** (1967). Full Scale Investigation of the Aerodynamic Characteristics of a Model Employing a Sailwing Concept. NASA-TN-D-4062.

[56] **Fisher, D.H. and Blick, E.F.** (1966). Turbulent Damping by Flabby Skins. Journal of Aircraft. 3(2), pp163-164.

[57] **Flechner, S.G. and Jacobs, P.F. and Whitcomb, R.T.** (1976). A High Subsonic Speed Wind Tunnel Investigation of Winglets on a Representative Second Generation Jet Transport Wing. NASA TN D-8264.

[58] **Fung, Y.C.** (1955). An Introduction to the Theory of Aeroelasticity. Galcit Aeronautical Series.

[59] **Gad-El-Hak, M.** (1994). Interactive Control of Turbulent Boundary Layers: A Futuristic Overview. AIAA Journal. 32(9), pp1753-1765.

[60] **Gaide, A.** (1985). Apparatus for Stabilising the Direction of Travel of Watercraft, Specifically a Sword or Fin for Sailboards. U. S. Patent 4,537,143.

[61] **Garrett, R.** (1987). The Symmetry of Sailing: The Physics of Sailing for Yachtsmen. Adlard Coles Nautical. ISBN 0 229 11759 7.

[62] **Gilmore, T.** (1991). Cutting Edge. Windsurf Magazine. 109, pp22 - 24.

[63] **Gratzer, L. B.** (1974). Analysis of Transport Applications for High Lift Schemes. AGARD Lecture Series no. 67. pp7-1 - 7-21. Von Karman Institute, Brussels, 1974

[64] **Gudgeon, J.** (1989). Fin Choice. Boards Magazine. 57, pp72-76.

[65] **Haddock, C. F.** (1980). Improvements in and Relating to Hydrofoils for Vessels. Australian Patent 1 567 395.

[66] **Hernandez, F. G.** (1982). Some Experiences with Sailing Hydrofoils. RINA Small Craft Group Conference on Sailing Hydrofoils.

[67] **Hiroyuki, H. and Taneda, S.** (1967). The Skin Friction Drag on Flat Plates Coated with a Flexible Material. Reports of Research Institute for Applied Mechanics. 15(49), pp1-15.

[68] **Holbrook, G.T., Dunham, D.M. and Greene, G.C.** (1985). Vortex Wake Alleviation Studies with a Variable Twist Wing. NASA Technical Paper 2442.

[69] **Holder, D. W. and Pankhurst, R. C.** (1952). Wind Tunnel Technique. Sir Isaac Pitman and Sons.

[70] **Honji, H. and Taneda, S.** (1967). The Skin Friction Drag on Flat Plates Coated with a Flexible Material. Reports of Research Institute for Applied Mechanics. XV, pp1-15.

[71] **Horton, H. P.** (1978). Fundamental Aspects of Flow Seperation Under High Lift Conditions. Von Karman Institute for Fluid Dynamics, Belgium.

[72] **Houghton, E. L. and Brock, A. E.** (1960). Aerodynamics for Engineering Students. Edward Arnold Publishers Ltd., London.

[73] **Housh, C.S. and Selberg, B.P. and Rokhsaz, K.** (1991). Aerodynamic Characteristics of Scissor Wing Geometries. Journal of Aircraft. 28(4), pp231-238.

[74] **Hoyt, S. W.** (1975). Hydrodynamic Drag Reduction due to Fish Slimes. Swimming and Flying in Nature. pp653-672.

[75] **Hoyt, S. W.** (1977). Polymer Drag Reduction - A Literature Review. 2nd International Conference on Drag Reduction Aug 31st - Sept 2nd, 1977. ppA1-1 - A1-19.

[76] **Hugo, R.J. and Jumper, E.J.** (1994). Loading Characteristics of Finite Wings Undergoing Rapid Unsteady Motions: A Theoretical Treatment. Journal of Aircraft. 31(3) pp495-502

[77] **Ishimitsu, K.K.** (1976). Aerodynamic Design and Analysis of Winglets. AIAA Paper 76-940, pp1-8.

[78] **Ismail, K. A. R.** (1972). The Hydrodynamic Theory of Vertical Swept Hydrofoils Near a Free Surface and Comparison with Measurement. Ph.D. Thesis, University of Southampton, England.

[79] **Jones, D.J. and Khalid, M.** (1985). Analysis of Experimental Data for a 21% Thick Natural Laminar Flow Airfoil NAE 68-060-21:1. NAE-AN-34, NRC No. 25076.

[80] **Kasprowicz, M.** (1989). Fin-esse. Windsurf Magazine. 87, pp76-71.

[81] **Kasprowicz, M.** (1990). The Hobert Fin. Windsurf Magazine. 87, pp4.

[82] **Kasprowicz, M.** (1992). Push Through Fins. Windsurf Magazine. 92, pp15-16.

[83] **Kato, H. and Miura, M. and Miyanaga, M and Yamaguchi, H.** (1989). Drag Reduction by Intentional Cavitation. Cavitation and Multiphase Flow Forum. pp65-69.

[84] **Kay, H. F.** (1971). The Science of Yachts, Wind and Water. G. T. Foulis and Co. Ltd., Oxfordshire. ISBN 0 85429 1148.

[85] **Kerwin, J.E. and Lewis, S.D. and Mandel, P.** (1972). An Experimental Sudy of a Series of Flapped Rudders. Journal of Ship Research. December 1972, pp221-239.

[86] **Kinnaird, A. T.** (1992). Variable Geometry Windsurf Fin. U. K. Patent Application GB 2 255 937 A.

[87] **Kramer, M.O.** (1957). Boundary Layer Stabilisation by Distributed Damping. Journal of Aeronautical Sciences. 24, pp459-460.

[88] **Kramer, M.O.** (1961). The Dolphin's Secret. American Society of Naval Engineers. 2, pp103-107.

[89] **Kramer, M.O.** (1965). Hydrodynamics of the Dolphin. Advances in Hydroscience. 2, pp111-130.

[90] **Lan, C. E. and Roskam, J.** (1985). Airplane Aerodynamics and Performance. Ruskam Aviation and Engineering.

[91] **Landahl, M.T.** (1962). On the Stability of a Laminar Incompressible Boundary Layer Over a Flexible Surface. Journal of Fluid Mechanics. Part 13, pp609-632.

[92] **Lang, T.G.** (1972). Speed, Power and Drag Measurements of Dolphins and Porpoises. In Swimming and Flying in Nature, Volume 2, pp553-572.

[93] **Levinsky, E. S. and Palko, R. I.** (1982). Tests of an Improved Computer Controlled Self Optimising Variable Geometry Wing. AIAA 82-0599, pp215-223.

[94] **Liebeck, R. H.** (1973). A Class of Airfoils Designed for High Lift in Incompressible Flow. Journal of Aircraft, vol 10 no 10. pp610-617.

[95] **Lighthill, M. J.** (1974). Aerodynamic Aspects of Animal Flight. Fifth Fluid Science Lecture at the Royal Institution, June 1974.

[96] **Lodey, P.** (1988). Lodey on Sails. Boards Magazine. 54, pp67-70.

[97] **Ma, E.C.** (1989). The Effect of Wing Tip Strakes on Wing Lift - Drag Ratio. Journal of Aircraft.. 26(5), pp410-416.

[98] **Mandel, P.** (1982). Water, Air and Interface Vehicles. Massachessetts Institute of Technology Press.

[99] **Marchaj, C.A.** (1979). Aero-Hydrodynamics of Sailing. 2nd Edition. Adlard Cole Nautical. ISBN 0-7136-3740-4.

[100] **McRae, D. M.** (1970). Aerodynamics of Mechanical High Lift Devices. AGARD Lecture Series no. 43. pp1-1 - 1-21. Von Karman Institute, Brussels, 1970

[101] **Menear, M.J.** (1975). Aircraft. G. B. Patent Specification 1,406,240.

[102] **Mineck, R.E. and Hartwich, P.M.** (1996). Effect of Full Chord Porosity on Aerodynamic Characteristics of the NACA 0012 Airfoil. NASA Technical Paper 3591.

[103] **Molland, A. F.** (1981). The Free Stream Characteristics of Ship Skeg-Rudders. Ph.D. Thesis, University of Southampton, England.

[104] **Moxon, J.** (1985). Mission Adaptive Wing. Flight International, vol 128, pp22-25.

[105] **Munk, M. M.** (1921). The Minimum Drag of Airfoils. NACA Report 121

[106] **Neto, M. M., Miranda, C. A. J., Cruz, J. R. B. and Silviera, R. C.** (1996). Collpase of a Ring-Stiffened Cylindrical Shell Under External Hydrostatic Pressure - Comparison Between FEA and Analytical Formulae. Computer Aided Engineering in the 21st Century Conference and Exhibition, May 20-22, 1996, Pittsburgh, PA. 1, pp1.353 - 1.358.

[107] **Newman, J.** (1977). Marine Hydrodynamics. The Massachusetts Institute of Technology. ISBN 0-262-14026-8.

[108] **Pendleton, E., Lee, M. and Wasserman, L.** (1991). An Application of the Active Flexible Wing Concept to an F-16 Derivative Wing Model. AIAA-91-0987. pp1855-1868.

[109] **Pillet, X.** (1995). Voici Le Matos Du XXIe Siecle. Planchemag. 170, pp44-51

[110] **Poll, D.I.A., Danks, M. and Humphreys, B.E.** (1992). The Aerodynamic Performance of Laser Drilled Sheets. European Forum on Laminar Flow Technology. pp274-277.

[111] **Poll, D.I.A, Danks, M. and Davies, A.J.** (1992). European Forum on Laminar Flow Technology. The Effect of Surface Suction Near the Leading Edge of a Swept Back Wing. pp278-293.

[112] **Popelka, D., Baker, D.J., Berry, V., Lindsay, D. and Parham, T.** (1995). Results of an Aeroelastic Tailoring Study for a Composite Tiltrotor Wing. In American Helicoptor Society 51st Annual Conference, May 1995. pp1117-1131.

[113] **Private Communication** (1997). Deepak Ganjoo, Swanson Analysis Systems, USA.

[114] **Private Communication** (1996). Martin Peters, Martello Design, England.

[115] **Private Communication** (1993). Mr. Hobert, Cherbourg, France.

[116] **Rao, A. J.** (1989). Variable Camber Wings for Transport Aircraft. Ph.D. Thesis, Cranfield Institute of Technology, College of Aeronautics.

[117] **Redecker, G., Oelker, H. C. and Wichmann, G.** (1986). Aerodynamic Investigation Toward an Adaptive Airfoil for a Transonic Transport Aircraft. Journal of Aircraft, vol23 no 5. pp398-403.

[118] **Reshotko, E.** (1977). Drag Reduction in Water by Heating. 2nd International Conference on Drag Reduction Aug 31st - Sept 2nd, 1977. pp E2-11 - E2-21.

[119] **Richards, M.** (1989). Smooth Operators. Windsurf Magazine. 10(2), pp30-31.

[120] **Rogallo, F. M., Croom, D. R. and Sleeman, W. C.** (1972). Flexible Wings for Transportation. Intersociety Conference on Transportation. pp237-247.

[121] **Rogers, K.** (1989). Fintech. Boards Magazine. 62, pp44-52.

[122] **Russel, C.** (1978). Model Testing Requirements and Techniques for High Lift Schemes: Three Dimensional Aspects. pp6-1 - 6-19

[123] **Russell, D.** (1985). Sailboards, Inventions, Yachts and Exotic Craft. In The Seventh Chesapeake Sailing Yacht Symposium, pp31-42.

[124] **Saltzman, E.J. and Hicks, J.W.** (1994). In Flight Lift Drag Characteristics for a Forward Swept Wing Aircraft. NASA Technical Paper 3414.

[125] **Shareef, N. H., Levine, D. L. and Swarts, D. F.** (1996). Stress Analysis of the Extensively Porous Coated Hip Stem Push-Out Test Specimens - A Comparison Between a Multi-Interface FEA and Experimental Results. Computer Aided Engineering in the 21st Century Conference and Exhibition, May 20-22, 1996, Pittsburgh, PA. vol1, pp1.257 - 1.273.

[126] **Shen, Y. T. and Dimotakis, P. E.** (1989). Viscous and Nuclei Effects on Hydrodynamic Loadings and Cavitation of a NACA 66(mod) Foil Section. Journal of Fluids Engineering, vol 111, pp306 - 316.

[127] **Short, B.** (1992). Blade Running. Windsurf Magazine. 113, pp22-26.

[128] **Siewart, R. F. and Whitehead, R. E.** (1978). Analysis of Advanced Variable Camber Concepts for Combat Aircraft. Naval Research Reviews. vol 31. pp1-16.

[129] **Smith, A.M.O.** (1972). Aerodynamics of High Lift Airfoil Systems. AGARD Paper CP-102, pp10-1 - 10-24.

[130] **Smith, A.M.O.** (1974). High Lift Aerodynamics. In Proceedings of The 37th Wright Brothers Lecture, American Institute of Aeronautics and Astronautics, Aircraft Design, Flight Test and Operations Meeting 1974, pp1-44.

[131] **Smith, H.C.** (1980). Method for Reducing Tangential Velocities in Aircraft Trailing Vortices. Journal of Aircraft. 17(12), pp861-866.

[132] **Smith, S. C. and Kroo, I. M.** (1990). A Closer Look at the Induced Drag of Crescent-Shaped Wings. AIAA-90-3063.

[133] **Somers, D.M.** (1981). Design and Experimental Results for a Flapped Natural Laminar Flow Airfoil for General Aviation Applications. NASA TP 1865.

[134] **Spillman, J.J.** (1978). The Use of Wing Tip Sails to Reduce Vortex Drag. Aeronautical Journal. pp387-395.

[135] **Sutherland, L.S.** (1993). Windsurfer Fin Hydrodynamics. M.Sc. Thesis. Department of Ship Science, Southampton University, England

[136] **Taylor, D. A.** (1983). Sailwing Construction. U. K. Patent Application GB 2 100 687 A.

[137] **Thain, J. A.** (1973). Reynolds Number Effects at Low Speeds on the Maximum Lift of Two Dimensional Aerofoil Sections Equipped with Mechanical High Lift Devices. Quarterly Bulletin National Aerospace Establishment, Ottawa. pp1-24.

[138] **Thomas, A.** (1978). Aircraft Drag Reduction Technology. AGARD. pp11-1 - 11-12.

[139] **Ulrich, J.** (1996). Static and Dynamic Flow Simulation of Microvalves using a Fluid-Structural Coupling. In Conference Proceedings. The Future of Simulation Tools: Computer Aided Design in the 21st Century. Pittsburgh, May 1996. (2), pp2.391 - 2.395.

[140] **Van Dam, C.P.** (1987). Induced Drag Characteristics of Crescent Moon Shaped Wings. Journal of Aircraft. 24(2), pp115-119.

[141] **Van Dam, C.P., Vijgen, P.M.H.W. and Holmes B. J.** (1989). Aerodynamic Characteristics of Crescent and Elliptical Wings. In 7th AIAA Applied Aerodynamics Conference, Seattle, 31st July to 2nd August 1989. pp763-774.

[142] **Van de Voorde, C. B.** (1975). Review of Hydrofoil Craft Development. Institute of Mechanical Constructions Report 11246/1.

[143] **Van Oossanen, P.** (1985). The Development of the 12 Meter Class Yacht 'Australia II'. In The Seventh Chesapeake Sailing Yacht Symposium. pp81-101.

[144] **Venn, M.** (1991). Fin Rules. Windsurf Magazine. 110, pp26-30.

[145] **Vijgen, P.M.H.W., Holmes, B.J. and Van Dam, C.P.** (1990). Wind Tunnel Investigation on the Effect of the Crescent Planform Shape on Drag. AIAA 90-0300.

[146] **Wadlin, K. L., Fontana, R. E. and Shuford, C. L.** (1951). The Effect of End Plates, End Struts and Depth of Submergence on the Chracteristics of a Hydrofoil. NACA RM 151B13.

[147] **Wanstall, B.** (1986). BERP Blades, the Key to the 200kn Helicoptor. Interavia. 3, pp322-324.

[148] **Widnall, S. E., Widnall, W. S., William, E. G. and Evernham, J. T.** (1993). Flexible Tailored Elastic Airfoil. U. S. Patent 5,181,678.

[149] **Wilkie, D. R.** (1960). Man as an Aero Engine. Journal of Aeronautical Society. Volume 64, August 1960.

[150] **Wilson, M. B.** (1982). Experimental Performance of a Flapped Hydrofoil in Calm Water at Low Froude Numbers. Naval Ship Research and Development Centre, Maryland. Report Number DTNSRDC-82/002

[151] **Wright, E. M.** (1966). Variable Camber Airfoil. U. S. Patent 1,406,240.

[152] **Zimmer, H.** (1977). The Significance of Wing End Configuration in Airfoil Design for Civil Aircraft. Dorneir GmbH, Friedrichshafen, Germany. NASA-TH-75711.

APPENDIX A

Hardware and Software Specifications

SILICON GRAPHICS Indy Workstation

R5000 'MIPS' Processor @ 100 Mhz

64 M Byte RAM

4 G Byte Hard Drive

24 Bit Graphics

17" Colour Monitor

SILICON GRAPHICS Irix 6.2 Operating System with Indigo Magic Desktop

ANSYS Revision 5.2. SWANSON Analysis Systems, Houston, Pa.

Flotran Revision 2.1. SWANSON Analysis Systems, Houston, Pa.

APPENDIX B

Airfoil Data

Airfoil E 472

Airfoil E 472 satisfies the requirements mentioned in the Directory 6.1. It has, near zero-lift, short laminar regions on both surfaces. At high c_l, the lower surface becomes laminar up to the trailing edge. The bubble warnings are, therefore, not significant.

E 472 12.1%

Separation bubble warning
△ upper surface
▽ lower surface

T. = boundary layer transition
S. = boundary layer separation
U. = upper surface
L. = lower surface

APPENDIX IV

NACA 0006 Wing Section (Continued)

453

THEORY OF WING SECTIONS

NACA 0006 Wing Section

452

NACA 0009 Wing Section (Continued)

455

NACA 0009 Wing Section

454

APPENDIX IV

457

Section drag coefficient, c_d

Moment coefficient, $c_{m_{c/4}}$

Section lift coefficient, c_l

NACA 0010-34 Wing Section (Continued)

Standard roughness

6.0 × 10⁶

R	a.c. position x/c	y/c
9.0 × 10⁶		.018
6.0		.001
3.0		.055

THEORY OF WING SECTIONS

Section lift coefficient, c_l

Moment coefficient, $c_{m_{c/4}}$

Section angle of attack, α_0, deg.

NACA 0010-34 Wing Section

0.20c simulated split flap deflected 60°

Standard roughness
6 × 10⁶

Standard roughness
6.0 × 10⁶

456

246

APPENDIX IV

Section drag coefficient, c_d

Moment coefficient, $c_{m\,a.c.}$

Section lift coefficient, c_l

NACA 0012 Wing Section (Continued)

403

THEORY OF WING SECTIONS

Section lift coefficient, c_l

Moment coefficient, $c_{m\,c/4}$

Section angle of attack, α_0, deg.

NACA 0012 Wing Section

402

APPENDIX IV

NACA 23012 Wing Section (Continued)

499

THEORY OF WING SECTIONS

NACA 23012 Wing Section

498
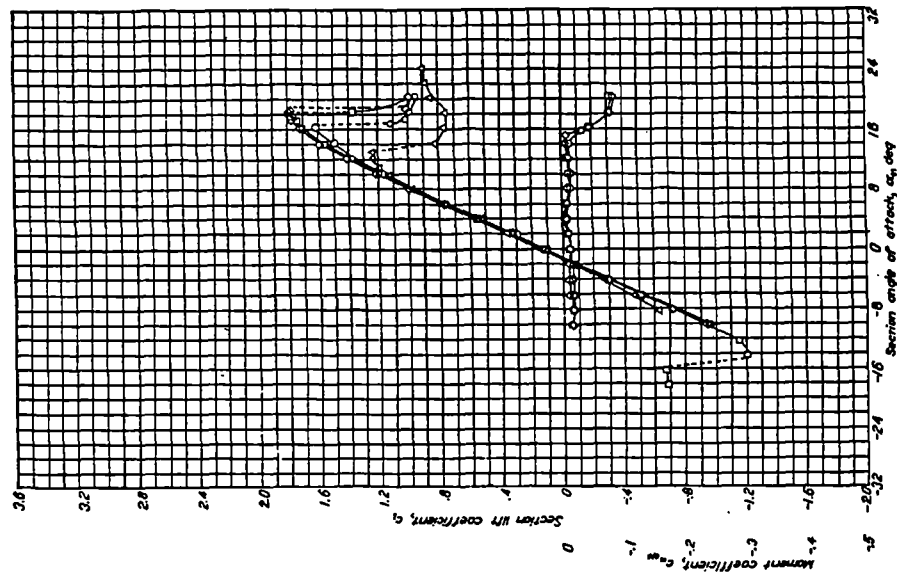
APPENDIX C

Publications

Conference Proceedings
Volume 2

ANSYS
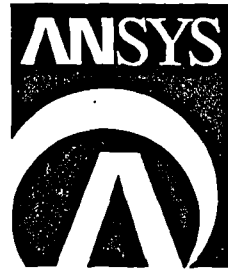
the future of

simulation tools:

computer

aided

engineering

in the 21st

century

Conference and Exhibition

MAY 20-22
1996 The Pittsburgh
Hilton & Towers

COUPLED FLUID FLOW AND NON-LINEAR ANALYSIS
OF AN ADVANCED HYDROFOIL

Simon Fagg
Department of Product Design and Manufacture
Bournemouth University
Bournemouth, UK

Xavier Velay
Department of Product Design and Manufacture
Bournemouth University
Bournemouth, UK

ABSTRACT

Small marine vehicles such as boats and particularly windsurfers, employ winglike lifting surfaces, such as daggerboards, rudders and fins, on the underside of the hull to resist the sideways force of the sail, and also for directional control. Due to the requirement for these lifting surfaces to operate on both tacks, a geometrically symmetrical cross-section is normally used, which inhibits the maximum values of lift that can be generated by a given surface area. To increase the maximum attainable lift, it is necessary to employ a cross-section with camber, although this presents a problem for a lifting surface which has to operate on both tacks. This paper discusses the way in which ANSYS 5.1 and FLOTRAN are being used as design and analysis tool in the development of a reversible cambered lifting surface for windsurfers and similar marine vehicles.

NOMENCLATURE

C_D = Drag Coefficient for cross-section
C_L = Lift Coefficient for cross-section
S = Surface Area of lifting surface
V = Velocity of lifting surface in fluid
c = Chord length of cross-section
t = Thickness of cross-section
α = Angle of attack
ρ = Density of fluid

INTRODUCTION

The sport of windsurfing started in the late 1960's and has since evolved into a mass participant sport with competitions at regional, national and international levels. The equipment used comprises a sail assembly and a board assembly which are joined by a universal joint of a mechanical or flexible elastomer design. The sail assembly comprises a mast, sail and boom, and the board assembly comprises the board, footstraps and, on the underside one or more fins. The complete assembly is controlled by the sailor through angulations of the sail assembly, footsteering of the board, and changes in the position of the bodyweight.

The continual evolution of the sport and particularly the equipment has enabled the windsurfer to become one of the fastest sail powered marine vehicles, with attainable speeds approaching 50 knots. The ultimate performance of the assembly is highly dependent on the individual components and as such much attention is being focused on the ways in which new technologies can be incorporated into the design and fabrication of the necessary equipment.

To consider the effect of the individual components on the operation of the complete windsurf assembly, a Global Model has been developed, (as illustrated in Figure 1), which shows the interaction of the various forces. From this it can be seen that the power for the windsurfer is provided by the sail assembly which generates a propulsive

force as a result of the air flow over its surfaces. This propulsive force can be resolved into components, one of which is useful and will drive the complete assembly in the direction of travel. The second component of the force acts at right angles and will normally push the assembly sideways; the third resists forward motion, and is normally referred to as drag. To avoid sideslip of the assembly, both the hull and the fins are used to counteract the sideways force generated by the sail. The modern day windsurfer will normally plane on only the last 30 cm or so of the hull as shown in Figure 2, and so the role of the fin(s) in counteracting the sideways forces of the sail is critical. This has meant that in recent years, much attention has been focused on the ways in which this part of the assembly can be made to operate with improved efficiency.

THE WINDSURF FIN

The lift and drag generated by a fin can be predicted with Formulae (1) and (2).

LIFT $= 0.5(\rho.V^2.S.C_L)$ (1)

DRAG $= 0.5(\rho.V^2.S.C_D)$ (2)

Because the windsurfer needs to sail on both tacks, the fin normally employs a symmetrical cross-section which limits the attainable C_L and associated C_D values. This can be explained by giving consideration to the effect of camber in the design of a lifting section.

Symmetrical Cross-Sections

At any distance from the leading edge to the tail of a lifting section it is possible to mark a point midway between the upper and lower surfaces (Figure 3a) and if a locus of these points is generated along the length of the lifting section, a median line is generated. If this median line is straight (0% camber) then the section is symmetrical. It is generally valid to assume that at low incidence angles the lift generated by a symmetrical foil section is the same as that given by a flat plate at the same incidence angle, with a slight compensation for the effects of foil thickness. Formula (3) takes account of the foil thickness ratio (t/c) of the lifting section giving.

$C_L = 0.11(1+t/c)\alpha$ (3)

This serves to illustrate the point that the C_L value for a symmetrical section is governed primarily by the angle of incidence, as well as the thickness ratio (t/c). This thereby limits the scope for increasing the C_L value as it has been shown that the optimum thickness ratio (t/c) for

symmetrical lifting sections is in the region of 12% and that the maximum value of C_L normally occurs at a stalling angle of approximately 15 degrees. Therefore another approach is needed to increase the C_L value.

Asymmetric Cross-Sections

If the median line of a lifting section deviates from a straight line (Figure 3c), then it is said to be asymmetric and indicates that the lifting section is cambered. This median line (Figure 3b) is normally given a percentage value to indicate the maximum value of deviation from the straight line of a symmetrical section in relation to the chord length. The general effect of camber is to move the coefficient of lift versus angle of attack curve for a given section to the left (as detailed in Figure 4), with the rise in the C_L value being proportional to the camber percentage. Therefore for a given range of angles of attack, a cambered lifting section will have a larger coefficient of lift (C_L) value than a comparable symmetrical section.

Reversible and Variable Camber Cross-Section

To create a cambered section it is normal to use variable geometry devices such as mechanically hinged leading and trailing edge flaps. A design solution using this approach for the windsurf fin has already been developed whereby the sailor uses a hinged deck mechanism on the board to activate the flaps on the fin. As an alternative approach to a hinge and flap system a new concept is proposed in which the pressure difference between the two surfaces of the lifting section is used to invoke and control the operation of the camber device, thereby removing the requirement for an additional activating mechanism. The functioning of this device is analogous to that of a traditional fabric sail whereby the cloth will billow to one side of the mast and form a cambered section as a result of its angle of incidence to the airflow and the induced pressure distribution over its surfaces. However, for proprietary reasons it is not possible to discuss the exact nature of the mechanism that is under development.

To test the feasibility of the concept, a series of evaluation prototypes have been produced. From the initial testing of these prototypes, the location and value of the maximum camber seems to have crucial effect on the functioning of the device. It is however difficult to fully appreciate the exact manner in which the device operates when in use, due to the interaction between the fluid flow and the structural deformations of the section. Therefore an additional design tool is required to assist in the design and development process.

2. 342

ADVANCED FLUID ANALYSIS

Fluid-Structural Coupled Analysis

The use of traditional tank testing techniques to evaluate potential concepts for the camber device was judged to be prohibitive and so it has been necessary to develop an alternative computational based process to consider the coupling effect between a fluid flow and a structure immersed in the flow. This process needs to combine Computational Fluid Dynamics (CFD) and Finite Element Analysis (FEA) packages into an iterative algorithm in which the effect of the pressure distribution on the structure is calculated, in addition to considering the effects of the induced changes in the structural geometry and the flow regime. To do this an ASCII program file has been created to control the operation of the CFD (FLOTRAN) package and the FEA (ANSYS) package. The program file has been written such that all the data for the section, camber device and flow regime is fully paramaterised as this minimises the required levels of user interaction, which in turn allows for rapid modifications to the computer model and analysis process.

Coupled CFD/FEA. The ASCII program file essentially consists of a number of looping operations, as is shown in Figure 5. This illustrates the way in which the two packages are made to interact and the manner in which data is transferred from one part of the analysis to another. In essence, the whole process can be broken down into four distinctive parts:

(a) Definition of the initial geometry,
(b) Flow analysis,
(c) Structural analysis,
(d) Convergence of the coupled analysis.

Initially, the user needs to define the starting geometric features of the foil section along with the associated material properties and flow regime. From this data, the program automatically generates the CFD and FEA models with appropriate meshes. To avoid ambiguity, all parameters, ordinates, data and results are in SI units (meters, seconds, kilograms, Newtons and Pascals) except for the angle of attack which is entered in degrees but is converted into radians in the program.

To govern the accuracy and reliability of the final solution, appropriate convergence checks are used. These convergence checks, as well as the number of loop iterations are parameterised so that rapid modifications to the operation of the program can be made with minimal effort. In addition the gravitational acceleration effect is set to zero for the current scenario. After the CFD solution, a review of the results is provided on screen for visual checking by the user.

To perform the structural analysis, the mesh representing the flow space is deleted and the remaining fluid elements are changed to structural solid element (PLANE42). Thus the program redefines the material properties of the elements representing the cross section of the fin and its camber device. The pressure distribution calculated by FLOTRAN is automatically transferred to ANSYS and applied to the corresponding elements as the load set for the subsequent structural analysis. When this analysis is completed, a displacement and stress plot are displayed on the screen for visual checking before continuation. Additionally, the positions of the nodes and their respective displacements are stored in arrays so they can be accessed in the next stage of the analysis by the program.

At this stage, the program returns to FLOTRAN to perform another flow analysis, on the deformed shape calculated by the previous structural analysis. To obtain the deformed shape a new set of keypoints is generated in FLOTRAN by using the array and spline functions, as well as the stored nodal data. It is then necessary to generate a revised mesh, apply the boundary conditions and define the flow regime before a further fluid analysis is performed. Based on the assumption that the geometry of the section is different from the previous flow analysis, a change in the pressure distribution should be apparent. The new pressure distribution is again stored so that it can be used as the load set for the subsequent structural analysis.

Due to the large scale deformations in the structure, non-linear behaviour is expected in certain regions. Currently the program uses a low Young's modulus and a high Poisson's coefficient to simulate this effect, although a part of the program is being modified to use experimental stress-strain data to derive a set of Mooney-Rivlin hyperelastic material constants.

As has previously been discussed, the program operates in a series of loops (IF/THEN/ELSE) which continue until convergence checks are satisfied. The convergence check in the global loop is based upon the change of the coefficient of lift (ΔC_L) between the current (j) and the previous (j-1) loop as shown in Formula (4).

$$\Delta C_L = C_{Lj} - C_{Lj-1} \qquad (4)$$

From the initial work with the program it is normal to expect a satisfactorily converged solution within 10 global iterations.

2. 343

252

User interaction and Parametric technology. The program is essentially a list of commands and arguments from the ANSYS and FLOTRAN software. The program is written with an ASCII text editor and hence is easily modified or customised for a particular application. All the parameters used in the analysis are located at the beginning of the program for easy access and are also fully annotated for clarity. Furthermore, by using the ANSYS Parametric Design Language (APDL) it has been possible to reduce the size of the program and improve its structure by locating commonly used routines in macros. The benefits of this type of programming become apparent when it is necessary to make major modifications to the section and/or flow regime. An example of this is when a new section is to be evaluated which simply requires the user to create a new macro or input file. In the near future a user interface will be developed for the program in which a windows type front end will be employed.

Validity and Accuracy

The validity of a model depends on how faithfully the physical problem is represented in the computer, whilst the accuracy depends on how close the resulting solution is to a theoretically derived value. Validity and accuracy are dependent upon:

(a) how the model mathematically mirrors the geometric and material properties of the actual product,

(b) how the boundary condition assumptions reflect the actual loading,

(c) how the method of discretization has been implemented,

(d) how the iteration method is controlled.

Geometric and Material properties. As a model becomes more complex it is normal to make geometrical approximations. At an element level, complex shapes and particularly small features in a model might not be represented precisely by the elements, since even the most advanced elements can only take up limited shapes. This is due to errors which are introduced into the approximation when the elements are distorted, as a result of skew, taper, wrapage and aspect ratio effects on the faces and sides of the elements. According to M.J. Fagan, some guidelines can be followed for distorted elements, but, since allowable limits for the angles and ratios depend on the field variable distribution and the order of the elements under consideration, it is difficult to perform a check as this procedure becomes almost impossible when the number of elements is important. For this reason the program is designed to map the mesh through specified line lengths and divisions thereby controlling the element

size and shape. These lines start from the fin profile and finish at the boundary of the flow space, with the starting point of the line corresponding with the point at which there is a significant change in radius of the splines. With this method most of the element distortion is controlled. The outer shape of the fin is constructed with splines at the modelling stage, resulting in a mesh consisting of small and straight lines on the element faces (Figure 6). However, due to the relatively small scale of this geometric approximation the overall flow characteristics around the fin are not adversely affected.

The fluid properties are accurately defined and can be rapidly checked by listing the various parameters. Normally the fin will be used in sea water at an ambient temperature and a speed no greater than 50 knots. Therefore with such a low mach number the fluid is considered to be incompressible, with a constant density of $1024 kg/m^3$ and a constant dynamic viscosity of $0.001 kg/m.s$.

Boundary Conditions. The setting of the flow and boundary conditions is critical in ensuring a meaningful solution is derived. To ensure the flow and boundary conditions are valid, the program automatically identifies the appropriate nodes in the mesh by using the select functions. Then for each node a parameterised velocity, pressure or displacement value is assigned before the solution is performed. To simulate an external flow in FLOTRAN, the boundaries are located many multiples of chord length from the fin, the inlet is set to a parameterised constant velocity, the outlet pressure is set to zero and the external nodes of the fin are set to zero velocity. In order to save computing time and disk space, the angle of attack is defined by changing the direction of the inlet velocity, as opposed to altering the attitude of the fin within the mesh. The pressures calculated by the CFD analysis are in terms of nodal pressure forces and, by using an intelligent and consistent numbering system, these forces can be transferred to the corresponding structural model as surface loads. Finally, the environment of use means that the flow is set to be adiabatic and turbulent, and a steady state solution is used because of the relatively instant operation of the camber device.

Discretisation. The mesh quality plays a significant role in the accuracy of the results. The percentage error of the final solution can be reduced greatly by using three techniques for refining the mesh. Firstly, the geometry can be divided into smaller elements so the mesh density is increased (h-refinement). Secondly, the accuracy of the elements themselves can be improved by using higher-order interpolation functions (p-refinement) and thirdly the nodes can be relocated to reduce the size of the

2. 344

253

elements (r-refinement). Because the last two methods are not available for the fluid elements, h-refinement is used in a parameterised format to control the mesh. By changing the mesh divisions on specific lines, the mesh density can be adapted for the solution. In the fluid analysis it is important to ensure a high quality mesh is used in regions of rapidly changing velocity and pressure as this is where a poor mesh will lead to large scale calculation errors or solution divergence. For the current analysis this means that the mesh is made very fine in and around the fin whereas larger meshing is used towards the external limits of the flow regime. It is acceptable to use meshing with an aspect ratio of up to 1/100 as long as the longer element face is in the direction of the flow, although this is not so crucial for the elements towards the external limits of the flow. This controlling of the mesh density and the mesh division ensures the solution is valid.

Iterations. The number of iterations in the program is critical for obtaining an accurate solution. The iteration value is stored as a parameter so the operation of the program can be altered with ease. By using this approach the best compromise between accuracy, computing time and memory space can be determined. Within the FLOTRAN package it has been found that approximately 350 iterations are required for a converged solution. This is however critically effected by the size and quality of the mesh, as a poor mesh can cause the solution to diverge.

CASE STUDY

CFD/FEA

The creation of a successful variable camber lifting section relies heavily upon the shape of the camber line (Figure 3b) as this influences the following:

      (a) Chordwise load distribution,
      (b) Angle of zero lift,
      (c) The pitching moment coefficient.

In general, the leading edge camber helps to reduce the magnitudes of C_D whereas the trailing edge camber increases the C_L value with the preferred position of maximum camber being in the forward third of the section. If the maximum camber is too far forward however it can cause a severe stall due to leading edge separation. Based upon these and other design considerations for cambered lifting sections, potential mechanisms can be proposed and evaluated with the design tool. To demonstrate the functioning of the design and analysis tool, a sample run using a lifting section with an unsuccessful concept for the mechanism is provided

(the internal mechanism is not shown for proprietary reasons).

Figure 7 shows the undeformed external geometry in the initial flow condition, with the expected pressure distribution for a symmetrical section on the upper and lower surface.

This pressure distribution is then used as the load condition for a structural analysis (as shown in Figure 8). As a result of the loading, the foil section experiences structural deformations (as shown in Figure 9).

The result of this deformation is that the foil section becomes asymmetric with camber. However, due to the changes in the external foil geometry, it is necessary to run a subsequent flow analysis to see the effect that this has on the flow regime and pressure distribution. This process of toggling between FLOTRAN and ANSYS is repeated until a satisfactorily stabilised solution is determined. Figure 10 shows the pressure distribution on the deformed foil shape for a final iteration which clearly illustrates the modification to the pressure distribution with the negative pressure peak reducing in intensity and moving rearwards in the expected manner. From this final solution the nodal pressure forces are summated and used in formulae (1) and (2) to determine the C_L and C_D values for the deformed shape.

Table 1 shows a comparison of the C_L and C_D values calculated at the end of the first and eighth CFD loops in which it can be seen that the C_L value for the section has increased as a result of the modifications to the section geometry.

Validity

To check the validity of the program, a cross-section has been analysed at varying angles of attack for a direct comparison with the available empirical data. Each C_L value at a certain angle of attack has been calculated by summating the (x) and (y) components of the surface nodal forces and then collated in Table 2 along with the known C_L values for the section. By comparing these figures the relative accuracy of the process can be determined. This shows that the C_L value is generally overestimated and would seem to indicate that the accuracy of the FLOTRAN process improves with an increasing angle of attack.

CONCLUSION

ANSYS and FLOTRAN are being used to aid in the design, development and analysis of a novel variable

2. 345

camber lifting section. The selection of these packages has been due to the ease with which they can be tailored to the problem in hand enabling the development of a coupled fluid flow and structural analysis. Based upon the results of an analysis, modifications to the section geometry and camber mechanism can be made prior to a subsequent evaluation. By using this process a clear understanding of the operation of this type of device will be developed, with the aim of creating a commercially viable product for the sport of windsurfing and other related marine applications.

Although the initial variable cambered lifting sections are intended for use in the small marine vehicle market, additional application areas are being investigated. The described design tool may also be applied to similar design problems, in which the coupling effect between a fluid flow and a structure is of interest, such as the foil systems on racing cars, rudders for small marine vehicles and the lifting surfaces of light aircraft.

2. 346

FIGURES

FIGURE 1. FORCES ON THE COMPLETE ASSEMBLY

FIGURE 2. PLANING WINDSURF BOARD

2. 347

256
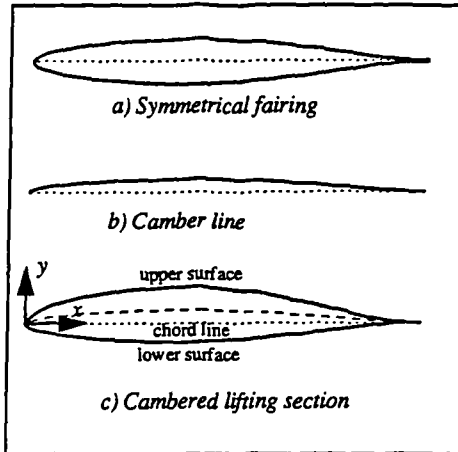
FIGURE 3. SYMMETRICAL AND CAMBERED LIFTING SECTION
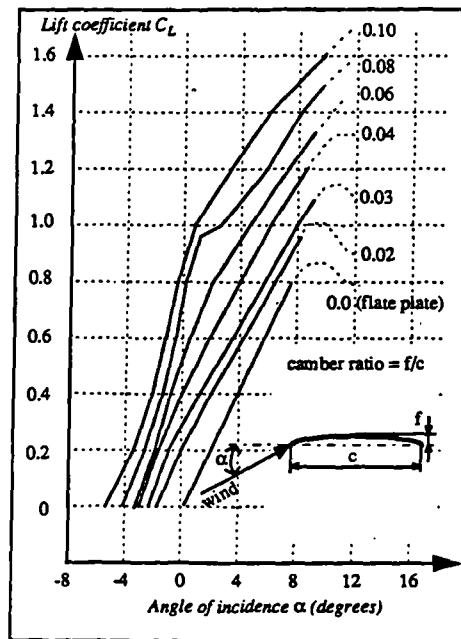
FIGURE 4. EFFECT OF CAMBER ON C_L

2. 348

257
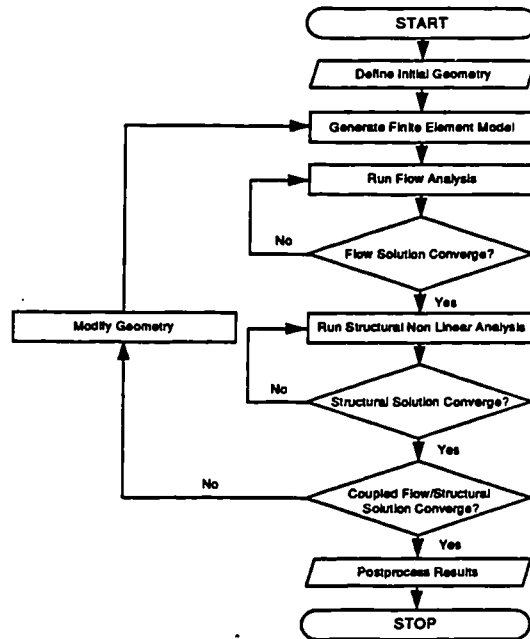
FIGURE 5. GENERAL FLOWCHART FOR COUPLED FLUID FLOW AND NON-LINEAR ANALYSIS

FIGURE 6. MESH QUALITY

2. 349

JAN 17 1996
18:01:19
NODAL SOLUTION
STEP=1
SUB =1
PRES
RSYS=0
SMN =-84900
SMX =56808

ZV =1
-DIST=0.079771
-XF =0.033711
-YF =0.013
CENTROID HIDDEN
-84900
-69155
-53409
-37664
-21917
-6173
9572
25317
41063
56808
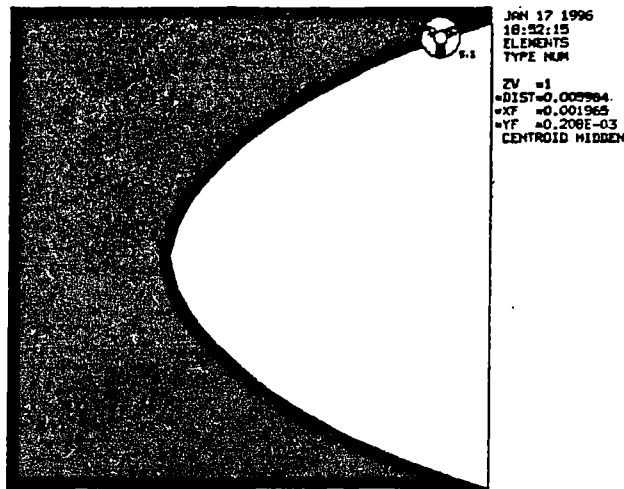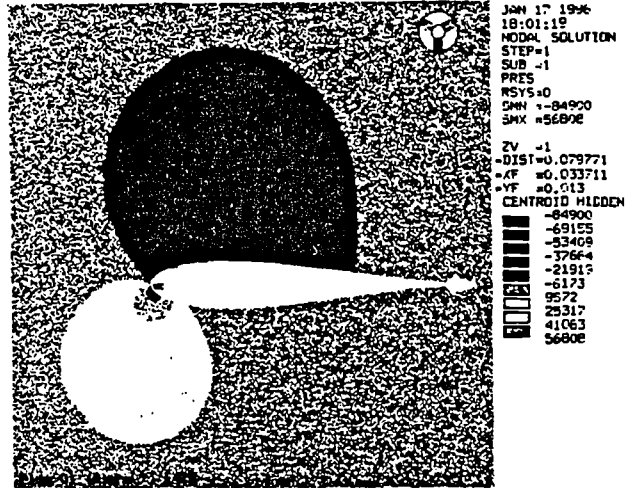
FIGURE 7. PRESSURE DISTRIBUTION ON THE UNDEFORMED GEOMETRY

JAN 17 1996
18:40:51
NODES
TYPE NUM
PRES

ZV =1
DIST=0.055
XF =0.05
CENTROID HIDDEN

Stru 01 (Alpha 7) E478
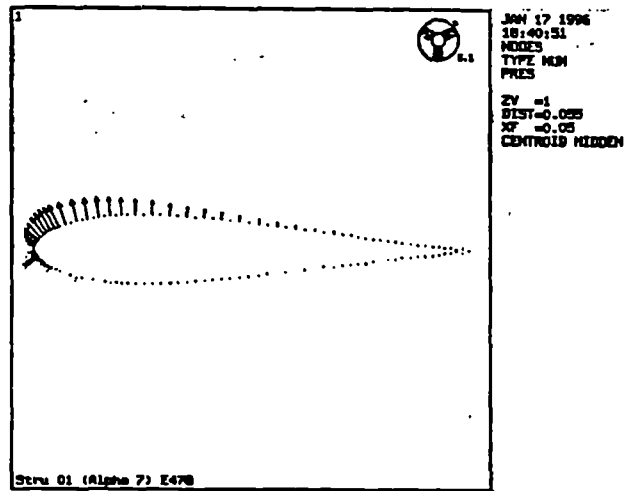
FIGURE 8. PRESSURE LOADING FOR THE STRUCTURAL ANALYSIS

2. 350
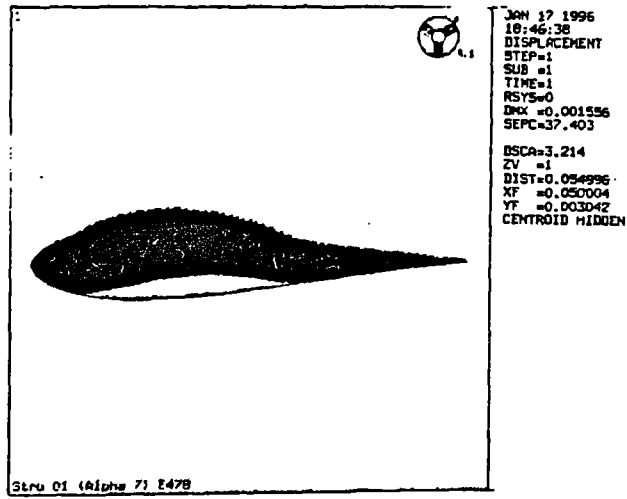
FIGURE 9. STRUCTURAL DEFORMATION
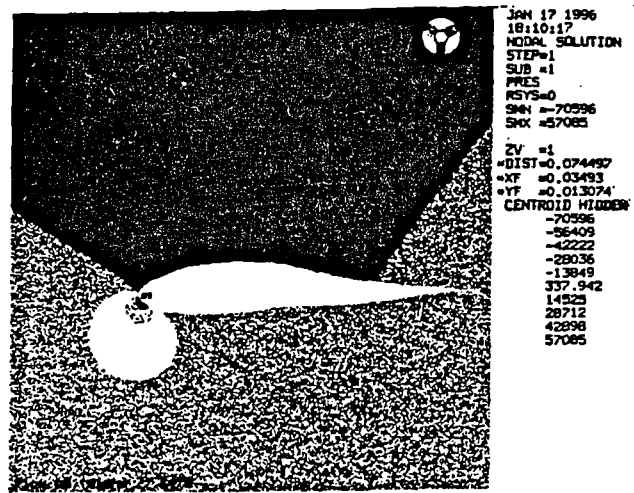
FIGURE 10. PRESSURE DISTRIBUTION AFTER SOLUTION CONVERGENCE

2. 351

TABLES

	C_L	C_D
Symmetrical Section (1st loop)	0.767	0.033
Cambered Section (8th loop)	0.870	0.046

TABLE 1. SYMMETRICAL AND CAMBER SECTION COMPARISON

Incidence Angle	Empirical Data (C_L)	FLOTRAN (C_L)	Error %
3	0.315	0.336	6.67 %
5	0.530	0.564	6.42 %
6	0.625	0.670	7.20 %
7	0.750	0.767	2.27 %
8	0.850	0.841	1.06 %

TABLE 2. RESULTS COMPARISON OF THE C_L VALUE.

ACKNOWLEDGEMENTS

REFERENCES

Abbott, I. H., Von Doenhoff, A. E., 1959, "Theory of Wing Sections", Dover Publications, New York, USA.

Dugdale, C., 1994, "Marine Steering Systems", Patent Application, UK.

Eppler, R., 1990, "Airfoil Design and Data", Springer-Verlag, Berlin, Germany.

Fagan, M. J., 1992, "Finite Element Analysis, Theory and Practice", Longman Scientific and Technical, Harlow, UK.

Ferris, J. C., 1977, "The Wing Tunnel Investigation of a Variable Camber and Twist Wing", NASA Langley, USA.

Marchaj, C. A., 1993, "Aero-Hydrodynamics of Sailing", Adlard Coles Nautical, London, UK.

Sutherland, L., 1993, "Windsurfer Fin Hydrodynamics", M.Sc. Thesis, University of Southampton, UK.

2. 352

1996 IEEE
AEROSPACE APPLICATIONS
CONFERENCE

PROCEEDINGS

Volume 3 of 4

CONFERENCE DIRECTOR:
ROBERT A. PROFET

PROGRAM CHAIR:
G. EDWARD BRYAN

DEPUTY PROGRAM CHAIR:
SOHRAB MOBASSER

Sponsor:

IEEE Aerospace and Electronics Systems Society

Simulating the Operation of a Novel Variable Camber Hydrofoil

Simon Fagg and Xavier Velay

Bournemouth University

12 Christchurch Road

Bournemouth BH1 3NA, UK

+44 1202 503750

sfagg@bmth.ac.uk

xvelay@bmth.ac.uk

Abstract—Small marine vehicles such as boats and particularly windsurfers, employ winglike lifting surfaces, such as daggerboards, rudders and fins, on the underside of the hull to resist the sideways force of the sail and also for directional control. Because these lifting surfaces must operate on both tacks, a geometrically symmetrical cross-section is normally used, which inhibits the maximum values of lift that can be generated by a given surface area. To improve the performance it is proposed to develop a cross-section with camber, even though this presents a problem for a lifting surface which has to operate on both tacks. This paper discusses the process and reasoning behind the development of a cambered lifting section for marine vehicles and the way in which aerodynamic data, theory and computational techniques are being applied in this process.

TABLE OF CONTENTS

1. INTRODUCTION

The sport of windsurfing started in the late 1960's and has since evolved into a mass participant sport, with competitions at regional, national and international levels. The equipment used comprises a sail assembly and a board assembly which are joined by means of a universal joint. The sail assembly is a mast, sail and boom and the board assembly is the board, footstraps and fin(s) on the underside, with the universal joint being of a mechanical or rubber type. The complete assembly is controlled by the sailor through angulations of the sail assembly, footsteering of the board and changes in the position of bodyweight. The equipment itself has so dramatically improved over the last twenty-five years that the board has developed from a displacement type hull into a highly efficient planing hull and the original floppy triangular cloth sails have evolved through the use of modern materials and design techniques into rigid foil structures. This has enabled the windsurfer to become one

of the fastest sail powered marine vehicles, with top speeds approaching 50 knots.

The power for the windsurfer is provided by the sail assembly, which generates a propulsive force from the air flow over its surfaces. This propulsive force can be resolved into three components, one of which is useful and will drive the complete assembly in the direction of travel, a second which acts at right angles and will normally push the assembly sideways, and a third which resists forward motion and is normally referred to as drag. To avoid sideslip, both the hull and the fins are designed to counteract the sideways force generated by the sail. In the early days of the sport when a displacement type hull was used for the board, the speeds were limited and the forces experienced by the fin(s) were low, as the large waterline of the hull served to counteract most of the sideways force of the sail. However, the modern day windsurfer will normally plane on only the last 30 cm or so of the hull (as shown in Figure 1), and the role of the fin(s) in counteracting the sideways forces of the sail has therefore been elevated. The result is that in recent years much attention has been focused on the ways in which this part of the assembly can be made to operate with improved efficiency, both through the use of new design techniques and through the use of new materials.

The designing of fins for windsurfers is not as simple as may be first anticipated due to the different disciplines found within the sport. This scenario is similar to the world of cycling where a pursuit bike would be unsuitable for off-road use and vice versa and also in the world of skiing where the varying disciplines govern the characteristics of the skis that are used [1]. In the sport of windsurfing there are three distinct disciplines, each of which require specific types of equipment to optimise performance. These disciplines are described as follows.

Figure 1. Planing windsurf board

Racing

With this discipline, the sailor is looking to complete a course in the quickest time possible. The course is normally triangular and requires the sailor to perform on all points of sailing, which means that on the upwind leg the fin needs to generate large values of lift, whilst on the downwind leg excessive lift will cause control and handling problems. To overcome these requirements the variable geometry fin has been developed by Dan Kinnaird [2], although this device has not been widely used in the sport.

Wave Sailing

Wave sailing requires the sailor to perform surfing type manoeuvres on the wave face, as well as using the wave as a launch ramp for jumping tricks. Ultimate performance and efficiency is therefore less of an issue and

manoeuvrability and user-friendliness taking precedence.

Recreational Sailing

The recreational sailor is looking for a compromise between high performance and manoeuvrability. For simplicity this paper will only discuss the development of fins for the high performance racing discipline.

2. AERO/HYDRODYNAMICS OF THE BOARD ASSEMBLY

As has already been discussed the fin of the windsurf board serves to counteract the sideways forces of the sail and to provide directionally stability. This is achieved by sailing the board at a leeway angle which in turn means that the fin is set at an incidence angle to the water. To develop a better understanding of the forces acting on the fin it is convenient to start by considering the forces acting on the complete assembly. Figure 2 shows a schematic representation of the complete windsurf assembly with the major forces clearly identified.

This global model has been used to develop a steady state program [3] based upon typical sailing conditions in which parameters such as the wind velocity, board speed, sail size, sailor weight and leeway angle are input and used to determine a state of equilibrium. Assuming a steady state and the necessity for equilibrium, the program generates values for the lift and drag of the fin in a specific scenario, the values of which show satisfactory correlation with empirically derived values [4]. Typically the fin accounts for approximately 25% of the drag of the complete assembly. Therefore any performance improvements to the fin will need to be significant if a noticeable effect on the overall performance of the complete assembly is to be found, although at the highest competitive level of the sport minor

improvements to the equipment can have a large influence.
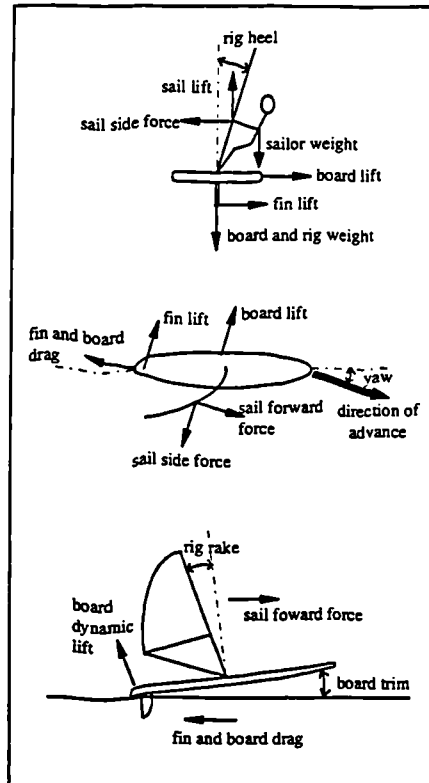
Figure 2. Forces on the complete assembly

3. THE WINDSURF FIN

The windsurf fin and its key geometric features as shown in Figure 3 can be directly compared with the wing of an aircraft, except that it works in a different orientation and in a fluid with a higher density.

It has therefore been possible to apply the knowledge as well as the computational and design techniques of the subsonic aircraft industry to the design of the windsurf fin.

263

In the first instance it is desirable to ascertain the manner in which specific geometric features and/or combinations of features influence the hydrodynamic performance of the fin and then to establish the methods that can be employed to optimise specific performance characteristics. The easiest method for doing this is to consider the formulae (1) and (2) for predicting the magnitudes of lift and drag produced by a nominal lifting surface;

$$LIFT = 0.5(\rho.V^2.S.C_L) \qquad (1)$$
$$DRAG = 0.5(\rho.V^2.S.C_D) \qquad (2)$$

Where:

C_L = Lift Coefficient based on three dimensional flow effects,

C_D = Drag Coefficient based on three dimensional flow effects,

S = Surface Area of lifting surface,

V = Velocity of lifting surface in fluid,

ρ = Density of fluid.

From these two formulae it is possible to identify the parameters that can be altered in the pursuit of improved performance and those parameters over which there is little scope for control.
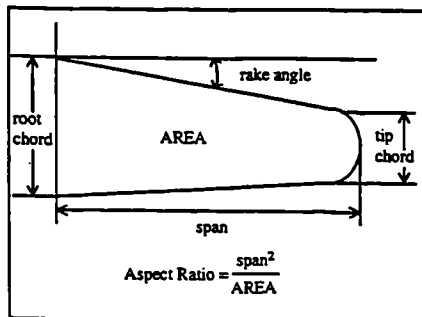
Figure 3. Geometry of the fin

Fluid Density

The initial limiting factor for the design of the

fin is the density of the water in which it will be used. The water will have a nominal density value between 1000kg/m³ for fresh water, to 1025 kg/m³ for water with a saline content.

Velocity

The velocity at which the fin travels through the water is governed by a number of factors, the most important of which is the ability level of the sailor. In addition to this factors, the wind strength and sea state will also govern the speed at which the sailor can navigate the assembly. Therefore an assumption has to be made based upon the anticipated conditions of usage, which then relies upon the ability of the sailor to attain these operational speeds.

Surface Area

The surface area of the fin has a direct influence on the magnitude of lift and drag that is produced. In general, the size of the fin is matched to the size of the sail on the premise that a smaller sail will generate a smaller sideways force and as such will require smaller fin. This again causes a problem as the size of sail that is used by a sailor will again be governed by sailor weight and ability, wind strength, sea state and envisaged discipline of use. To overcome this problem it is normal to have a range of sized fins wherein the emphasis is on the sailor to select the correct size for the sail that is being used. This is similar to the way in which a bike rider will select a frame, or a skier will select a ski length based upon their ability level and anatomical dimensions.

Coefficients of Lift and Drag

These coefficient values are governed by the lifting cross-section and planshape of the fin. The lifting section most suitable for hydrofoil applications is that which can be operated with the maximum craft speed without cavitation and which can tolerate the wide velocity

264

266

fluctuations imposed by rough waters or during manoeuvring [5]. The windsurf fin normally employs a symmetrical cross-section due to the requirement for the fin to operate on both tacks, which limits the attainable C_L and associated C_D values. Due to the finite length of the fin, three dimensional flow effects will further reduce the theoretical two dimensional C_L value, as well as increasing the C_D value [6]. Therefore the planshape is normally optimised to minimise the three dimensional flow effects by increasing the aspect ratio (AR), reducing the rake angle and by ensuring a semi-elliptical type loading in keeping with the theories of Lanchester and Prandtl for constant downwash across the span. Due to the plating action of the board, the effective AR for a windsurf is approximately double that of its geometric value [6], which means that performance fins normally have an effective AR of 8. When considering the effect of AR on C_L it can be seen that beyond an AR value of 6, the improvements in efficiency with increasing AR show decreasing returns [6]. In addition, an increasing AR serves to increase the span of the fin which in turn makes it more difficult to sail, as well as increasing the stresses in the structure and at the board/fin interface.

From the factors that govern the magnitude of lift and drag generated by a fin the most critical are the surface area and the section C_L and C_D values. Based on the assumption that a sized range of fins is normally provided to cater for varying sailor sizes, the focus of the work has been to establish the ways in which the section C_L and C_D values can be optimised. This work is only considering the two dimensional operation of the lifting section and therefore is not at the present time concerned with minimising the three dimensional flow effects of a finite length lifting surface.

4. LIFTING SECTION CHARACTERISTICS

At any distance from the leading edge to the tail of a lifting section it is possible to mark a point midway between the upper and lower surfaces and if a locus of these points is generated along the length of the lifting section, a median line is generated. If this median line is straight (0% camber) then the section is symmetrical (Figure 4a). Based on the fact that a symmetrical section is normally employed in the design of windsurf fins, consideration is initially given to this type of design.

a) Symmetrical fairing

b) Camber line

c) Cambered lifting section
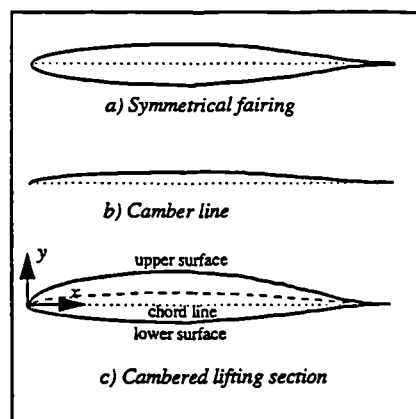
Figure 4. Symmetrical and cambered lifting sections

It is generally valid to assume that at low incidence angles the lift generated by a symmetrical foil section is the same as that given by a flat plate at the same incidence angle. Formula (3) gives a reasonable approximation for the performance of a flat plate at low incidence angles.

$$C_L = 0.1\alpha \qquad (3)$$

$$\alpha = \text{angle of attack}$$

265

267

For a symmetrical foil type section Formula (3) is modified to take account of the thickness ratio (t/c) of the lifting section giving Formula (4).

$$C_L = 0.11(1+t/c)\alpha \qquad (4)$$

Formula (4) serves to illustrate the point that the C_L value for a symmetrical section is governed primarily by angle of incidence, as well as by the thickness ratio. This thereby limits the scope for increasing the C_L value as it has been shown that the optimum thickness ratio for symmetrical lifting sections is in the region of 12% and that stall normally occurs at approximately 15 degrees. Therefore another approach is needed to increase the C_L value.

If the median line of a lifting section deviates from a straight line (Figure 4b), then it is said to be asymmetric and indicates that the lifting section is cambered as is shown in Figure 4c. The general effect of camber is to move the coefficient of lift versus angle of attack curve for a given section to the left as shown in Figure 5, with the rise in the coefficient of lift value being proportional to the camber percentage. Figure 6 illustrates the point that the total C_L value can be considered as being composed of two components, namely the lift due to camber and the lift due to incidence alone. This means that for a given range of angles of attack, a cambered lifting section will have a larger coefficient of lift value than a comparable symmetrical section, which would seem to offer a solution to the design problem. Formula (5) takes account of the effects of camber.

$$C_L = 0.11(1+t/c)(\alpha-\alpha_0) \qquad (5)$$
$$\alpha_0 = \text{angle of zero lift}$$
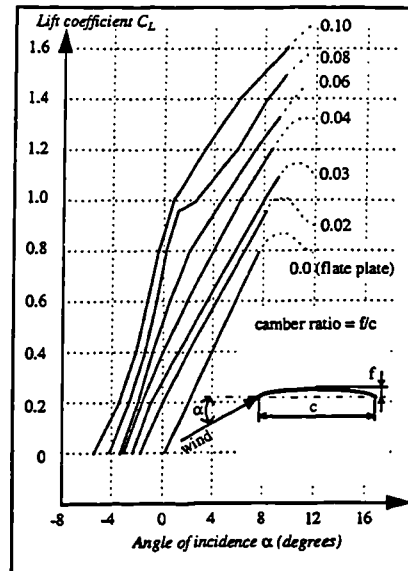
Figure 5. Effects of camber on C_L
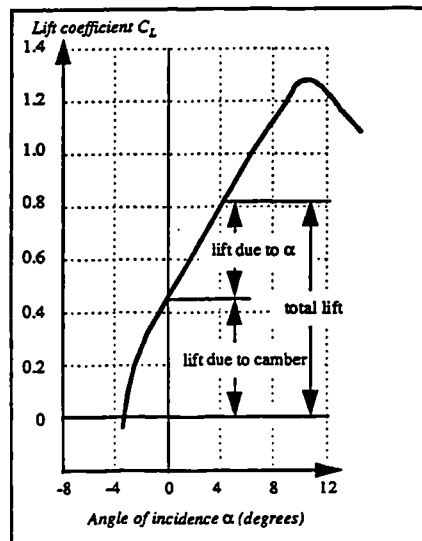
Figure 6. Lift due to camber

266

268

In addition to increasing the attainable C_L value, camber can have a beneficial influence on the C_D as shown in Figure 7. This is attributed to the effects of leading edge camber in promoting a favourable flow regime with a reduced low pressure suction peak[7].
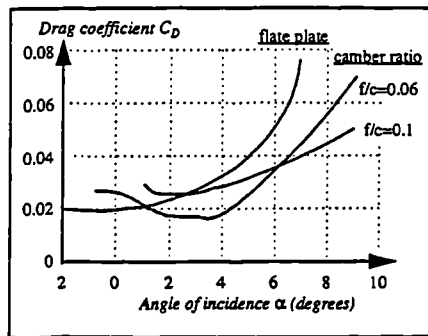
Figure 7. Effects of camber on C_D

5. VARIABLE CAMBER DEVICES

The drawback with most lifting sections is that they have to overcome the conflict of varying environmental conditions and will only operate optimally at a specific angle of attack. To overcome this, it is normal to use variable geometry devices. Based upon the fact that the use of camber in the lifting section is the only realistic method for improving the C_L and C_L/C_D ratio, methods for incorporating camber in the design are investigated.

The most commonly used approach in the world of aeronautics is that of the mechanically hinged leading and trailing edge devices. A design solution using this approach for the windsurf fin is cited [8] whereby the sailor uses a hinged deck mechanism on the board to activate the flaps on the fin. This system requires a specially modified board and has not been developed into a commercial product at the present time. Similar flapped systems have been incorporated in the design of rudders for larger sailing craft [6] although the

International Yacht Racing Union (IYRU) has outlawed their use in most forms of racing. Alternative approaches to this problem are also cited [9]&[10] although they all rely upon the use of an activating mechanism and are therefore not regarded as suitable for incorporation in a windsurf fin, as this would require modifications to the board.

As an alternative approach to the current variable camber lifting sections, a new concept is proposed, in which the pressure difference between the two surfaces of the lifting section is used to invoke and control the operation of the device, thereby removing the requirement for an activating mechanism. The operation of this device is analogous to the operation of a traditional fabric sail whereby the cloth will billow to one side of the mast and form a cambered section as a result of the airflow and induced pressure distribution over its surfaces. Initial prototypes have been produced to evaluate the potential for this concept, with varying success and it is now necessary to develop an analytical process for the design, development and evaluation of subsequent .concepts.

6. ANALYTICAL SOLUTION

The development of the analytical process is required so that the operation and functioning of potential concepts for a variable camber lifting section can be evaluated without the need for expensive empirical test methods. It is however a complex problem to determine the manner in which this type of device will behave because as the structural geometry changes so too does the pressure distribution over the two surfaces and hence the load distribution on the lifting section. Therefore, to create a successful device it is necessary to consider the coupling effects between the fluid flow and structural changes in normal operating conditions.

267

The Program

For this design tool a Computational Fluid Dynamics (CFD) and Finite Element Analysis (FEA) have been combined to create an analytical iterative process. By integrating FLOTRAN (CFD) and ANSYS (FEA) a design tool has been developed specifically for the problem inhand, although it is also possible to evaluate the performance of related coupled analysises. The development of this design tool is described, although for proprietary reasons the nature and operation of the camber device is not described.

To integrate ANSYS and FLOTRAN an ASCII program file has been created. The program is a list of commands and arguments from the ANSYS and FLOTRAN software. The program is written with an ASCII editor and hence can be easily modified or customised for the application. The program algorithm has four distinct parts [11].

    (1) Definition of the initial geometry,
    (2) Flow analysis,
    (3) Structural analysis,
    (4) Convergence of the coupled analysis.

Definition of the Initial Geometry—In the first instance, the user needs to define the initial geometric features of the foil section, along with the material properties and flow regime. From this initial data, the program automatically generates the CFD and FEA models. To avoid ambiguity, all parameters, ordinates, data and results, are in SI units (meters, seconds, kilograms, Newtons and Pascals) except for the angle of attack which is entered in degrees.

Flow Analysis—Some solution controls are added to control the convergence, the reliability and the accuracy of the solution. The number of iterations and its criteria are parameterised and the gravitational acceleration effect is set to zero. Because the fluid problem is non-linear and convergence is not guaranteed, a relaxation technique is used to slow down and stabilise the solution.

After the CFD solution, a quick review of the results is performed in the postprocessor for visual checking. A few lines of programming allows the user to see the warnings (or errors) printed during the solution, the pressure distribution of the overall flow region and a zoomed view of the distribution around the foil section.

Structural Analysis—The structural analysis is performed using the ANSYS FEA software. The program redefines the material properties of the elements representing the cross section of the fin. The camber device is composed of a number of parts which are nominally rigid, with moveable sections and a flexible covering of an elastomer-type material. Due to the large scale deformations in the structure, non-linear behaviour is expected. At the present moment the program uses a low Young's modulus and a high Poisson's coefficient. To simulate an hyperelastic behaviour, a part of the program is being modified to use experimental stress-strain data to derive a set of Mooney-Rivlin hyperelastic material constants.

When the structural analysis is completed a displacement and stress plot are displayed on the screen for visual checking before continuation of the analysis.

Convergence of the Coupled Analysis—At this point of the analysis, the deformed shape is imported to FLOTRAN for a new flow analysis, with the modifications to the foil geometry being updated automatically.

A new flow analysis is started in which a revised mesh is generated. The boundary conditions are again applied along with the

268

270

flow characteristics, before the next solution is performed. The coupled analysis is then continued by transferring the new pressure distribution to the current deformed geometry of the fin for a subsequent structural analysis.

The loop between the fluid and the structural analysises is controlled by looping commands (such as IF/THEN/ELSE) and a convergence check, based upon the change in deflections (Δu) between the current (j) and the previous (j-1) loop as shown in Formula (6).

$$\Delta u = u_j - u_{j-1} \qquad (6)$$

Sample Analysis

The creation of a successful variable camber lifting section relies heavily upon the shape of the camber line as this influences the following [12]:

(1) Chordwise load distribution,
(2) Angle of zero lift,
(3) The pitching moment coefficient.

In general the leading edge camber helps to reduce the magnitudes of C_D whereas the trailing edge camber increases the C_L value [13] with the preferred position of maximum camber being in the forward third of the section [6]. If the maximum camber is too far forward however, it can cause a severe stall due to leading edge separation [12]. Based upon these and other design considerations for cambered lifting sections potential mechanisms can be proposed and evaluated with the design tool.

To demonstrate the functioning of the design and analysis tool, a sample run using a lifting section with an unsuccessful concept for the mechanism is provided (the internal mechanism is not shown for proprietary reasons). Figure 8 shows the undeformed external geometry in the initial flow condition, with the expected pressure distribution for a symmetrical section on the upper and lower surface.
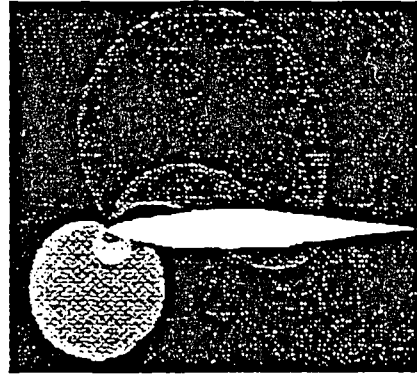
Figure 8. Pressure distribution on the undeformed geometry

This pressure distribution is then used as the load condition for a structural analysis, as shown in Figure 9.
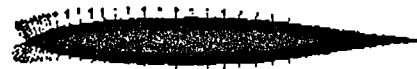
Figure 9. Pressure distribution for the FEA

As a result of the loading, the foil section experiences structural deformations, as shown in Figure 10.

Figure 10. Structural deformations

269

The result of this deformation is that the foil section becomes asymmetric with camber. However, due to the changes in the foil geometry, it is necessary to run a subsequent flow analysis to see the effect that this has on the pressure distribution. Figure 11 shows the pressure distribution on the deformed foil shape, which clearly illustrates the modification to the pressure distribution, with the negative pressure peak reducing in magnitude and moving rearwards in the expected manner. This iterative process is continued until a successfully converged result is found and the C_L and C_D values calculated by summating the (x) and (y) components of the surface nodal forces.
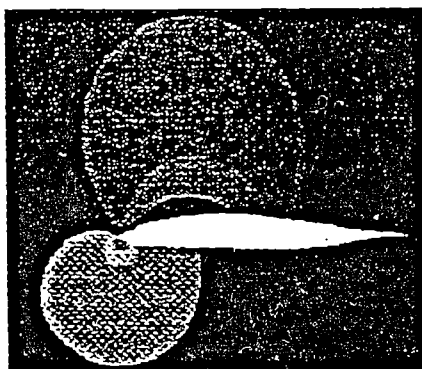
Figure 11. Pressure distribution on the deformed geometry

Based upon the results of an analysis, modifications to the section geometry and camber mechanism can be made prior to a subsequent evaluation. By using this process a clear understanding of the operation of this type of device will be developed, with the aim of creating a commercially viable product for the sport of windsurfing and other related marine applications.

7. CONCLUSION

ANSYS and FLOTRAN have been used to aid in the design, development and analysis of a novel variable camber lifting section. This has been due to the ease with which the packages can be linked to develop a coupled fluid flow and structural analysis. Although the initial variable cambered lifting sections are intended for use in the small marine vehicle market, additional application areas are being investigated. The described design tool may also be applied to similar design problems, in which the coupling effect between a fluid flow and a structure is of interest, such as the foil systems on racing cars, rudders for small marine vehicles and the lifting surfaces of light aircraft.

REFERENCES AND NOTES

[1] E. D. Pilpel, "Expanded Design Analysis of the Use of Composite in Determining Snow Ski Characteristics", 27th National SAMPE Symposium, May 4-6, 1982.

[2] A. T. Kinnaird, "Variable Geometry Windsurfer Fin", UK Patent Application (GB 2 255 937 A), May 21, 1991.

[3] L. Sutherland, "Windsurfer Fin Hydrodynamics", MSc Thesis, University of Southampton (UK), June, 1993.

[4] T. W. Chiu, C. A. M. Broers, A. H. C. Walker & C. R. Baller, "An Experimental Study of the Effects of Deformable Tip on the Performance of Fins and Finite Wings", AIAA 24th Fluid Dynamics Conference, July 6-9, 1993.

[5] R. Eppler & Y. T. Shen, "Wing Sections for Hydrofoils - Part 1: Symmetrical Profiles", Journal of Ship Research, Vol. 23, No. 3, 209-217, September, 1979.

[6] C. A. Marchaj, Aero-hydrodynamics of Sailing, London: Adlard Coles Nautical, 1993.

[7] R. H. Liebeck. "A Class of Airfoils Designed for High Lift in Incompressible Flow", *Journal of Aircraft*, Vol. 10, No. 10, 610-617, October 1973.

[8] C. Dugdale, "Marine Steering Systems", UK Patent Application, June, 1994.

[9] M. Fink, "Full Scale Investigation of the Aerodynamic characteristic of a Model Employing a Sailwing Concept", NASA Langley, 1967.

[10] G. F. Moss, "Variable Aerofoil Mechanism (RAEVAM)", RAE, 1972.

[11] S. Fagg & X. Velay, "Coupled Fluid Flow and Non-Linear Analysis of an Advanced Hydrofoil", To be proceeded at the 7th International ANSYS Conference, May 20-22, 1996.

[12] I. H. Abbott & A. E. Von Doenhoff, *Theory of Wing Sections*, New York: Dover Publication, 1959.

[13] J. C. Ferris, "The Wing Tunnel Investigation of a Variable Camber and Twist Wing", NASA Langley, August, 1977.

Simon Fagg is a Technology Demonstrator in Computer Aided Design and Science and Technology. After finishing his B.Sc. (Hons) degree, his interest and participation in the sport of windsurfing led him to investigate the ways in which the hydrodynamic performance of the equipment could be improved. He is currently developing a new type of windsurf fin in which a variable camber device is being employed, as part of his Ph.D. "The Optimisation of Windsurf Fins" at Bournemouth University (UK).

Xavier Velay is a researcher in design optimisation with artificial intelligence and a consultant in FEA analysis. He is currently developing a fully integrated design system which incorporates CAD and FEA from a computer aided engineering package with an expert system. After his engineering education in France he moved to England to study a B.Eng. and a M.Sc. in computer aided engineering at Coventry University (UK). He is in the process of finishing his Ph.D. in "Design Visualisation and Optimisation" at Bournemouth University (UK).

271

273

Advances in Fluid Mechanics Series
Volume 9
Series Editor: M. Rahman

Advances in
Fluid Mechanics

Editors:

M. Rahman
Technical University of Nova Scotia, Canada

C.A. Brebbia
Wessex Institute of Technology, UK
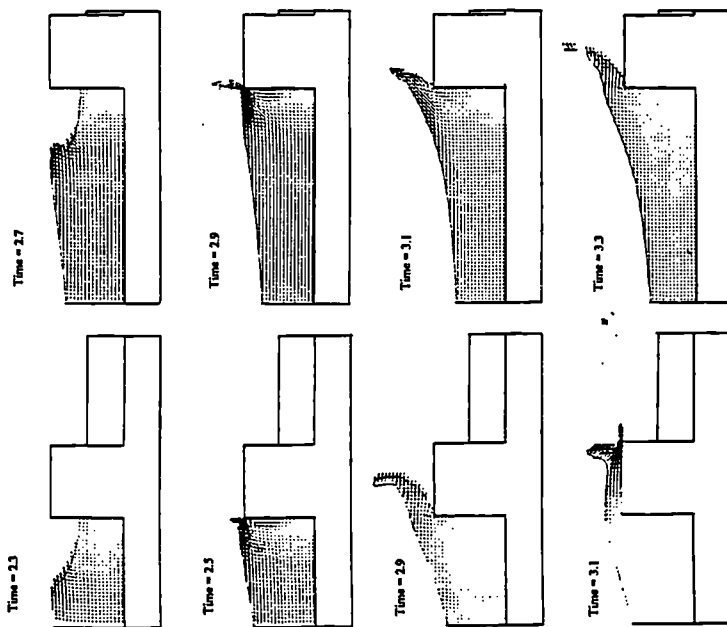
The development of a coupled fluid flow and structural analysis tool

S. Fagg, X. Velay
Department of Product Design and Manufacture, Bournemouth University, Bournemouth BH1 3NA, UK

Abstract

Hydrofoils, rudders, fins and the like are used on sail powered marine vehicles to resist the sideways force generated by the sail and also to give directional control. These hydrofoils need to operate on both tacks and so a symmetrical cross-section is normally employed which tends to limit the overall hydrodynamic performance. To realise further performance gains, a novel design approach is proposed to incorporate camber in the cross-section by means of a reversible and variable camber device. The device functions by using the surface pressure forces on the foil to invoke controlled structural deformations in the hydrofoil cross-section, with the amount of deformation being a function of the velocity and the angle of incidence of the section to the freestream. To predict the manner in which the device operates it has been necessary to develop an analytical computer tool in which the coupling effect between a fluid flow and a structure immersed in the flow is considered. This paper discusses the development of a novel hydrofoil for sail powered marine vehicles and the manner in which modern computational techniques are being applied to the problem.

1 Introduction

Modern day sailing and windsurfing is becoming increasingly competitive with the operation of the equipment becoming as influential as the skill and ability level of the sailor. The successful operation of any sail powered marine vehicle is dependent upon the efficient transfer of the energy gained from the wind into a useful directional motion over the water. This process involves the interaction of many force components both above and under the water and so the starting point for any design problem is to establish the magnitude and

Figure 3. Sequence of velocity and free-surface configuration plots for case 4 (left) and case 6 (right).

influence of the individual variables on overall performance. To assist in this process, a number of theoretical models have been developed to illustrate the forces acting on boats [1] and windsurfers from which it is possible to establish the dynamic operation of each component and the techniques which may be used to improve the overall performance.

The sail assembly on a boat or windsurfer will generate a propulsive force when set at an incidence angle to the wind. This propulsive force can be resolved into three distinct components; one will be useful and drive the assembly in a forward direction, a second will act in a rearwards direction and is referred to as drag and a third will push the assembly sideways. To resist this sideways force of the sail, hydrofoils are used on the underside of the hull to provide an opposing hydrodynamic force. These hydrofoils are required to operate on both tacks and so a symmetrical cross-sectioned design is used.

2 Hydrofoil optimisation

As part of the ongoing research at Bournemouth University, an investigation into the performance of hydrofoils and the factors which influence performance has been undertaken with the aim of establishing the suitability of incorporating various alternative design features. From this work it has been established that the use of devices such as laminar flow profiles, tip vortex suppression devices, compliant surfaces, surface coatings and electromagnetic damping [2] are either impractical to implement and/or unlikely to result in noticeable performance gains when used individually or collectively. However, as a result of this investigation it was possible to establish that the use of a symmetrical cross-sections in small marine craft hydrofoils is the greatest limiting factor on performance. To overcome this limitation it is advantageous to use camber in the design of the cross-section. Traditional methods for achieving this involve the use of flapped trailing and leading edge devices as is most commonly employed in aeronautical applications. The flaps on aircraft are normally actuated and controlled by hydraulically driven linkages and mechanisms, although in the intended environment of use it is not deemed appropriate to use the same type of system.

Reversible and variable camber

As an alternative approach to the mechanically driven flaps, a novel device is proposed which functions in a manner analogous to the traditional fabric sail to create a variable camber line. In operation the fabric sail has a neutral and floppy shape when at rest, but billows to one side of the mast to take on a cambered form when set at an incidence angle to the wind. The proposed reversible camber device uses the surface pressure loads to invoke controlled and predetermined structural deformations in the same manner as the fabric

sail, when set at at an incidence angle to the freestream, although the techniques used to realise a successfully operating device are somewhat different. The magnitude of the structural deformations in the section are finitely variable up to a certain limit and are a function of both its incidence angle to the freestream as well as the velocity of the section in the freestream. For proprietary reasons the exact nature of the device will not be expanded upon.

3 Coupled fluid-structural analysis

The operation of the proposed camber device is difficult to predict as it involves a coupling effect between the forces generated by a fluid flow and the resulting physical deformations of a multi-component structure. One way to assess and develop the camber device could be with the use of emperical tank testing and evaluation methods, although cost makes this process prohibitive. In addition, for each modification to the device, it would be necessary to construct a further prototype and submit it to further tank testing. Therefore, as an alternative to emperical test methods, a computer based two dimensional analytical process has been developed. This process considers the coupling effect between the fluid flow and the induced structural deformations in the cross-section by combining the two distinctive and seperate disciplines of Finite Element Analysis (FEA) and Compuational Fluid Dynamics (CFD) into a single algorithm. With this algorithm it is possible to predict the pressure distribution around the cross-section and then calculate the manner in which the geometry will change as a result of the surface pressure loadings. However, the modified section geometry will then effect the pressure distribution and so a subsequent flow analysis is required. The algorithm repeats this process in which the mutual effects of changing geometry and flow pattern are considered until the section settles into a nominal shape. When a solution has been calculated it is then possible to calculate the coefficient of lift (C_L) and the coefficient of drag (C_D) values for the deformed shape.

4 The problem

As has been outlined, it is necessary to develop a computer based analytical process in which the mutual coupling effect between a fluid flow and a structure in the flow is considered. With any computer based analysis certain assumptions and approximations are made when modelling the environment due to the limitations imposed by both the available computer hardware and software. It was therefore essential that the correct decisions were made as to the most suitable way in which to model the problem computationally. In addition, the development of a successfully operating variable camber cross-section involves the interaction of many individual factors and components, each one of which could have an influence on the overall operation of the device. Because of this it is necessary to ensure that the analytical process is

126   Advances in Fluid Mechanics

flexible enough to accommodate rapid changes to the flow regime or section geometry with minimal time and effort before the running of a subsequent analysis.

Successful modelling of the problem domain

The validity and accuracy of the modelling solution is highly dependent on the assumptions made during it's conception. Before the computer tool was developed it was necessary to establish the exact nature of the problem in hand by:

Understanding the problem;
- the physical phenomena being modelled,
- the flow regime,
- the desired outcome.

Establishing the finite element modelling factors;
- the physical size of the model,
- the resolution of the mesh,
- the boundary conditions.

Selecting suitable analysis controls and convergence checks;
- solution controls,
- iteration check.

Using the solution data;
- understanding the solution results,
- postprocessing the data and modifying the cross-section.

Once these were established it was possible to start on the creation of the analysis tool.

5 The Program

The fluid-structural analysis tool has been created by linking a CFD (FLOTRAN) and a FEA (ANSYS) program into a single iterative algorithm as is shown schematically in Figure 1. This has been achieved by creating a seperate program file which autonomously operates and controls the two individual software applications. By using this process the data used in the analysis is managed by the program and is processed automatically, thereby reducing the required level of user interaction. In addition, the data used to define the section geometry, material characteristics, flow regime and solution controls are stored within the program in a parameterised format so that changes to the model can be realised and assessed rapidly.

Advances in Fluid Mechanics   127

The analysis algorithm can be considered as having four distinctive parts;
- the definition of the initial model,
- the CFD flow analysis,
- the FEA structural analysis,
- the convergence checks.

Initially the primary geometric features of the cross-section, the material properties and the flow regime need to be defined. This data is stored in a parameterised format in separate reference files from which the program is able to generate the initial CFD and FEA models. To ensure consistency in this process all the data is stored in SI units (meters, seconds, kilograms, Newtons and Pascals) except for the angle of attack which is entered in degrees but converted to radians at a later stage.

The Initial model

The initial model is generated by using a series of user-defined keypoints to generate the geometry of the cross-section and the flowspace. The keypoints for the flowspace are created automatically and are a direct function of the geometry of the cross-section. Using this model it is then possible to predict the flow patterns and associated pressure distribution around the cross-section in the CFD package.

The CFD analysis

The validity and accuracy of the CFD analysis is highly dependent on the quality of the mesh, therefore consideration needs to be given to the manner in which the model and particularly the mesh is generated. Due to computing limitations it is not possible to mesh the entire model in a comprehensive manner and so techniques for optimising the meshing process are used. Generally, the mesh requirements in any area of the model are a function of the rates of change of flow in that area. Therefore it is necessary to increase the density of mesh in regions where large changes in the flow velocity are expected. In the case of the CFD model, the meshing requirements are more stringent than for structural analyses [3] and so the mesh density is refined in the immediate vicinity of the cross-section (Figure 2) and made coarser towards the external limits of the flowspace. By using this approach it is possible to ensure that the solution is valid. In the CFD package, the mesh density is controlled by using division spacing techniques on the individual lines of the model and through experience it has been possible to select the most suitable values for these divisions. In addition to the mesh density, it is important to ensure that the correct element shapes arranged in uniform patterns are used in the CFD model and so starburst type patterns are to be

128 Advances in Fluid Mechanics

avoided. In a flow analysis it is essential the elements are aligned with the general flow direction and the aspect ratio of the individual elements is kept to about 10:1, although it is possible to increase the aspect ratio to around 100:1 if the long side of the element is aligned with the flow direction and the included angles are not greater than about 25 degrees.

Boundary conditions and solution controls

When the model has been satisfactorily meshed it is necessary to apply the boundary conditions and define the convergence controls so the solution can be performed. To ensure the predicted flow pattern and pressure distribution is accurate, it is vital the flow boundary conditions and other external effects are applied correctly. By using a number of element and node selection techniques it is possible to associate the correct pressure and velocity values to the appropriate nodes in the model. This process is again controlled automatically and is only made possible by the parameterised nature of the data and structure of the program. To simulate an external flow, the boundaries are located at a large distance form the cross-section, the inlet is set to have a constant velocity, the outlet is set to have a zero pressure value and the nodes representing the external geometry of the cross-section are set to a value of zero velocity. In order to save computing time and space, the angle of attack of the cross-section to the freestream is defined by varying the direction of the inlet velocity instead of remodelling the cross-section in the flowspace.

Before the CFD analysis is performed, convergence checks and solution controls need to be set as these are critical for an accurate solution. By having these solution controls stored as parameters it is easier to determine the most suitable compromise between accuracy, computing time and memory space for a particular analysis. It is therefore a rapid process to change these values should the solution start to diverge, although it must be remembered the solution controls are dependent on the mesh quality. This means that a continually diverging solution cannot be resolved simply by changing the solution controls and may require the mesh to be refined further. From experience it has been found that at least 350 iterations are required in the flow analysis to ensure a meaningful result is calculated. Due to the envisaged environment of use for the current cross-section, the flow is set to be adiabatic and turbulent before the solution is started.

The CFD solution

Following a successful CFD analysis, the user is provided with an onscreen plot of the pressure forces acting on the cross-section for visual checking (Figure 3). Assuming that the result is valid, the user can then instruct the program to proceed. For the next stage of the analysis the pressure forces at

Advances in Fluid Mechanics 129

each nodal location on the external surface of the cross-section need to be determined. These pressure forces are required for the subsequent stages of the coupled analysis and so are stored in a results file using an intelligent numbering system.

The FEA solution

To perform the structural analysis the mesh representing the flow space is no longer required and so is deleted leaving just the area representing the cross-section itself. The next step is to define the material properties of the cross-section and to apply the appropriate loadings and boundary conditions. The nodal pressure distribution calculated in the previous CFD analysis is automatically transferred to the FEA model and assigned to the corresponding nodes by virtue of the consistent numbering system that is employed. In addition to these external nodal pressure forces it is necessary to apply boundary conditions to specific regions of the internal structure. When this is completed the solution controls can be set before the execution of the analysis. Due to the large scale deformations in certain regions of the structure, non-linear material behaviour is expected. Currently this is simulated by using a low Young's modulus and a high Poisson's coefficient, although in the near future the accuracy of the process will be improved through the use of experimental stress-strain data to derive a set of Mooney-Rivlin hyperelastic material constants.

With the analysis completed the user is again provided with an onscreen plot for visual checking in which the displacement and stress plots are shown (Figure 4).

The deformed cross-section

Due to the surface pressure loadings the cross-section will experience structural deformations in certain regions. These deformations will change the flow pattern in the flow regime and so it is necessary to transfer the deformed geometry to the CFD package for a subsequent analysis. The generation of this deformed shape requires the creative use of programming commands because it is necessary to save the nodal co-ordinates on the external faces of the cross-section and their respective displacements (UX, UY) in the form of an array. These two arrays are then combined to provide the data from which a set of new keypoints can be generated to represent the deformed shape in the next CFD analysis.

The global convergence check

The analysis tool continues to loop in an iterative manner between the CFD and FEA packages until a satisfactorily converged solution is derived. The convergence check is based upon the change of the coefficient of lift (ΔC_L) between the current (j) and the previous (j-1) loop as shown in Equation (1).

$$\Delta C_L = C_{L,j} - C_{L,j-1} \qquad (1)$$

When the change in the coefficient of lift between the current and the previous loop is less than a predetermined value, the solution is said to have converged.

Validity and accuracy

The analysis tool has been used to assess potential devices for a variable camber cross-section for small marine vehicles. Initially the validity of the data produced by the tool had to be determined and so it was necessary to compare the predicted results from the tool with emperically available data. This was achieved by calculating the C_L values for an airfoil shape at various angles of attack and then comparing the results with reference values (Table 1) [4]. With the accuracy of the process established, the data obtained for potential camber devices can be considered qualitatively. By using the analysis tool it has been shown that the C_L value for a potential variable camber cross-section increases in the expected manner as the geometry of the cross-section changes (Table 2).

Incidence Angle	Experiment	FLOTRAN	Error %
3	0.315	0.336	6.67
5	0.530	0.564	6.42
6	0.625	0.670	7.20
7	0.750	0.767	2.27
8	0.850	0.841	1.06

Table 1. Results comparison.

	C_L	C_D
Symmetrical Section (1st loop)	0.767	0.033
Cambered Section (8th loop)	0.870	0.046

Table 2. Symmetrical and camber section comparison.

6 Conclusion

As a result of research at Bournemouth University into the performance of small sail powered marine vehicles and the manner in which their hydrofoil's performance can be optimised, a novel reversible and variable camber cross-section has been developed. As part of the development process an analytical computational process to predict the coupling effect between a fluid flow and a structure has been created. The result of this research is the development of a hydrofoil cross-section which has superior performance characteristics compared to geometrically symmetrical cross-sections.

A fin for the sport of windsurfing is under development from which a commercially successful product is envisaged. Following on from this alternative application areas will be sought for both the cross-section and the coupled fluid-structural analysis tool.

References

1. Marchaj, C.A., *Aero-Hydrodynamics of Sailing*, Adlard Coles Nautical, London, 1993.

2. Fagg, S., *The Optimisation of Windsurf Fins*, Interim Report, Bournemouth University, Bournemouth, UK, 1995.

3. Swanson Analysis Systems, *Advanced Flotran (ANSYS)*, Swanson Analysis Systems Inc, Houston, USA, 1994.

4. Eppler, R., *Airfoil Design and Data*, Springer-Verlag Publishing, Berlin, Germany, 1990.

Figure 3: Pressure distribution on the undeformed geometry.
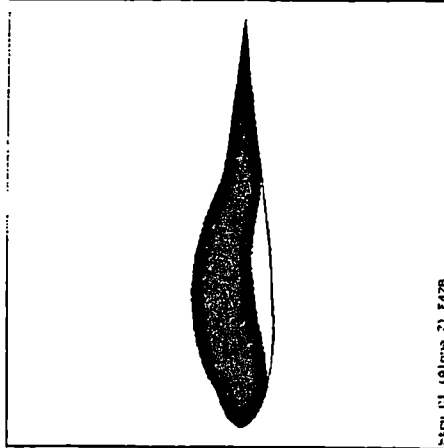
Figure 4: Structural deformation (exaggerated for clarity).

START

Define Initial Geometry

Generate Finite Element Model

Run Flow Analysis

Flow Solution Converge?

Run Structural Non Linear Analysis

Structural Solution Converge?

Coupled Flow/Structural Solution Converge?

Postprocess Results

STOP

Modify Geometry

Figure 1: Flowchart for coupled fluid flow and non-linear structural analysis.

Figure 2: Mesh quality.

FIFTH INTERNATIONAL CONFERENCE ON COMPUTER AIDED
DESIGN IN COMPOSITE MATERIAL TECHNOLOGY

CADCOMP 96

ORGANISING COMMITTEE

W.R. Blain
Wessex Institute of Technology, UK

W.P. De Wilde
Vrije Universiteit Brussels, Belgium

C.A. Brebbia
Wessex Institute of Technology, UK

INTERNATIONAL SCIENTIFIC ADVISORY COMMITTEE

M.C. Altan	R. Keunings
R. Dechaene	I. Marshall
O.H. Griffin, Jr	M. Maier
P. Hamelin	E. Onate
S.V. Hoa	C. Oomens
J.M. Kenny	H. Sol
V.E. Verijenko	

Organised by:
Wessex Institute of Technology, UK

The development of a novel composite material hydrofoil through advanced computational techniques

S. Fagg, X. Velay
Department of Product Design and Manufacture, Bournemouth University, Bournemouth, BH1 3NA, UK

Abstract

The fin(s) on a windsurfer are employed to resist the sideways force generated by the sail and also to give directional stability. The design of the fins normally incorporate a symmetrical cross-section as the craft must operate on both tacks. It is recognised that the use of camber in the design of the cross-section can increase the lift generated by a given surface area, as witnessed by the use of variable geometry flaps on aircraft. However the use of flaps requires the implementation of an actuating mechanism, which is impractical for the proposed environment of use. A reversible variable camber lifting section is therefore proposed in which the pressure difference between the two surfaces invokes and controls an internal camber mechanism. This concept uses the angle of incidence to regulate the pressure loads on the surfaces which are transmitted to the internal mechanism thereby controlling the magnitude of deformations and hence the camber in the cross-section. The design and evaluation of the concept requires the use of new computational techniques to consider the coupling effect between a fluid flow and the induced structural deformations in the section, as well as an investigation into the most suitable material combinations to realise a functioning device.

1 Introduction

The modern day windsurfer is a wind powered marine vehicle capable of speeds approaching 50 knots. To achieve this the sailor uses his bodyweight, footsteering, angulations of the rig and balance to control and transmit the propulsive force of the sail into forward motion. When consideration is given to the number of different forces that are acting on the complete assembly at any one time, windsurfing can be seen as a highly skilled task [1].

most sports are now played can be attributed in part to the development of the equipment.

The windsurf fin

The materials used in the construction of the windsurf fin have changed over the years in response to the increasing dynamic loads. In the early days of the sport, the displacement type hull provided large magnitudes of resistance to the sideways force of the sail and so the main role of the fin was to provide directional stability. For this purpose it was sufficient to produce fins using injection moulding techniques. The materials used in this process varied from ABS to fibre reinforced plastics. However, as the sport advanced, a new type of planing hull developed in which the vertical support force is generated dynamically by the board as the assembly skims across the water. These early planing hulls had the sail assembly situated towards the front of the board and so again there was a large area of the hull engaged in the water, which helped to resist the sideways sail force. The use of plastic fins was now starting to reach a practical limit with increased loading and so the first fibre reinforced composite fins were produced. These early Glass Fiber Reinforced (GFR) fins were fabricated by producing a large slab of material from glass fibre and resin from which the individual fins could be crafted either manually or through Numerically Controlled (NC) machining techniques.

The design of the planing hull changed again in the early nineties as a result of developments in sail design. The new board designs are wider towards the tail which has enabled the sail to be located further rearwards thereby reducing the wetted area of the hull. With such a small wetted area the fin has become a highly stressed part of the assembly and so further techniques have been used to improve its structural integrity.

In the first instance, a new type of material known as G10 has emerged from which the majority of fins are now machined. The G10 material consists of many layers of glass fibre in a resin matrix and is, in essence, a thicker version of the material used for Printed Circuit Boards (PCB). This material has a high fibre content and as such provides a high degree of stiffness. However, there are limitations with using G10 as a fin material as the stiffness of the structure is a feature of the material thickness, which is governed by the hydrodynamic shaping of the design. This limitation in controlling the stiffness within the fin has lead to the development of moulded GFR fins in which the reinforcement can be aligned to counteract the expected loading. The actual processes and moulding techniques used by the individual fin manufacturers are closely guarded secrets although it is known that wet layup, Resin Transfer Moulding (RTM) and prepreg processes are commonly employed.

The power for the windsurfer is provided by the sail assembly, which generates a propulsive force from the air flow over its surfaces. This propulsive force can be resolved into three components, one of which is useful and will drive the complete assembly in the direction of travel, a second which acts at right angles and will normally push the assembly sideways, and a third which resists forward motion and is normally referred to as drag. To avoid sideslip, both the hull and the fins are designed to counteract the sideways force generated by the sail. The modern day windsurfer will normally plane on only the last 30 cm or so of the hull and so the fin has a crucial effect on the overall performance of the complete assembly as it represents the major part of the assembly in contact with the water. In the past considerable time and effort has been spent on improving the board and sails, but little work has been undertaken into the design of the fins. This has changed in recent years and the fin has become the focus of attention with new design techniques and materials being investigated in the pursuit of improved efficiency [2].

2 Materials in sports equipment

Until recently, the use of organic materials such as wood and animal based products were most prominent in the fabrication of sporting equipment. However these traditional materials are increasingly being challenged by the introduction of modern composite materials [3].

Sport equipment optimisation

Composite materials are commonly considered as consisting of a reinforcing fibre or filament embedded in a supporting matrix material, although any combination of two or more separate materials can be considered as a composite. Composites are used as alternatives for conventional materials because of the manner in which their stiffness and strength can be tailored in an anisotropic manner to resist the expected usage loading. As a result of this application efficient construction, composite material products are often lighter than alternatives made with traditional isotropic type materials.

With most sports, the weight of the equipment will have a critical effect on the performance of the athlete. It is no longer the case that the fittest or most skilled person will succeed as performance is highly dependent on the efficiency of the energy transfer between the human body and the equipment used. This therefore adds another dimension to any sport as the ability and skill of the equipment designer becomes a major influencing factor. Therefore one of the primary roles of the designer is to reduce the weight of the equipment whilst still maintaining the structural integrity of the product. For most applications this is an ongoing process as the knowledge base for optimising the use of composite materials in the product is expanded. The increasing speeds at which

As a result of these new moulding techniques, the modern windsurf fin is nearer to an optimal design in its current format. To realise further improvements to the operation of the fin it is necessary to consider alternative design features which will improve the hydrodynamic performance of the device.

3 Windsurf fin hydrodynamics

The windsurf fin generates a lifting force to counteract the sideways force of the sail by virtue of the water flow over its surfaces. The magnitude of the lifting force generated by a finite length fin is given by Equation (1).

$$Lift = 0.5(\rho.V^2.S.C_L) \qquad (2)$$

From this it can be seen that the magnitude of lift generated by a fin is a function of [4]:

- the density of the water (ρ)(sea water is denser than fresh water),
- the square velocity of the fin through the water (V^2),
- the planshape and surface area of the fin (S),
- the design of the cross section (C_L)(coefficient of lift).

Therefore to change the performance of the fin, the designer has the scope to change the planshape, surface area and cross-section of the fin, assuming the speed it travels through the water is influenced by the ability level of the sailor. From years of continual refinement, a series of optimal planshapes have been developed for the windsurf fin and there is limited scope for expanding upon these shapes. This continual refinement has been almost exclusively concerned with the planshape, with the cross-section of the fin being largely overlooked as a variable with which the designer can work.

The cross-section of a windsurf fin is normally symmetrical in design due to the requirement that it must be able to operate on both tacks. This is a limiting factor on the efficiency of the fin as it is known that the coefficient of lift (C_L) value for a symmetrical section is a function of the angle of attack and velocity of the section to the freestream and is nominally the same as that produced by a flat plate [4]. To further increase the C_L value of the section it is necessary to incorporate camber into the design so the section takes on an asymmetric form. By using camber in the design, the C_L value is increased further as a function of the percentage camber, up to a finite limit.

In most aerospace applications, the provision of camber is provided by mechanically flapped wing devices which are controlled and powered by a separate actuating system. These systems allow the pilot to vary the camber and lift of the wing, thereby optimising the performance of the aircraft for the

various stages of the flight (take-off, cruise and landing). It is also a requirement in the sport of windsurfing that the fin produces varying levels of lift depending on whether it is sailing to windward or downwind. Currently the sailor varies the amount of lift generated by the fin by changing its angle of attack to the freestream with footsteering techniques. To gain a performance advantage it would be beneficial to develop a variable camber system, although, because it is inappropriate to use the same mechanical flaps as used on aircraft, an alternative approach is required.

To create a variable and reversible camber device for the windsurf fin a new approach is under development in which the pressure difference between the two surfaces of the fin are used to invoke controlled structural deformations in the structure of the cross-section. These deformations will change the overall geometry of the section thereby making it asymmetric in design and hence cambered. The operation of the device is similar to the functioning of a conventional sail, in which the cloth will billow from one side of the mast to the other to form a cambered shape when it is set at an angle of attack to the wind. In the windsurf fin a similar phenomenon is realised in a smaller scale by using suitable materials and structural combinations that exhibit predetermined structural deformations as a result of the surface loadings. This therefore provides the sailor with a reversible and variable camber fin which generates more lift than a conventional type design. The magnitude of camber is governed by both the incidence angle of the section and its velocity to the freestream and, because of its autonomous operation, the sailor can control it with conventional footsteering techniques without the need for an additional actuating mechanism. For proprietary reasons it is not possible to discuss in detail the exact nature of this device.

4 Advanced computational techniques

Development of the analytical process is required so the operation and functioning of potential concepts for a variable camber lifting section can be evaluated without the need for expensive empirical test methods. It is however a complex problem to determine the manner in which this type of device will behave because as the structural geometry changes so too does the pressure distribution over the two surfaces and hence the load distribution on the lifting section. Therefore, to create a successful device it is necessary to consider the coupling effects between the fluid flow and structural changes in normal operating conditions.

This process needs to combine Computational Fluid Dynamics (CFD) and Finite Element Analysis (FEA) packages into an iterative algorithm in which the effect of the pressure distribution on the structure is calculated in addition to considering the effects of the induced changes in the structural geometry and the flow regime. To do this an ASCII program file has been created to control the

operation of the CFD package (FLOTRAN) and the FEA package (ANSYS) [5]. The program file has been written such that all the data for the section, camber device and flow regime is fully parameterised as this minimises the required levels of user interaction, which in turn allows for rapid modifications to the computer model and analysis process.

Computational fluid dynamics

The flow space surrounding the fin is divided into finite elements to create a mesh. Each element is categorised by the velocity-pressure approximation allowed in the elements. Therefore the finite element equations are obtained by weighted residual methods [6]. To minimise computing time and memory requirements, the flow domain is idealised to a two dimensional problem. Nevertheless the fluid properties are accurately defined. Normally the fin will be used in sea water at an ambient temperature with a speed no greater than 50 knots. Therefore the flow is subsonic (mach number less than about 0.3) and the fluid is considered to be Newtonian, adiabatic and incompressible, with a constant density of 1024kg/m³ and a constant dynamic viscosity of 0.001kg/m.s. To activate the camber device an angle of attack is input to the flow. Results from the flow analysis include the velocity vectors, pressure contours and streamline vorticity. The pressure distribution at the surface of the fin is derived and computed to give the coefficient of lift and drag (C_L and C_D). The drag generated by a fin can be predicted using Equation (2).

$$Drag = 0.5(\rho.V^2.S.C_D) \qquad (2)$$

Structural analysis

The structural part of the coupled analysis is performed with the finite element method. The initial mesh, representing the flow space is then deleted and the fin cross-section remeshed with solid elements categorised by their degrees of freedom in X and Y directions. The program then redefines the material properties of the elements representing the cross section of the fin and its camber device. The pressure distribution calculated by the flow analysis is automatically transferred to the surface of the fin and applied to the corresponding elements as the load set for the subsequent structural analysis. When this analysis is completed, a displacement and stress plot can be obtained for visual checking before continuation. Additionally, the positions of the nodes and their respective displacements are stored in arrays so they can be accessed by the program in the next stage of the analysis.

Coupled analysis

At this point of the analysis, the deformed shape is imported into FLOTRAN for a new flow analysis with the modifications to the foil geometry being updated

automatically. After a revised mesh has been generated for the analysis, the boundary conditions are again applied along with the flow characteristics, before the next solution is performed. The coupled analysis is then continued by transferring the new pressure distribution to the current geometry of the fin for a subsequent structural analysis. The loop between the fluid and the structural analyses is controlled by looping commands and a convergence check, based upon the change in deflections between the current and the previous loop.

Analysis improvements

Due to the large scale deformations in certain regions of the structure, non-linear material behaviour is expected. Currently the program uses a low Young's modulus and a high Poisson's coefficient to simulate this effect, although a part of the program is being modified to use experimental stress-strain data to derive a set of Mooney-Rivlin hyperelastic material constants. Nevertheless, for non-linear problems it is important to perform a preliminary linear analysis to reveal which regions of the model will first experience non-linear response and at what load levels these non-linearities will come into play. It is important to identify the non-linear regions to improve the mesh density because with large deflections, individual elements cannot deform by more than 30 degrees for an accurate solution.

Improved accuracy and understanding of the fluid flow surrounding the fin could be achieved by using a three dimensional analysis. The ANSYS program provides 3-D fluid element. However to model and mesh accurately the geometry of the fin, its camber device and the external flow space, a large number of elements and therefore degrees of freedom are required. Although today's workstations are now more powerful than mainframe computers of only a few years ago, this kind of analysis could not be supported in an economic way.

Alternatively the composite materials used in the camber device and the fin could be modelled by using specialised 'layered' elements. Composites are somewhat more difficult to model than isotropic materials such as iron or steel because special care should be taken in defining the properties and orientations of the various layers since each layer may have different orthotropic materials properties. But once again for this particular analysis the hardware capability and availability are critical. ...

5 Example of a coupled CFD/FEA analysis

The creation of a successful variable camber lifting section relies heavily upon the shape of the camber line as this influences the following:
- Chordwise load distribution,
- Angle of zero lift,
- The pitching moment coefficient.

Composite Material Technology; V   *175*

5 Conclusion

With the knowledge of new material usage in water sports and the help of advanced computational techniques, it has been possible to design a novel variable camber hydrofoil. The design tool (coupled analysis) allowed the most suitable materials and design to be chosen before any costly manufacturing. Thus, with the help of computer aided design and analysis (CADA) tools, the cost for advanced design has been considerably reduced and a preliminary mould has been produced. Based upon initial test results the authors expect only a small redesign to the structure of this initial prototype fin before a commercially viable product is realised.

An improvement to the CADA tool is expected in the near future with the availability of new element technology and cheaper computing hardware. The universal element has not been found yet but interest and research in exotic uses of FEA (such as coupled problems and new applications) is increasing. Further improvements are expected from new meshing techniques, such as p-elements (polynomial elements) and from improved hardware performance with parallel computers (parallelization of processors).

References

1. Sutherland, L., *Windsurfer fin hydrodynamics*, M.Sc. Thesis, University of Southampton, Southampton, 1993.

2. Chiu, T.W., Broers, C.A.M., Walker, A.H.C. & Baller, R.C., An experimental study of the effects of deformable tip on the performance of fins and finite wings, *Proceedings of the 24th AIAA Conf. on Fluid Dynamics*, Orlando, USA, 1993.

3. Engineers guide to composite materials, American Society of Metals, 1987.

4. Marchaj, C.A., *Aero-Hydrodynamics of Sailing*, Adlard Coles Nautical, London, 1993.

5. Fagg, S. & Velay, X., Coupled fluid flow and non-linear analysis of an advanced hydrofoil, *Proceedings of the 7th Int. ANSYS Conf.*, Pittsburgh, USA, 1996.

6. Brauer, J.R., *What Every Engineer Should Know About Finite Element Analysis*, Marcel Decker Inc, New-York, 1993.

174   *Composite Material Technology; V*

In general, the leading edge camber helps to reduce the magnitudes of C_D whereas the trailing edge camber increases the C_L value with the preferred position of maximum camber being in the forward third of the section. If the maximum camber is too far forward however it can cause a severe stall due to leading edge separation. Based upon these and other design considerations for cambered lifting sections, potential mechanisms can be proposed and evaluated with the design tool.

To demonstrate the functioning of the design and analysis tool, a sample run using a lifting section with an unsuccessful concept for the mechanism is provided (the internal mechanism is not shown for proprietary reasons).

Figure 1 shows the undeformed external geometry in the initial flow condition with the expected pressure distribution for a symmetrical section on the upper and lower surface.

This pressure distribution is then used as the load condition for a structural analysis (as shown in Figure 2). As a result of the loading, the foil section experiences structural deformations (exaggerated for clarity in Figure 3).

The result of this deformation is that the foil section becomes asymmetric with camber. However, due to the changes in the external foil geometry, it is necessary to run a subsequent flow analysis to see the effect that this has on the flow regime and pressure distribution. This process of toggling between FLOTRAN and ANSYS is repeated until a satisfactorily stabilised solution is determined. Figure 4 shows the pressure distribution on the deformed foil shape for a final iteration which clearly illustrates the modification to the pressure distribution with the negative pressure peak reducing in intensity and moving rearwards in the expected manner. From this final solution the nodal pressure forces are summated and used in Equations (1) and (2) to determine the C_L and C_D values for the deformed shape.

Table 1 shows a comparison of the C_L and C_D values calculated at the end of the first and eighth CFD loops in which it can be seen that the C_L value for the section has increased as a result of the modifications to the section geometry.

	C_L	C_D
Symmetrical Section (1st loop)	0.767	0.033
Cambered Section (8th loop)	0.870	0.046

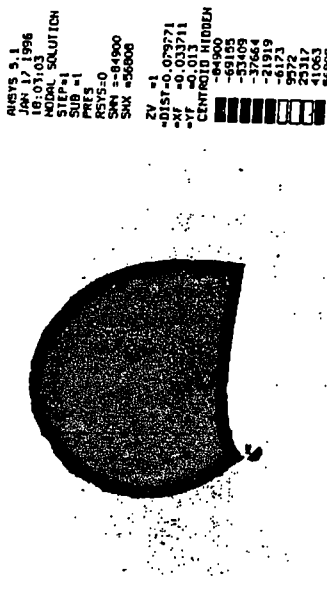Table 1: Symmetrical and camber section comparison.

Figure 3: Structural deformation.

Figure 4: Pressure distribution after solution convergence.

Figure 1: Pressure distribution on the undeformed geometry.

Figure 2: Pressure loading for the structural analysis.

APPENDIX D

Program Listings

FLOW-1ST.PRO

```
!################################################################
!#                                                              #
!#                          ANSYS INPUT                         #
!#                                                              #
!#   Filemane:        flow04                                    #
!#                                                              #
!#   Purpose:         Coupled Fluid-Non linear Structural Analysis #
!#                    of an Advanced Airfoil Design             #
!#                                                              #
!#   Created By:      Simon Fagg & Xavier Velay                 #
!#                    School of Design Engineering & Computing  #
!#                    Departement of Product Design & Manufacture #
!#                    Bounrnemouth University                   #
!#                    Bournemouth BH1 3NA                       #
!#                    United Kingdom                            #
!#                                                              #
!#                    Tel:   +44 1202 503750                    #
!#                    Fax:   +44 1202 503751                    #
!#                    Email: sfagg@bmth.ac.uk                   #
!#                           xvelay@bmth.ac.uk                  #
!#                    http:  www.bournemouth.ac.uk             #
!#                                                              #
!#   Input runs at:   Revision 5.1                             #
!#                                                              #
!#   Other files:     flow-1st.pro  stru-1st.pro               #
!#                    flow-2nd.pro  stru-2nd.pro               #
!#                    runflow.mac   newshape.mac  mesh-fin.mac #
!#                    1st.par       2nd.par                    #
!#                                                              #
!#   Comments:        This program is under a UK Patent        #
!#                    This program may be used or copied only in #
!#                    accordance with the authors              #
!#                                                              #
!#   Last Modified:   20/12/95        By:   SF & XV(mod fin geometry) #
!#                                                              #
!################################################################
/FILNAM,flo1                     !Set filename to pro1.db
!--------------------------------------------------------------
!|                      PARAMETERS  (SI Units)                |
!--------------------------------------------------------------

velocity=10                 !Velocity of the fluid
alpha=7                     !Angle of attaque
outpre=0.0                  !Pressure on the outlet
height=2                    !Height of the flowspace
length=2                    !Length of the flowspace
divi=30                     !Mesh division
densi=3000                  !Density parameter
!
*DIM,xkpt,ARRAY,31           !X coordinate of the airfoil E236 12.66%
xkpt(1)=0.1,0.099636,0.098576,0.09634,0.094634,0.091838,0.088551,0.084843,0.080789,0.076465
xkpt(11)=0.071945,0.067277,0.062490,0.057615,0.052684,0.047730,0.042784,0.037891,0.033106,0.028
480
```

```
xkpt(21)=0.024064,0.019906,0.016049,0.012535,0.009397,0.006669,0.004376,0.002539,0.001176,0.000
307
xkpt(31)=0
!
*DIM,ykpt,ARRAY,31                 !Y coordinate of the airfoil E236 12.66%
ykpt(1)=0,0.000022,0.000118,0.000312,0.000593,0.000956,0.001413,0.001966,0.002599,0.003286
ykpt(11)=0.003983,0.004633,0.005200,0.005662,0.006006,0.006223,0.006320,0.006310,0.006205,0.006
009
ykpt(21)=0.005727,0.00550,0.00525,0.00505,0.00470,0.00436,0.00408,0.00372,0.00282,0.00155
ykpt(31)=0


!-------------------------------------------------------------------
!|      PRE-PROCESSING, SOLUTION & POST-PROCESSING OF THE 1ST CFD     |
!-------------------------------------------------------------------

/PREP7                             !Enter the Pre-Processing
*DO,I,1,31                         !Generate keypoint 1 to 31
    K,I,xkpt(I),ykpt(I)            !using the array xkpt() and ykpt()
*ENDDO
*DO,I,32,60                        !Generate keypoint 32 to 60
    K,I,xkpt(I-(2*(I-31))),-ykpt(I-(2*(I-31)))
*ENDDO

RUNFLOW                            !See the runflow.mac macro

/POST1                             !Enter the Post-Processing
ESEL,S,MAT,,1                      !Select only the flow space (Material No1)
/ZOOM,1,RECT,-0.8,0.6,0.7,-0.6     !Zoom around the X-section
/EDGE,1,0,0                        !Select the edges
/GLINE,1,-1                        !Turn the line off
SET,LAST                           !Select the last results set
PLNSOL,PRES,                       !Plot the pressure distribution
FINISH                             !Leave the Post-Processing
!find a solution to stop process/print a plot
!-------------------------------------------------------------------
!|            PREPARATION FOR THE 1ST STRUCTURAL ANALYSIS            |
!-------------------------------------------------------------------

/PREP7                .            !Enter the Pre-Processing
!ACLEAR,1,16,1                     !Clear the meshes in areas 1 to 16
!ETCHG                             !Change elements of area 17 to Plane42
!SAVE                              !Save the database
!FINISH         .                  !Leave the Pre-Processing
*MSG,NOTE,                         !Note message
      You must QUIT FLOTRAN and ENTER ANSYS %/ with the input file: STRU-1ST.PRO



RUNFLOW.MAC

!This is a MACRO for STRU-1ST.PRO, STRU-2ND.PRO, etc...

!----- Create spline for the hydrofoil Xsection -----
/PREP7                             !Enter the Pre-Processing
BSPLIN,1,2,3,4,5,6                 !Create line1 between kpt 1 to 8
*REPEAT,5,5,5,5,5,5,5              !Repeat 5 times, increment 5
BSPLIN,26,27,28,29                 !Create line6 between kpt 26 to 29
BSPLIN,29,30,31                    !Create line7 between kpt 29 to 31
BSPLIN,31,32,33                    !Create line8 between kpt 31 to 33
BSPLIN,33,34,35,36                 !Create line9 between kpt 33 to 36
BSPLIN,36,37,38,39,40,41           !Create line10 between kpt 36 to 41
*REPEAT,4,5,5,5,5,5,5              !Repeat 4 times, increment 5
BSPLIN,56,57,58,59,60,1            !Create line14 between kpt 1 to 8

!----- Generate flowspace keypoints -----
```

289 ·

```
K,131,-length/2,0              !Create keypoint 131
K,129,-length/2,height/4       !Create keypoint 129
K,126,-length/2,height/2       !Create keypoint 126
K,121,-length/4,height/2       !Create keypoint 121
K,116,0,height/2               !Create keypoint 116
K,111,length/10,height/2       !Create keypoint 111
K,106,length/5,height/2        !Create keypoint 106
K,101,length/4,height/2        !Create keypoint 101
K,96,length/2,height/2         !Create keypoint 96
K,91,length/2,0                !Create keypoint 91
K,133,-length/2,-height/4      !Create keypoint 133
K,136,-length/2,-height/2      !Create keypoint 136
K,141,-length/4,-height/2      !Create keypoint 141
K,146,0,-height/2              !Create keypoint 146
K,151,length/10,-height/2      !Create keypoint 151
K,156,length/5,-height/2       !Create keypoint 156
K,161,length/4,-height/2       !Create keypoint 161
K,166,length/2,-height/2       !Create keypoint 166


!----- Generate flowspace lines -----
LSTR,1,101                     !Create line15 from kpt 1 & 101
*REPEAT,6,5,5                  !Repeat 6 times, increment 5
LSTR,29,129                    !Create line21 from kpt 29 & 129
*REPEAT,3,2,2                  !Repeat 3 times, increment 2
LSTR,36,136                    !Create line24 from kpt 36 & 136
LSTR,41,141                    !Create line25 from kpt 41 & 141
*REPEAT,4,5,5                  !Repeat 4 times, increment 5
LSTR,1,161                     !Create line29 from kpt 1 & 161
LSTR,1,91                      !Create line30 from kpt 1 & 91
LSTR,91,96                     !Create line31 from kpt 91 & 96
*REPEAT,7,5,5                  !Repeat 7 times, increment 5
LSTR,126,129                   !Create line38 from kpt 126 & 129
LSTR,129,131                   !Create line39 from kpt 129 & 131
LSTR,131,133                   !Create line40 from kpt 131 & 133
LSTR,133,136                   !Create line41 from kpt 133 & 136
LSTR,136,141                   !Create line42 from kpt 136 & 141
*REPEAT,6,5,5                  !Repeat 6 times, increment 5
LSTR,91,166                    !Create line48 from kpt 91 & 166


!----- Generate flowspace areas -----
AL,30,31,32,15                 !Create area1 from lines
AL,1,15,33,16                  !Create area2 from lines
*REPEAT,14,1,1,1,1             !Repeat 14 times, increment 1
AL,30,29,47,48                 !Create area16 from lines


!----- Define mesh division -----
*DO,I,15,29                    !For line 15 to 29
    LESIZE,I,,,divi,densi      !do 30 divisions with a density of 3000
*ENDDO
LESIZE,31,,,divi,densi         !Line 31, divi 30, densi 3000
LESIZE,48,,,divi,densi         !Line 48, divi 30, densi 3000
LESIZE,30,,,length*8,10        !Line 30, divi 30, densi 3000
LESIZE,32,,,length*8           !Line 32, divi 30, densi 3000
LESIZE,47,,,length*8           !Line 47, divi 30, densi 3000
*DO,I,1,12                     !For line 2 to 13 and line 34 to 45
    LESIZE,1+I,,,6             !do 6 divisions
    LESIZE,33+I,,,6
*ENDDO
LESIZE,1,,,3                   !Line 1, divi 3
LESIZE,33,,,3                  !Line 33, divi 3
LESIZE,14,,,3                  !Line 14, divi 3
LESIZE,46,,,3                  !Line 46, divi 3


!----- Mesh all areas -----
```

```
ESHAPE,2,0                          !Set elements to BRICKS only
ET,1,141                            !Element type 1 Fluid141
AMESH,ALL                           !Mesh all the flow space


!----- Mesh of the X-section -----
ESHAPE,0,0
LSEL,S,LINE,,1,14,1,0               !Select the fin X-section
AL,ALL                              !Create area 17
ALLSEL                              !Select all

!LSTR,26,36                         !Create line 49
!AL,6,7,8,9,49                      !Create area18
!LSTR,11,51                         !Create line 50
!AL,1,2,50,13,14                    !Create area 19

K,500,0.004,0,0                         !CENTRE OF CIRCLE
K,501,0.065,0,0                         !CENTRE OF REAR AREA

CIRCLE,500,0.003,,,,,                   !CIRCLE AT FRONT OF SECTION
AL,49,50,51,52                          !CREATE AREA FROM CIRCLE

LSTR,11,501                             !CREATE NEW LINE AT REAR
LSTR,501,51                             !CREATE SECOND LINE AT REAR
AL,1,2,53,54,13,14                      !CREATE AREA AT REAR

AOVLAP,17,18,19                     !Overlap and create area 18,19,20
LESIZE,49, , ,4,1,                  !Division on line 49
LESIZE,50, , ,4,1,                  !Division on line 50

K,502,0.011,-0.002,0
K,503,0.011,0.002,0
K,504,0.030,0.002,0
K,505,0.030,-0.002,0

LSTR,502,503
LSTR,503,504
LSTR,504,505
LSTR,505,502
AL,55,56,57,58

ASBA,20,17,,KEEP,DELETE                  !Take away space from body

ET,1,141                            !Element type 1 Fluid141
MAT,2                               !Material No2
AMESH,18,19,1                       !Mesh area 18, 19
MAT,3                               !Change material type
AMESH,20,,1                         !Mesh area 20


!----- Apply the boundary conditions -----
LSEL,S,LOC,X,-length/2,,,1                   !Select the inlet
D,ALL,VX,velocity*COS(alpha*(3.1415/180))   !Velocity in X
D,ALL,VY,velocity*SIN(alpha*(3.1415/180))   !Velocity in Y
LSEL,S,LOC,Y,height/2,,,1                    !Select the top
D,ALL,VX,velocity*COS(alpha*(3.1415/180))   !Velocity in X
D,ALL,VY,velocity*SIN(alpha*(3.1415/180))   !Velocity in Y
LSEL,S,LOC,Y,-height/2,,,1                   !Select the bottom
D,ALL,VX,velocity*COS(alpha*(3.1415/180))   !Velocity in X
D,ALL,VY,velocity*SIN(alpha*(3.1415/180))   !Velocity in Y
LSEL,S,LOC,X,length/2,,,1                    !Select the outlet
D,ALL,PRES,outpre                            !Pressure = 0
LSEL,S,LINE,,1,14,1,0                        !Select the fin X-section
NSLL,S,1                                     !Select nodes attached to lines
D,ALL,VX,0                                   !Velocity in X
```

```
D,ALL,VY,0                           !Velocity in Y
ALLSEL                               !Select all

!----- flotran conditions -----
FLDA,SOLU,TRAN,0                     !Steady state
FLDA,SOLU,FLOW,1                     !Solve flow equations
FLDA,SOLU,TEMP,0                     !Adiabatic
FLDA,SOLU,TURB,1                     !Turbulent
FLDA,SOLU,COMP,0                     !Incompressible
FLDA,SOLU,SWRL,0                     !No swirl
FLDA,SOLU,SPEC,0                     !???????

FLDA,ITER,EXEC,200,                   !Global iterations 30
FLDA,ITER,CHEC,0,                    !No overwrite of .rfl file
FLDA,ITER,APPE,0,                    !No append of .rfl file
FLDA,TERM,PRES,1e-08,                !Pressure termination criteria
FLDA,OUTP,SUMF,50,                   !Output summary frequency 50

FLDA,PROP,DENS,0
FLDA,VARY,DENS,0
FLDA,PROT,DENS,CONSTANT              !Set the density constant
FLDA,NOMI,DENS,1024,                 !1024kg/m^3
FLDA,PROP,VISC,0
FLDA,VARY,VISC,0
FLDA,PROT,VISC,CONSTANT              !Set the viscosity constante
FLDA,NOMI,VISC,0.001,                !0.001 kg/m.s
FINISH                               !Leave the Pre-Processing

/SOLU                                !Enter the Solution
SOLVE                                !Run the Solution of the CFD analysis
SAVE                                 !Save the database
FINISH                               !Leave the Solution


STRU-1ST.PRO

!This program is an ANSYS input after the run of FLOW-1ST.PRO
/FILNAM,stru1
RESUME,flo1,db,,0
!-------------------------------------------------------------------
!| PRE-PROCESSING, SOLU & POST-PROCESSING OF THE 1ST STRUCTURAL ANALYSIS |
!-------------------------------------------------------------------

/PREP7                               !Enter the Pre-Processing
ALLSEL                              !Select everything
UIMP,2,EX, , ,5000000,               !Young's Modulus for material No2
UIMP,2,NUXY, , ,0.49,                !Poisson's Coefficient for material No2
UIMP,3,EX, , ,5000000,               !Young's Modulus for material No3
UIMP,3,NUXY, , ,0.49,                !Poisson's Coefficient for material No3
FINISH                               !Leave the Pre-Processing

/SOLU                                !Enter the Solution
DDELE,ALL,ALL                        !Delete all BC fron the previous CFD
LDREAD,PRES,last,, , ,flo1,rfl,      !Import the pressure from the CFD

CLAMPING                             !Call proceedure for applying boundary conditions

/STAT,SOLU
SOLVE                                !Run the Solution of the structural analysis
FINISH                               !Leave the Solution

/POST1                               !Enter the Post-Processing

PLDISP,2                             !Plot the displacement
```

```
FINISH                          !Leave the Post-Processing

!----------------------------------------------------------------
!|                   PREPARATION FOR THE 2ND CFD                 |
!----------------------------------------------------------------

NEWSHAPE                        !See the newshape.mac macro

*DIM,xkparray,ARRAY,60,1,1      !Create an array for the 60 X coordinate
*VGET,xkparray(1),KP,1,LOC,X,,,,2!of the keypoints
*DIM,ykparray,ARRAY,60,1,1      !Create an array for the 60 Y coordinate
*VGET,ykparray(1),KP,1,LOC,Y,,,,2!of the keypoints
PARSAV,ALL,first,par,,          !Save parameter & array on file: 1st.par
SAVE                            !Save the database
*MSG,NOTE,                      !Note message
You must QUIT ANSYS and ENTER FLOTRAN %/ with the input file: FLOW-2ND.PRO



NODECATCHER

*DIM,xnode,ARRAY,10000,1,1,
*VGET,xnode(1),NODE,1,LOC,X, , , ,2
*DIM,ynode,ARRAY,10000,1,1,
*VGET,ynode(1),NODE,1,LOC,Y, , , ,2
ACLEAR,ALL
ADELE,ALL, , ,1

KPX1=1
KPY1=1
KPX6=(((length*8)+1)*(divi+1))+1
KPY6=(((length*8)+1)*(divi+1))+1
KPX11=KPX6+(3*(divi+1))
KPY11=KPY6+(3*(divi+1))


K,1,xnode(1),ynode(1)
k,6,xnode(KPX6),ynode(KPY6)
k,11,xnode(KPX11),ynode(KPY11)



NEWSHAPE.MAC

!This is a MACRO for STRU-1ST.PRO, STRU-2ND.PRO, etc...

/PREP7                          !Enter the Pre-Processing
*DIM,xnode,ARRAY,10000,1,1,     !Create an array for the X coordinate
*VGET,xnode(1),NODE,1,LOC,X,,,,2 !of each nodes
*DIM,ynode,ARRAY,10000,1,1,     !Create an array for the Y coordinate
*VGET,ynode(1),NODE,1,LOC,Y,,,,2 !of each nodes

*DIM,dispX,ARRAY,10000,1,1,     !Create an array for the displacement
*VGET,dispX(1),NODE,1,U,X,,,,2  !in X of each nodes
*DIM,dispY,ARRAY,10000,1,1,     !Create an array for the displacement
*VGET,dispY(1),NODE,1,U,Y,,,,2  !in Y of each nodes

ACLEAR,ALL                      !Clear all meshes
ADELE,ALL, , ,1                 !Clear all areas and lines
KDELE,ALL                       !Clear all keypoints

KP1=1                           !Create parameters to find the node
KP6=(((length*8)+1)*(divi+1))+1 !number of the nodes related to the
KP11=KP6+(3*(divi+1))           !previous keypoints 1, 6, 11, etc
KP16=KP11+(6*(divi+1))          !The node number is dependant of the
KP21=KP16+(6*(divi+1))          !mesh division and the first keypoint
```

```
KP26=KP21+(6*(divi+1))          !to be mesh (here kp1 = node1)
KP29=KP26+(6*(divi+1))
KP31=KP29+(6*(divi+1))
KP33=KP31+(6*(divi+1))
KP36=KP33+(6*(divi+1))
KP41=KP36+(6*(divi+1))
KP46=KP41+(6*(divi+1))
KP51=KP46+(6*(divi+1))
KP56=KP51+(6*(divi+1))


K,1,xnode(KP1)+dispX(KP1),ynode(KP1)+dispY(KP1)          !Create the
K,6,xnode(KP6)+dispX(KP6),ynode(KP6)+dispY(KP6)          !keypoints by
K,11,xnode(KP11)+dispX(KP11),ynode(KP11)+dispY(KP11)     !additioning the
K,16,xnode(KP16)+dispX(KP16),ynode(KP16)+dispY(KP16)     !node position
K,21,xnode(KP21)+dispX(KP21),ynode(KP21)+dispY(KP21)     !and the node
K,26,xnode(KP26)+dispX(KP26),ynode(KP26)+dispY(KP26)     !displacement
K,29,xnode(KP29)+dispX(KP29),ynode(KP29)+dispY(KP29)
K,31,xnode(KP31)+dispX(KP31),ynode(KP31)+dispY(KP31)
K,33,xnode(KP33)+dispX(KP33),ynode(KP33)+dispY(KP33)
K,36,xnode(KP36)+dispX(KP36),ynode(KP36)+dispY(KP36)
K,41,xnode(KP41)+dispX(KP41),ynode(KP41)+dispY(KP41)
K,46,xnode(KP46)+dispX(KP46),ynode(KP46)+dispY(KP46)
K,51,xnode(KP51)+dispX(KP51),ynode(KP51)+dispY(KP51)
K,56,xnode(KP56)+dispX(KP56),ynode(KP56)+dispY(KP56)


BSPLINE,1,6,11,16        !Create a spline between kpt 1,6,11,16
BSPLINE,16,21,26         !Create a spline between kpt 16,21,26
BSPLINE,26,29,31         !Create a spline between kpt 26,29,31
BSPLINE,31,33,36         !Create a spline between kpt 31,33,36
BSPLINE,36,41,46         !Create a spline between kpt 36,41,46
BSPLINE,46,51,56,1       !Create a spline between kpt 46,51,56,1


KDELE,6         !Delete keypoint 6
KDELE,11        !Delete keypoint 11
KDELE,21        !Delete keypoint 21
KDELE,29        !Delete keypoint 29
KDELE,33        !Delete keypoint 33
KDELE,41        !Delete keypoint 41
KDELE,51        !Delete keypoint 51
KDELE,56        !Delete keypoint 56


*DO,I,1,14              !Create 14 keypoints (kpt2 to kpt15)
KL,1,(1/15)*I,I+1       !on line1, with a space of 1/15
*ENDDO
*DO,I,1,9              !Create 9 keypoints (kpt17 to kpt25)
KL,2,(1/10)*I,I+16     !on line2, with a space of 1/10
*ENDDO
*DO,I,1,4             !Create 4 keypoints (kpt27 to kpt30)
KL,3,(1/5)*I,I+26     !on line3, with a space of 1/5
*ENDDO
*DO,I,1,4             !Create 4 keypoints (kpt32 to kpt35)
KL,4,(1/5)*I,I+31     !on line4, with a space of 1/5
*ENDDO
*DO,I,1,9              !Create 9 keypoints (kpt37 to kpt45)
KL,5,(1/10)*I,I+36    !on line5, with a space of 1/10
*ENDDO
*DO,I,1,14             !Create 14 keypoints (kpt47 to kpt60)
KL,6,(1/15)*I,I+46    !on line6, with a space of 1/15
*ENDDO
LDELE,1,6             !Delete line 1 to 6
```